KAUNAS UNIVERSITY OF TECHNOLOGY

TITAS BRAUKYLA

SYNTHESIS AND INVESTIGATION OF FUNCTIONAL TRÖGER'S BASE MOLECULES FOR OPTOELECTRONIC APPLICATIONS

Doctoral Dissertation
Natural Sciences, Chemistry (N 003)

2019, Kaunas

The present work was carried out at Kaunas University of Technology, Faculty of Chemical Technology, Department of Organic Chemistry, in the period of 2013–2019. It was supported by the Research Council of Lithuania, European Union Seventh Framework Programme [FP7/2007-2013] under grant agreement of the MESO project and European Union's Horizon 2020 research and innovation programme under grant agreement of the PerTPV project.

Dissertation was prepared externally.

Scientific Consultant:
Prof. Dr. Vytautas GETAUTIS (Kaunas University of Technology, Natural Sciences, Chemistry, N 003).

Edited by: Brigita Brasienė and Inga Nanartonytė (Publishing Office "Technologija").

Dissertation Defence Board of Chemistry Science Field:
Prof. Dr. Saulius GRIGALEVIČIUS (Kaunas University of Technology, Natural Sciences, Chemistry, N 003) – **chairman**;
Prof. Dr. Linas LABANAUSKAS (Centre for Physical Sciences and Technology, Natural Sciences, Chemistry, N 003);
Prof. Dr. Vytas MARTYNAITIS (Kaunas University of Technology, Natural Sciences, Chemistry, N 003);
Prof. Dr. Habil. Vytautas MICKEVIČIUS (Kaunas University of Technology, Natural Sciences, Chemistry, N 003);
Prof. Dr. Edvinas ORENTAS (Vilnius University, Natural Sciences, Chemistry, N 003).

The official defence of the dissertation will be held at 11 a.m. on 20th of September, 2019 at the public meeting of Dissertation Defence Board of Chemistry Science Field in the Dissertation Defence Hall at Kaunas University of Technology.

Address: K. Donelaičio St. 73-403, 44249 Kaunas, Lithuania.
Tel. no. (+370) 37 300 042; fax. (+370) 37 324 144; e-mail doktorantura@ktu.lt.

Doctoral dissertation was sent on 20th of August, 2019.
The doctoral dissertation is available on the internet http://ktu.edu and at the library of Kaunas University of Technology (K. Donelaičio St. 20, 44239 Kaunas, Lithuania).

© T. Braukyla, 2019

ISBN 978-609-02-1633-0

The bibliographic information about the publication is available in the National Bibliographic Data Bank (NBDB) of the Martynas Mažvydas National Library of Lithuania.

KAUNO TECHNOLOGIJOS UNIVERSITETAS

TITAS BRAUKYLA

TRIOGERIO BAZĖS FRAGMENTĄ TURINČIŲ FUNKCINIŲ MOLEKULIŲ OPTOELEKTRONIKAI SINTEZĖ IR TYRIMAS

Daktaro disertacija
Gamtos mokslai, chemija (N 003)

2019, Kaunas

Disertacija rengta 2013–2019 metais Kauno technologijos universiteto Cheminės technologijos fakulteto Organinės chemijos katedroje. Moksliniai tyrimai buvo remiami Lietuvos mokslo tarybos, Europos Sąjungos 7-osios bendrosios programos FP7 projekto „Superstruktūros hibridiniai saulės elementai (MESO)“ ir Europos Komisijos finansuojamo mokslo projekto „Perovskitiniai plonasluoksniai fotovoltiniai elementai (PerTPV)“ lėšomis.

Disertacija ginama eksternu.

Mokslinis konsultantas:

Prof. dr. Vytautas GETAUTIS (Kauno technologijos universitetas, gamtos mokslai, chemija, N 003), 2013-2018 m. – mokslinis vadovas.

Redagavo: Brigita Brasienė ir Inga Nanartonytė (leidykla „Technologija“).

Chemijos mokslo krypties disertacijos gynimo taryba:
Prof. dr. Saulius GRIGALEVIČIUS (Kauno technologijos universitetas, gamtos mokslai, chemija, N 003) – **pirmininkas**;
Prof. dr. Linas LABANAUSKAS (Fizinių ir technologijos mokslų centras, gamtos mokslai, chemija, N 003);
Prof. dr. Vytas MARTYNAITIS (Kauno technologijos universitetas, gamtos mokslai, chemija, N 003);
Prof. habil. dr. Vytautas MICKEVIČIUS (Kauno technologijos universitetas, gamtos mokslai, chemija, N 003);
Prof. dr. Edvinas ORENTAS (Vilniaus universitetas, gamtos mokslai, chemija, N 003).

Disertacija bus ginama viešame chemijos mokslo krypties disertacijos gynimo tarybos posėdyje 2019 m. rugsėjo 20 d. 11 val. KTU Disertacijų gynimo salėje.

Adresas: K. Donelaičio g. 73-403, 44249 Kaunas, Lietuva.
Tel. +370 37 300 042; faks. +370 37 324 144; el. paštas doktorantura@ktu.lt.

Disertacija išsiųsta 2019 m. rugpjūčio 20 d.
Su disertacija galima susipažinti interneto svetainėje http://ktu.edu ir Kauno technologijos universiteto bibliotekoje (K. Donelaičio g. 20, 44239 Kaunas).

© T. Braukyla, 2019

ISBN 978-609-02-1633-0

Leidinio bibliografinė informacija pateikiama Lietuvos nacionalinės Martyno Mažvydo bibliotekos Nacionalinės bibliografijos duomenų banke (NBDB).

CONTENTS

1. INTRODUCTION 10
2. LITERATURE REVIEW 14
2.1. Tröger's base. Introduction and structure 14
2.2. Synthesis of Tröger's base 16
2.3. Reactions and modification of methanodiazocine subunit 18
2.4. Reactions and modifications of aromatic rings of Tröger's base 21
2.5. Fused Tröger's base analogs 24
2.6. Heterocyclic Tröger's base analogs 26
2.7. Applications of Tröger's base and its analogs 28
2.8. Tröger's base in optoelectronic applications 33
2.9. Conclusions 34
3. RESULTS AND DISCUSSION 35
3.1. Small-molecular hole transporting materials containing triphenylamine moieties conjoined by Tröger's base core 35
3.1.1. Synthesis of novel Tröger's base compounds and investigation of their structure 36
3.1.2. Thermal and optical properties 39
3.1.3. Photoelectrical properties 40
3.2. Hole transporting materials containing Tröger's base core and phenylethenyl moieties 43
3.2.1. Synthesis of novel Tröger's base derivatives containing phenylethenyl moieties 43
3.2.2. Thermal and optical properties 44
3.2.3. Photoelectrical properties 47
3.2.4. Testing compounds in perovskite solar cells 50
3.3. Hole transporting TPD derivatives conjoined by Tröger's base core 52
3.3.1. Synthesis of compounds 53
3.3.2. Thermal and optical properties 55
3.3.3. Photoelectrical properties 61
3.3.4. Testing compounds in perovskite solar cells 64
3.4. Hole transporting materials containing Tröger's base core and enamine–linked diphenyl branches 66

3.4.1. Synthesis of novel Tröger's base compounds 67
3.4.2. Thermal and optical properties 69
3.4.3. Photoelectrical properties 71
3.4.4. Testing compounds in perovskite solar cells 73
3.5. Sensitizers for dye-sensitized solar cell based on Tröger's base scaffold 74
3.5.1. Synthesis of novel Tröger's base scaffold based dyes 76
3.5.2. Optical properties 78
3.5.3. Photoelectrical properties 82
3.5.4. Quantum chemistry calculations 84
3.5.5. Photovoltaic performance in dye-sensitized solar cells 87
3.6. Improved sensitizers for dye-sensitized solar cells based on Tröger's base scaffold 89
3.6.1. Synthesis of novel dyes based on Tröger's base scaffold 89
3.6.2. Optical properties 92
3.7. Light emitting materials containing tetraphenylethenyl fragments and Tröger's base core 93
3.7.1. Synthesis of novel Tröger's base compounds 94
3.7.2. Thermal and optical properties 96
3.7.3. Photoelectrical properties 100
4. EXPERIMENTAL PART 102
4.1. Instrumentation 102
4.2. Materials 108
5. MAIN RESULTS AND CONCLUSIONS 149
6. SANTRAUKA 151
Įvadas 151
1. Skyles pernešantys organiniai puslaidininkiai, turintys Triogerio bazės fragmentą 155
1.1. Mažamolekulių skyles pernešančių medžiagų, turinčių Triogerio bazės karkasu susietų trifenilamino grupių, sintezė 155
1.2. Terminės ir optinės savybės 156
1.3. Fotoelektrinės savybės 157
2. Skyles pernešančios medžiagos, turinčios Triogerio bazės karkasą ir feniletenilpakaitus 158
2.1. Naujų Triogerio bazės fragmentą turinčių junginių sintezė 158

2.2. Terminės ir optinės savybės 159
2.3. Fotoelektrinės savybės.....159
2.4. Perovskitiniai saulės elementai.....160
3. Skyles pernešantys TPD tipo junginiai, sujungti Triogerio bazės fragmentu..161
3.1. Naujų Triogerio bazės fragmentą turinčių junginių sintezė.....161
3.2. Terminės ir optinės savybės 163
3.3. Fotoelektrinės savybės.....164
3.4. Perovskitinių saulės elementų konstravimas 166
4. Skyles pernešantys puslaidininkiai, turintys Triogerio bazės fragmentą ir šoninius enamino pakaitus.....167
4.1. Naujų Triogerio bazės fragmentą turinčių junginių sintezė.....167
4.2. Terminės ir optinės savybės 168
4.3. Fotoelektrinės savybės.....168
4.4. Junginių išbandymas perovskitiniuose saulės elementuose 169
5. Triogerio bazės karkasą turintys dažikliai įjautrintiems saulės elementams ...170
5.1. Naujų Triogerio bazės karkasą turinčių dažiklių sintezė.....171
5.2. Optinės savybės.....172
5.3. Fotoelektrinės savybės.....173
5.4. Kvantinės chemijos skaičiavimai 174
5.5. Dažikliais įjautrinti saulės elementai.....175
6. Patobulinti TB karkasą turintys dažikliai įjautrintiems saulės elementams 176
6.1. Triogerio bazės karkasą ir tiofeno ar hidrazono fragmentą turinčių dažiklių sintezė.....176
6.2. Optinės savybės.....178
7. Spinduoliai, turintys tetrafeniletenilo fragmentų ir Triogerio bazės karkasą ..179
7.1. Naujų Triogerio bazės fragmentą turinčių spinduolių sintezė.....179
7.2. Terminės ir optinės savybės 181
7.3. Fotoelektrinės savybės.....183
Pagrindiniai rezultatai ir išvados 184
7. REFERENCES 187
8. CURRICULUM VITAE..... 209
9. LIST OF PUBLICATIONS AND CONFERENCES..... 210
10. ACKNOWLEDGEMENTS..... 212

LIST OF ABBREVIATIONS AND PHYSICAL UNITS

μ	charge carrier mobility;
δ	chemical shifts parameter;
ν	wavelength in cm^{-1};
λ	wavelength;
μ_0	zero field charge carrier mobility;
^{13}C NMR	carbon (^{13}C) nuclear magnetic resonance;
^{1}H NMR	proton nuclear magnetic resonance;
A	acceptor;
Ac	acyl;
ACQ	aggregation-caused quenching;
AEE	aggregation-enhanced emission;
AIE	aggregation-induced emission;
Ar	aromatic;
BODIPY	boron-dipyrromethene;
$CDCl_3$	deuterated chloroform;
CSA	(±)-camphor-10-sulfonic acid;
CV	cyclic voltammetry;
D	donor;
d	layer thickness;
DCM	dichloromethane;
DMF	*N*,*N*-dimethylformamide;
DMSO	dimethyl sulfoxide;
DNA	deoxyribonucleic acid;
DSC	differential scanning calorimetry;
DSSC	dye sensitized solar cell;
E	electric field;
EA	electron affinity;
ee	enantiomeric excess;
E_g	energy band gap;
E_g^{opt}	optical band gap;
Fc	ferrocene;
FF	fill factor;
FL	fluorescence;
FTO	fluorine-doped tin oxide;
HOMO	highest occupied molecular orbital;
HTM	hole transporting material;
ICT	intramolecular charge transfer;
I_p	ionization potential;
IPCE	incident photon to current conversion efficiency;
IR	infrared;
ITO	indium tin oxide;
J	coupling constant in Hz;
J_{sc}	short circuit current;

LUMO	lowest unoccupied molecular orbital;
NBS	*N*-bromosuccinimide;
NIR	near-infrared;
NMR	nuclear magnetic resonance;
o-DCB	*o*-dichlorobenzene;
OLED	organic light-emitting diode;
PCE	solar-to-electric power conversion efficiencies;
PC-Z	bisphenol Z polycarbonate;
PESA	photoelectron spectroscopy in air;
Ph	phenyl;
PH	phosphorescence;
PL	photoluminescence;
ppm	parts per million;
PS	polystyrene;
PSC	perovskite solar cells;
PV	photovoltaic;
SCE	standard-reference Calomel electrode;
SHE	standard hydrogen electrode;
Sphos	2-dicyclohexylphosphino-2',6'-dimethoxybiphenyl;
spiro-OMeTAD	2,2',7,7'-tetrakis-(*N*,*N*-di-*p*-methoxyphenylamine)-9,9'-spirobifluorene;
ssDSSC	solid-state dye-sensitized solar cell;
T	temperature;
t	time;
TB	Tröger's base;
t-Bu	*tert*-butyl;
T_{dec}	decomposition temperature;
TFA	trifluoroacetic acid;
T_g	glass transition temperature;
TGA	thermogravimetric analysis;
THF	tetrahydrofuran;
TLC	thin layer chromatography;
T_m	melting point;
TMS	trimethylsilane;
TPA	triphenylamine;
TPD	*N,N'*-bis(3-methylphenyl)-*N,N'*-diphenylbenzidine;
TPE	tetraphenylethene;
UV-Vis	ultraviolet-visible;
V_{oc}	open circuit photovoltage;
XPhos	2-dicyclohexylphosphino-2',4',6'-triisopropylbiphenyl;
XTOF	xerographic time of flight technique;
ε	extinction coefficient;
η	solar energy to electricity conversion efficiency;
Φ_F	fluorescence quantum yield.

1. INTRODUCTION

Technological progress is making various devices an inseparable part of daily life, consequently raising the demand of new materials for their manufacturing. In the recent years, considerably more attention is paid to organic materials for their use in electronics and optoelectronics. The employing of organic compounds in devices has some advantages, as such devices or their parts can be cheaper, flexible (due to amorphousness of materials), lighter, require less energy to produce, and offer a way to overcome the problem of rare materials, as these compounds consist of abundant chemical elements. These organic compounds find their use in various applications such as organic light emitting diodes (OLEDs), photovoltaic cells, electrophotography, field-effect transistors, and others [1].

The well performing optoelectronic devices can as well contribute to finding a two-sided solution to the problem of increasing energy demand caused by the growing human population and intensifying usage of various technologies, as energy consumption is predicted to increase to 56% by 2040 [2]. This challenge can be addressed by providing a cheap and convenient access to the renewable source of solar power and decreasing energy wasted by the inefficient devices. The harnessing of solar power seems to be a desired option, because it is the primal and direct energy source from which the majority of other renewable energy sources originate; furthermore, solar cells directly transform it into electricity: a form that is the most suitable for transfer, accumulation, and usage. Organic and hybrid solar cells are earning their place in a market of photovoltaic cells, mainly dominated by the already well developed inorganic cell technology and offer an alternative of inexpensive, flexible, light, less fabrication energy and expensive chemical elements demanding technology [3]. Among the most popular of them are dye sensitized solar cells (DSSC) and perovskite solar cells (PSC), i.e., a rapidly developing technology that is already holding the performance record of 23.2% efficiency [4]. A flip-side solution to the energy problem would be the development and implementation of energy saving technologies, and illumination is a suitable field for innovation due to artificial lighting that is a major source of electricity demand globally, accountable for 15% of global electricity consumption [5, 6]. Light emitting diodes (LEDs) and their organic counterparts (OLEDs) offer high power to light conversion ratio, allowing cutting the energy demand by multiple times while maintaining the same illumination. OLEDs as well have the benefits of organic electronics, lightness and flexibility among others, allowing manufacture of thin, large-area devices, sheets, and panels. The main functions of organic compounds in all these optoelectronic devices are charge transport, light emission, and charge generation. Therefore, the development of high-performing materials with desired characteristics is essential for the production of high-performance devices.

Tröger's base (TB) is V-shaped C_2-symmetric chiral molecule consisting of a bicyclic aliphatic methanodiazocine unit fused with two aromatic rings, their planes nearly perpendicular to each other. Such structure of rigid V-shaped molecular scaffold allows it be used as a core and provide angle orientation for the substituents,

such as conjugated π-systems, attached to it. It was as well reported that, besides connecting aromatic fragments only geometrically, the non-conjugated bridge in Tröger's base can bestow electronic coupling for conjoined fragments in the absence of a π-linker [7]. Hence, Tröger's base offers itself as a unique, nanometer-sized building block for unusual molecular design, granting the possibility to bestow compounds with desired, yet uncommon, properties. Although Tröger's base is already well studied and found applicability in different areas such as molecular recognition, supramolecular chemistry, biological labeling, ligand design (especially for asymmetric catalysis), DNA interactions, or even as drug candidates, its use in optoelectronics was not widely described, leaving this field for further investigation and discovery. Hence, the field of interest presented in this work is the synthesis and investigation of novel functional Tröger's base compounds for optoelectronic applications: charge generating double-acceptor TB dyes for dye-sensitized solar cells, solid-state light emitting Tröger's base derivatives for OLEDs, and well performing amorphous hole transporting materials for perovskite solar cells.

The main aim of this work is the synthesis and investigation of the V-shaped Tröger's base derivatives as charge generating, transporting, and light emitting materials.

The tasks proposed for the achievement of the above stated aims were as follows:

1. Synthesis and investigation of small-molecular HTMs containing triphenylamine moieties conjoined by Tröger's base core;
2. Synthesis and investigation of HTMs consisting of photoconductive TPD-type (*N*,*N'*-bis(3-methylphenyl)-*N*,*N'*-diphenylbenzidine) moieties conjoined by Tröger's base core;
3. Synthesis and investigation of HTMs containing Tröger's base core and enamine–linked diphenyl branches;
4. Synthesis and investigation of sensitizers based on Tröger's base scaffold;
5. Synthesis and investigation of light emitting materials containing TPE (tetraphenylethene) fragments and TB core.

Scientific novelty: the series of novel HTMs based on Tröger's base core have been synthesized, and the influence of the substituents on thermal and photoelectrical properties of these compounds has been investigated. It was determined that synthesized Tröger's base compounds incorporating triphenylamine fragments with methyl- and methoxy- substituents qualify as HTMs and have quite favorable physical properties, are stable, mainly amorphous and readily soluble, making them decent candidates for the use in optoelectronics. In addition, the synthesis and investigation of these compounds provided useful research information and some insight for further development in HTM molecular design.

The novel V-shaped hole-transporting compounds based on Tröger's base core and phenylethenyl substituted triphenylamine moieties were synthesized and studied. Tröger's base core significantly increases glass transition temperatures of the HTMs,

which is especially apparent when compared to non-TB analogues, while phenylethenyl moieties provide structural bulk, decrease crystallinity, and considerably contribute to the size of the π-conjugated system of molecules. These HTMs were investigated and tested in perovskite solar cells, concluding that they are promising candidates for application in organic and hybrid optoelectronic devices, as they can be handled in the air, are thermally stable, require no high temperature annealing steps, can be solution deposited, and possess comparatively high mobility (up to 0.011 $cm^2 V^{-1} s^{-1}$).

Novel HTMs based on the concept of TPD-type moieties conjoined by a Tröger`s base core have been synthesized and investigated. The TB core provides orientation for TPD fragments angle-wise towards each other and hampers the crystallization processes, rendering the investigated compound fully amorphous, while oriented *para*- substituted TPD-type moieties provide high charge mobility. These HTMs are promising candidates for the application in organic and hybrid optoelectronic devices due to their stability, amorphousness, high glass transition temperatures, ability to be solution deposited, and comparatively high charge mobility (up to 0.036 $cm^2 V^{-1} s^{-1}$), exceeding that of the corresponding non-TB methyl and methoxy TPD analogues by more than two orders of magnitude. The preliminary testing in perovskite solar cells indicates that this class of TB-linked molecules can function effectively as HTM in the device.

New V-shaped Tröger's base derivatives having the enamine-linked diphenyl branches were synthesized by using a simple and convenient procedure and yielding compounds with decent HTM properties. The synthesis of these materials does not require palladium catalysts and corresponding ligands, inert atmosphere conditions, and, consequently, no palladium residue in the reaction mixture allows easy separation, evading extensive purification by column chromatography. These hole-transporting materials are thermally stable, solution processable and have a relatively high hole-drift mobility, making these compounds attractive for various applications in optoelectronics. When tested in perovskite solar cells, the best performing material in this group demonstrated very high efficiency, rivaling that of the state-of-the-art Spiro-OMeTAD, and even outperformed it by 1.6 times in a dopant-free PSC composition.

A set of novel metal-free di-anchoring organic dyes based on a Tröger's base scaffold, possessing triphenylamine donor and rhodanine-3-acetic acid as acceptor/anchoring group, linked by the poly[n]enic (n = 0–2) chain, have been designed and synthesized. The investigation of the influence of the polymethine chain length and number of the anchoring groups on the photophysical, electrochemical, and photovoltaic properties of these V-shape sensitizers, as well as testing in DSSCs, showed that the extended polymethine chains ensure flexibility of these units and allow the interaction between two chromophores, hence promoting aggregate formation and impairing their performance. Such findings encourage the replacement of polymethine backbones with rigid bulky structural spacers, which could prevent aggregate formation in di-anchoring organic TB dyes. Novel structurally improved di-anchoring Tröger's base dyes with thiophene and phenyl-branched hydrazone spacers were designed; their synthetic pathways were discovered, and the

investigation of properties was performed. It was found that even though thiophene fragment bestowed the compounds with superior light absorption properties, it still does not offer sufficient structural stiffness to prevent intra-anchoring. On the contrary, phenyl-branched hydrazone unit successfully provided both the rigid structure and structural bulk, hampering these unfavorable interactions. These dyes are promising candidates for the DSSC applications.

Novel Tröger's base compounds with TPE side-arms were synthesized and investigated. These compounds are thermally stable, soluble and possess aggregation induced emission (AIE) properties, allowing them to be used in forming pristine solid-state layers in light emitting devices. Even though quantum efficiency values of these compounds were not as high as expected, the research results revealed some structure-properties relations that allows further improvement and optimization in the molecular design of the future light emitting TB compounds with AIE properties.

The main statements of doctoral dissertation are the following:

1. The newly synthesized small-molecular HTMs containing triphenylamine fragments conjoined by Tröger's base core, varying in substituents on outer phenyl rings, are thermally stable, solution processable, and possess comparatively high mobility ($1.2 \cdot 10^{-5}$–$3.3 \cdot 10^{-4}$ cm^2/Vs), thus making them promising candidates for the application in optoelectronic devices.
2. HTMs containing Tröger's base core and phenylethenyl side-branches are thermally stable, solution processable, and possess comparatively high mobility (up to 0.011 $cm^2\ V^{-1}\ s^{-1}$), thus making them promising candidates for the application in the perovskite solar cells (PSC).
3. The TB core provides orientation for para- substituted TPD fragments angle-wise towards each other, yielding stable, fully amorphous materials with comparatively high charge mobility (up to 0.036 $cm^2\ V^{-1}\ s^{-1}$), indicating that this class of TB-linked molecules can function effectively as HTM in the PSC devices.
4. Tröger's base formation and modification allow easy three-step transition-metal-free synthesis of efficient HTMs with TB core and enamine-linked diphenylamine moieties that can outperform the state-of-the-art Spiro-OMeTAD in efficiency in perovskite solar cells.
5. Tröger's base can be used as a core for molecular design of novel solid-state light emitting compounds with AIE properties and sensitizers for dye sensitized solar cells.

2. LITERATURE REVIEW

2.1. Tröger's base. Introduction and structure

In 1887, Carl Julius Ludwig Tröger made a publication on condensation reactions between aromatic amines and methylal (dimethoxymethane) [8], hence starting the history of Tröger's base (TB). During the experiment, an unexpected product was isolated from the reaction between *p*-toluidine and methylal (which is hydrolyzed to formaldehyde and methanol in reaction mixture) in aqueous HCl, and it was described as "base $C_{17}H_{18}N_2$". It took almost half a century, in 1935, the exact chemical structure was determined by Spielman, who carefully analyzed the reactivity of the substance and assigned TB **1** as racemic 2,8-dimethyl-6*H*,12*H*-5,11-methanodibenzo[*b*,*f*][1,5]diazocine ((±)-**1**) (Figure 2.1) [9].

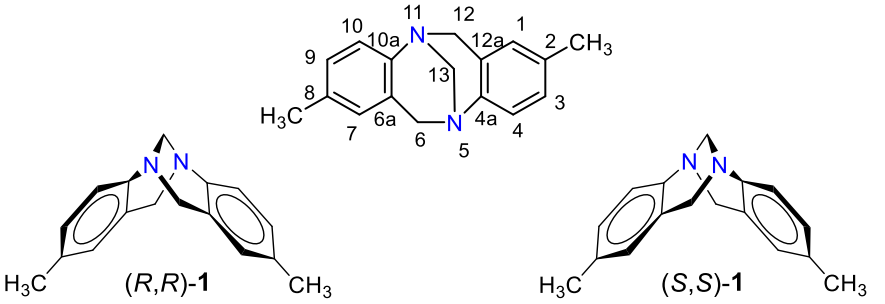

Figure 2.1. Tröger's base ((±)-**1**) and the structures of its (*R*,*R*) and (*S*,*S*) enantiomers

A few months later in the same year, a condensation mechanism, according to which the forming of Tröger's base **1** occurs, was proposed by Wagner (Scheme 2.1) [10].

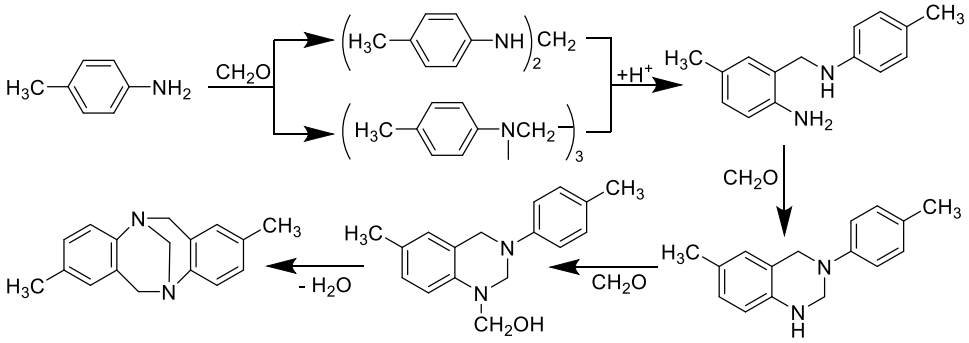

Scheme 2.1. Mechanism of Tröger's base formation proposed by Wagner

The next big event in the history of Tröger's base occurred in 1944, when Vladimir Prelog performed and published separation of Tröger's base **1** into its mirror-image components by chromatography on a column of lactose hydrate [11], pioneering the process and making TB one of the first compounds resolved on an enantiopure stationary phase. Due to that, TB **1** was used mainly for the evaluation of

new separation techniques until the 1980s [12]. The exploration of TB chirality was the first of many landmarks in stereochemistry, a field that became identified with Prelog's name, and discoveries in this field ultimately won him Nobel Prize in Chemistry in 1975 [13]. Tröger's base appeared interesting in other aspects as well, and the attention to its derivatives started to grow as the field of supramolecular chemistry, specifically molecular recognition, was evolving. In 1986, the structure, proposed by Spielman half century earlier, was unquestionably confirmed by single-crystal X-ray diffraction analysis by Wilcox [14], which later led to the conclusion that (+)-TB had the *S,S* configuration [15]. The XRD structure of the Tröger's base framework and several simple but unprecedented TB analogs synthesized by Wilcox [16] and his colleagues started a new wave of research of TB, followed by a series of publications, bearing some remarkable results and including the renowned Wilcox molecular torsion balance, allowing the measurement of "intermolecular" interactions [17, 18]. Later, various research interests emerged and were explored by using TB as building blocks in various fields of chemistry, investigation fields, including receptors, biological labeling, ligand design for asymmetric catalysis, DNA interactions, and even drugs and medical applications.

The Tröger's base consists of a bicyclic aliphatic unit fused with two aromatic rings. The central methanodiazocine unit orientates the aromatic rings in a nearly perpendicular fashion, making TB a rather rigid V-shaped molecule, its angular orientation of aromatic rings creating a hydrophobic cavity (Figure 2.1). Tröger's base is C_2-symmetric; therefore, it is a chiral molecule. The methylene fragment impedes pyramidal inversion of the bridged nitrogen atoms, creating configurationally stable stereogenic centers. TB is known as one of the first molecules having such N atoms to be discovered. These stereogenic nitrogen atoms are bridgehead atoms, hence allowing only the enantiomers of either *R,R* or *S,S* configuration to exist (Figure 2.1), and diastereomeric (*R,S*)-TB is being geometrically impossible.

Prelog has successfully isolated both enantiomers from the racemate, enabling the investigation of optically active (+)-**1** and (–)-**1**. The enantiomers were found to be stable to the extent that they could be sublimed without any observable racemization, yet this stability does not persist once the molecules are in contact with the diluted acidic media. He reported that TB slowly racemizes and postulated that the configurational inversion takes place due to the reversible formation of the methylene-iminium ion **2** (Scheme 2.2) as a key intermediate [11].

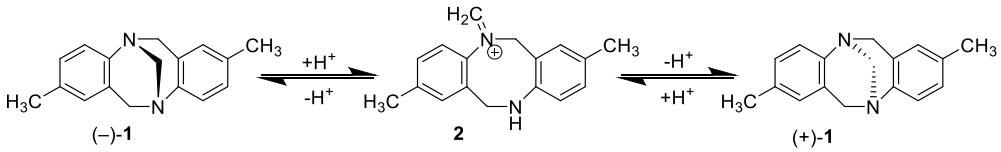

Scheme 2.2. Proposed acid-catalyzed racemization of TB in acidic media

Even though no spectroscopic evidence of such an intermediate compound had been observed [19], it was proposed that the iminium compound exists only transiently and in undiscoverably low concentrations. It was as well noticed that ethano-bridged TB analogs are configurationally stable to acidic conditions as they

are unable to form such stabilized iminium, and this indirectly supports the reported mechanism of TB racemization [20–22]. However, in the concentrated acid media, both TB nitrogen atoms are protonated, making the formation of the iminium intermediate impossible, likely due to no free electron pair available for the opening of the bridge, and no racemization occurs [19].

2.2. Synthesis of Tröger's base

Tröger's base condensation resulting in such structure was first achieved between *p*-toluidine and methylal [8]. Now, after the reaction mechanism was discovered and widely studied, it can be theorized that, in principle, any aromatic or heteroaromatic amine can serve as a possible precursor of TBs; hence, starting aromatic amines could be fully substituted, except for one *ortho* position that is required for the desired cyclization reaction [12]. The first synthesis of polysubstituted Tröger's base analogs was published in 1948 by Smith and Schubert [23]. These authors as well highlighted the necessity of strong acid reaction conditions for the formation of Tröger's bases, as reaction was conducted in diluted hydrochloric acid yields dihydroquinazolines and tetrahydro-quinazolines as major products. Each discovery led to the developing of various methodologies for the synthesis of TB analogs, variating in their original conditions. Despite their variety, the general preparation methods of TB derivatives are based on an acid-induced reaction of aromatic amine with formaldehyde or its equivalent, such as paraformaldehyde, hexamethylene-tetraamine [24], or dimethoxymethane [8, 25], while reaction acidic conditions usually maintained in aqueous or alcoholic HCl solutions, acetic acid, trifluoroacetic acid (TFA), or methanesulfonic acid (Scheme **2.3**) [16, 26–30]. Alternative synthetic protocols are still being discovered and improved, such as methods employing DMSO as a methylene synthetic equivalent [31, 32]. Moreover, the advances in Lewis acid- catalyzed TB synthesis [33, 34], the use of diglycolic acid/polyphosphoric acid [35], or super-acidic conditions [36], and unusual condensation media, such as ionic liquids, have been reported [37].

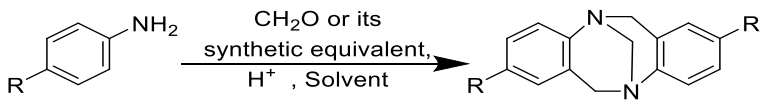

Scheme 2.3. The condensation of Tröger's base

TB condensation based on this synthetic protocol has demonstrated high sensitivity to factors concerning the electronic properties of aniline substituents and their substitution positions. It was presumed that the aromatic ring substituents should have the electron-donating properties, as reactions involving electron-withdrawing groups were noticed to be slow and resulted in the low-yields [38, 39]. Furthermore, it was thought that unsubstituted *para* position should be avoided to prevent polymerization [12].

An important advancement in TB synthesis happened when a new condensation protocol for the synthesis of halogenated TB analogs was developed and introduced by Wärnmark in 2001 [40]. The reaction performed with paraformaldehyde in TFA

removes the limitation of amines having electron-withdrawing substituents and allows synthesis of substituted TB analogs having halogen in nearly any position of the aromatic ring [29], consequently making this protocol to become the most commonly used method among its analogs. Not only does this methodology allow scaling synthesis and obtain multiple grams of halogenated TB analogs [41–43], but it permits the inclusion of a variety of substituents, both electron-donating and electron-withdrawing ones, for example: alkyl chains, MeO and MeS, COOR, CF_3, and even NO_2, which possesses strong electron-accepting properties [35, 44–47]. Notably, this protocol was as well efficient for the condensation of unsubstituted aniline, yielding the TB analog with no methyl groups in a noteworthy 78% [48], hence proving the need of *para*-substitution, as the anti-polymerization measure, unnecessary.

This advancement was achieved by the detailed investigation of the reaction mechanism and taking steps to improve the synthetic protocol further. The first attempt to describe reaction series between *p*-toluidine and formaldehyde, leading to TB condensation, was made by Wagner [10]. This proposed sequence of reactions was reexamined later on by Farrar [49] and Wagner himself [26, 50], leading to the development of reaction mechanism describing the formation of the methano[1,5]diazocine skeleton. The formation consists of a chain of electrophilic aromatic substitution reactions as key steps and assumes the involvement of four main intermediates (**3**–**6**, Scheme 2.4).

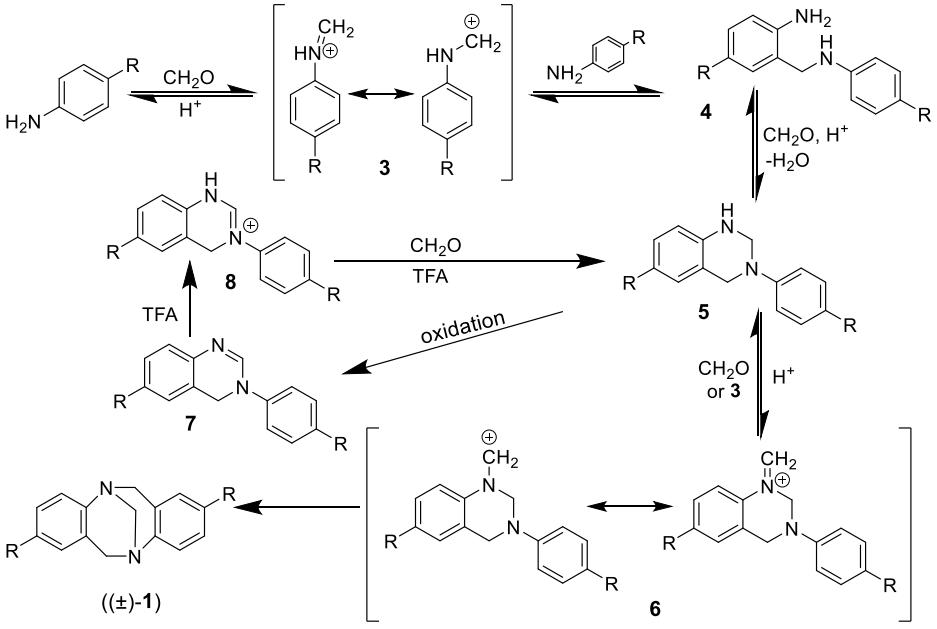

Scheme 2.4. Improved Tröger's base condensation reaction mechanism proposed by Wagner and Farrar

During the first step of the mechanism (R = CH_3), an acid-catalyzed condensation between *p*-toluidine and formaldehyde took place, forming the iminium ion **3**, which then reacts with another equivalent of aniline compound resulting in

intermediate **4** [51]. Two successive additions of methylene were each followed by a cyclization yield TB through intermediate compounds **5** and **6**. The bottleneck of the reaction sequence is the conversion of tetrahydroquinazoline compound **5** into the intermediate **6** and the electrophilic aromatic substitution that follows. The presence of electron-withdrawing substituents of the aniline component decreases the nucleophilicity of the secondary amine in **5**, causing a further decreased rate of the intramolecular electrophilic substitution, consequently promoting to the formation of the dihydroquinazoline **7** as a side reaction (Scheme 2.4). Wärnmark and his group proposed that the presence of paraformaldehyde in TFA increases the concentration of protonated formaldehyde comparative to CH_2O/HCl in ethanol and thus increases the reaction rate for the formation of **6** [40]. Moreover, TFA supports the reduction of dihydroquinazoline **7** to tetrahydroquinazoline **5** by protonation induced by the comparatively strong acid TFA, causing formation of **8**, and is followed by hydride transfer from paraformaldehyde. This reaction mechanism was as well supported by the work of other researchers detecting the intermediate compounds [52] or even isolating and reintroducing them to reaction afterwards to obtain compound **1** [53].

The molecules that are analogous to compound **4** can be obtained by other methods (examples in Scheme 2.5) and then used for the preparation of the Tröger's bases by the previously analyzed condensation principle. Such stepwise method allows obtaining compounds with groups that are more sensitive to relatively harsh reaction conditions and have been used by Wilcox for the synthesis of unsymmetrical analogs of TB. Unsymmetrical molecules are synthesized by employing intermediate analogs of **4** produced from two differently substituted aniline derivatives, followed by cyclization with formaldehyde (Scheme 2.5) [48, 54].

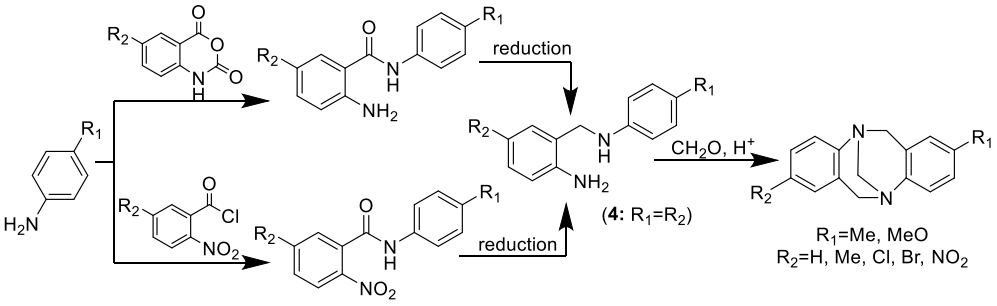

Scheme 2.5. Alternative Wilcox synthesis of TB derivative through the analog of **4**

2.3. Reactions and modification of methanodiazocine subunit

The center of the Tröger's base is a rigid bicyclic aliphatic unit fusing with two aromatic rings. This part of the molecule plays an essential part in defining the shape and properties of the molecule; hence, its chemical reactivity and modification perspectives are of reasonable interest. The methanodiazocine bridge linking two nitrogen atoms into bicyclic structure of **1** is rather sturdy and remains unaffected by sodium and boiling ethanol or, for the most part, Sn/HCl [9]. It is not oxidized by mercury oxide in Et_2O or silver nitrate/ammonia. It does degrade, however, when heated with HI/red-P at high temperature it is resulting in 2,4-dimethylaniline as a

single isolable product (Scheme 2.6). The procedure of refluxing **1** with HI firstly and then reducing it with Sn/HCl allows getting the reduced product and increases its yield [9].

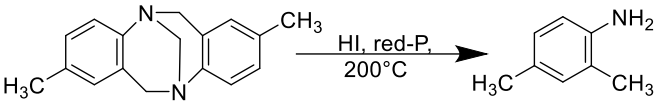

Scheme 2.6. Degradation of methanodiazocine ring

The tertiary amines of the methanodiazocine subunit are potential targets for the TB functionalization. Monoquaternary salts of TB can be easily prepared by reaction with the appropriate alkyl or benzyl bromide (Scheme 2.7, a) [27, 55–57]. Double TB quaternization, involving both nitrogen atoms, was argued to be unattainable because of the strong negative inductive effect caused by the first formed quaternary nitrogen atom, assumedly eliminating the nucleophilicity of the remaining tertiary nitrogen atom. Nonetheless, Lenev and coworkers have synthesized and reported the dimethylated TB analog after obtaining it by using dimethyl sulfate [21]. Tröger's base **1** can as well undergo acetylation and benzoylation, as it was performed by Spielman during the clarification of the structure [9], hence obtaining the diacylated derivative by removing carbon atom of methylene bridge in the form of formaldehyde (Scheme 2.7, b).

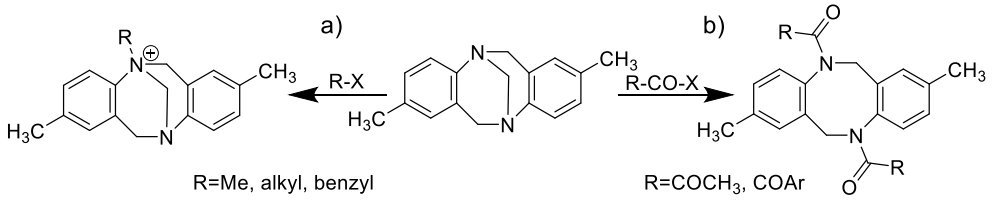

Scheme 2.7. Alkylation, benzylation, and acylation of TB aliphatic unit

Spielman has as well performed and reported nitrosation of TB, during which the methylene bridge is detached [9]. The resulting di-*N*-nitroso analog was converted into diamine in reaction with CuCl/HCl (Scheme 2.8), reported by Cooper and Partridge [58]. The obtained diamine was used in condensation with different ketones and aldehydes, resulting in TB analogs possessing functionalized methylene bridges. Such stepwise method later was employed as a general procedure for the preparation of various analogs of Tröger's base, having one or two substituents attached to the methylene bridges [19, 59].

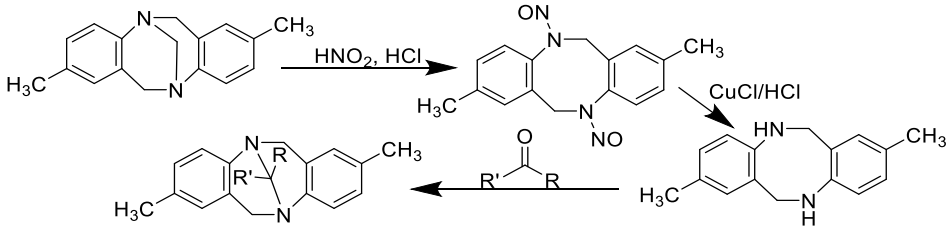

Scheme 2.8. Stepwise synthesis of TB analogs with substituted methano bridges

Periasamy and coworkers have reported a simple one-pot method for substitution reactions with aromatic carbonyl compounds in the presence of $TiCl_4$ or $POCl_3$, making alterations of the methanodiazo fragment possible with no prior removal of the methano bridge needed (Scheme 2.9) [60].

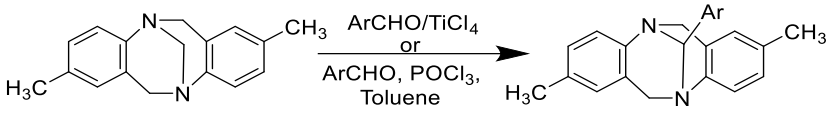

Scheme 2.9. Synthesis of TB analogs with aromatic substituent attached to methano bridge

In addition, they obtained the corresponding TB analog under Vilsmeier-Haack conditions, proving that TB reaction employing DMF as the carbonyl partner in the presence of $POCl_3$ is possible. Furthermore, the regioselective synthesis of dialkylamino-substituted TB analogs under Vilsmeier-Haack conditions was reported by Reddy and coworkers [61]. The reaction of TB analogs with substituents on their aromatic rings and various formamide derivatives in the presence of $POCl_3$ resulted in TB analogs with arylalkylamino-substituted methano bridges in yields of 53–83% range. The usage of $POBr_3$ as a substitute for insertion of *N*,*N*-disubstituted amines presented similar results [62].

A different approach to modify the methano bridge through its cleavage was proposed by Hamada and Mukai [20]. They reported a method of treatment of (+)-**l** with 1,2-dibromoethane in the presence of lithium carbonate in DMF to afford the desired ethano- Tröger's base in 76% yield (Scheme 2.10). It is assumed that the "bridge-replacement" takes place through ammonium ion and dibromide intermediates before the formation of the ethano-TB analog along with dibromomethane.

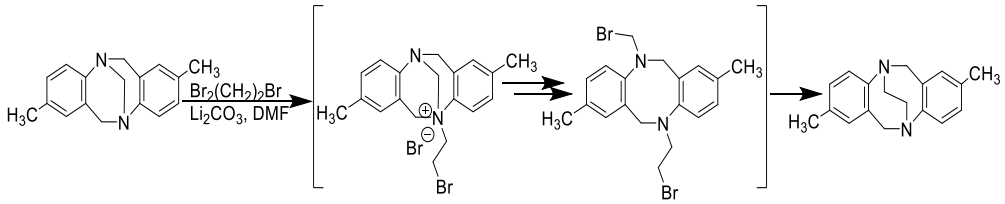

Scheme 2.10. Synthesis of ethano-Tröger's base

Other possible position within the central heterocyclic subunit of Tröger's base that could be interacted chemically are the atoms of methylenes that are adjusted directly to aromatic rings. Even though TB analogs with substituents in these positions had already been indirectly synthesized previously [63, 64], Harmata and coworkers pioneered the derivatization of the benzylic methylene components of TB molecule itself [65, 66]. Earlier, Harmata's methodology involved metalation of the benzylic methylene groups by treatment of TB (**1**) with $BF_3{\cdot}OEt_2$, followed by reaction with *n*BuLi, and quenching by electrophile, therefore obtaining the *exo*-monosubstituted species. Both sided *exo*, *exo*-disubstitution can be done likewise by repeated

monometalation and electrophilic quenching (Scheme 2.11), yet the need to conduct the synthesis in a sequential manner consequentially decreased the overall yields [67].

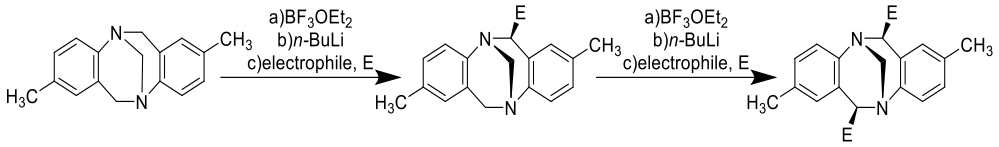

Scheme 2.11. Modification of TB by mono- and di-substituting the *exo* positions of the benzylic methylenes

Cvengroš and coworkers reported a simple direct approach of oxidative acetoxylation and azidation of benzylic methylene groups in Tröger's base analogs promoted by *N*-bromosuccinimide (NBS) and $Pd(OAc)_2$ under mild conditions (Scheme 2.12). This method is centered on NBS oxidizing the carbon atoms next to the nitrogen atoms in the presence of $Pd(OAc)_2$, followed by a reaction with oxygen- or nitrogen-based nucleophiles such as KOAc or NaN_3, yielding either the mono- and bisacetoxylated or azidated TB derivatives in a stereo- and chemoselective manner. X-Ray crystallographic analyses of obtained compounds provided an unambiguous proof that the acetoxylation occurred only at the benzylic carbons, hence leaving the methylene-bridge carbon untouched [68].

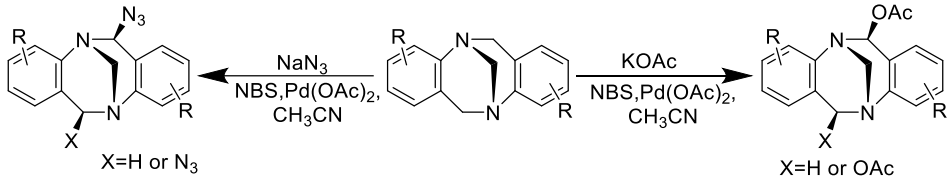

Scheme 2.12. Oxidative acetoxylation and azidation of benzylic methylene groups

2.4. Reactions and modifications of aromatic rings of Tröger's base

Aromatic system is the other part of the Tröger's base molecule; thus, a significant part of research and reports involving the derivatization of TB are mostly focused on the aromatic rings, a tendency mostly attributable to the easy access to halogenated analogs of Tröger's base, as mentioned before [29, 41, 43–48, 69]. Even though most of the methods obtain Tröger's base analogs directly from corresponding halogenated anilines, various studies on the direct halogenation of the aromatic rings of TB analogs have been reported. Didier and Sergeyev proposed a method for the 8-bromo-2-iodo-substituted TB analog from the di-demethylated analog of TB by sequential iodination and bromination (Scheme 2.13) [48]. Try and coworkers analyzed the mono- and dichlorination and -bromination of di-demethylated TB analogs and differently substituted analogs of TB, resulting in moderate overall yields of halogenated TB analogs [70].

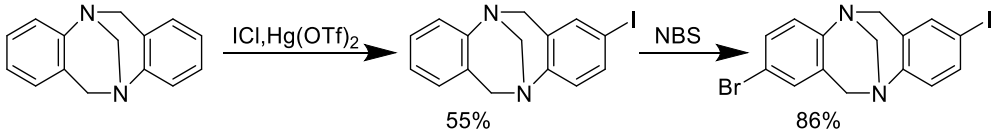

Scheme 2.13. Sequential halogenation of di-demethylated TB

The more practical and arguably the most popular method is the direct path of synthesis of halogenated analogs of TB that was introduced by Wärnmark [40]. The same article as well reported that halogenated TB analogs offer access to various other functional groups via the introduction of ethynyl substituents by Corriu–Kumada cross-coupling (Scheme 2.14, a). Moreover, various research groups have used halogenated TB analogs in a series of transition-metal-catalyzed C-C cross-coupling reactions. Wärnmark and coworkers as well employed Sonogashira coupling reactions to introduce substituted alkynyl groups to halogenated TB analogs (Scheme 2.14, b) [43, 69, 71]. Lützen reported the usage of arylboronic acids as coupling reagents for arylation reactions by Suzuki–Miyaura coupling (Scheme 2.14, c) [41, 71, 72]. Wärnmark has published a report comparing different palladium-catalyzed cross-coupling techniques used for the introduction of aryl and heteroaryl groups through metalated TB analogs (Scheme **2.14**, d); it was shown that the Suzuki coupling method is superior paralleled to others, as it gives excellent yields, while Stille and Negishi coupling offers moderate to good yields [72]. Besides these classical cross-coupling methods, C-C bond formation was achieved by palladium-catalyzed cyanation and reported by Didier and Sergeyev (Scheme 2.14, e) [73, 74].

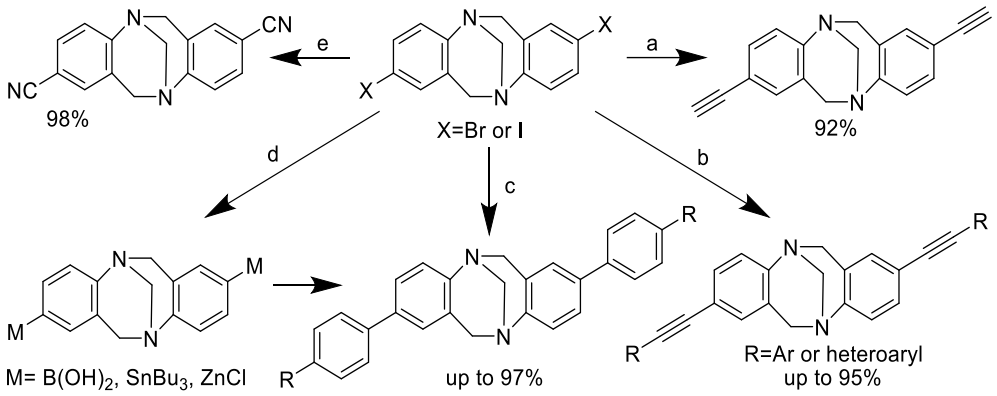

Scheme 2.14. Main examples of transition-metal-catalyzed transformations with halogenated analogs of TB. Reaction conditions: a) HC≡CMgBr, $Pd(PPh_3)_4$; b) $Pd(PhCN)_2Cl_2$, P(*t*Bu)$_3$, alkyne-R substrate, CuI; c) $Pd[P(tBu)_3]_2$, substituted phenylboronic acid, CsF; d) e.g.: *n*BuLi, THF, –78 °C, $B(OCH_3)_3$; then $Pd[P(tBu)_3]_2$, substituted halobenzene, CsF; e) $Zn(CN)_2$, Zn, $[Pd_2(dba_3)]$, dppf.

Transition-metal-catalyzed reactions have been reported as a viable method for carbon-heteroatom bond formation in halogenated analogs of TB. As such, C–O bond formation was reported in method by employing Ullmann coupling conditions (Scheme **2.15**, a) [71, 75]. The formation of C–N bonds from halogenated TB analogs can as well be achieved by Buchwald–Hartwig protocols such as Cu catalyzed amidation [73] and Pd-catalyzed amination (Scheme 2.15, b) [73, 74, 76–81].

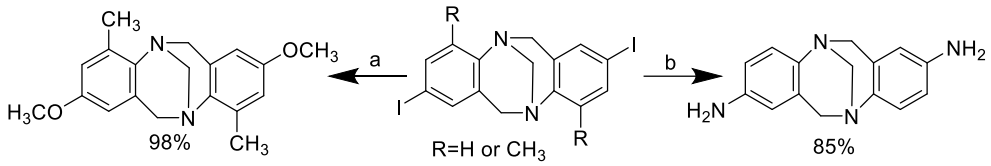

Scheme 2.15. Examples of transition-metal-catalyzed reactions for carbon–heteroatom bond formation. Reaction conditions: a) $NaOCH_3$, CuCl, MeOH/DMF; b) 1) $Pd_2(dba)_3$, BINAP, NaO*t*Bu, benzophenone imine, toluene; 2) HCl_{aq}, THF.

Wärnmark and coworkers have developed a different method to produce valuable mono- and disubstituted analogs of TB [82]. Symmetrical disubstituted analogs of Tröger's base were achieved by double halogen/lithium exchange with 2.4 equiv. *n*-BuLi followed by electrophilic quenching. (Scheme 2.16, a). Alternatively, analogous conditions with only 1.1 equiv. of *n*-BuLi results in asymmetrically monosubstituted analog of TB instead (Scheme 2.16, b). The selectivity for the single bromine/ lithium exchange was attributed to the solvent effect. It was proposed that dilithiated molecules were better solvated in THF compared to Et_2O. This solvation difference causes higher difference in energy between mono- and dilithiated species in the solvent mixture of THF/Et_2O compared to THF. A second bromine/lithium exchange performed with the monosubstituted TB analog and subsequent electrophilic quenching allowed obtaining asymmetric disubstituted TB analogs.

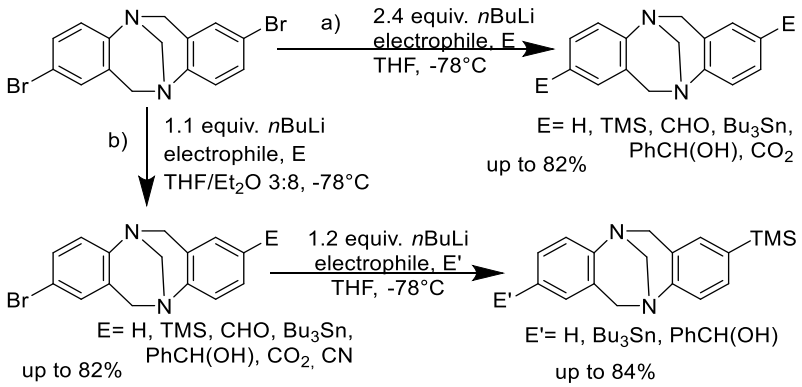

Scheme 2.16. Halogen/lithium exchange protocol for the synthesis of symmetric and asymmetric analogs of TB.

The formation of C–N bonds from halogenated TB analogs as well were reported by Wärnmark [83], done via halogen/lithium exchange followed by quenching with TSN_3 and subsequent reduction of the corresponding azide, thus providing a flexible method suitable for obtaining either mono- or diamino-substituted TB analogs. The synthesis of 2-amino-8-bromo-substituted analogs of TB by this monosubstitution protocol (Scheme 2.17, a) plays a significant role in the synthesis of fused analogs of tris-TB [69, 83]. However, the double halogen/lithium protocol

allowed to synthesize the 2,8- diamino-substituted TB (Scheme 2.17, b), making it an alternative to the palladium-catalyzed Buchwald-Hartwig coupling (Scheme 2.15, b).

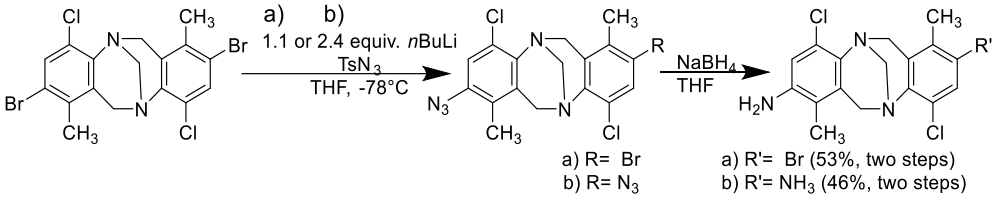

Scheme 2.17. Synthesis of mono- or di- amino-substituted TB analogs based on changes of bromine/lithium exchange protocol

In another approach to amino-substituted TB analogs, Lützen and coworkers synthesized the diamino-substituted TB (Scheme 2.18) by the reduction of the dinitro-substituted derivatives, which were synthesized earlier by the TB condensation from the corresponding nitroanilines. This simple method resulted in good yields of TB derivatives that are easily further modifiable via the introduced amino groups [84].

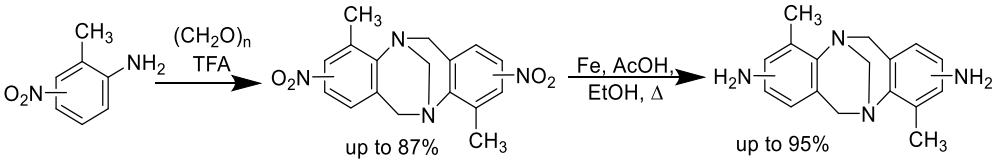

Scheme 2.18. Synthesis of diamino-substituted TB analogs via reduction of nitrogroups

2.5. Fused Tröger's base analogs

TB condensation and formation of the methano[1,5]diazocine frame is not limited to the single unit merging with two aromatic rings at both of its sides. There are molecules having at least one aromatic ring fused into two, or even three, TB structural analogs. A fused TB analog is a TB that contains more than one methanodiazocine unit and has an aromatic ring fused to more than one of such units. "Bis-", "tris-", and "oligo-" fused TB analogs refer to molecules containing two, three, or more methanodiazocine units. In order to obtain such molecules, a suitable number of amino groups are needed in the proper positions for multiple instances of TB cyclization to occur. It can be achieved by the stepwise introduction of new amino groups through the substitution into TB derivative after the first TB cyclisation and preparing the molecule structurally for the consecutive one (Scheme 2.19, route A). Alternatively, it can be achieved by performing a simultaneous TB condensation with compounds having multiple "cyclisation sites", structurally comparable to dimers or trimers of compound **4** (Scheme 2.19, route B).

Pardo was the first one who synthesized the molecule containing two methanodiazocine units fused to the same aromatic ring in 2001 [85]. It was achieved via the approach similar to the stepwise procedure for the synthesis of unsymmetrical TB analogs (see Scheme 2.5). In that research, mono-TB analog was modified stepwise to undergo second TB cyclisation and form bis-TB analog (Scheme 2.19,

route A) in the forms of the *syn* and *anti* diastereoisomers. Both symmetrical (R=R') and unsymmetrical (R≠R') analogs could be synthesized.

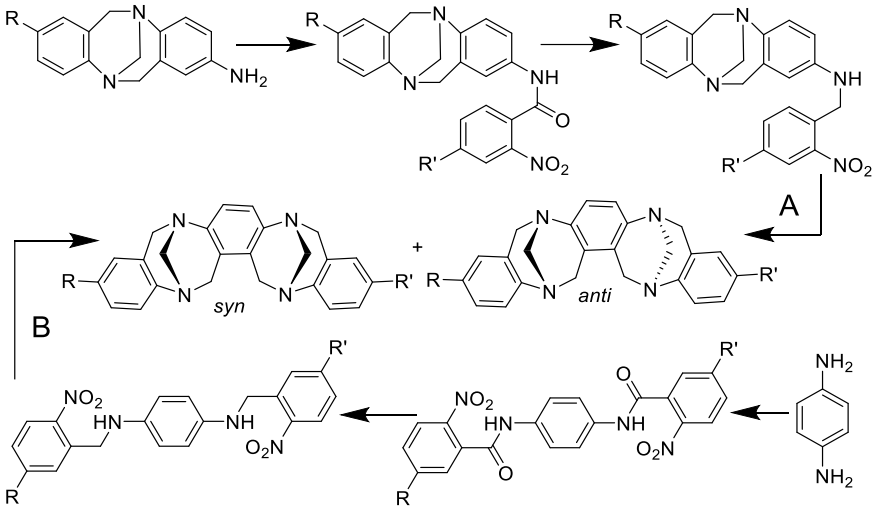

Scheme 2.19. Preparation of fused bis-TB analogs by stepwise (A) and simultaneous (B) route

A shorter "simultaneous" synthetic route to obtain fused bis-TB analogs starting from 1,2-, 1,3-, and 1,4-diaminobenzenes was reported later (Scheme 2.19, route B) [86–88].

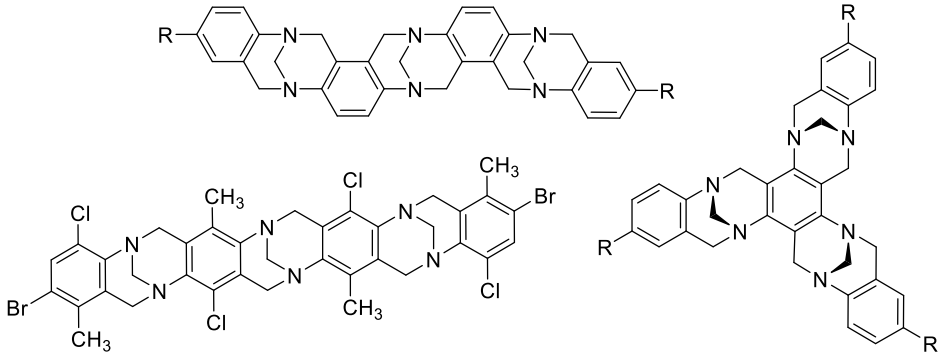

Figure 2.2. Few examples of fused TB analogs

Fused Tröger's base analogs might undergo these synthetic routes multiple times, especially route A, each new methanodiazocine fragment adding new aromatic ring attached to the molecule in an angular manner, consequently forming sophisticated molecular structures (Figure 2.2, Figure 2.3). Modeling such structures allow obtaining molecular cavities of desired shape and size, a valuable feature for supramolecular chemistry [89]. Dolenský and coworkers have reviewed the progress in fused TB chemistry [90], including synthesis, structures, properties, applications, and perspectives.

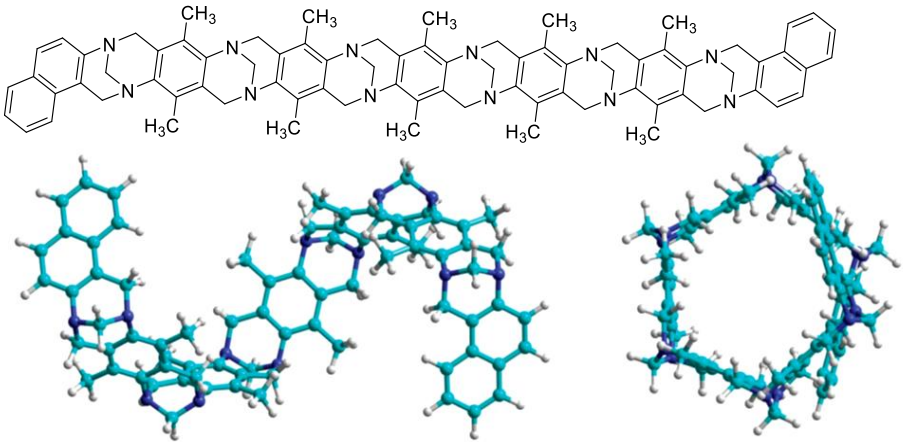

Figure 2.3. Illustration of the helical shape of syn,syn,syn,syn,syn-Z-hexa-TB [90]

2.6. Heterocyclic Tröger's base analogs

Aromatic heterocycles are known for a variety of useful properties and vast application perspectives; a possibility to fuse such molecules angle-wise via methanodiazocine unit, hence expanding these fields even further through new interesting structural possibilities, was seen as a chance not to be missed. Yashima and coworkers stepped into this field of possibilities by condensing 5-amino-1,10-phenanthroline with formaldehyde (aq. HCl in EtOH) and thus synthesizing the first aromatic heterocyclic analog of TB (Scheme 2.20) [91].

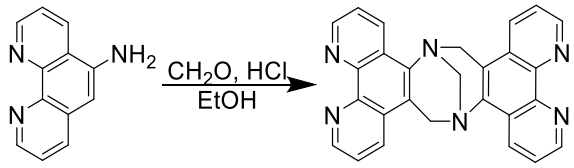

Scheme 2.20. TB condensation of 5-amino-1,10-phenanthroline

After such start, more aromatic heterocycles were employed in TB condensation resulting in new TB analogs possessing aromatic heterocyclic moieties (Figure 2.4). Pardo and coworkers reported azolyl-based derivatives (Figure 2.4,compounds **10**–**12**) providing unusual early examples of direct cyclisation of TB analogs possessing σ-electron-withdrawing groups. Johnson and coworkers managed to accomplish the comparable result by reporting TB analogs based on 3-picoline (Figure 2.4, compound **20**) [59]. Cudero and coworkers pioneered the synthesis of the first TB analog where a heterocyclic aromatic framework is directly fused to the methanodiazonic subunit (Figure 2.4, compound **13**) [39]. They as well provided the analysis and comparison of the reactivity of heterocycles, both π-excessive (azoles) and π-deficient (azines) via the usage of different acid and methylene source, either of HCl and formaldehyde or TFA and hexamethylenetetramine, respectively (Figure 2.4, compounds **9**, **13**–**19)**. Surprisingly, the usage of **13** as starting material and TFA as the acid resulted in no occurring reaction. All the azines had low reactivity of π-deficient heterocycles

towards electrophilic substitution, hence they were isolated from the reaction mixtures unchanged, as suspected. Abonia and coworkers had studied the TB condensation of heterocyclic amines later by using **27** and **28** as starting materials together with formaldehyde and acetic acid [92]. It was suggested that the probable formation of stable side-products caused the low yields, as intermediate compounds were not reacting any further. Several years later, Wu and coworkers introduced some new members of the five-atom- ring class heterocyclic-ring-fused TB analogs by an analogous synthetic approach (Figure 2.4, compounds **28**, **41**–**43**) [93]. After this, various heterocyclic analogs of TB, as shown in Figure 2.4, have been synthesized in one-step TB cyclisation [30, 38, 39, 85, 92–96]. Some of these TB analogs were obtained by using biologically active molecules possessing free aromatic amine groups (Figure 2.4, compounds **24**, **29**–**35** [30, 94–96]; **37**–**39** [97]) as starting materials.

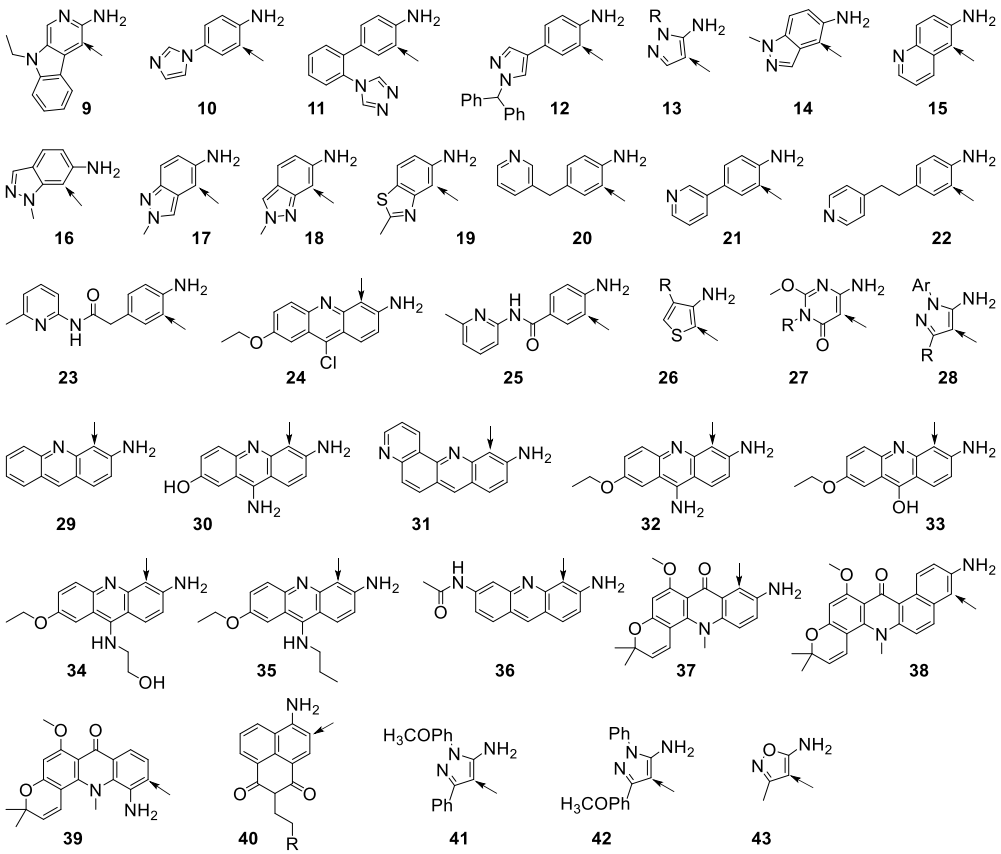

Figure 2.4. Instances of molecules containing aromatic heterocycles that were employed in Tröger's base cyclisation. The arrows indicate the positions of reaction with formaldehyde equivalent [98, 99]

A great advancement in one-step direct TB condensation is achieved, but still a more universal protocol, like the one developed by Wärnmark for non-heterocyclic

TBs, needs to be found. So far, no universal solution exists, and more complex compounds require precise optimization and manipulation by changing acid, formaldehyde source, and solvent; yet, some achievements, like a direct TB condensation of heterocyclic system of [2-aminotetraarylporphyrinato(2–)]nickel [100] looks really promising. Regardless, some of π-deficient heterocycles has their properties expressed to the extent where the synthesis of heterocyclic TB analogs by one-step protocols are inconceivable. A solution to this problem can be found by modifying the formed TB analog via attachment or modification of the heterocyclic functional group. Such approach was used for the synthesis of various heterocyclic TB analogs, including aminopyridine derivatives (as well obtained by one-step method) [101], bis-pyridinium analogs [102], and benzodiazolium TB analogs [103].

2.7. Applications of Tröger's base and its analogs

The remarkable structure of Tröger's base offers to use it in various applications, both as molecule itself and as a building block for various functional molecules for the fields of supramolecular chemistry, molecular recognition, enzyme inhibitors, as chiral hosts and metal ion ligands, for catalysis, etc.

TB that is known for its chirality due to the work performed by Prelog was used as a standard for the evaluation of new chiral chromatographic techniques.

Tröger's base analogs found use in the field of hydrogen-bonding receptors. In 1989, Wilcox and Adrian reported carboxylic-acid-substituted TB derivatives (compounds by formula **44**, Figure 2.5) that aimed to simultaneously form four hydrogen bonds with cyclic urea compounds and adenine base moieties [104]. The binding process was investigated by UV/fluorescence and NMR spectroscopy techniques in solvents of different polarities and hydrogen bonding capabilities. This system was as well used for investigating the effect of water on the binding abilities of similar hosts [28]. The report of the TB amidopyridine analog **45** (Figure 2.5) [101, 105], proven by complexation studies of the recognition of dicarboxylic acids, showed it as selective host for suberic acid in the presence of other α,ω-diacids. Wärnmark and coworkers investigated the C_2-symmetric bis(crown ether) TB analog **46** (Figure 2.5) and its use for the recognition studies of chiral and achiral primary bisammonium salts [106].

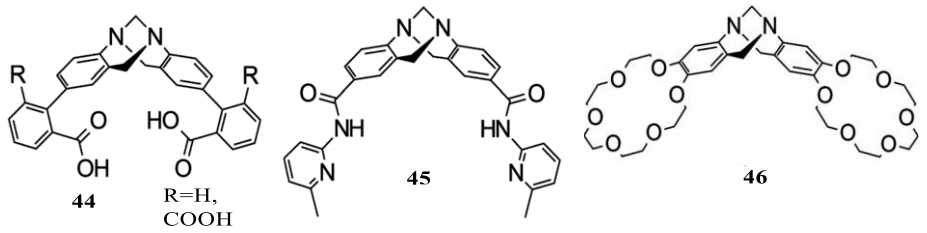

Figure 2.5. Hydrogen-bonding Tröger's base analogs used as receptors

Metal-containing porphyrins and their coordination abilities have as well been explored while fused into a TB scaffold. Different TB analogs were synthesized in which methanodiazocine subunit is fused into two tetraarylporphyrins, forming a

molecule with well-defined chiral cleft structure [107–109]. A series of these bisporphyrino-TB analogs containing inserted metal ions demonstrated strong affinities with diverse selectivities towards diamine guests such as α,ω-diaminoalkanes of different lengths [107], as well as towards lysine and histidine esters [108]. Molecules of analog of TB (**47,** Figure 22) were not only binding simple diaminoalkanes but as well encapsulated a tetramine dendrimer, while forming a spherical cage [109]. A report based on similar structures by Crossley group demonstrated ditopic binding of an α,ω-dicarboxylic acid within the cavity when the porphyrin rings had $Sn(OH)_2$ coordinated to them [110].

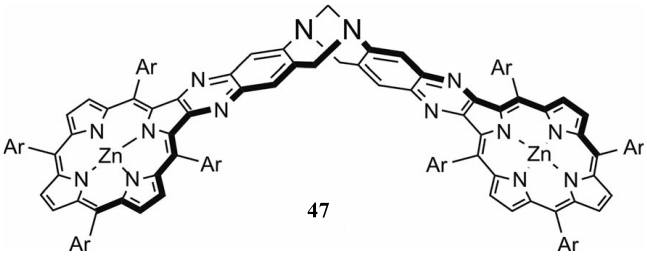

Figure 2.6. A TB analog of metal-containing porphyrin, used as a receptor

Molecular torsion balances, designed by Wilcox and coworkers, are perhaps the most elegant among the applications of TB analogs. Employing molecular structures such as of TB analog **48** (Figure 2.7) allowed for the measurement of weak forces (e.g., CH–π interactions [18] or aromatic edge-to-face interactions [17]) that are believed to heavily influence protein folding. Later improvements give rise to water-soluble structures, thus removing the need for corrections for the change in the direction of the dipoles between folded and unfolded conformers [111]. Diederich and coworkers synthesized molecular balances for research of the interactions between the amide group and "organic" fluorine atoms [112].

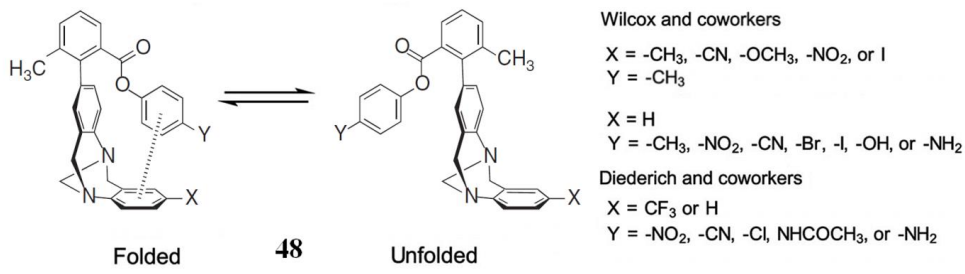

Figure 2.7. TB molecular torsion balances used for the quantification of aromatic edge-to-face interactions [17, 18, 113]

Chirality, rigid structure, and the presence of sites for binding with transition metals (provided by nitrogen atoms) make TB and its analogs decent candidates as the ligands in asymmetric catalysis. Nevertheless, the applications in this field have

not been widely investigated. The first such use of TB derivative was reported in hydrosilylation of terminal alkynes [114]. The complex TB·2$RhCl_3$ (**49**, M = Rh, Figure 2.8) demonstrated catalytic activity, resulting in thermodynamically not so stable *cis* products with selectivity up to 95%. Enantiopure (+)-**1** was used as an additive in hydrogenation reaction of ethyl pyruvate with the Pt/Al_2O_3, resulting in 65% *ee* of ethyl lactate [115]. The same enantiomer used in the amine-promoted aziridation of chalcones as well presented *ee*s of up to 67% [116], while (–)-**1** used as an additive in the 1,4-addition of alkyllithium species increased *ee* to a 57% of resulting α,β-unsaturated *tert*-butyl esters [117]. The induction of asymmetry in catalytic processes was a field where various TB analogs have been studied. The effect of different TB chiral ligands for aromatic aldehydes as the addition to Et_2Zn were investigated by Harmata [65]. Even though enantiopure TB **1** gave poor enantioselectivity in the resulting alcohol, 6-*exo*-substituted TB analog **50** (Figure 2.8), however, afforded up to 86% *ee* in the product alcohol. Furthermore, the substituted pyrazole analogs of TB (compound **51**; Figure 2.8) were employed as organic catalysts for one-pot Mannich reactions between aniline derivatives, aromatic aldehydes, and cyclohexanone in aqueous media, thus resulting in very good yields and remarkable *anti*/*syn* stereoselectivity of the products [93]. The palladium complex **52**, based on the dimeric architecture of the same pyrazole TB skeleton, was employed as a catalyst in the C-C coupling Mizoroki–Heck reaction, displaying high catalytic activity and substantial selectivity towards the formation of *trans*-stilbenes with 89–93% conversion (Figure 2.8) [118].

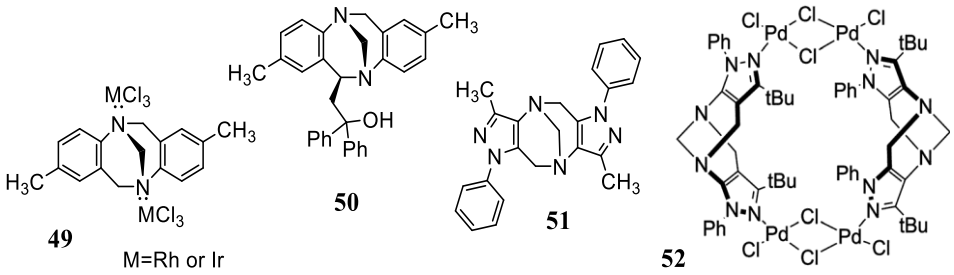

Figure 2.8. Tröger's base analogs used in the selective catalysis

TB analogs containing aromatic heterocyclic rings have shown great ability to interact with DNA. The first TB analog of this group was introduced by Yashima and coworkers (compound **53**; Figure 2.9); this phenanthroline analog showed higher affinity towards DNA compared to the parent 1,10-phenanthroline [91]. This field was widely explored by Demeunynck and Lhomme [30, 94–96, 119, 120]. The proflavine TB analog **54** (Figure 2.9) is a characteristic example. Compound (–)-**54** was reported to bind to calf thymus B-DNA in a sequence-selective fashion [94, 96], and it was found that some identifiable sequences bound preferably to it. Another research of DNA interaction including the non-symmetric proflavine-phenanthroline TB **55** (Figure 2.9) showed that the acridine ring intercalates between the DNA pairs as the phenanthroline moiety resides in one groove of the DNA [95].

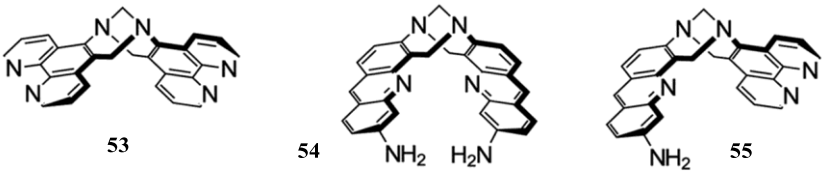

Figure 2.9. Phenanthroline and proflavine analogs of TB exhibiting affinity towards DNA

The affinity to DNA and the ability to bestow molecules with fluorescence via substitution suggest TB analogs for a field of cell imaging. Veale and Gunnlaugsson reported the synthesis of a small library of fluorescent 1,8-naphthalamide analogs of TB (compounds a) (Figure 2.10) [121]. As it was predicted, all three of these compounds were strongly binding to the phosphate backbone of DNA at physiological pH showing high affinities.

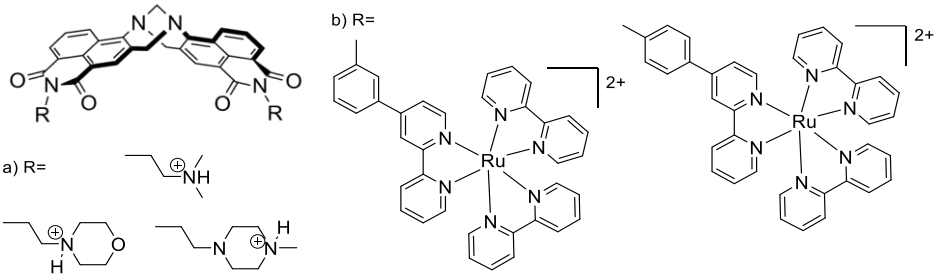

Figure 2.10. Fluorescent analogs of TB for cancer cell imaging

Fluorescence imaging studies of TB analogs (Figure 2.10, a) demonstrated the rapid uptake by cancer cells and that the compounds become localized within the nuclei. Likewise, Gunnlaugsson, Williams and coworkers have developed several 1,8-naphthalimide based Tröger's base derivatives conjugated with Ru(II)-polypyridyl complexes (Figure 2.10, b) [122]. It was found that the luminescence of these complexes was much less affected upon binding to DNA than the corresponding conjugates of Ru(II)–naphthalimide. Moreover, both of these conjugates were readily taken up by the cervical cancer cell lines, opening up the use of these complexes for imaging and therapeutic purposes.

Several TB-derivatives incorporating various amino acids and peptide have been developed by Gunnlaugsson and coworkers. Compound **56** (Figure 2.11) is formed from synthons that possess amino acid or peptide residues side chains and have demonstrated to be highly active anticancer agents in resilient cancer cell lines such as the chronic myeloid leukemia based K562 cell line [123]. As an addition to compounds having these properties, TB analogs bearing the cytotoxic acronycine motif, such as compound **57** (Figure 2.11), have been reported to be cytotoxic against L-1210 leukemia and KB-3-1 solid tumor cell lines [97]. Furthermore, a library of structurally diverse Tröger's base analogs has been synthesized via amination of methylene bridge, employing Vilsmeier–Haack conditions **58** as well as by the incorporation of five and six membered heterocycles on the aromatic core of Tröger's

base framework **59** [124]. Seven of the thirty compounds that were synthesized and evaluated were found to possess cytotoxicity that is equivalent or better than the standard drug Doxorubicin against breast cancer MDAMB-231 cell line.

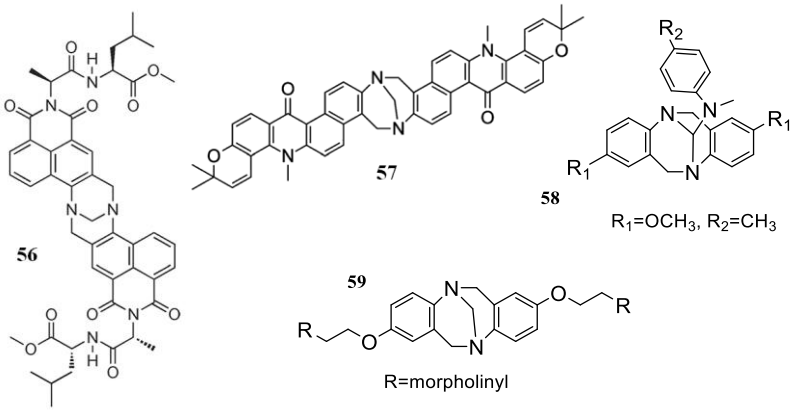

Figure 2.11. TB analogs with reported cytotoxicity against cancer cells

The rigid V-shaped structure of TB has been employed for building elaborated metallomacrocycles. The first example of these structurally marvelous complexes was reported by Mirkin, as a phosphane/thioether ligand containing the TB motif **60** (Figure 2.12), when coordinated to CuI, formed a dimeric metallocycle [125]. However, when coordinated with RhI, a mixture of trimer and tetramer was obtained. Since the discovery of this phenomenon, TB analogs have been investigated for the supramolecular self-assembly, a wide-ranging field covering the helix of DNA, as the inclusion compounds. It is generally considered as the process through which the defined aggregates are formed from individual molecules, and then can self-organize to form higher-order structures.

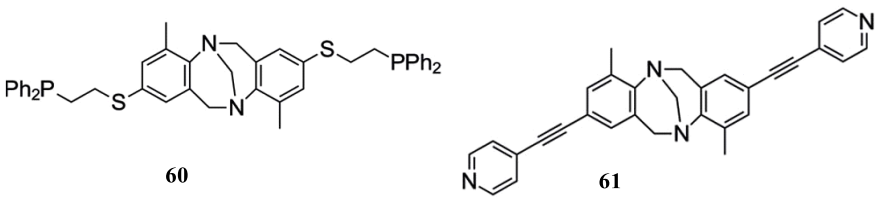

Figure 2.12. TB ligands used for building metallomacrocycles

Two very significant observations on self-assembled TB metallohelicates were made by Lützen. The first one relates to the absence or presence of diastereoselectivity in the process of self-assembly. He showed that some TB ligands containing 2-pyridylmethanimine or 2,2'-bipyridine moieties self-assembled into dinuclear double-stranded helicates when coordinated to CuI and AgI [44]. The complexation of the metal ion by the racemic ligand is diastereospecific in a self-recognition manner, hence producing diastereomerically pure complexes [44, 84, 126, 127].

Likewise, the groups of Lützen and Wärnmark wave built a metallomacrocycle from a racemic bis(4-pyridyl-alkyne)-derived TB analog 61 (Figure 2.12), and $(dpp)Pt(OTf)_2$ in a diastereoselective self-discrimination process, which formed exclusively the heterochiral R,R,S,S isomer [102]. Wärnmark showed that the resulting formed metallocyclic cage displayed greatly enhanced fluorescence compared to the TB ligand alone. The second observation of Lützen, together with Piguet this time, was established on experimental and theoretical analysis of metal–metal interactions in solution. Two effects opposing each other were noted by these researchers: Coulombic interactions causes large short-distance intermetallic repulsion, and solvation effects produce big intermetallic attractions for small pseudo-spherical ions with short intermetallic separations [128].

2.8. Tröger's base in optoelectronic applications

The first examples of Tröger's base derivatives designed as materials for optical and optoelectronic applications have been suggested only quite recently [129]. Initial applications of TB analogs in this field have been reported in recent years and were reviewed by Yuan and coworkers [130]. Among these compounds, some are noteworthy due to their luminescent properties. The TB bis-pyridinium-derived analog **62** (Figure 2.13) demonstrates aggregation-induced light emission in the solid state, but it is practically non-emissive in solution: a feature that is not observed in its planar non-TB counterpart [131]. Yuan as well reported BODIPY dyes based **63** (Figure 2.13) on TB that is showing high solid-state fluorescence [132]. Fluorene-derived TB analogs as well demonstrated potentially beneficial photophysical and electroluminescent properties [133]; for example, compound **64** (Figure 2.13) exhibit strong fluorescence emission in both dilute solutions and aggregated states. Organic light emitting diodes (OLEDs) that is assembled by using these TB analogs demonstrate high brightness, high efficiency, and low turn-on voltage.

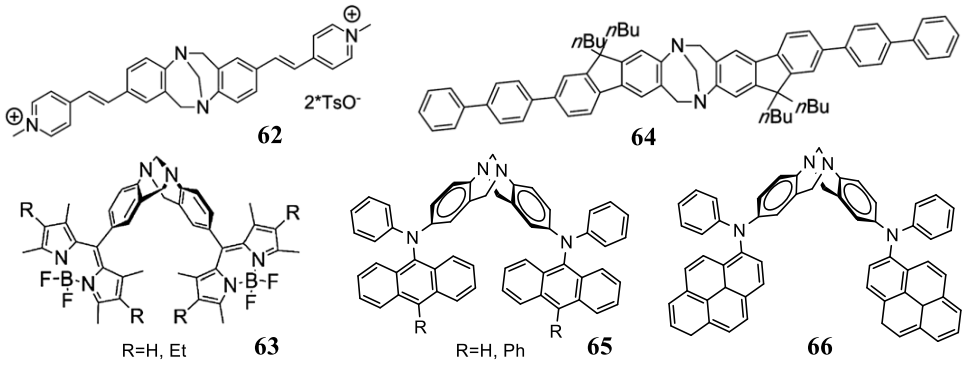

Figure 2.13. TB analogs demonstrating light emission in the solid state

Three bifunctional TB derivatives **65**–**66** (Figure 2.13) [134] were synthesized and tested in simple double layer OLED devices with no additional HTMs, thus demonstrating the functionality of these compounds both as HTMs and emissive materials. These compounds are fully amorphous with considerably high glass

transition temperatures, and one of them (**56**, R=Ph, Figure 2.13) is especially noteworthy due to its electroluminescence manifesting in rare pure yellow emission.

The charge transfer properties of other Tröger's base derivatives were as well noticed and reported [7, 135], but this field has barely started to be investigated; hence, only some of compounds were synthesized and studied.

2.9. Conclusions

Since its discovery, Tröger's base has fascinated chemists with its unusual molecular structure and properties, yet its uncommon features, such as the structure that took a half-century to reveal and the lack of chemical methods for efficient modifications, left its full potential unrealized. The properties of TB, as a rigid chiral molecule, with aromatic rings oriented angle-wise and a cavity, together with the synthetic methods already discovered by the scientific community, offers new applications and high possibilities of countless TB analogs. Moreover, as different researchers have started to explore the use of TB as building blocks in various fields such as receptors, molecular torsion balance, ligand design for asymmetric catalysis, DNA interactions, and even drugs candidates; they barely scratched the surface of some potentially beneficial applications. The field of TB research for applications in optoelectronic devices is not widely explored. While there are some interesting TB derivatives that have been discovered and started to be applied in this field, it mostly covers luminescent and few charge-transporting materials, mainly in the field of OLEDs. This still leaves topics such as solar cells unexplored and unpublished; hence, the TB research in solar cell applications proposes scientific novelty and possibilities of noticeable discoveries.

3. RESULTS AND DISCUSSION

3.1. Small-molecular hole transporting materials containing triphenylamine moieties conjoined by Tröger's base core

Electronic and optoelectronic devices which are using organic materials as active elements, such as organic light-emitting diodes, organic photovoltaic devices, organic field-effect transistors, etc., involve charge transport as an essential operation process and, hence, require charge-transporting materials [136]. Therefore, the development of high-performance charge-transporting materials is a key issue for the fabrication of high-performance devices [137, 138]. The realization of organic electronics potential as an inexpensive technology as well requires the ability to use simple processing techniques such as device formation by solution deposition methods, preferably using simple, cheap, easily purified materials [139, 140]. Small-molecule hole transporting materials exhibit many outstanding advantages over polymers, such as structural versatility, exact molecular weight, and relatively easy purification by chromatography, crystallization, or vacuum sublimation [141, 142]. Unfortunately, a significant number of these HTMs have low glass transition temperatures (T_g) [139, 140, 143] which can result in the conversion from glass to liquid or crystalline state and potentially reduce the device characteristics [144, 145].

The V-shaped structure of Tröger's base allows it be used as a core and provide angle orientation for the conjugated π-systems that are attached to it. Recent investigations have as well revealed that the rigidity of the TB scaffold and high molecular mass via its 2-fold functionalization impairs crystallization, making the TB derivatives highly amorphous, and significantly increase glass transition temperature [134, 146, 147]. These findings prompt interest in the synthesis and investigation of the new HTMs containing the TB core.

A large group of nitrogen-containing triarylamine compounds has long been known as hole-transporting materials for the active layer of OLEDs, organic photoreceptors, and organic solar cells. This group of compounds shows very good solubility in common organic solvents, stability towards air and humidity [139–141], and adequately high charge-carrier mobility (μ= 0.01 cm^2V^{-1} s^{-1} in vapor-deposited [148] and spin-coated [149] films). Although high-mass materials such as conjugated polymers of triphenylamine (TPA) represent part of this group [150], the other part consists of smaller compounds. Unlike polymers, small molecules have well-defined molecular structures and exact molecular weights, thus avoiding batch-to-batch variations in solubility, different processing properties, and performance. They can be purified by column chromatography, crystallization from solution, or vacuum sublimation. All these factors allow for more reproducible fabrication protocols and better understanding of the relationships between molecular structure and properties that it bestows.

Among a wide variety of organic semiconductors usually possessing large conjugated π electron systems, there are some noteworthy small-system exceptions [148, 151] (Figure 3.1) demonstrating semiconducting properties (especially charge mobility) rivalling those of counterpart compounds containing large conjugated π-systems.

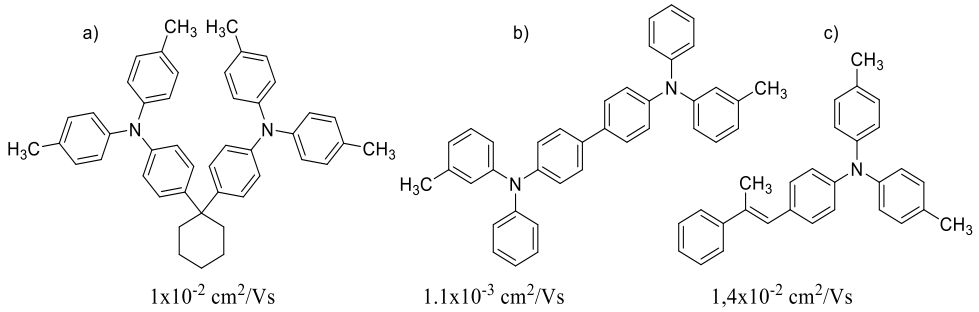

Figure 3.1. Examples of small-molecular HTMs having high charge mobility

Some of these compounds (Figure 3.1 a.) have the planes of their small π-systems oriented at an angle-fashion one towards another bestowing the coupling between them. The structure of Tröger's base allows using it as a core providing angle orientation for the conjugated π-systems attached to it and, therefore, potentially creating coupling between them. Some recent researches have reported properties of a compound containing two triphenylamine fragments conjoined by Tröger's base core, and the further investigation of it shows that, besides connecting aromatic fragments only geometrically, the non-conjugated bridge in Tröger's base can as well bestow electronic connecting of conjoined fragments in the absence of a π-linker [7]. Such phenomena as well as technologically more favorable physical properties compared to non-conjoined "half" counterparts draw attention to Tröger's base compounds of such structure as promising candidates for the HTM applications.

For the development and further investigation of improved compounds with such structure, the influence of small substituents should not be underestimated. There are some cases reported where the addition of substituents such as methyl-, methoxy-, or a mere change in their position (*p*-, *m*-, or *o*-) can have a significant change in ionization potential and charge mobility, bestow highly improved performance as HTM, or suppress crystal growth in the HTM layer, hence significantly increasing solar cells' resistance to thermal stress and the overall lifetime of the ssDSSC device [144, 152, 153]. This chapter is dedicated to the synthesis and investigation of small-molecular Tröger's base compounds containing two triphenylamine fragments and methyl- or methoxy- substituents.

3.1.1. Synthesis of novel Tröger's base compounds and investigation of their structure

Novel Tröger's base-based compounds 4,10-dimethyl-N^2,N^2,N^8,N^8-tetraphenyl-6*H*,12*H*-5,11-methanodibenzo[*b*,*f*][1,5]diazocine-2,8-diamine (**1a**), N^2,N^2,N^8,N^8-tetrakis(4-methoxyphenyl)-4,10-dimethyl-6*H*,12*H*-5,11-methanodibenzo[*b*,*f*][1,5]diazocine-2,8-diamine (**1b**), N^2,N^8-bis(4-methoxy-3-methylphenyl)-N^2,N^8-bis(4-methoxyphenyl)-4,10-dimethyl-6*H*,12*H*-5,11-methanodibenzo[*b*,*f*][1,5]diazocine-2,8-diamine (**1c**), and N^2,N^8-bis(4-methoxyphenyl)-4,10-dimethyl-N^2,N^8-di-p-tolyl-6*H*,12*H*-5,11-methanodibenzo[*b*,*f*][1,5]diazocine-2,8-diamine (**1d**) have been synthesized (Scheme 3.1) by obtaining brominated Tröger's base (**1'**) from 4-bromo-2-

methylaniline [40], and its reaction with corresponding diphenylamine (diphenylamine, bis(4-methoxyphenyl)amine [154], 4-methoxy-*N*-(4-methoxyphenyl)-3-methylaniline [144], 4-methoxy-*N*-(*p*-tolyl)aniline [155]) via palladium catalyzed C–N cross-coupling reaction.

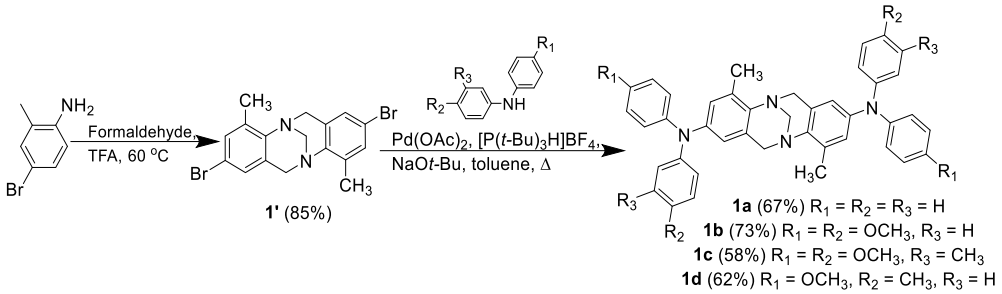

Scheme 3.1. Synthesis of novel compounds **1a**–**d** containing Tröger's base core

The structure of TB derivatives **1a**–**1d** was confirmed by ^{1}H and ^{13}C NMR and elemental analysis. The NMR signal pattern displayed in the interval of 3.8–4.6 ppm in the ^{1}H NMR spectrum is characteristic for the methanodiazocine bridge, indicating the presence of the TB core. Methylene bridge appears as a singlet at 4.32 ppm, and protonic signals of benzylic-type methylenes (Ar-CH_2-N) show two doublets at 3.89 and 4.48 ppm, indicating *endo* and *exo* hydrogens respectively [156] (Figure 3.2), signifying that these protons are magnetically nonequivalent due to the rigid structure of the TB. In the aromatic and most heteroaromatic TB derivatives, the lower field doublet was assigned to the *exo* and the higher field doublet to the *endo* protons, whose signal is always broader than the signal of the *exo* protons because of the long range coupling between the *endo* protons and the corresponding anti proton of the methylene bridge [12].

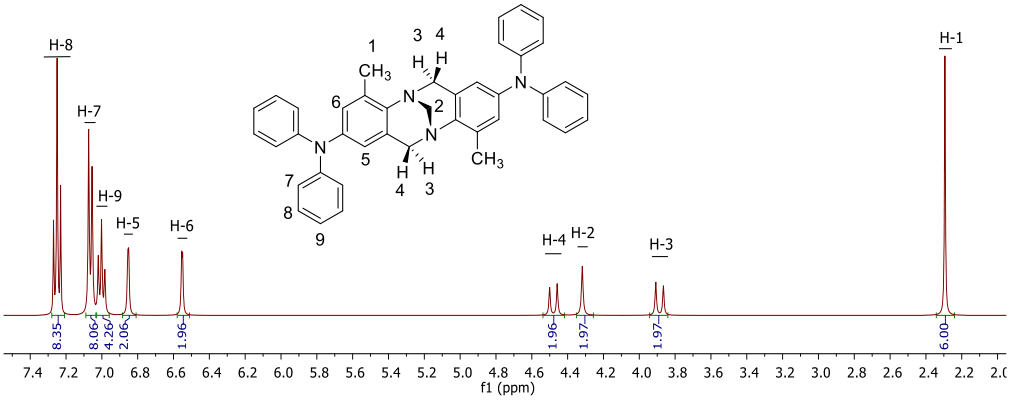

Figure 3.2. ^{1}H NMR spectrum (400MHz, $CDCl_3$) of compound **1a**

Compound **1a** is crystalline; therefore, mono crystal was grown and analyzed by X-ray diffraction, detecting molecular configuration, and confirming its structure

(Figure 3.3)[1]. The core of the molecule has a typical Tröger's base structure of two planes of phenyl groups fused in nearly perpendicular fashion by methanodiazocine unit, while terminal phenyls are twisted in a way that they do not form one plane neither with central phenyl fragments, nor with each other. The study of the crystal structure (Figure 3.4) reveals that molecules are arranged in a manner that plane of aromatic rings in the core unit is parallel to the one of another molecule nearby, while terminal phenyl groups of two opposite molecules are oriented towards each other forming a cavity in between them. Such pattern of molecular arrangement provides a crystal with parallel pseudo-hexagonal tube shape cavities, making its structure resemble that of the honeycomb just with double-layered walls. Such cavities inside the crystal could possibly host small molecules (e.g. some solvents) or allow their transition as some of such signals were observed during the experiment, but they were unidentified.

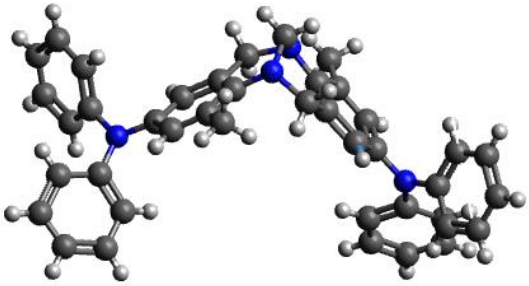

Figure 3.3. Molecular structure of compound **1a**

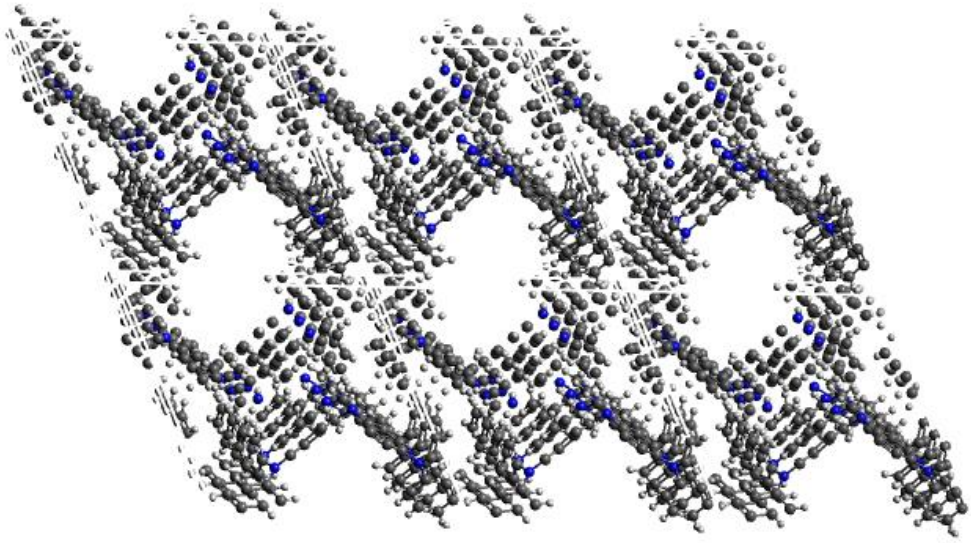

Figure 3.4. Projection of the crystal structure of compound **1a**

[1] Measurements were performed in the Department of Polymer Chemistry and Technology, KTU, by Dr. G. Bagdžiūnas

3.1.2. Thermal and optical properties

The successful application of hole transporting materials in devices requires the formation of homogeneous and thermally stable layers. The thermal characteristics of synthesized compounds defining their crystallinity and glass-transition temperature were obtained by differential scanning calorimetry (DSC) (Table 3.1, Figure 3.5).

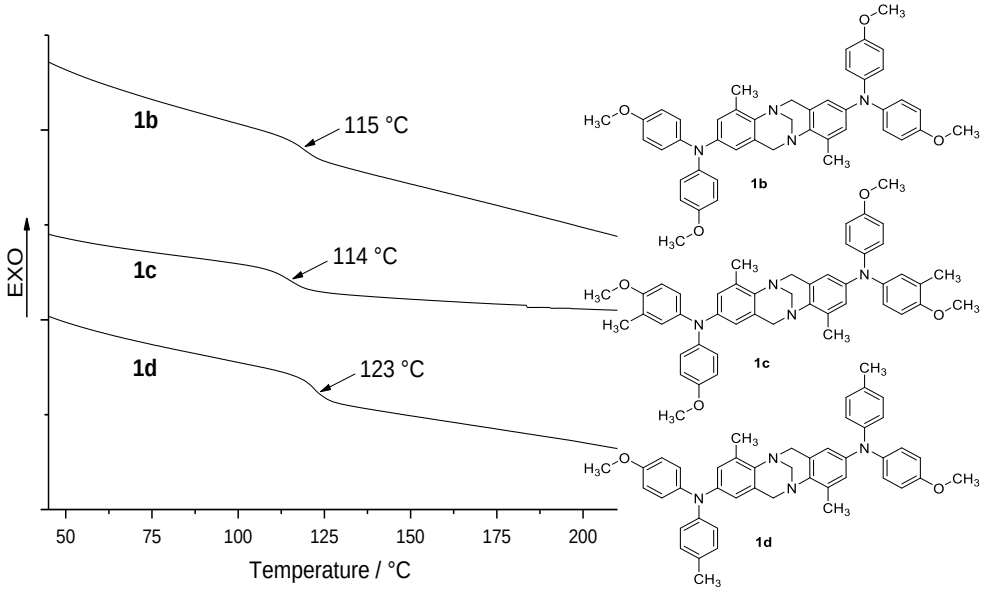

Figure 3.5. DSC curves indicating T_g of compounds **1b–d**; 10 K/min; second run

DSC measurements revealed high crystallinity that is distinctive to compound **1a**, the only compound that has no substitutes attached to its outer phenyl groups, registering melting of the crystals (T_m) at 158 °C. It is interesting that derivative **1c**, possessing substitutes in both *p*- and *m*- positions of outer phenyl groups, exist both in crystalline and amorphous state; therefore, during the first heating melting of the crystals (T_m) at 162 °C, it is observed, but no crystallization takes place during cooling or second heating scans, and only glass transition (T_g) at 114 °C is detected during the second heating (Table 3.1). Compounds **1b** and **1d** remain completely amorphous during DSC experiments, and only glass transition is registered during heating and cooling runs (Table 3.1, Figure 3.5).

Table 3.1. Thermal properties of TB derivatives **1a–d**

Compound	T_m [°C] [a]	T_g [°C] [b]	T_{dec} [°C] [c]
1a	158	-	371
1b	-	115	378
1c	162	114	370
1d	-	123	387

[a] Melting point was only detected during the first heating 10 K/min.
[b] Determined by DSC: scan rate, 10 K/min; N_2 atmosphere; second run.
[c] Onset of decomposition determined by TGA: heating rate, 10 K/min; N_2 atmosphere.

Thermogravimetric analysis reveals high decomposition temperatures (Table 3.1) suggesting very good thermal stability of the investigated compounds.

The UV-VIS absorption bands of the compounds **1a–d**, measured in tetrahydrofuran solutions (c=10^{-4}mol/l, d=1mm) (Figure 3.6), indicate absorption in near-UV region (210 nm) that corresponds to n-σ* electron transitions in the proximity of central nitrogen atoms, and the absorption in longer wavelengths (300 nm) correspond to the π–π* electron transitions of the conjugated system. Practically no bathochromic shift of the absorption maximum (303 nm) is observed as the size of the π-conjugated system is the same, but the absorption intensity slightly differs among the compounds depending on the substituents attached to them. The highest hyperchromic shift is observed in compound **1d,** containing one methyl- and one methoxy- substituent attached to each TPA fragment in p- positions.

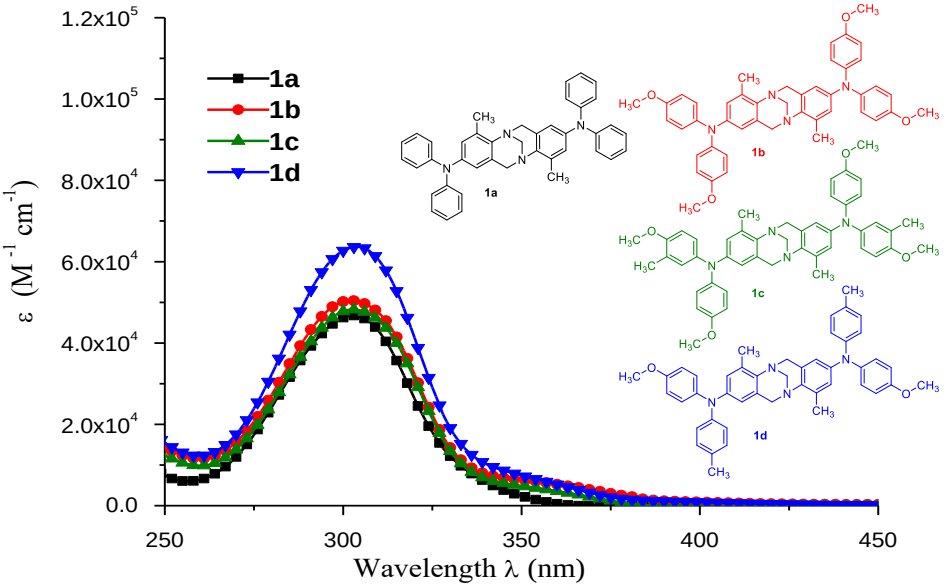

Figure 3.6. Absorption spectra of 1×10^{-4} M THF solutions of compounds **1a–d**

3.1.3. Photoelectrical properties

Solid-state ionization potential (I_p) it is a crucial parameter when the use of an organic materials for the hole-transport applications is considered. This factor can help in identifying suitable partner organic transport and inorganic electrode materials in the optoelectronic device. The ionization potentials of the synthesized molecules were measured by the photoelectron spectroscopy in air (PESA) method (Figure 3.7)[1], and the results are presented in Table 3.2; the measurement error is evaluated as 0.03 eV.

[1] Measurements of ionization potential were performed at the Department of Solid State Electronics, Vilnius University, by Dr. V. Jankauskas, E. Kamarauskas.

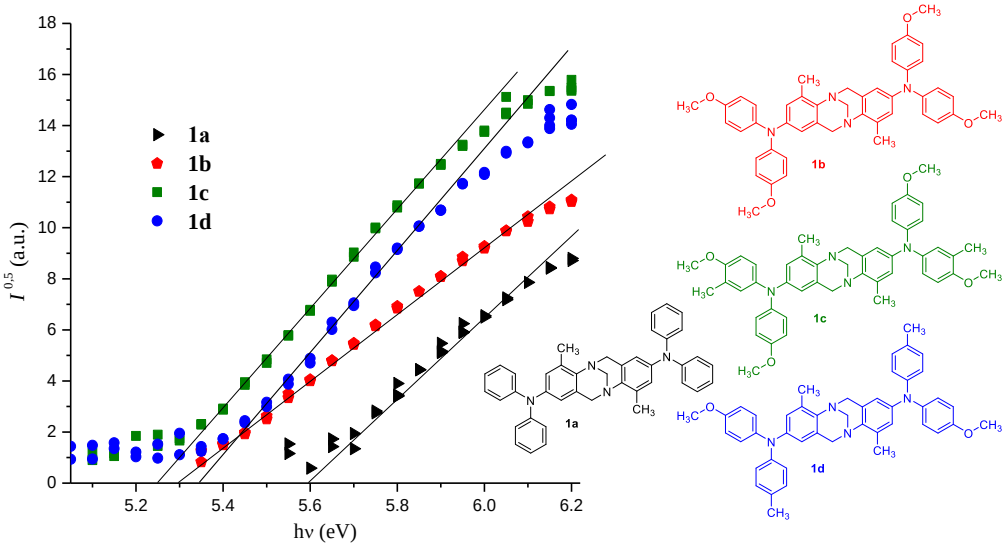

Figure 3.7. Photoemission in air spectra of Tröger's base derivatives **1a–d**

Table 3.2. Energy level and hole mobility data for compounds **1a–d**

Compound	I_p [eV] [a]	μ_0 [cm^2/Vs][b]	μ (6.4×10^5 V/cm) [cm^2/Vs][c]
1a	5.60	$3.8\cdot10^{-7}$ [d]	$4.5\cdot10^{-6}$ [d]
1b	5.30	$3\cdot10^{-8}$	$1.3\cdot10^{-4}$
1c	5.25	$1\cdot10^{-7}$	$1.2\cdot10^{-5}$
1d	5.34	$3\cdot10^{-6}$	$3.3\cdot10^{-4}$

[a] Solid state ionization potential (I_p) was measured by the photoemission in the air method from films.
[b] Mobility value at zero field strength.
[c] Mobility value at 6.4×10^5 V cm^{-1} field strength.
[d] **1a** mobility values were measured from the mixture of compound **1a** and PC-Z (1:1).

One of the main parameters, defining if material qualifies for the applications of hole transport, is charge mobility. Charge transport properties of the synthesized Tröger's base derivatives were measured by the xerographic time-of-flight (XTOF) technique (Figure 3.8)[1]. The values of charge mobility defining parameters: zero field mobility (μ_0) and the mobility at the electric field of 6.4×10^5 V cm^{-1} for the compounds **1a–d** are given in Table 3.2. Poor quality films of the **1a** were obtained; therefore, a mixture of **1a** and polycarbonate (PC-Z) in weight ratio 1:1 was used in order to obtain uniform layers. As a result, the absolute mobility results for **1a** are lower (approximately one order of magnitude) due to the presence of nonconductive polymer.

[1] Charge mobility measurements were performed at the Department of Solid State Electronics, Vilnius University, by Dr. V. Jankauskas, E. Kamarauskas.

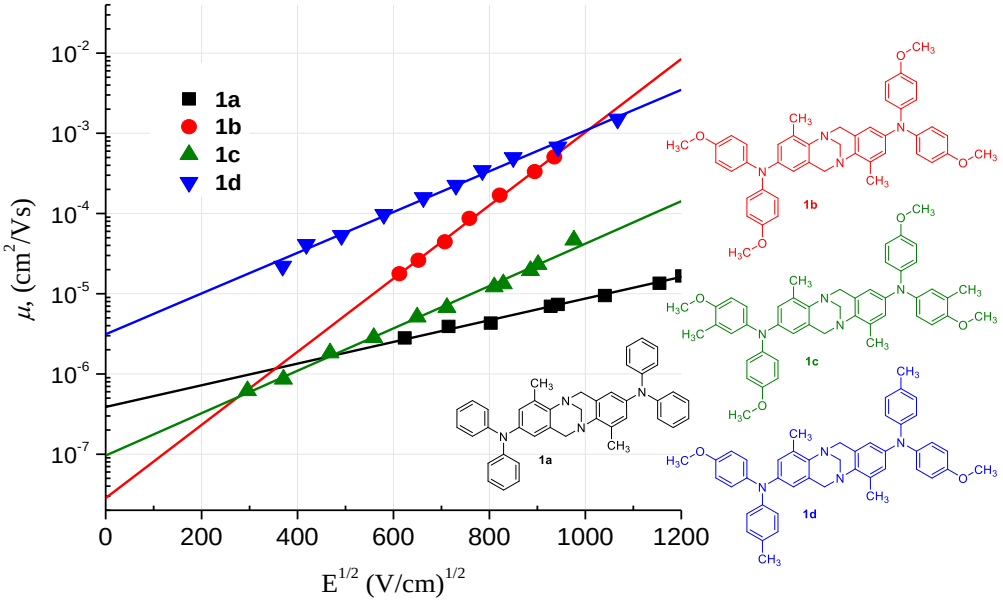

Figure 3.8. Electric field dependencies of the hole drift mobilities (μ) in the charge-transport layers of Tröger's base derivatives **1a–d**. Mobility values of **1a** were measured from the mixture of compound **1a** and PC-Z (1:1)

Hole-drift mobility of the compound **1d**, measured at room temperature, was $3.3 \cdot 10^{-4}$ cm^2 V^{-1} s^{-1} at strong electric fields, and it is the best result among all three pure materials (**1b-d**), comparable to some industrial HTMs reported in the literature. Compound **1c** demonstrated the lowest charge mobility in the pure material group, and such results could be explained, because additional methyl- substituent in *m*-position adversely affects charge mobility, most likely by the manner in which molecules' organization in layer is altered unfavorably.

Concluding this chapter of the research, it is worth saying that synthesized Tröger's base compounds with methyl- and methoxy- substituents do qualify as HTM and have quite favorable physical properties, are stable, mainly amorphous (**1a** excluded), and readily soluble. Even though zero field mobility (μ_0) of these compounds is not sufficient for the application in solar cells, as competition with materials such as Spiro-OMeTAD ($\mu_0 = 4.1 \times 10^{-5}$ cm^2/Vs) makes their attractiveness in this niche quite limited; there are other fields (e.g. electrophotography) where these compounds could be successfully used. In addition, synthesis and investigation of these compounds provided useful research information and some insight for further development in their molecular design. It can be assumed that the main concept of molecule is promising, but it could potentially be improved by replacing small substituents with larger moieties, hence expanding π-conjugated system, thus tuning the properties of the compound favorably.

3.2. Hole transporting materials containing Tröger's base core and phenylethenyl moieties

As it was already noticed, Tröger's base compounds could be promising candidates as hole transporting materials for the optoelectronic applications. Seeking further improvement in the molecular design of synthesized and analyzed in the previous chapter compounds, some efficient, and preferably convenient, methods need to be found. One of such methods was reported, and it demonstrates that the addition of the phenylethenyl groups to the molecule noticeably extended π-conjugated system by improving the properties of charge-transporting materials and bestowed them comparatively high hole drift mobilities (up to 0.017 $cm^2 V^{-1} s^{-1}$) [157, 158]. This method uses a simple one-step reaction to expand conjugated *π*-system by attaching phenylethenyl moieties due to the condensation with corresponding aldehyde.

It was as well noticed that such structural improvement could bestow compounds with other desirable properties [158] as additional bulky diphenylethenyl fragments attached to triphenylamine core increased both glass transition temperature and thermal stability. A similar approach was utilized in the current investigation as phenylethenyl groups have been incorporated into the Tröger's base core containing molecule **1a**, as well possessing triphenylamine fragments, in order to expand π-conjugated system, hopefully improving hole drift mobility and other properties desirable for HTMs.

This chapter is dedicated to the synthesis and investigation of V-shaped charge transporting molecules consisting of Tröger's base core and phenylethenyl moieties. The presented results were published in a journal article as well[159].

3.2.1. Synthesis of novel Tröger's base derivatives containing phenylethenyl moieties

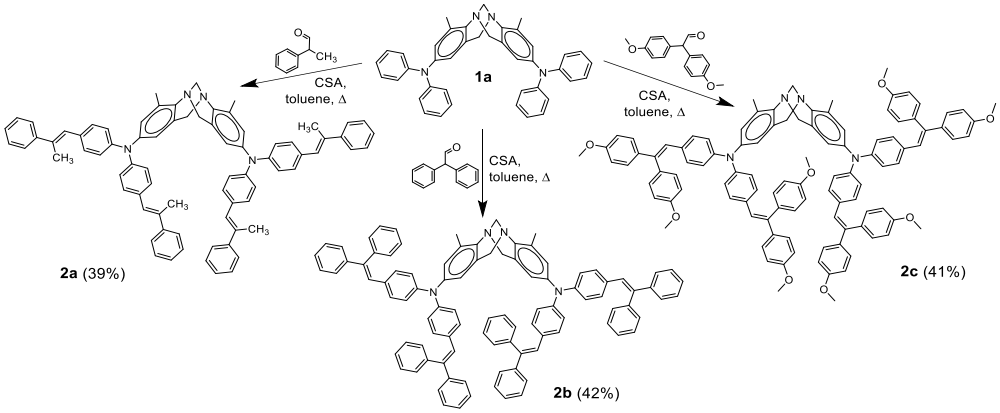

Scheme 3.2. Synthesis of compounds **2a–c** containing Tröger's base core and phenylethenyl moieties

Novel compounds 4,10-dimethyl-N^2,N^2,N^8,N^8-tetrakis(4-((*E*)-2-phenylprop-1-en-1-yl)phenyl)-6*H*,12*H*-5,11-methanodibenzo[*b*,*f*][1,5]diazocine-2,8-diamine (**2a)**, N^2,N^2,N^8,N^8-tetrakis(4-(2,2-diphenylvinyl)phenyl)-4,10-dimethyl-6*H*,12*H*-5,11-

methanodibenzo[*b*,*f*][1,5]diazocine-2,8-diamine **(2b)** and N^2,N^2,N^8,N^8-tetrakis(4-(2,2-bis(4-methoxyphenyl)vinyl)phenyl)-4,10-dimethyl-6*H*,12*H*-5,11-methanodibenzo[*b*,*f*][1,5]diazocine-2,8-diamine **(2c)** have been synthesized from already investigated compound **1a** by the condensation with corresponding aldehyde (methylphenyl-, diphenyl- or di(4-methoxy)phenylacetaldehyde) in toluene at the reflux temperature in the presence of (+/-)-camphor-10-sulfonic acid (CSA) (Scheme 3.2). The reaction occurs through intermediate hydroxyl group containing compound, which undergoes dehydration catalyzed by CSA; the water generated in the reaction was removed by Dean-Stark trap at reflux temperature. This method was chosen due to its efficiency that was reported in the literature [158].

^{1}H and ^{13}C NMR as well as elemental analysis data confirmed the structure of newly synthesized Tröger's base derivatives **2a–c**. The signal pattern of ^{1}H NMR spectrum in the region between 3.6–4.5 ppm is crucial for the identification of the methylene bridge, indicating the presence of the TB core. In ^{1}H NMR spectrum of compound **2b** (Figure 3.9), the bridging methylene protons (Ar-CH_2-N) show two doublets at 4.38 and 3.79 ppm, *exo* and *endo* hydrogens respectively, signifying that these protons are magnetically nonequivalent due to the rigid structure of the TB. The singlet for the two protons of the other bridging methylene carbon (N-CH_2-N) is observed at 4.21 ppm. Singlet indicating protons in H-9 position of phenylethenyl fragment is observed at 6.93 ppm. Compounds **2a** and **2c** exhibit similar structural properties, however, due to the presence of a large number of conformers, signals are less resolved, and multiplets are observed.

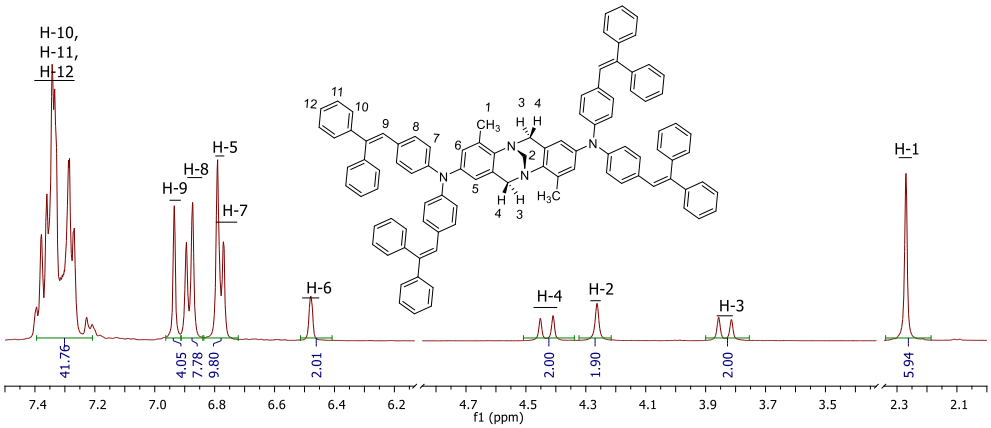

Figure 3.9. ^{1}H NMR spectrum (700 MHz, $CDCl_3$) of compound **2b**

3.2.2. Thermal and optical properties

DSC measurements reveal that structural bulk and presence of a large number of conformers hampers the crystallization processes in the investigated compounds, as only compound **2a** exist both in crystalline and amorphous state (Figure 3.10), an effect especially noticeable compared to highly crystalline **1a**. During the first heating, the melting of the crystals (T_m) at 204 °C is observed, no crystallization takes place during cooling or second heating scans, and only glass transition (T_g) at 132 °C is

registered during the second heating (Figure 3.10 a, Table 3.3). Small intensity of the melting peak and absence of the crystal formation or melting signals during the subsequent scans indicate that the crystallization of **2a** is slow and does not proceed readily under the temperatures above T_g. Compounds **2b** and **2c** remain completely amorphous during the DSC experiments, and only glass transition is registered during the heating and cooling runs (Table 3.3, Figure 3.10 b, c). Compared with analogous HTMs without TB core, [160] T_g increases from 1 °C to 132 °C for **2a** and twofold for **2b** and **2c**.

Thermogravimetric analysis reveals high decomposition temperatures (Table 3.3), suggesting very good thermal stability of the investigated compounds.

Table 3.3. Optical and thermal characteristics of **2a–c**

Comp.	T_g [°C] [a]	T_m [°C] [b]	T_{dec} [°C] [c]	λ_{max}^{abs} [nm] [d]	ε [$M^{-1}cm^{-1}$]	λ_{max}^{FL} [nm] [e]	Φ_F [%]
2a	132	204	378	353	8.49×10^4	432	37
2b	152	–	413	393	9.56×10^4	479	9
2c	146	–	321	377	7.25×10^4	471	20

[a] Determined by DSC: scan rate, 10 K/min; N_2 atmosphere; second run. [b] Melting point was only detected during the first heating; the compound vitrified on cooling to room temperature with 10 K/min. [c] Onset of decomposition determined by TGA: heating rate, 10 K/min; N_2 atmosphere. [d] UV-Vis spectra were measured in 10^{-4} M THF solution. [e] Fluorescence spectra were measured in 10^{-5} M toluene solution.

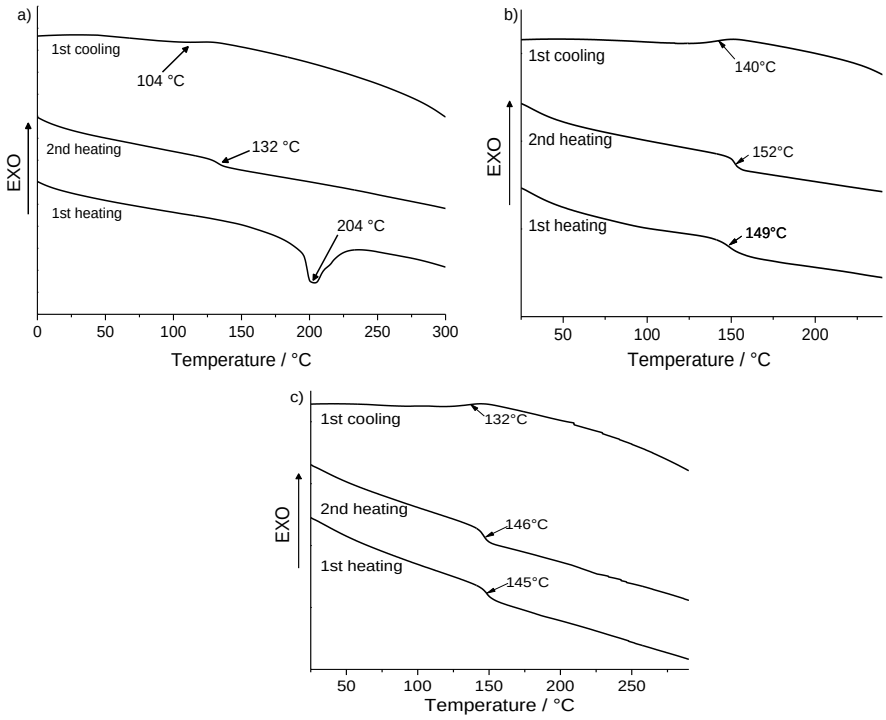

Figure 3.10. DSC curves for the **2a** (a), **2b** (b), and **2c** (c)

The UV-VIS absorption bands of the compounds **2a**–**c**, measured in 10^{-4} M tetrahydrofuran solutions, are shown in Figure 3.11 and summarized in Table 3.3. The bathochromic shift of the absorption maximum of **2a**–**c**, compared to that of intermediate **1a**, is attributed to the extension of the π-conjugated system by the phenylethenyl units. The maximum of the absorption spectrum of compound **2a** is red shifted by about 49 nm compared with that of the intermediate **1a**. In line with the expectations, additional phenyl groups in **2b** increase the conjugated system even further, and bathochromic shift of about 90 nm, compared with **1a**, is registered. Additional methoxy groups in **2c** yield hypsochromic shift of 15 nm compared with **2b**, indicating that **2c** adopts a less planar configuration, due to these extra moieties. It is worth noticing that in their pristine undoped form, **2a**–**2c** absorb mostly in the UV region below 450 nm, making these hole conductors a particularly interesting option for solid-state dye-sensitized and perovskite solar cells as they do not significantly interfere with the absorption of the sensitizer.

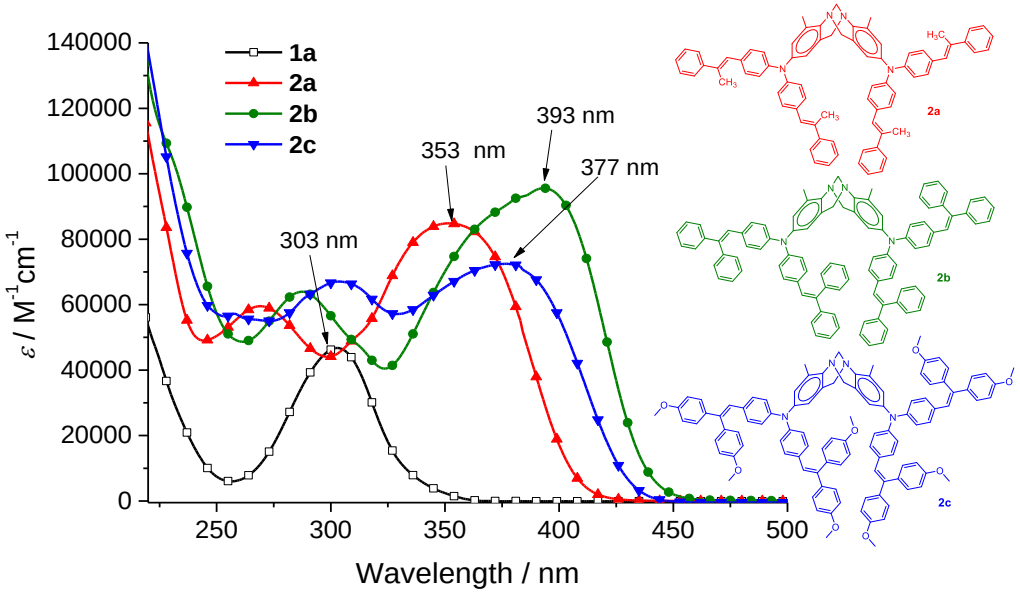

Figure 3.11. Absorption spectra of 1×10^{-4} M THF solutions of the **2a–c**. The absorption spectrum of **1a** is shown for comparison

Thin film UV-Vis absorption spectra of the synthesized materials have been investigated as well (Figure 3.12). From the absorption spectra, it is evident that only in case of **2c**, somewhat more significant blue shift (≈15 nm) from solution (1×10^{-4} M in THF) to the solid state is observed, suggesting some degree of intermolecular interactions in the solid state and the formation of the H-aggregates (Figure 3.12 c). Very little change in absorption spectra of **2a** and **2b** is detected, indicating much weaker intermolecular interactions in the solid state.

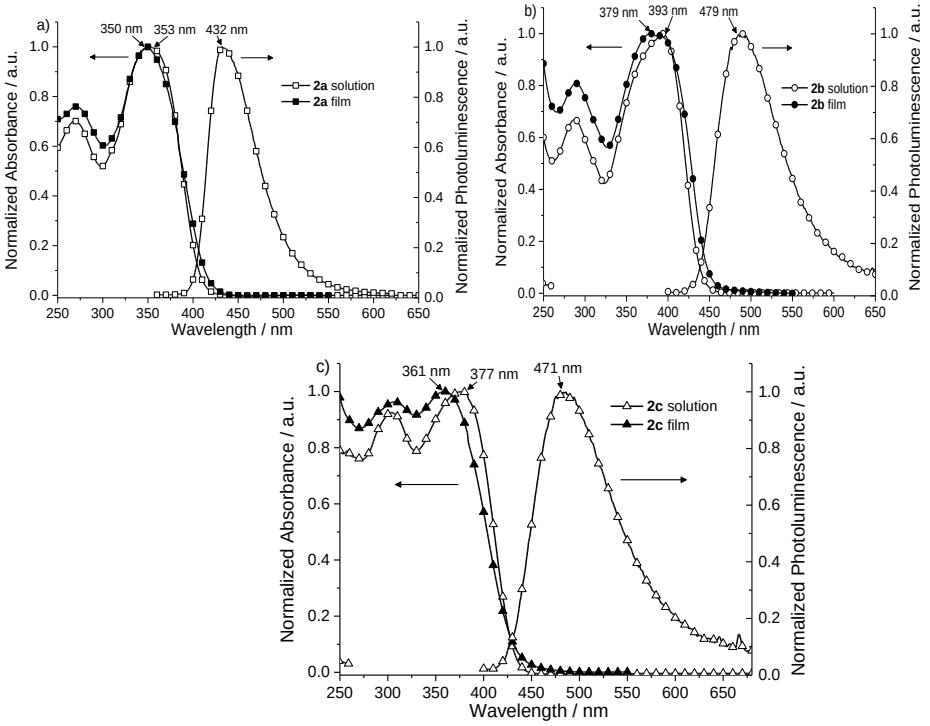

Figure 3.12. Absorption and emission spectra of the **2a–c**

The fluorescence band maximum of the methylphenylethenyl substituted TB derivative **2a** is located at ~432 nm (Figure 3.12 a), and the fluorescence quantum yield (Φ_F) of the dilute solution is 37%. The introduction of the second phenyl into the compound **2b** resulted in the redshift of fluorescence band by ~50 nm. A similar behavior was as well observed for **2c,** containing diphenylethenyl fragments with methoxy groups (Figure 3.12 c). Additional phenyl moiety detrimentally affected Φ_F of the **2b** and **2c** (Table 3.3): Φ_F dropped from 37% down to 9% for **2b**. This significant reduction of Φ_F is attributed to the second phenyl induced steric hindrance effect, which activates phenyl vibrations/torsions and thus promotes radiationless decay [161]. Note that the reduction of Φ_F for the compound **2c** is smaller than for **2b**, since the phenyl motions are somewhat impeded by the presence of methoxy moieties.

3.2.3. Photoelectrical properties

The ionization potential of compounds **2a–c** was measured by the PESA method (Figure 3.13)[1], and the results are presented in Table 3.4; the measurement error is evaluated as 0.03 eV. Methyl and phenyl substituted derivatives **2a** and **2b** have very similar I_p values, while the addition of methoxy groups in **2c** lowers I_p by ~0.2 eV.

[1] Measurements of ionization potential were performed at the Department of Solid State Electronics, Vilnius University, by Dr. V. Jankauskas, E. Kamarauskas.

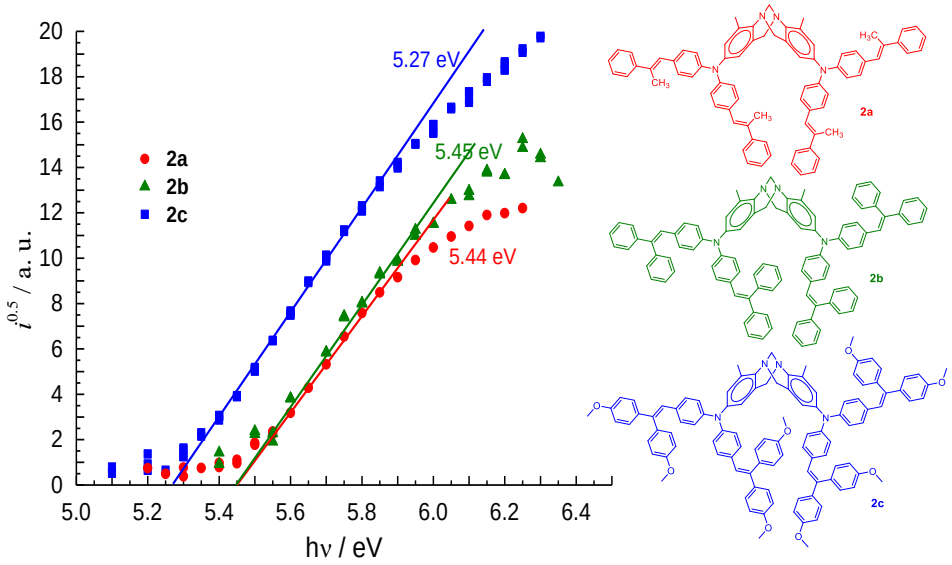

Figure 3.13. Photoemission in air spectra of **2a–c**

Table 3.4. Energy level and hole mobility data for **2a–c** [a]

Compound	E_g^{opt} [eV][b]	E_{HOMO} [eV] [c]	E_{LUMO} [eV] [d]	I_p [eV][e]	EA [eV][f]	μ_0 [$cm^2 V^{-1} s^{-1}$][g]	μ_h [$cm^2 V^{-1} s^{-1}$][h]
2a	3.05	5.38	2.33	5.44	2.39	1.5×10^{-3}	0.011
2b	2.82	5.35	2.53	5.45	2.63	1.3×10^{-4}	0.005
2c	2.87	5.29	2.42	5.27	2.40	3.9×10^{-5}	0.002

[a] The CV measurements were carried out at a glassy carbon electrode in dichloromethane solutions containing 0.1 M tetrabutylammonium hexafluorophosphate as electrolyte and $Ag/AgNO_3$ as the reference electrode. Each measurement was calibrated with ferrocene (Fc). Potentials measured vs Fc+/Fc. [b] The optical band gaps E_g^{opt} estimated from the edges of electronic absorption spectra in solution. [c] Conversion factors: ferrocene in DCM vs SCE 0.46 [162], SCE vs SHE: 0.244 [163], SHE vs. vacuum: 4.43 [164]. [d] E_{LUMO} calculated from the equation $E_{LUMO} = I_p - E_g^{otp}$. [e] Solid-state ionization potential (I_p) was measured by the photoemission in the air method from films. [f] EA calculated from the equation $EA = E_{HOMO} - E_g^{otp}$ [g] Mobility value at zero field strength. [h] Mobility value at 6.4×10^5 V cm^{-1} field strength.

The ground-state oxidation potentials of the HTMs were measured employing the cyclic voltammetry (CV) technique (Figure 3.14, Table 3.4). These values do not represent any absolute solid-state or gas-phase ionization energies, but can be used to compare different compounds that are relative to one another. All three HTMs have similar oxidation potentials in the solution, although a slight decrease of E_{HOMO} is observed due to additional phenyls in **2b** and methoxy groups in **2c**. The structure/energy level transition is more clearly defined in solvated molecules compared with the ones tightly packed in the films. Measured I_p values are slightly higher than the HOMO levels found in the CV experiments. The difference may result from different measurement techniques and conditions (solution in CV and a solid film in the photoemission method).

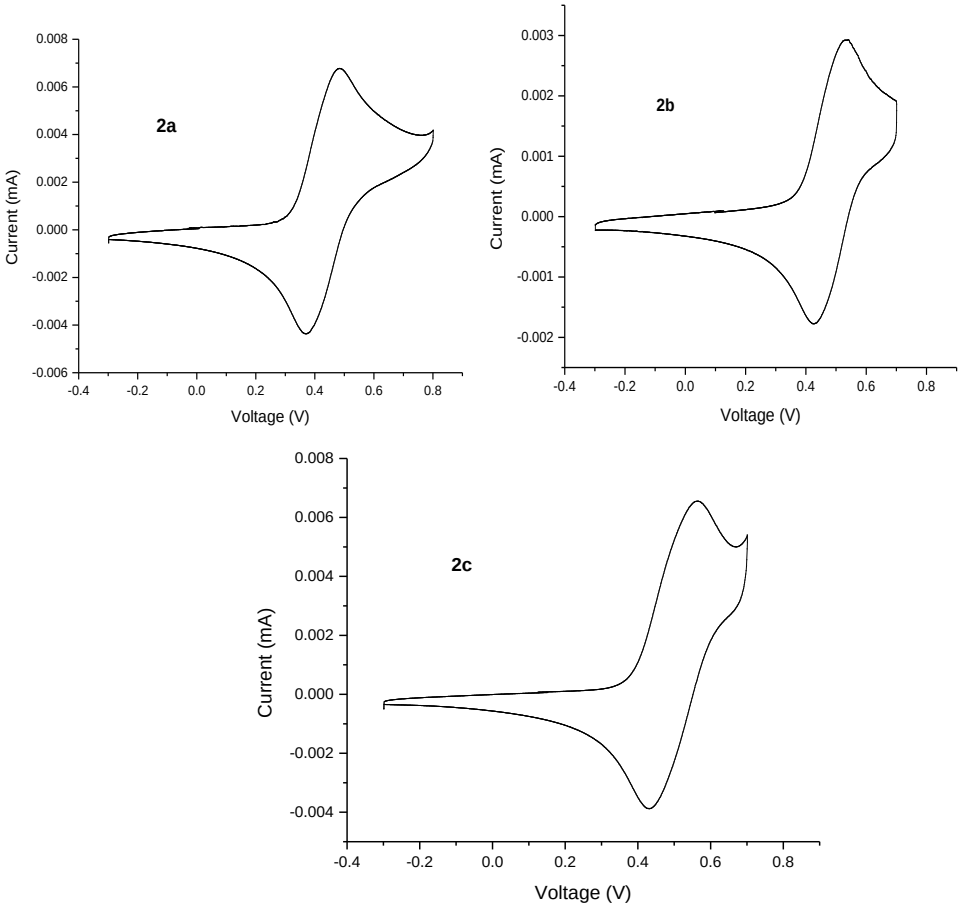

Figure 3.14. First oxidation waves of **2a–c** (scan rate = 50 mV·s^{-1}) in argon-purged dichloromethane solutions

Charge transport properties of the synthesized Tröger's base derivatives were analyzed by the XTOF technique (Figure 3.15) [1]. The values of charge mobility defining parameters: zero field mobility (μ_0) and the mobility at the electric field of 6.4×10^5 V cm^{-1} for the compounds **2a**–**c** are given in the Table 3.4. The room temperature hole-drift mobility of **2a** was 0.011 cm^2 V^{-1} s^{-1} at strong electric fields, and it is approximately five times higher than that of the methoxy-substituted analogue **2c**. Compound **2b** demonstrated intermediate performance, and μ_h of 0.005 cm^2 V^{-1} s^{-1} was reached. Additional structural bulk in the molecules of **2b** and **2c** adversely affects charge mobility; most likely, the manner in which molecules organize in the layer is altered unfavorably by the addition of the phenyl groups and methoxy groups.

[1] Charge mobility measurements were performed at the Department of Solid State Electronics, Vilnius University, by Dr. V. Jankauskas, E. Kamarauskas.

It has to be noted that these results were achieved by using spin-coated films as it has been recognized that the materials that are deposited by using solution-based techniques offer better processability potential compared to the ones that are formed employing deep vacuum methods. Materials, deposited this way, however, demonstrate lower carrier mobility. The decrease in mobility is generally attributed to the higher structural disorder that reduces intermolecular π-orbital overlap. Compared with other low molecular weight hole transporting materials [140, 143, 160, 165–167], Tröger's base phenylethenyl derivatives demonstrate comparatively high hole drift mobility.

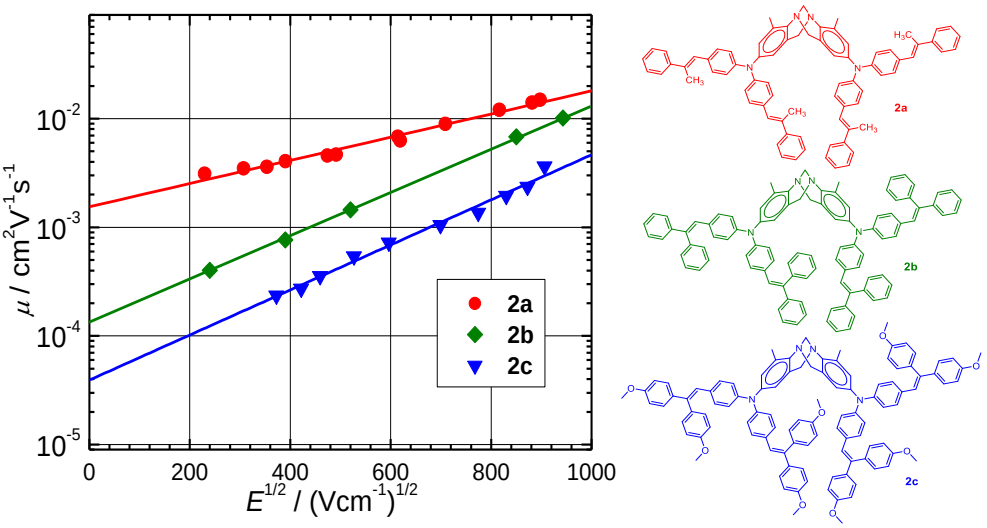

Figure 3.15. Electric field dependencies of the hole drift mobilities (μ) in the charge-transport layers of Tröger's base derivatives **2a**–**c**

The ionization potential values for **2a**–**c** are close to I_p of charge generation materials that are widely used in electrographic photoreceptors such as titanyl phthalocyanines, perylene pigments, and bisazo pigments (5.1–5.6 eV) [168]. This observation combined with very good charge transporting properties indicates that the synthesized compounds can be used as HTM in the electrophotographic photoreceptors.

Compounds **2a**–**2c** can apparently be used as hole transporting materials in organic light emitting diodes. Their I_p values are rather close to that of indium tin oxide (–4.8 eV), which is used as anode in electroluminescent devices.

3.2.4. Testing compounds in perovskite solar cells

In order to examine in-device application possibilities and compatibility with other materials synthesized TB derivatives, **2a–c** have been preliminary tested as hole transporting semiconductors for the perovskite solar cells (PSC) [1]. The experiments

[1] Solar cells fabricated and tested in the Department of Physics, Clarendon Laboratory, University of Oxford, by Prof. H. J. Snaith, Dr. N. Sakai.

were carried out by using perovskite precursor containing a cation and anion mixture in a device stack of fluorine doped tin oxide(FTO)/compact TiO_2/ perovskite/HTM/Ag (Figure 3.16). All the fabrication details are described in the experimental section.

Corresponding maximum power conversion efficiency of 11.09% under AM 1.5 G illumination was recorded in the perovskite device, containing **2c** as hole transporting material. The measured fill factor was 0.6, the current density (J_{sc}) 20.1 mA cm^{-2}, and the open-circuit voltage (V_{oc}) 923 mV (Figure 3.17). For comparison, 2,2′,7,7′-tetrakis(*N*,*N*-di-*p*-methoxyphenylamine)-9-9′-spirobifluorene (Spiro-OMeTAD) was used as a reference material, and the device from the same batch of solar cells, prepared by following the same device fabrication procedure, but using Spiro-OMeTAD as hole-extracting layer, displayed a PCE of 15.34%. Unfortunately, **2a** and **2b** did not function in the tested solar cell setup because of the energy level mismatch between perovskite and HTMs (Figure 3.16). The energy offset of the I_p (ca. -5.45 eV) relative to that of the $MAPbI_xCl_{3-x}$ (–5.40 eV) [137] does not present enough driving force for the charge injection process.

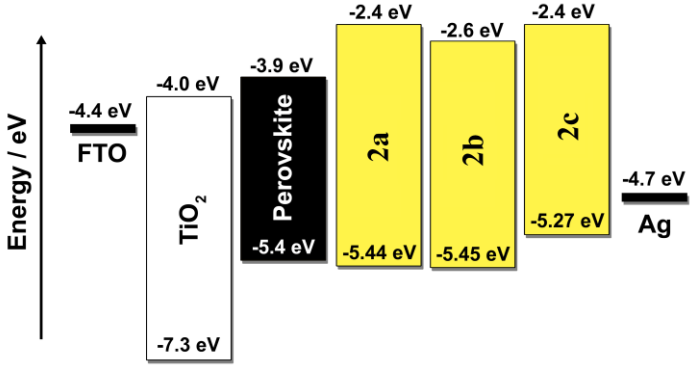

Figure 3.16. Energy level diagram for the PSC devices constructed using **2a**–**c**

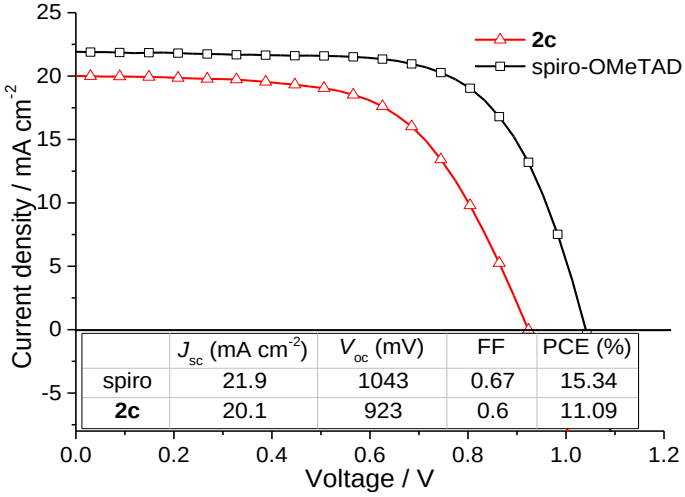

	J_{sc} (mA cm^{-2})	V_{oc} (mV)	FF	PCE (%)
spiro	21.9	1043	0.67	15.34
2c	20.1	923	0.6	11.09

Figure 3.17. Best performing perovskite solar cells current density-voltage characteristics with **2c** and spiro-OMeTAD as hole transporting materials

In conclusion, this simple synthetic procedure has been proven efficient and fruitful in obtaining solution processable V-shaped hole-transporting compounds based on Tröger's base core and phenylethenyl substituted triphenylamine moieties. TB core significantly increases the glass transition temperatures of the HTMs, which is especially apparent when compared to non-TB analogues, while phenylethenyl moieties provide structural bulk, decrease crystallinity, and contribute considerably to the size of the π-conjugated system of molecules. The investigated hole transporting materials are promising candidates for the application in organic and hybrid optoelectronic devices as they can be handled in the air, are thermally stable, require no high temperature annealing steps, can be solution deposited, and possess comparatively high mobility (up to 0.011 $cm^2 V^{-1} s^{-1}$).

3.3. Hole transporting TPD derivatives conjoined by Tröger's base core

Among various electronic and optoelectronic devices, hybrid perovskite solar cells (PSC) are one of the most dynamic and rapidly evolving areas of research [169–172]. The efficiency of the perovskite solar cell is highly dependent on the used HTM, which is expected to have good hole-drift mobility and high morphological stability as well as to meet certain energy level requirements. Among a considerable number of hole-transporting materials that were investigated, spiro-OMeTAD stands out as one of the most efficient and most widely used small-molecule HTMs in both solid-state dye-sensitized solar cells (ssDSSCs) [173, 174] and PSCs [175–179].

Despite its widespread popularity as a material of choice for PSCs, spiro-OMeTAD has flaws of its own. Spiro-OMeTAD is found to have a high tendency to crystallize in the device, thus impairing cell's performance [144]. The crystallization of the hole conductor in the layer is undesirable because it would impair the formation of a good contact between the active layer and back contact electrodes [180]. Additionally, spiro-OMeTAD is synthesized in five reaction steps that require sensitive (*n*-butyllithium or Grignard reagents) and aggressive (Br_2) reagents, low temperature (-78 °C) conditions which make it quite costly [181]. Such findings encourage the search for easier to synthesize novel HTM alternatives with improved thermal stability and charge mobility.

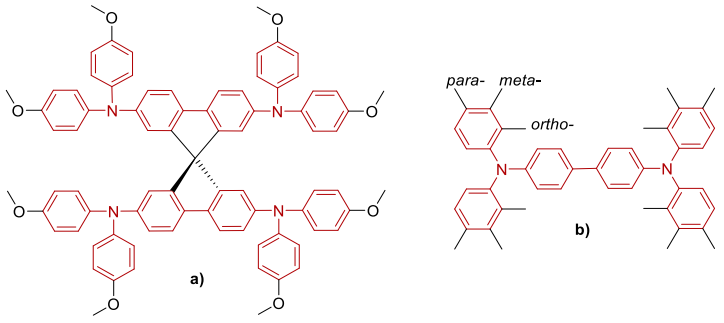

Figure 3.18. a) spiro-OMeTAD; b) TPD-type molecule with methyl groups at different positions

The link between spiro-OMeTAD structural features and its high efficiency as HTM in PSC is as well of significant importance. It is considered that spiro-OMeTAD (Figure 3.18) is mostly conceptually derived from the respective *N,N,N′,N′*-tetraarylbenzidine-type (TPD) compounds that are conjoined by spiro center orientating TPD moieties perpendicularly to one another [146].

The concept of conjoined TPDs suggests that the investigation of alternative ways to connect these compounds in non-planar manner could afford the materials with improved performance in PSCs, and Tröger's base provides a valuable opportunity as its structure allows it to be used as a core and provide angle orientation for the conjugated π-systems that is attached to it. Recent investigations have revealed that the rigidity of the TB scaffold and high molecular mass via its 2-fold functionalization impart crystallization, significantly increase glass transition temperature, and render TB derivatives highly amorphous and thermally stable [134, 146, 147]. Additionally, the work on HTMs containing TB core that have already been presented in previous chapters encourages further work in this field as the presented compounds had comparatively high charge mobility and very good thermal and morphological stability.

A study by Nukada *et al*. showed how seemingly insignificant methyl groups at different positions (Figure 3.18 b) of TPD molecule can influence the hole-drift mobility, allowing for maximized charge transport properties when substituents are present in *para*- positions [153]. Therefore, it is of interest to investigate how HTM characteristics are influenced by different functional groups at *para*- position of the phenyls.

This chapter is dedicated to the synthesis and investigation of the V-shaped charge transporting molecules consisting of TPD-type moieties containing different functional groups at *para*- position of the phenyl rings and conjoined by Tröger's base core. The results that are presented in this work were published in a journal article as well [182].

3.3.1. Synthesis of compounds

Novel Tröger's base core containing TPD compounds N^4,$N^{4'}$-(4,10-dimethyl-6*H*,12*H*-5,11-methanodibenzo[*b*,*f*][1,5]diazocine-2,8-diyl)bis-N$^{4'}$-(4-methoxyphenyl)-N^4,$N^{4'}$-diphenyl-(1,1'-biphenyl)-4,4'-diamine (**3f**), N^4,$N^{4'}$-(4,10-dimethyl-6*H*,12*H*-5,11-methanodibenzo[*b*,*f*][1,5]diazocine-2,8-diyl)bis(N^4,$N^{4'}$,$N^{4'}$-tri-*p*-tolyl-[1,1'-biphenyl]-4,4'-diamine) (**3g**) and N^4,$N^{4'}$-(4,10-dimethyl-6*H*,12*H*-5,11-methanodibenzo[*b*,*f*][1,5]diazocine-2,8-diyl)bis(N^4,$N^{4'}$,$N^{4'}$-tris(4-methoxyphenyl)-[1,1'-biphenyl]-4,4'-diamine) (**3h)** have been synthesized via intermediate biphenyl compounds **3a**–**e** (Scheme 3.3).

Initially, biphenyl compounds **3a**–**b** were obtained from the 4,4'-dibromobiphenyl and the corresponding anilines employing Buchwald-Hartwig cross-coupling reaction. **3a**, **3b** and their commercially available analogue *N*,*N*-diphenylbenzidine were used in a Pd catalyzed cross-coupling reaction with appropriate aryl halides to isolate compounds **3c**–**e**, which in turn reacted with brominated Tröger's base [40] to obtain target compounds **3f**–**h**, having TPD fragments conjoined by Tröger's base core.

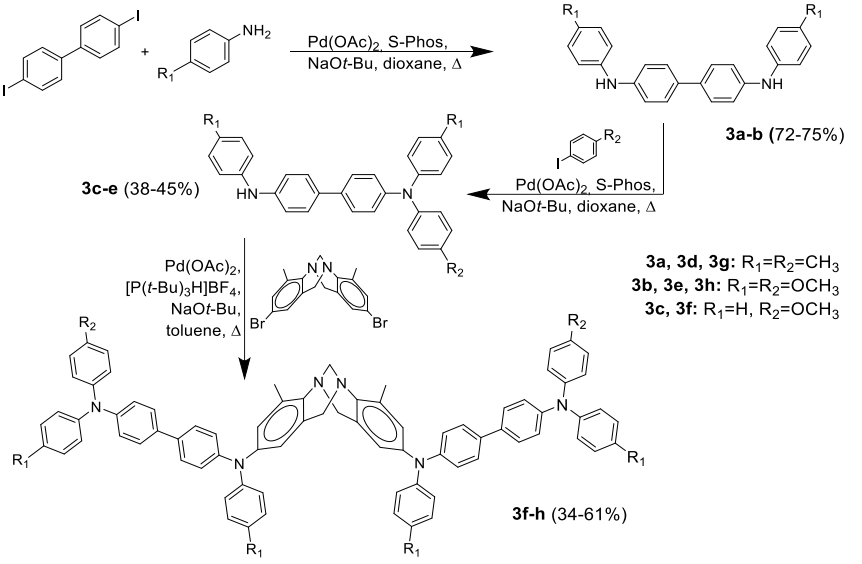

Scheme 3.3. Synthesis of compounds **3a**–**3h**

The structures of synthesized compounds were confirmed by NMR ^{1}H and ^{13}C spectroscopy as well as elemental analysis. The signal pattern of compounds **3f**–**h** in the interval of 3.85–4.50 ppm of ^{1}H NMR spectrum is essential for the identification of *methanodiazocine* bridge, proving the presence of the TB core (Figure 3.19). ^{1}H NMR spectra of **3f**–**3h** shows a doublet near each margin of the mentioned interval, and these two doublets, *endo* and *exo* hydrogens respectively, signify that the protons in bridging methylene part (Ar-CH_2-N) are magnetically nonequivalent due to the rigid structure of the TB. As a contrasting example, the signals of two protons of the other bridging methylene carbon (N-CH_2-N) can be observed as a singlet at 4.30 ppm. The signal of protons in methoxy groups is detected as sharp singlet at 3.80 ppm, neighboring signal of hydrogens in *endo* position.

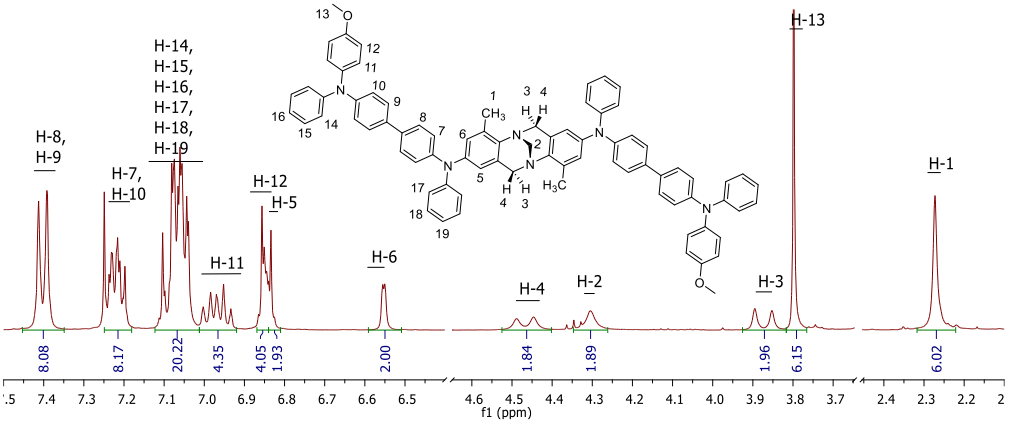

Figure 3.19. ^{1}H NMR spectrum (400MHz, $CDCl_3$) of compound **3f**

As the investigation of compounds **3f**–**h** was advancing, the compound **3h** was showing the most promising results, therefore suggesting that methoxy substituents on TPD fragments bestow the final compound with most favorable properties. Hence, a plan to synthesize molecules containing two or four methoxy substituted TPD fragments (*via* reaction with intermediate **3e)** fused by TB in a different way was created. The synthesis of such compounds was executed by synthesizing two brominated TB cores, **3i**–**j**, having bromine substituents in a different positions compared to the previously used core; these core molecules underwent reaction with **3e** via Buchwald-Hartwig cross-coupling, affording materials **3k**–**l** (Scheme 3.4).

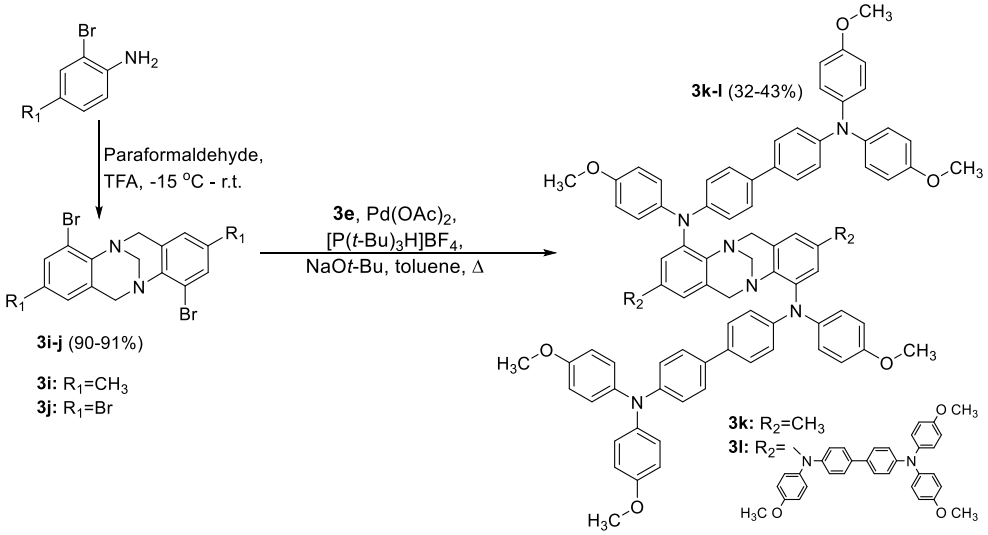

Scheme 3.4. Synthesis of compounds **3i**–**l**

The structures of synthesized compounds were confirmed by NMR ^{1}H and ^{13}C spectroscopy as well as elemental analysis; NMR results resemble that of **3f**–**h** and have proton signals typical for TB core, such as showing doublets for energetically nonequivalent *exo* and *endo* hydrogens in central fragment; the peaks of TPD fragments and methoxy groups were observed as well.

3.3.2. Thermal and optical properties

Non-planar structure of TB and subsequently TPD-type fragments oriented one towards another in angle fashion form a non-compact structural bulk which hampers the crystallization process in the investigated HTMs. DSC measurements reveal that all the investigated Tröger's base compounds **3f**–**3h** and **3k**–**l** exist only in amorphous state (Figure 3.20, Table 3.5).

During the first heating, a peak specific to glass transition (T_g) temperature can be observed, and no signals that show the melting of crystals is detected. No crystallization takes place during cooling or second heating scans, and only glass transition is registered at 167 °C, 177 °C, and 161 °C for **3f, 3g,** and **3h**, and 153 °C and 166 °C for **3k** and **3l**, respectively.

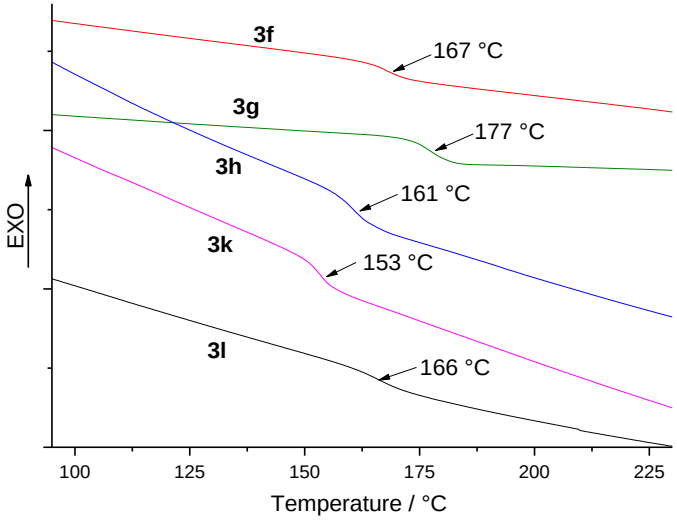

Figure 3.20. DSC curves of **3f**–**h** and **3k**–**l** indicating T_g. heating rate 10 K/min, second run

The thermogravimetric analysis of these compounds reveals high decomposition temperatures (Figure 3.21, Table 3.5), and in general, all the compounds within the series have demonstrated superior thermal stability, with initial destruction temperatures (corresponding to 5% weight loss) exceeding 400 °C, confirming that these TB derivatives are thermally very stable and are promising candidates for the practical applications. Slight weight loss (up to ~2%) observable for **3h** at ~130 °C is attributed to the evaporation of the traces of residual solvents that remained after the purification of material. It can be noticed that compounds with methoxy groups on all outer phenyls of TPD moieties have slightly lower initial destruction temperatures.

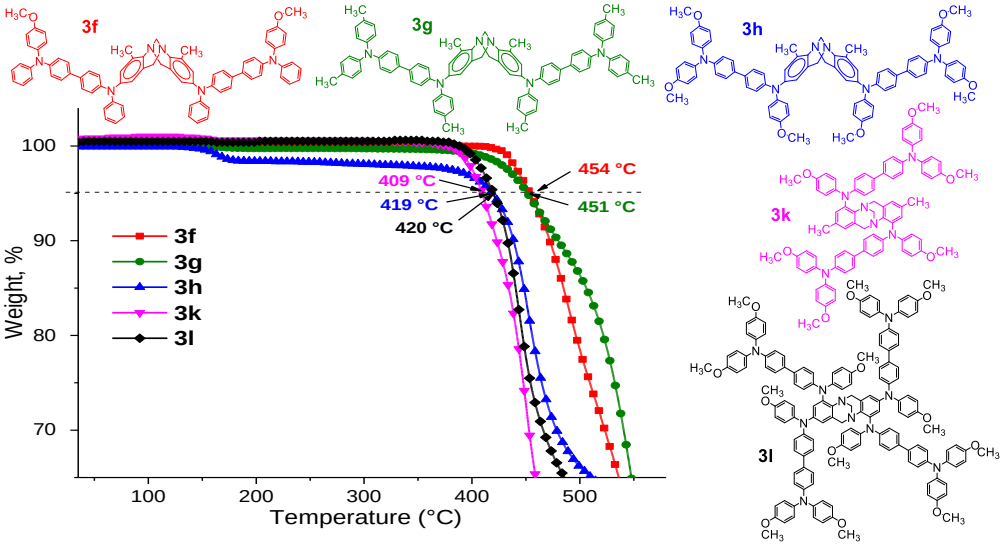

Figure 3.21. TGA curves for TB derivatives possessing TPD fragments

UV–VIS absorption spectra of Tröger`s base derivatives **3f**–**3h** and **3k**–**l** in 10^{-4} M THF solution (Figure 3.22), and emission spectra of **3f**–**h** measured in 10^{-6} M THF solution, polystyrene (PS) film and neat film are shown in Figure 3.23. Compounds **3f-h** show twofold absorption characteristics peaking at 303–305 nm and 354–355 nm, respectively, what is a typical feature of various triphenylamine-cored compounds [151, 183]. The absorption spectra of **3k** and **3l** show similar tendencies, except in this case, the first absorption peaks are slightly shifted bathochromicaly and located at 310nm. TB derivative **3l** have twice TPD fragments compared to the other measured molecules, bestowing it the absorption of nearly double the intensity compared to other compounds, but no significant bathochromic shift indicates that two neighboring TPD fragments in each side of the core do not form a single expanded conjugated system, likely due to the unfavorable twisting of fragments breaking the conjugation. UV–Vis–NIR absorption spectra of these compounds do not show any absorption in the NIR region of the spectrum, a property that would be beneficial for the application of these materials in the tandem solar cells.

Table 3.5. Thermal and optical properties of TB derivatives possessing TPD fragments

Comp.	T_g (°C)	T_{dec} (°C)	THF solution				PS film 0.1 wt %		Neat film		Zeonex film 1 wt %
			λ_{abs} (nm) [a]	ε (l mol^{-1} cm^{-1}) [b]	λ_F (nm) [c]	Φ_F (%) [d]	λ_F (nm) [c]	Φ_F (%) [d]	λ_F (nm) [c]	Φ_F (%) [d]	λ_{PH} (nm) [e]
3f	167	454	304	66391	413	44.5	403	42	418	2.3	523
			354	86250							
3g	177	451	305	63454	419	46.8	406	44.2	419	2.2	527
			356	77413							
3h	161	419	303	65804	424	52.1	413	50.2	428	3.9	529
			355	86485							
3k	153	409	310	59758	410	39.33					
			352	83109							
3l	166	420	310	11647	435	37.26					
			354	15466							

[a] Absorption maxima in THF solution. [b] Molar extinction coefficient of absorption in THF solution at peak positions. [c] Fluorescence maxima in THF solution, PS film (0.1 wt %), neat film. [d] Fluorescence quantum yield in THF solution, PS film, neat film. [e] Phosphorescence maxima in Zeonex film (1 wt %).

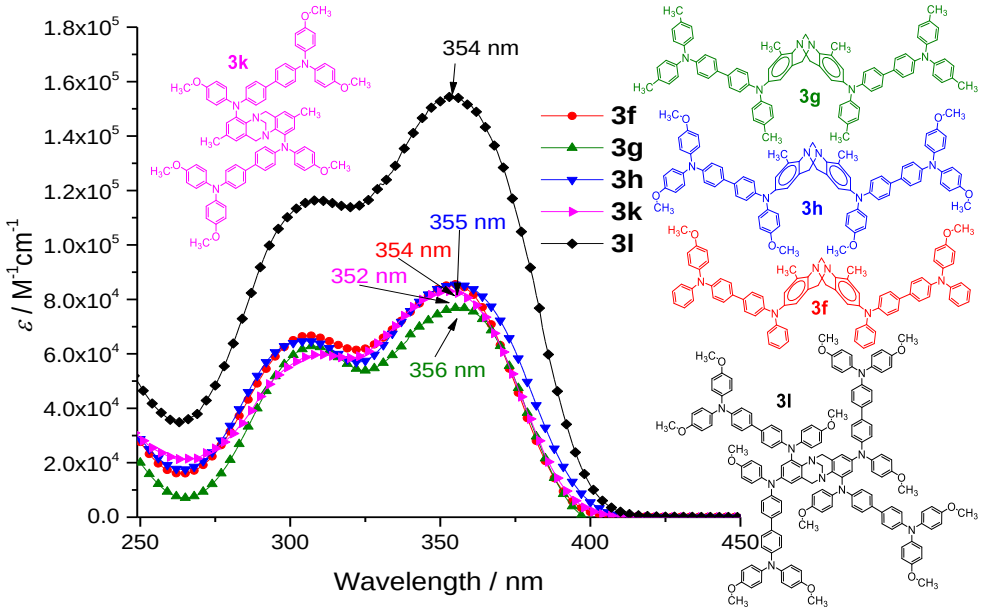

Figure 3.22. Absorption spectra of 1×10^{-4} M THF solutions of compounds **3f–h** and **3k–l**

The fluorescence of compounds **3f**–**h** in dilute THF (10^{-6} M) solutions, PS film (0.1 wt %), neat film, and phosphorescence in Zeonex (1 wt %) film were measured[1]. The fluorescence in solutions revealed that all three compounds exhibit deep-blue structure-less emission that peaked at 413–424 nm. The incorporation of different substituents at the *para*- position of the triphenylamine moiety in **3f**–**3h** has a noticeable impact on both absorption and emission properties of the molecules. The observed fluorescence redshift (of 10 nm) for the compound **3h** can be attributed to the polar nature of the methoxy substituents. Interestingly, all Tröger`s base derivatives **3f**, **3g,** and **3h** show relatively high fluorescence quantum yields (45 to 52%), which can be due to the restriction of the phenyl moiety torsion by bulky substituents [184]. This is supported by similar fluorescence properties of the compounds that were tested in a rigid PS matrix. The compounds exhibit strong room temperature phosphorescence that is recorded at 1 ms delay time after the excitation (Figure 3.23). The estimated triplet state energy shifts from 2.37 eV to 2.35 eV and 2.34 eV for compounds **3f**, **3g**, and **3h**, respectively. The triplet energy values are typical for TPA-cored compounds [185, 186]. Close molecular packing of the Tröger`s base derivatives in the neat films resulted only in minor redshift of the fluorescence, indicating restricted intermolecular interaction and exciton coupling (Figure 3.23). The fluorescence of the neat film of compound **3g** shows additional broad excimer emission that peaked at about 500 nm, which can be attributed to the absence of methoxy substituents.

[1] Fluorescence measurements performed in the Institute of Applied Research, Vilnius University, by Prof. S. Juršėnas, R. Komskis.

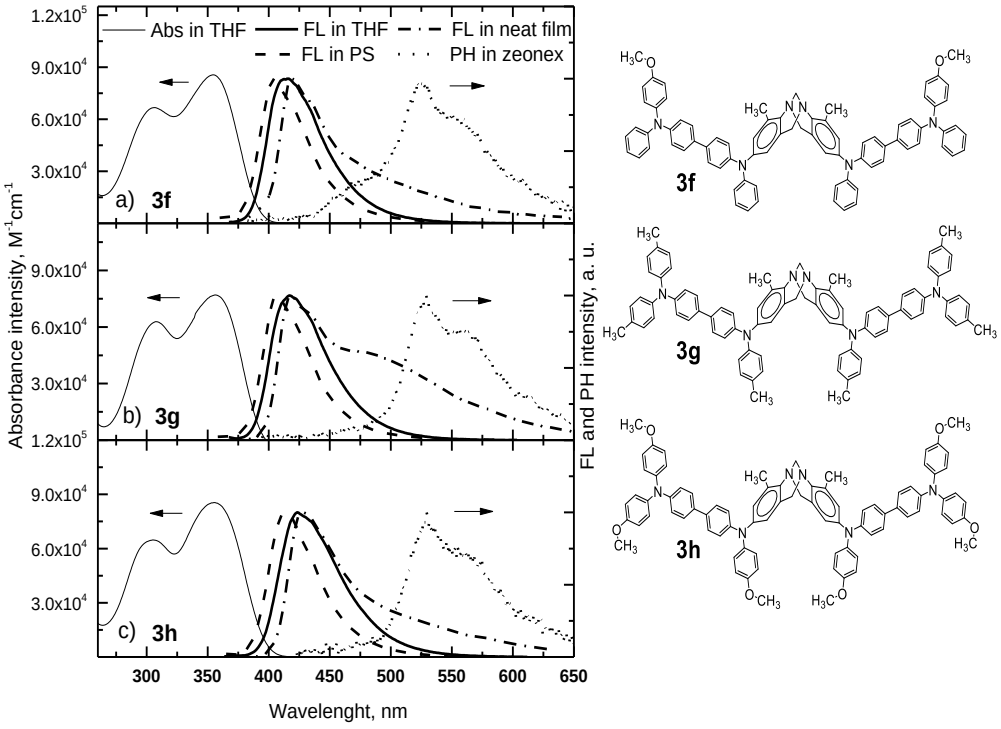

Figure 3.23. Absorbance (Abs) and emission-fluorescence (FL) and phosphorescence (PH) spectra of Tröger`s base derivatives **3f–h**

Fluorescence decay transient measurements were carried out in order to determine excited state relaxation dynamics (Figure 3.24, Table 3.6). All compounds demonstrate exponential fluorescence decay transients in THF solution with excited state decay constant 1.31 ns and 1.35 ns for compounds **3f** and **3g,** respectively, and similar radiative recombination decay constant (2.88 ns and 2.94 ns for **3f** and **3g**, respectively). The incorporation of methoxy substituents enhances relaxation time slightly (up to 1.58 ns) for **3h** (Table 3.6). Almost the same radiative recombination decay constant (3.03 ns) and slower nonradiative decay constant (3.30 ns) for **3h** implies on the restriction of molecular torsions in phenylamine moieties, which results in enhanced fluorescence quantum yield. The restriction of molecular torsions in a rigid polymer medium ensures faster fluorescence decay rate (0.99–1.08 ns) with exponential decay dynamics and similar fluorescence quantum efficiency. Meanwhile, the relaxation of excited state in the neat films demonstrates non-exponential decay characteristics and reduced quantum efficiency due to the enhanced exciton migration and trapping to the nonradiative states [187].

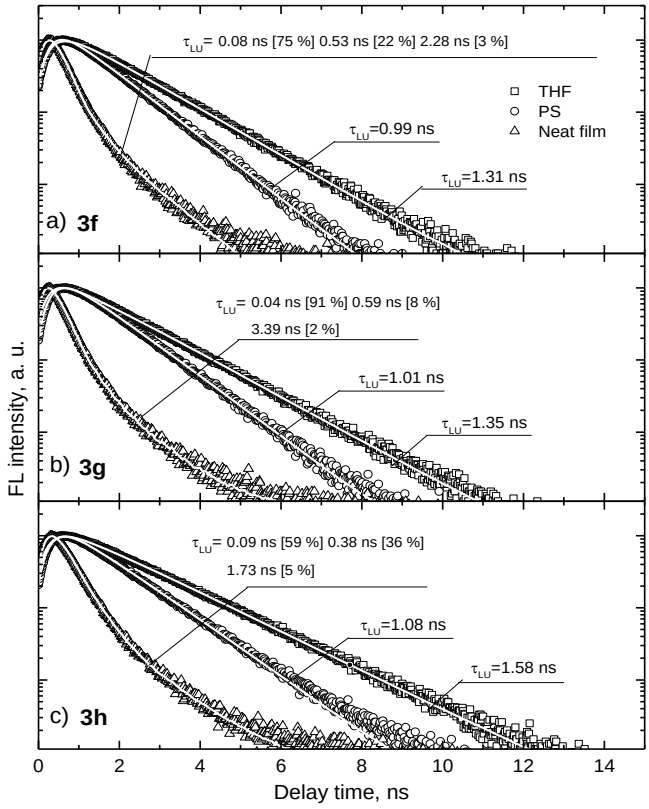

Figure 3.24. Fluorescence decay transients of Tröger`s base derivatives **3f** (a), **3g** (b), **3h** (c)

Table 3.6. Emission decay transient properties of derivatives **3f**–**h**

Comp.	THF solution				Neat film		PS film 0.1 wt %			
	τ_F (ns) [a]	τ_r (ns) [b]	τ_{nr} (ns) [c]	Φ_F (%) [d]	τ_F(ns) [a]	Φ_F (%) [d]	τ_F (ns) [a]	τ_r (ns) [b]	τ_{nr} (ns) [c]	Φ_F (%) [d]
3f	1.31	2.94	2.36	44.5	0.08 [75%] 0.53 [22%] 2.28 [3%]	2.3	0.99	2.36	1.71	42
3g	1.35	2.88	2.54	46.8	0.04 [91%] 0.59 [8%] 3.39 [2%]	2.2	1.01	2.29	1.81	44.2
3h	1.58	3.03	3.30	52.1	0.09 [59%] 0.38 [36%] 1.73 [5%]	3.9	1.08	2.15	2.17	50.2

[a] Exponential decay constant of fluorescence in THF solution, PS film (0.1 wt %), neat films. [b] Radiative recombination rate of fluorescence in THF solution, PS film (0.1 wt %), neat films. [c] Non radiative recombination rate of fluorescence in THF solution, PS film (0.1 wt %), neat films. [d] Fluorescence quantum yield in THF solution, PS film (0.1 wt %), neat films.

3.3.3. Photoelectrical properties

The ionization potential of the compounds **3f**–**h** and **3k**–**l** was measured by the PESA method (Figure 3.25)[1], and the results are presented in Table 3.7; the measurement error is evaluated as 0.03 eV.

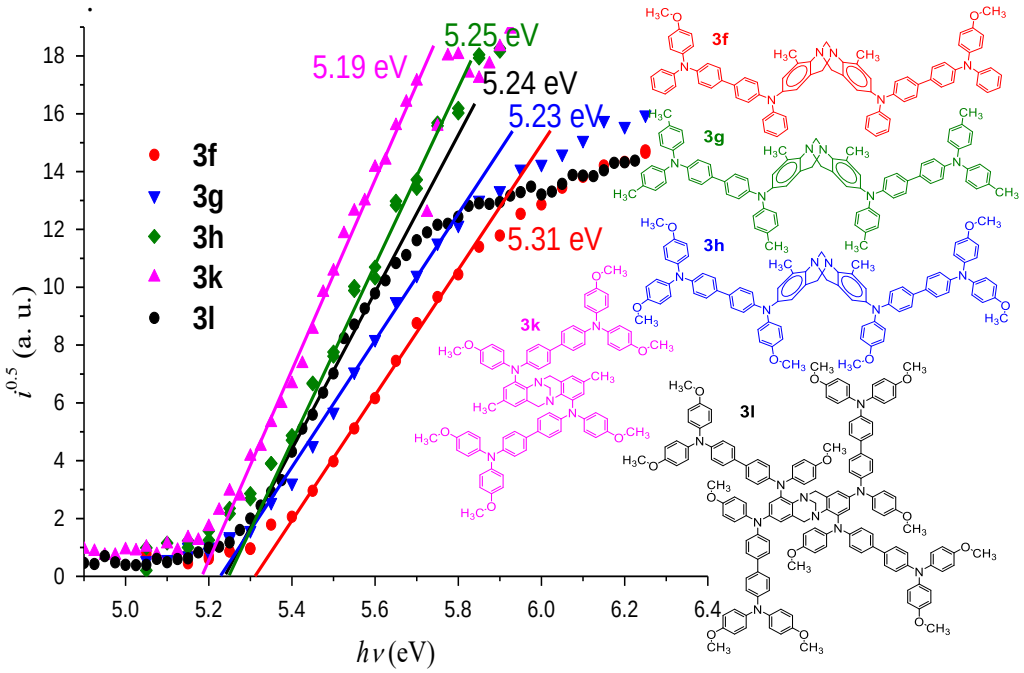

Figure 3.25. Photoemission in air spectra of **3f**–**3h** and **3k**–**l**

I_p values for TB derivatives **3f**–**3h** display the influence of methyl- and methoxy- substituents in phenyl groups. **3f** has four unsubstituted phenyl groups, and the highest I_p value (5.31 eV), *para*-substitution of all terminal phenyls with methyl groups in **3g** lowers I_p by 0.06 eV. The incorporation of six donating methoxy fragments in **3h** resulted in the lowest I_p among all three compounds (5.23 eV). The compounds **3k** and **3l** have their I_p values of 5.19 and 5.24 eV, respectively, showing that not only the amount of methoxy groups themselves determine their I_p values, but the location of group housing as well. Interestingly enough, compound **3k**, having TPD moieties attached in a different location (TB core substitution in 2,8- positions), demonstrated the lowest I_p in the group.

Ground-state oxidation potentials of the compounds **3f**–**h** and **3k**–**l** were measured by employing the cyclic voltammetry technique (Table 3.7). All five TB derivatives undergo reversible oxidation in their CV scans, indicating the electrochemical stability of the compounds (Figure 3.26). The observed CV results in the solution correlate well with the ionization potential measurement data that was obtained from films, indicating limited intermolecular interaction in the solid state.

[1] Measurements of ionization potential were performed at the Department of Solid State Electronics, Vilnius University, by Dr. V. Jankauskas, E. Kamarauskas.

Table 3.7. Energy level and hole mobility data for **3f**–**3h**[a] (spiro-OMeTAD given for comparison)

Compound	E_g^{opt} (eV) [b]	E_{HOMO} (eV)[c]	E_{LUMO} (eV)[d]	I_p (eV)[e]	μ_0 ($cm^2\ V^{-1}\ s^{-1}$)[f]	μ_h ($cm^2\ V^{-1}\ s^{-1}$)[g]
3f	3.16	5.24	2.08	5.31	4×10^{-8} h	4×10^{-6} h
3g	3.15	5.13	1.98	5.25	1.2×10^{-4}	0.004
3h	3.13	5.11	1.98	5.23	6×10^{-5}	0.036
3k	3.05	5.13	2.08	5.19	–[i]	–[i]
3l	3.01	5.19	2.18	5.24	1.1×10^{-5}	9.4×10^{-4}
spiro-OMeTAD	–	–	–	5.00	4.1×10^{-5}	5×10^{-4}

[a] The CV measurements were carried out at a glassy carbon electrode in dichloromethane solutions containing 0.1 M tetrabutylammonium hexafluorophosphate as electrolyte and Pt wire as the reference electrode. Each measurement was calibrated with ferrocene (Fc). Potentials measured vs Fc^+/Fc. [b] The optical band gaps E_g^{opt} estimated from the edges of electronic absorption spectra in solution. [c] Conversion factors: ferrocene in DCM vs SCE 0.46 [143], SCE vs SHE: 0.244 [166], SHE vs. vacuum: 4.43 [167]. [d] E_{LUMO} calculated from the equation $E_{LUMO} = E_{HOMO} - E_g^{otp}$. [e] Solid state ionization potential (I_p) was measured by the photoemission in the air method from films. [f] Mobility value at zero field strength. [g] Mobility value at 6.4×10^5 V cm^{-1} field strength. [h] **3f** mobility values were measured from the mixture of compound **3f** and PC-Z (1:1). [i] No layers suitable for measurements were obtained.

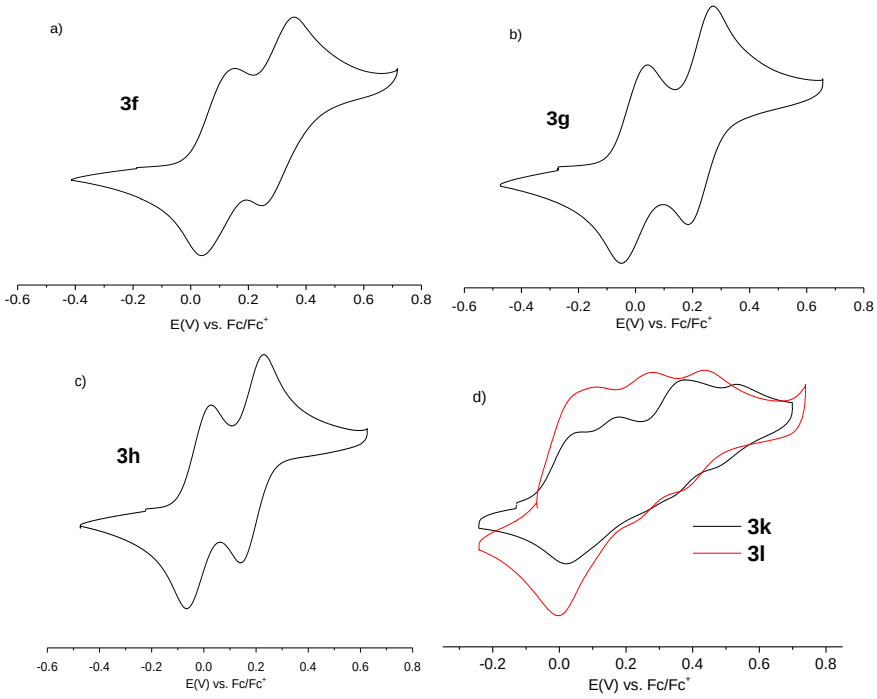

Figure 3.26. Oxidation waves of **3f** (a), **3g** (b), **3h** (c), and **3k**–**l** (d) (scan rate = 50 $mV \cdot s^{-1}$) in argon-purged dichloromethane solutions

The charge transport properties of synthesized compounds **3f**–**h** and **3k**–**l** were analyzed by XTOF technique[1]. The values of the charge mobility defining parameters: zero field mobility (μ_0) and the mobility in the electric field of 6.4×10^5 V cm^{-1} for the compounds **3f**–**h** and **3k**–**l** are given in the Table 3.7 and Figure 3.27. The best hole-drift mobility (0.036 cm^2 V^{-1} s^{-1} at strong electric fields) was measured in films with the methoxy-substituted **3h**. It is approximately nine times higher than that of the methyl-substituted analogue **3g,** which demonstrated intermediate performance, and μ_h of 0.004 cm^2 V^{-1} s^{-1} was reached. Compound **3l** showed even poorer results, despite having a double amount of TPD moieties fused into TB core; evidently, the additional presence of these fragments does not favor the charge mobility, a phenomena that might be explained by possible hindrance by additional fragments making the side arms of molecule too bulky, hence interfering favorable arrangement towards neighboring molecules. Poor quality films of the **3f** were obtained; therefore, a mixture of **3f** and polycarbonate (PC-Z) in weight ratio 1:1 was used in order to obtain uniform layers. Naturally, absolute mobility results for **3f** are lower (approximately one order of magnitude) due to the presence of a large portion of nonconductive polymer. Compound **3k** did not form a suitable uniform layer neat or in mixture with PC, disallowing to obtain any significant results.

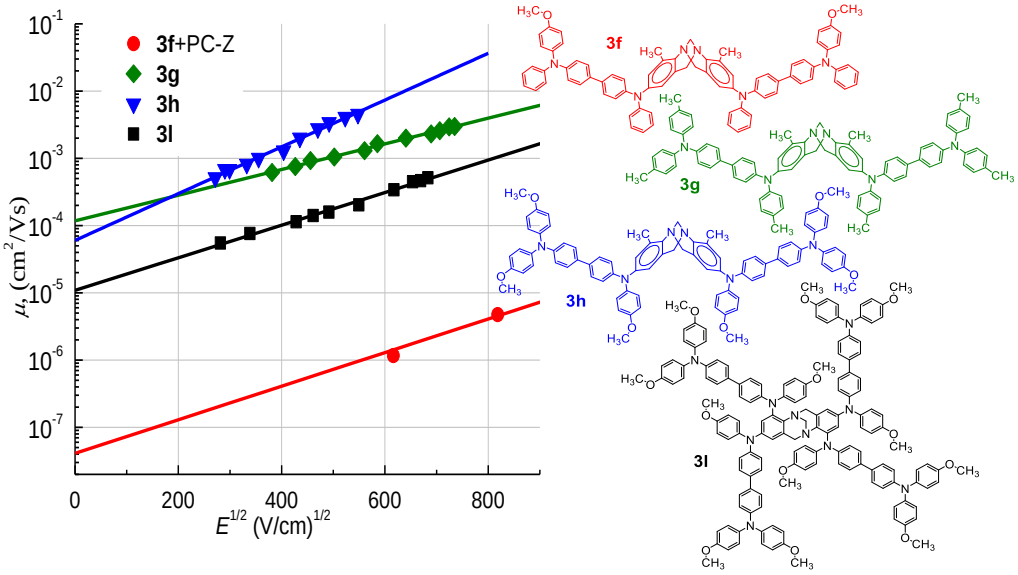

Figure 3.27. Electric field dependencies of the hole drift mobilities (μ) in the charge-transport layers of Tröger base derivatives **3f**–**3h** and **3l**. A mixture of compound **3f** and PC-Z (1:1) was used to obtain uniform layer

Compared with other low molecular weight hole transporting materials [143, 160, 165–167], the synthesized TB derivatives **3g** and **3h** demonstrate comparatively high hole drift mobility, exceeding that of the corresponding methyl and methoxy TPD analogues without TB core by more than two orders of magnitude [140, 188].

[1] Charge mobility measurements were performed at Department of Solid State Electronics, Vilnius University by Dr. V. Jankauskas, E. Kamarauskas.

An interesting phenomenon was observed in these compounds, the substitution of methyl- group to methoxy- did not cause decrease in charge mobility, which is usually a tendency. This phenomenon was as well observed in a number of other triphenylamine systems. The experimental data and theoretical calculations suggest that the enhancement of intramolecular interactions observed in methoxy- substituted triphenylamine compounds make a positive impact on the hole mobility of these materials [189–191].

I_p values of compounds **3f**–**h**, **3k**–**l** are in the range of 5.31–5.19 eV and do not exceed I_p values of perovskite compositions (~5.6–5.4 eV [192, 193]). This observation combined with very good charge transporting properties is suggesting that the synthesized hole transporting materials could be promising candidates for perovskite solar cells.

Derivatives **3k**–**l**, having two, or four, methoxy substituted TPD moieties linked into Tröger's base core in a different way, provided interesting results for the research and comparison with compounds such as **3g**–**h**. Despite having most of the thermal, optical, and photoelectrical properties equally suitable for optoelectronics, these materials were not be able to exceed the charge mobility results of **3g**–**h**. TB derivative **3k** did not form uniform layers, and hence falls behind in its potential applicability in perovskite solar cells.

3.3.4. Testing compounds in perovskite solar cells

As the most promising property-wise among the synthesized TB derivatives, **3g** and **3h** have been preliminary tested as hole transporting semiconductors for the perovskite solar cells[1].

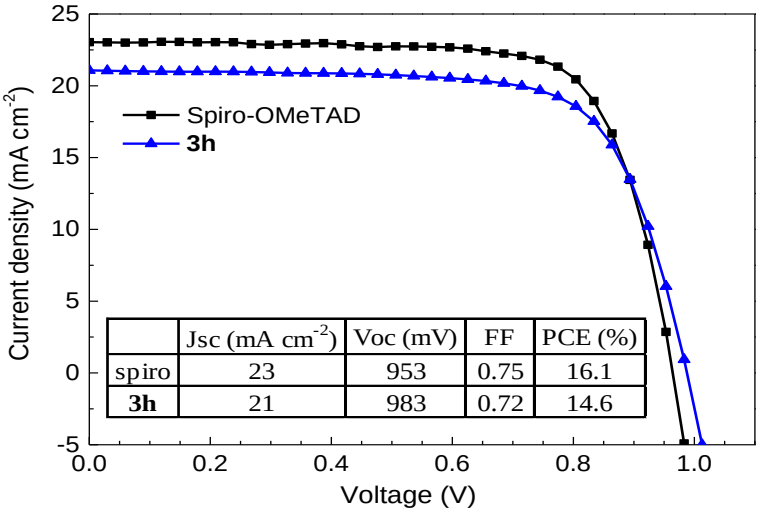

	Jsc (mA cm^{-2})	Voc (mV)	FF	PCE (%)
spiro	23	953	0.75	16.1
3h	21	983	0.72	14.6

Figure 3.28. Best performing perovskite solar cell current density-voltage characteristics with **3h** and spiro-OMeTAD as hole transporting materials

[1] Solar cells fabricated and tested in the Department of Physics, Clarendon Laboratory, University of Oxford, by Prof. H. J. Snaith, Dr. N. Sakai.

The experiments were carried out by using perovskite precursor containing a cation and anion mixture in a device stack of fluorine doped tin oxide (FTO)/compact SnO_2/C60/ perovskite/HTM/Ag. The devices with **3g** without methoxy groups demonstrated results that are more modest: the efficiency up to 10% was recorded. Respectable maximum power conversion efficiency of 14.6% under AM 1.5 G illumination was recorded in the best performing perovskite devices, containing **3h** as hole transporting material, indicating that the investigated TB-linked HTM can function effectively in PSC. An improved absolute PSC efficiency (by ~3.5%), compared with TB-based molecules investigated earlier, can be observed. The measured fill factor was 0.72, the current density (J_{sc}) 21.0 mA cm^{-2} and the open-circuit voltage (V_{oc}) 983 mV (Figure 3.28). Spiro-OMeTAD was used as a reference material and device from the same batch of solar cells, prepared following the same device fabrication procedure, but using Spiro-OMeTAD as hole-extracting layer displayed a PCE of 16.1%.

Compound **3l** have been device-tested as HTMs in the perovskite solar cells based on an optimized architecture of FTO/TiO_2 blocking layer/ mesoporous TiO_2 layer/ amorphous SnO_2 layer/ perovskite layer/ HTM/Au. Herein, the mixed perovskite films of $[(FAPbI_3)_{0.87}(MAPbBr_3)_{0.13}]_{0.92}(CsPbI_3)_{0.08}$ were used as a light harvester (Figure 3.29) [1].

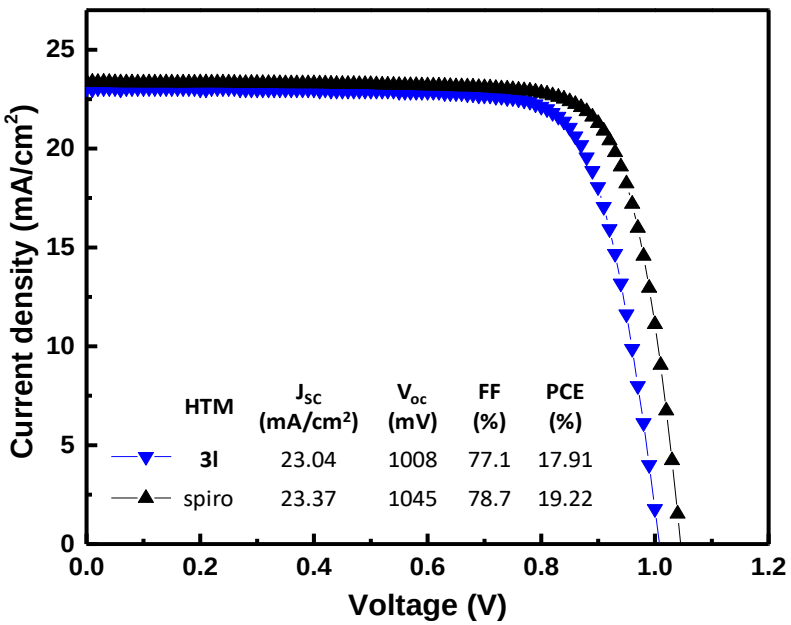

Figure 3.29. Best performing perovskite solar cell current density-voltage characteristics with **3l** and spiro-OMeTAD as hole transporting materials

[1]PSCs fabricated and tested in the Group for Molecular Engineering of Functional Materials, Institute of Chemical Sciences and Engineering, EPFL, by Prof. M. K. Nazeeruddin, R. Xia.

The devices with **3l** were performing really well: their maximum power conversion efficiency reaching 17.91% were achieved in the best performing perovskite devices, employing **3l** as HTM, comparable to that of spiro-OMeTAD (which has PCE of best performing device reaching 19.22%) that can be observed.

In conclusion, the concept of TPD-type moieties conjoined by a Tröger`s base core allowed to obtain solution processable HTMs with decent properties. TB core provides orientation for the TPD fragments angle-wise towards each other and hampers the crystallization processes rendering the investigated compound fully amorphous, while oriented *para*- substituted TPD-type moieties provide high charge mobility. These novel HTMs are promising candidates for the application in organic and hybrid optoelectronic devices, as they can be handled in the air, are amorphous, and require no high temperature annealing steps, have high glass transition temperatures, can be solution deposited. They as well possess high charge mobility (up to 0.036 $cm^2 V^{-1} s^{-1}$), thus exceeding that of the corresponding methyl and methoxy TPD analogues without TB core by more than two orders of magnitude. The preliminary testing in perovskite solar cells indicates that this class of TB-linked molecules can function effectively as HTM in the device. A noticeable improvement of mobility and PSC efficiency, compared with TB-based molecules that were investigated earlier and described in the previous chapter, indicates that the compounds with Tröger's base linking unit are a promising group of hole transporting materials, and with additional structural optimization, further improvements in device efficiency could be expected.

3.4. Hole transporting materials containing Tröger's base core and enamine–linked diphenyl branches

As hole transporting materials are an essential part of solar cell manufacturing, currently, they are a bottleneck for the realization of cost-effective and stable devices [194]. Despite significant efforts dedicated towards the development of new HTMs, the field is still dominated by costly small spiro-type molecules: spiro-OMeTAD, 2`,7`-bis(bis(4-methoxyphenyl)amino)spiro-[cyclopenta[2,1-b:3,4-b`]dithiophene-4,9`-fluorene] (FDT) and even more expensive macromolecule poly[bis(4-phenyl)(2,4,6-trimethylphenyl)amine] (PTAA) [137, 138, 195, 196]. The high cost of these HTMs is caused by expensive multi-step synthesis and costly purification procedures and is a limiting factor for their potential application in low-cost solar cells.

Simple synthesis and purification, as well as possibility to use cheap and accessible materials, makes compounds appealing for the commercial applications, and methods allowing that are highly sought after. One of such methods was reported, as new small-molecule enamine based hole conductor was prepared in one step without the use of expensive catalysts, column chromatography, or sublimation purification, resulting in material rivaling spiro-OMeTAD in properties and PSCs device performance [197]. In the reported case, a reaction of aldehyde and amino

group with CSA as a catalyst results in the formation of enamine and significant expansion of molecule's conjugated π-system by linking additional diphenylethenyl moieties in a single simple step. The reaction can be performed under ambient conditions, and water is the only by-product, making product purification uncomplicated [198].

Employing such reaction could allow linking primary amino substituents containing Tröger's base core with diphenylethenyl moieties, hence increasing both structural bulk and expanding conjugated π-system multiple times. The molecules that were obtained in this fashion structurally resemble compounds that have been already investigated in chapter 3.2, but unlike in the former case, the diphenylethenyl moieties are now connected directly to nitrogen without interlinking phenyl groups. Although losing a phenyl fragment in each branch partially lessens the conjugated π-system, the synthesis of these molecules no longer requires palladium catalysts and corresponding ligands, inert atmosphere conditions, and occurring crystallization of the product, and no palladium residue in the mixture allows easy separation of target compounds as no excessive purification through column chromatography is necessary.

This chapter is dedicated to the synthesis and investigation of V-shaped of Tröger's base derivatives with enamine-linked diphenyl branches. The presented results were published in a journal article as well [199].

3.4.1. Synthesis of novel Tröger's base compounds

Novel Tröger's base enamines N^2,N^2,N^8,N^8-tetrakis(2,2-diphenylethenyl)-4,10-dimethyl-6*H*,12*H*-5,11-methanodibenzo[*b*,*f*][1,5]diazocine-2,8-diamine (**4c**), N^2,N^2,N^8,N^8-tetrakis[2,2-bis(4-methylphenyl)ethenyl]-4,10-dimethyl-6*H*,12*H*-5,11-methanodibenzo[*b*,*f*][1,5]diazocine-2,8-diamine (**4d**), and N^2,N^2,N^8,N^8-tetrakis[2,2-bis(4-methoxyphenyl)ethenyl]-4,10-dimethyl-6*H*,12*H*-5,11-methanodibenzo[*b*,*f*][1,5]diazocine-2,8-diamine (**4e**) have been synthesized via intermediate TB derivatives **4a**–**b** (Scheme 3.5).

Initially, the nitro groups containing TB derivative **4a** were obtained from 2-methyl-4-nitroaniline and paraformaldehyde in trifluoroacetic acid. The reduction of nitro groups in compound **4a** followed as material was refluxed with iron powder that was suspended in a mixture of acetic acid and ethanol, affording diamino derivative **4b**. The synthesis of enamines **4c**–**e** was performed by the reaction of **4b** and the corresponding aldehyde (diphenyl-, bis(4-methylphenyl)-, or bis(4 methoxyphenyl)acetaldehyde) in THF at the reflux temperature in the presence of (+/-)-camphor-10-sulfonic acid (CSA).

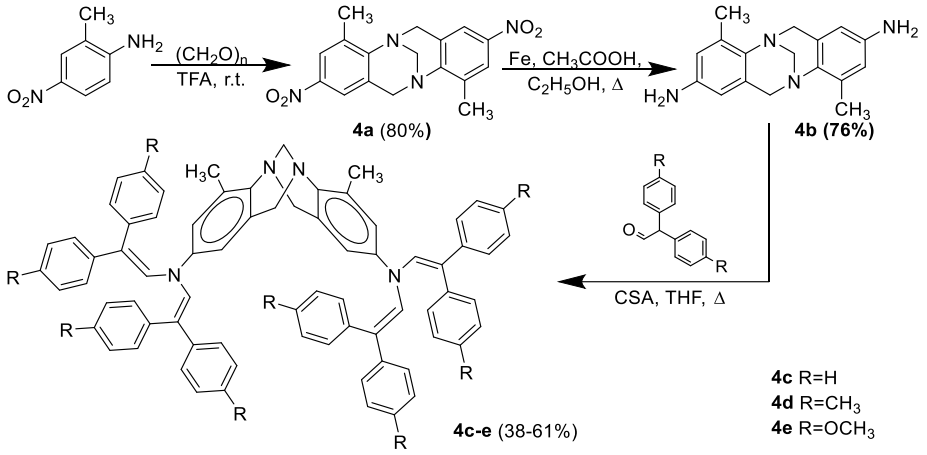

Scheme 3.5. Synthesis of Tröger's base compounds **4a–e**

^{1}H and ^{13}C NMR as well as elemental analysis data confirmed the structure of newly synthesized Tröger's base derivatives **4c**–**e**. The signal pattern of ^{1}H NMR spectrum in the region of 3.6–4.5 ppm is essential in identifying *methanodiazocine* bridge, proving the presence of the TB core. In ^{1}H NMR spectrum of compound **4d** (Figure 3.30), the bridging methylene protons (Ar-CH_2-N) show two doublets at 4.45 and 3.97 ppm, *exo* and *endo* hydrogens respectively, as these protons are magnetically nonequivalent due to the rigid structure of the TB. The singlet for the two protons of the other bridging methylene carbon (N-CH_2-N) is observed at 4.20 ppm. The singlet indicating CH-N protons of enamine groups is registered at 5.56 ppm. An interesting phenomenon is observed, as hydrogens of terminal methoxy groups have their proton signals split in two singlets at 3.67 and 3.81 ppm, indicating that due to molecular configuration, these protons become energetically unequal.

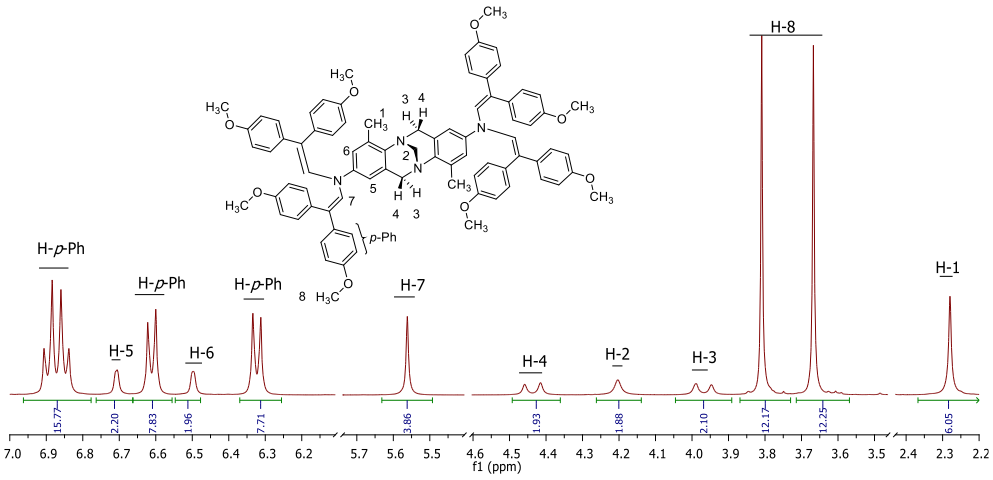

Figure 3.30. ^{1}H NMR spectrum (400MHz, $CDCl_3$) of compound **4e**

3.4.2. Thermal and optical properties

The DSC measurements of compounds **4c**–**e** were performed, and they reveal that the investigated compounds **4c** and **4e** exist both in crystalline and amorphous state (Table 3.8), as during the first heating, the melting of the crystals (T_m) was observed in compounds **4c** and **4e**. No melting in derivative **4d** was detected, but it might be due to narrower temperature interval, not exceeding 280 °C, as doing that could have potentially caused the decomposition of a compound (Figure 3.32, **4d**). No crystallization takes place during the cooling or second heating scans. Only glass transition (T_g) of compounds **4c**–**e** is registered during the second heating (Figure 3.31). The two states could be explained as crystallization is often observed in enamine compounds, and the amorphousness of compound is influenced by non-planar structure of TB core and structural bulk that is added by diphenylethenyl moieties. Compound **4d** is amorphous, likely due to eight substituting methyl groups attached to each of terminal phenyl, which influence the molecular packing, but unlike in the case of methoxy substituents, they do not induce hydrogen bonding and additional intermolecular interactions.

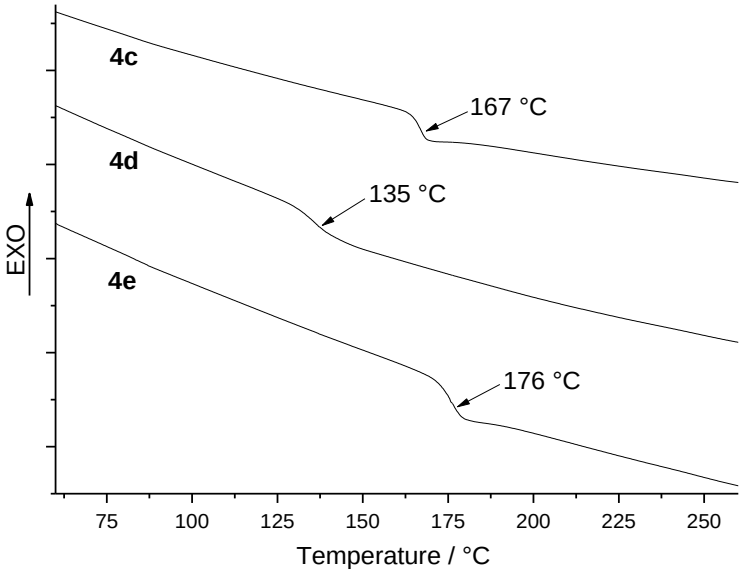

Figure 3.31. DSC curves of **4c**–**d** indicating T_g. Heating rate 10 K/min; second run

The thermogravimetric analysis of **4c**–**e** reveals high decomposition temperatures (Figure 3.32, Table 3.8) suggesting good or very good thermal stability of the investigated compounds.

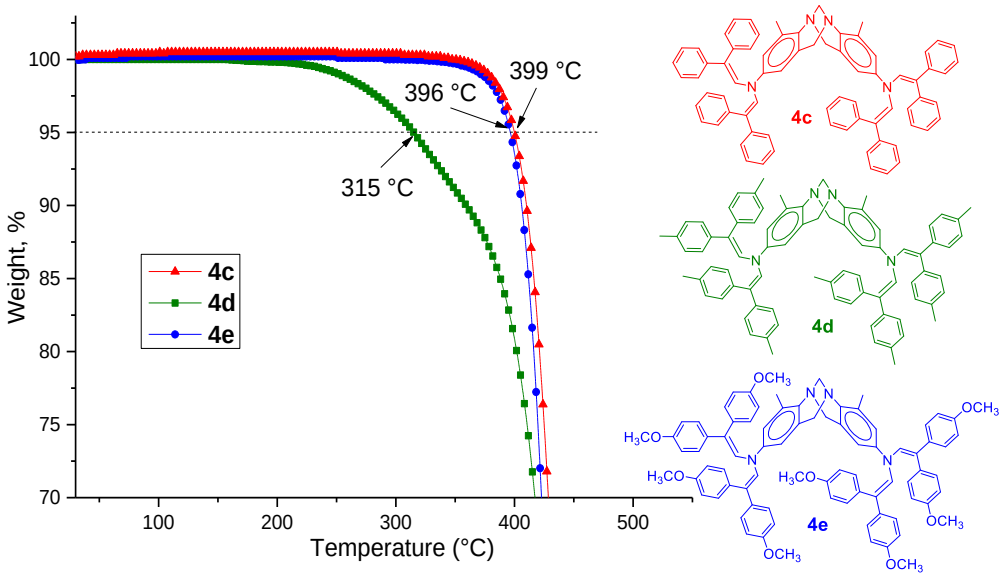

Figure 3.32. TGA curves for compounds **4c–e**

Table 3.8. Thermal and optical properties of TB derivatives

Compound	T_m [°C] [a]	T_g [°C] [b]	T_{dec} [°C] [c]	λ_{max}^{abs} [nm] [d]	ε [$M^{-1}cm^{-1}$]
4b				220; 252	25990;13834
4c	363	167	399	341	529280
4d	-	135	315	342	54850
4e	229	176	396	261; 343	69145; 55918

[a] Melting point was only detected during the first heating 10 K/min. [b] Determined by DSC: scan rate, 10 K/min; N_2 atmosphere; second run. [c] Onset of decomposition determined by TGA: heating rate, 10 K/min; N_2 atmosphere. [d] UV-Vis spectra were measured in 10^{-4} M THF solution.

The UV-VIS absorption bands of the compounds **4c**–**e**, measured in tetrahydrofuran solutions (c=10^{-4}mol/l, d=1mm) (Figure 3.33), indicate tremendous bathochromic and hyperchromic shifts when compared to starting diamino compound **4b**. Such difference in absorption accurately represents the expansion of the π-conjugated system that is achieved by enamine linking of diphenylethenyl branches. The differences between compounds **4c**–**e** are as well noticeable: even though aromatic part of the molecule is the same in all of them, *p*- substituents of terminal phenyl groups in **4c**, **4d**, and **4e** (none, methyl, and methoxy, respectively) cause slight bathochromic (~1nm difference) and hyperchromic shifts. The case of **4e** is especially interesting, as the absorption intensity in the range of 240–290 nm is increased, having maximum value at 261 nm that could correspond to n-σ* electron transitions in the proximity of oxygen atoms in methoxy substituents.

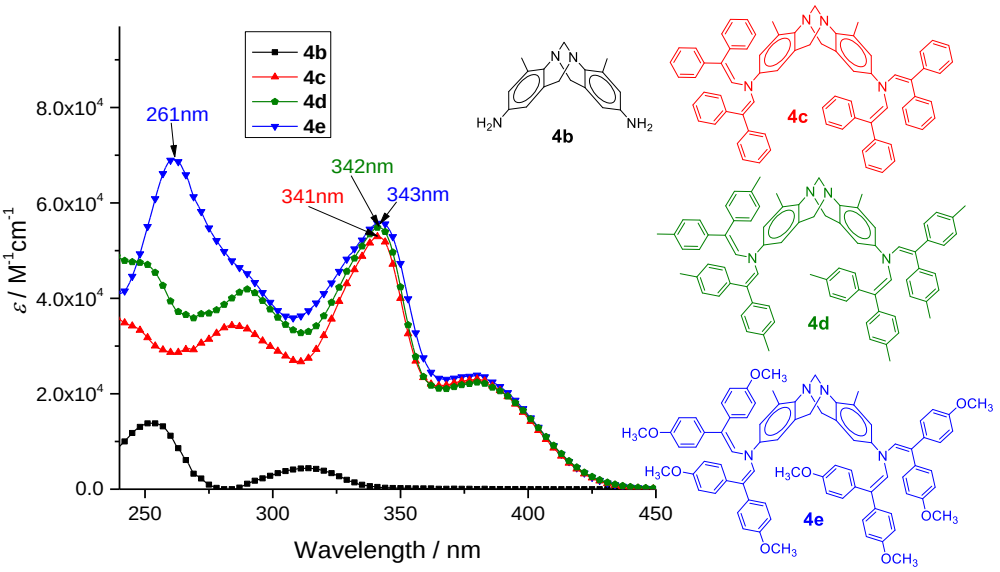

Figure 3.33. Absorption spectra of 1×10^{-4} M THF solutions of compounds **4b**–**e**

3.4.3. Photoelectrical properties

The ionization potential of compounds **4c**–**e** was measured by the PESA method (Figure 3.34, Table 3.9) [1]. The ionization potential of compound **4c** reaches value 5.54 eV, making its potential application in solar cells hardly possible. Electron donating methyl and methoxy groups attached to terminal phenyl groups lowers I_p by 0.1 eV and 0.29 eV, respectively resulting in 5.44 eV for **4d** and 5.25 eV for **4e**. Compound **4e** is particularly most promising for solar cell applications as its ionization potential makes it compatible with most of the materials that are used in this field.

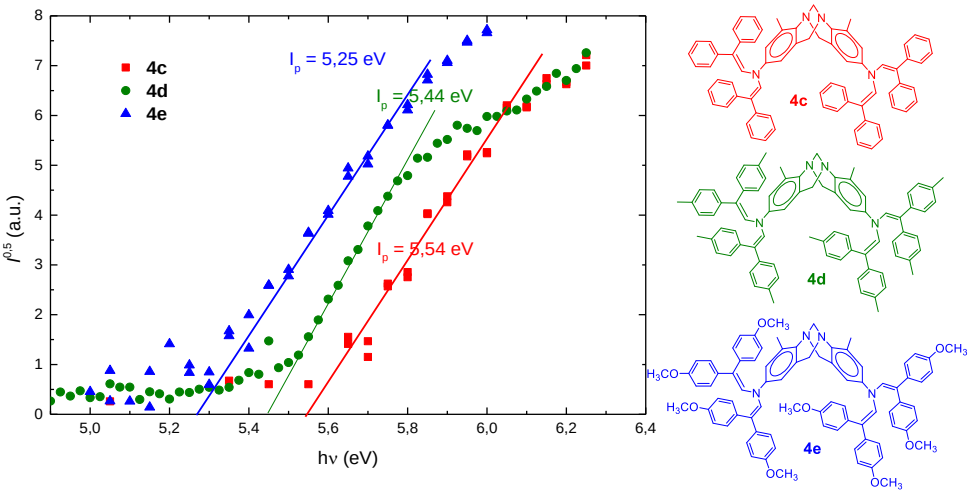

Figure 3.34. Photoemission in air spectra of Tröger's base derivatives **4c**–**e**

[1] Measurements of ionization potential were performed at the Department of Solid State Electronics, Vilnius University, by Dr. V. Jankauskas, E. Kamarauskas.

Table 3.9. Energy level and hole mobility data for compounds **4c**–**e**

Compound	E_g^{opt} (eV) [b]	E_{HOMO} (eV)[c]	E_{LUMO} (eV)[d]	I_p (eV) [e]	μ_0, cm²/Vs [f]	μ (6.4×10^5 V/cm), cm²/Vs [g]
4c	2.80	4.98	2.18	5.54	-[h]	-[h]
4d	2.80	4.84	2.04	5.44	$4\cdot10^{-6}$ [i]	$1.5\cdot10^{-5}$ [i], ~10^{-3} [h], [j]
4e	2.80	4.87	2.07	5.25	$2.1\cdot10^{-4}$	$3.35\cdot10^{-4}$

[a] The CV measurements were carried out at a glassy carbon electrode in dichloromethane solutions containing 0.1 M tetrabutylammonium hexafluorophosphate as an electrolyte and Pt wire as the reference electrode. Each measurement was calibrated with ferrocene (Fc). Potentials measured vs Fc^+/Fc. [b] The optical band gaps E_g^{opt} estimated from the edges of electronic absorption spectra in solution. [c] Conversion factors: ferrocene in DCM vs SCE 0.46[162], SCE vs SHE: 0.244[163], SHE vs. vacuum: 4.43[164]. [d] E_{LUMO} calculated from the equation $E_{LUMO} = E_{HOMO} - E_g^{otp}$. [e] Solid state ionization potential (I_p) was measured by the photoemission in the air method from films. [f] Mobility value at zero field strength. [g] Mobility value at 6.4×10^5 V cm^{-1} field strength. [h] No layer suitable for the measurements was obtained. [i] **4d** mobility values were measured from the mixture of compound **4d** and PC-Z (1:1). [j] Integral method was used to obtain results.

The charge transport properties of compounds **4c**–**e** were measured by the XTOF technique (Figure 3.35) [1]. The values of charge mobility defining parameters: zero field mobility (μ_0), and the mobility at the electric field of 6.4×10^5 V cm^{-1} for the compounds **4c**–**e** are given in the Table 3.9. Poor quality neat films of **4c** and **4d** were obtained; therefore, a mixture of compound and polycarbonate (PC-Z) in weight ratio 1:1 was used in order to obtain uniform layers. Even so, the quality of the layer with **4c** was not sufficient to obtain results. The absolute mobility results for such composite layer of **4d** are lower than that of neat material layer due to the presence of nonconductive polymer.

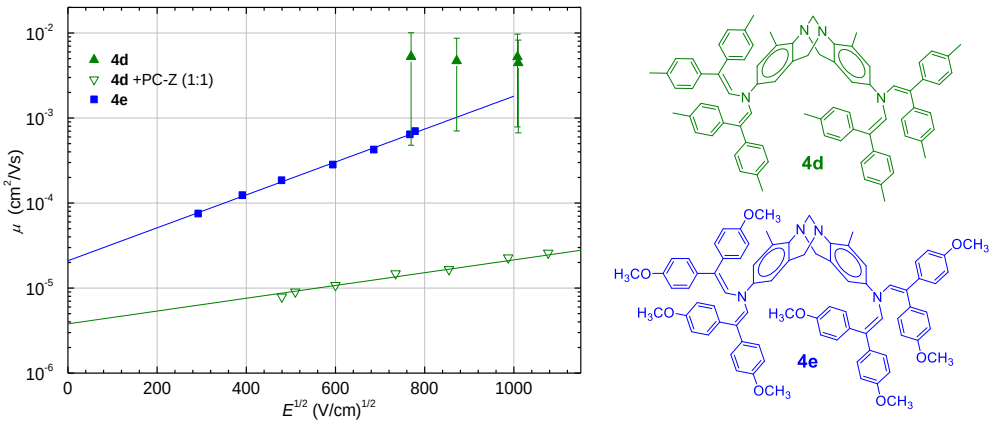

Figure 3.35. Electric field dependencies of the hole drift mobilities (μ) in the charge-transport layers of Tröger's base derivatives **4d**–**e**. Mobility values of **4d** were measured from the mixture of compound **4c** and PC-Z (1:1)

[1] Charge mobility measurements were performed at the Department of Solid State Electronics, Vilnius University, by Dr. V. Jankauskas, E. Kamarauskas.

Some results measured from the layer of neat **4d** show decent results, outmatching the ones of **4e**, but they are not very reliable due to poor layer and used integral method to determine results, which as well does not allow determining zero field mobility. The hole-drift mobility of the TB derivative **4e** is $3.35 \cdot 10^{-4}$ $cm^2 V^{-1} s^{-1}$ at strong electric fields. This result is sufficient for the application in solar cells as hole conductor and comparable to some reported HTMs that are used for this purpose. Even not that accurate, the measurement of neat **4d** show even better results, making it a promising candidate.

3.4.4. Testing compounds in perovskite solar cells

Although compound **4c** may have its ionization potential too high to find its use in conventional perovskite solar cells[1] and its charge mobility was not determined, compounds **4d** and especially **4e** looks promising for this feat. For the investigation and comparison, all three compounds have been device-tested as HTMs in the perovskite solar cells based on an optimized architecture of FTO, TiO_2 blocking layer, mesoporous TiO_2 layer, amorphous SnO_2 layer, perovskite layer, HTM, and Au. Herein, the mixed perovskite films of $[(FAPbI_3)_{0.87}(MAPbBr_3)_{0.13}]_{0.92}(CsPbI_3)_{0.08}$ are used as light harvester. As it was expected, the devices with **4e** were the best performing ones among the three, their power conversion efficiency reaching 18.62%.

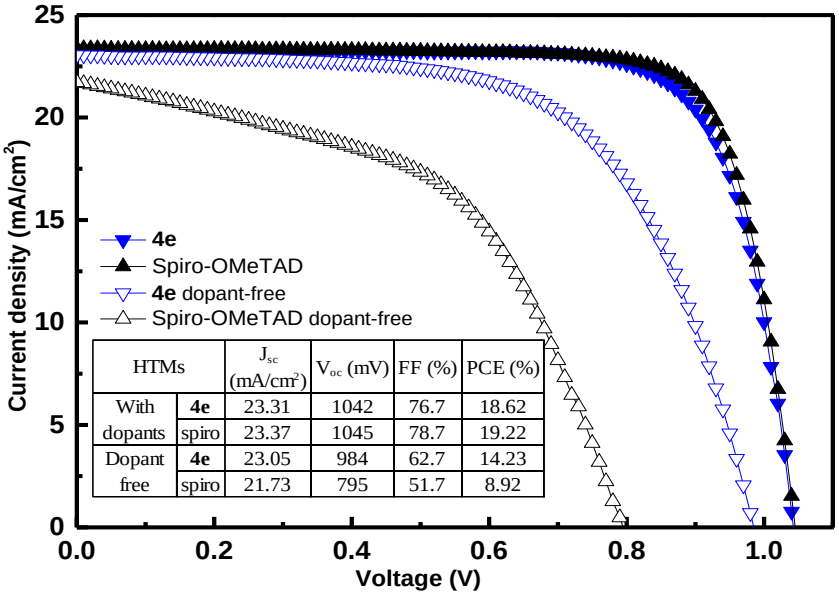

HTMs		J_{sc} (mA/cm²)	V_{oc} (mV)	FF (%)	PCE (%)
With dopants	**4e**	23.31	1042	76.7	18.62
	spiro	23.37	1045	78.7	19.22
Dopant free	**4e**	23.05	984	62.7	14.23
	spiro	21.73	795	51.7	8.92

Figure 3.36. Best performing perovskite solar cell current density-voltage characteristics with **4e** and spiro-OMeTAD as hole transporting materials

[1]PSCs fabricated and tested in Group for Molecular Engineering of Functional Materials, Institute of Chemical Sciences and Engineering, EPFL by Prof. M. K. Nazeeruddin, R. Xia.

Notably, the cells containing **4c** and **4e** performed considerably better than spiro-OMeTAD when they were used in PSCs of a dopant-free composition, showing enhanced short-circuit current generation (J_{sc}) and fill factor (FF). With dopants added, the devices based on **4c** and **4d** demonstrated comparatively lower results than spiro-OMeTAD, their PCE reaching 13.27% and 9.60%, respectively. Despite that, the maximum power conversion efficiency of 18.62% was achieved in the best performing perovskite devices employing **4e** as HTM, comparable to that of spiro-OMeTAD reaching 19.22% in champion-device (Figure 3.36), while the average PCE values 18.14% in **4e** devices are compared to 18.88% in spiro-OMeTAD devices.

The device stability test of the most efficient PSCs with **4e** and spiro-OMeTAD was performed. The devices were stored in the air with a relative humidity of ~50% (cells non-encapsulated) and regularly measured under 100 mW/cm^2 simulated sun irradiation (1.5 AM). The results of this test demonstrated enhanced PCE for both systems after the first 100 hours, but a remarkable difference after long-time periods. Interestingly, the efficiency of **4e** devices maintained >90% of the initial efficiency after 700 hours, while that of spiro-OMeTAD dropped to 65%.

In conclusion, the molecular concept of enamine-linked Tröger's base derivatives proven to be efficient and allowed to easily obtain stable HTMs with desirable properties, suitable for the optoelectronic applications. The testing in PSCs demonstrated that the devices with **4e** have high device efficiency (18.62% PCE), rivaling spiro-OMeTAD, and superior device stability, proving its suitability. Despite their lower efficiency in PSCs, compounds **4c** and **4d** can potentially find their use in other optoelectronic applications due to their decent properties and convenient synthesis.

3.5. Sensitizers for dye-sensitized solar cell based on Tröger's base scaffold

Among the emerging photovoltaic technologies, dye-sensitized solar cells (DSSCs) have attracted significant attention as one of the promising energy harvesting devices, since the report of Ru-based photosensitizers [200, 201]. After two decades of research and development, DSSCs with iodide/triiodide (I^-/I_3^-) liquid electrolyte have achieved record power conversion efficiency (PCE) over 13% based on Zn-porphyrin complex dyes [202, 203]. Compared with them, metal-free organic dyes have such advantages as relatively lower production cost, facile synthetic methodologies, and high molar extinction coefficient [204–206]. An impressive cell efficiency of 12.5% achieved by a novel metal-free alkoxysilyl carbazole dye ADEKA-1 demonstrated that metal-free dyes could be promising sensitizers for realizing highly efficient DSSCs [207]. Towards the realization of higher photovoltaic performance and durability in DSSCs, the development of the sensitizing dyes is one of the most important approaches.

It is well known that the most of the excellent sensitizers have the donor-π-acceptor (D-π-A) structures that facilitate effective photoinduced intramolecular charge transfer across the molecule [208–210]. However, the single 1D-π-1A sensitizer often has a rod-shaped structure, which may cause undesirable dye

aggregation and charge recombination [211]. In order to enhance the photovoltaic performance in DSSCs, considerable efforts have been devoted to optimize the structure of the organic dyes, such as increasing the amount of anchoring groups and/or extending π-conjugation to increase the molar extinction coefficient of the absorption band, which can improve the light harvesting ability of the dyes [204, 212]. The dye containing double/multiple anchor groups exhibited a unique advantage of stronger bonding with the TiO_2 surface. Strong binding improves adsorption and leads to red shift in absorption, efficient charge injection [204, 213], and photocurrent generation [204, 214].

Seeking to synthesize an efficient dye, the choosing of a proper anchoring group moiety is particularly important. In recent years, the importance of anchoring groups for photovoltaic applications was investigated by several research groups. Jia and Zheng reported that the PCE of the DSSC based on Y-shaped D-π-$(A)_2$ type phenthiozine dye ZJA2 (4.55%) was 67% higher than the DSSC based on single 1D-π-1A sensitizer ZJA1 (2.72%) [211]. The designed DSSCs of Abbotto et al. yielded power conversion efficiency up to 5.7% (4.9% with ionic liquid electrolyte) with increased photocurrent and enhanced stability under 1 sun conditions caused by the di-anchoring groups [215]. Sirohi and Lee concluded that the di-anchoring moiety in dye KS-5 caused strong binding to TiO_2, which forced the dye molecule to assume a non-planar conformation, thereby minimizing aggregation [216]. This factor together with an extended conjugated framework led to about 1.5 times higher efficiency of KS-5 compared to parent dye L1. Recently, Cao et al., reported that the novel metal-free organic dye is bearing two symmetric double donor-acceptor segments with an impressive power conversion efficiency, which is 22% higher than that of the mono-anchoring dye based counterpart [204].

One quite recent publication [217] reports a novel A-π-D-π-A metal-free organic dye with two anchoring groups for solid state DSSC (ssDSSC) with spiro-OMeTAD as HTM. As it was expected, this dye demonstrated the highest extinction coefficient of all the investigated D-π-A hydrazone dyes in that study, mostly due to the presence of two electron accepting units and larger change in the electronic charge distribution that is occurring during excitation. The device based on this material had the strongest and widest light absorbance from the whole series. However, the external quantum efficiency and ssDSSC performance decreased by more than 50% compared with analogues sensitizers, possessing one anchoring group. It was concluded that the D-(π-$A)_2$ molecule has a rod-shaped structure, which might cause undesirable dye aggregation that is promoted by carboxylic acid moieties not attached to the TiO_2 surface. The unbound anchoring group that is oriented by rod-shaped molecule could serve as a charge recombination in site between the HTM and dye layers, reducing the performance on the ssDSSC cell. The solution to this problem could be found by designing a molecule with an angular core fragment, preventing rod-shaped configuration, and Tröger's base offer such a structural feature.

This chapter is dedicated to the design and synthesis of Tröger's base scaffold-based metal-free sensitizers **5A**–**C** (Figure 3.37) with a triphenylamine donor group and rhodanine-3-acetic acid unit as the acceptor/anchoring group to investigate their

di-anchoring effect in DSSCs. The TB structure allows it to be used as a core and provide an angle (~ 90º) orientation for the conjugated π-systems conjoined by it [7, 218]. The non-planar structure of the TB and presence of two carboxyl groups should ensure two separate channels for charge transfer to TiO_2 and increase in the overall device efficiency. Dyes analogues **5D**–**F** (Figure 3.37) with one anchoring group were synthesized for comparison. These sensitizer series were as well designed to investigate the influence of the poly[n]enic (from n = 0 to 2) backbones and their anchoring effect in DSSCs.

The results are presented in this dissertation chapter and published in a journal article [219].

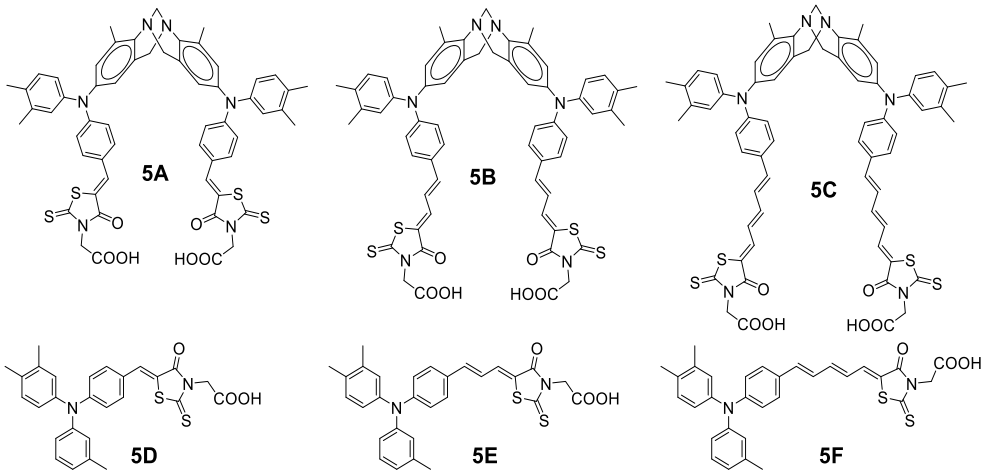

Figure 3.37. Molecular structures of investigated dyes **5A**–**F**

3.5.1. Synthesis of novel Tröger's base scaffold based dyes

The new metal-free di-anchoring organic dyes based on TB scaffold **5A**, **5B,** and **5C** were synthesized according to a six-step reaction as described in Scheme 3.6. Initially, Horner-Wittig condensation was made to increase the polyenic chain (from n = 0 to 2). The yield of 70–80% was achieved by palladium-catalyzed cross-coupling reaction between protected aldehydes **5c**, **5d**, and 3,4-dimethylaniline. The obtained corresponding diphenylamines **5e**, **5f**, and **5g** underwent reaction with 2,8-dibromo-4,10-dimethyl-6*H*,12*H*-5,11-methanodibenzo[*b*,*f*][1,5]diazocine (brominated Tröger's base derivative) [40] in the presence of palladium(II) acetate, tri-*tert*-butylphosphonium tetrafluoroborate, and sodium *tert*-butoxide to provide intermediates based on TB scaffold **5h**, **5i**, and **5j**. After the deprotection, the obtained penultimate dialdehydes **5k**–**m** were a common synthon, which were condensed with rhodanine-3-acetic acid to give sensitizers **5A**, **5B**, and **5C**.

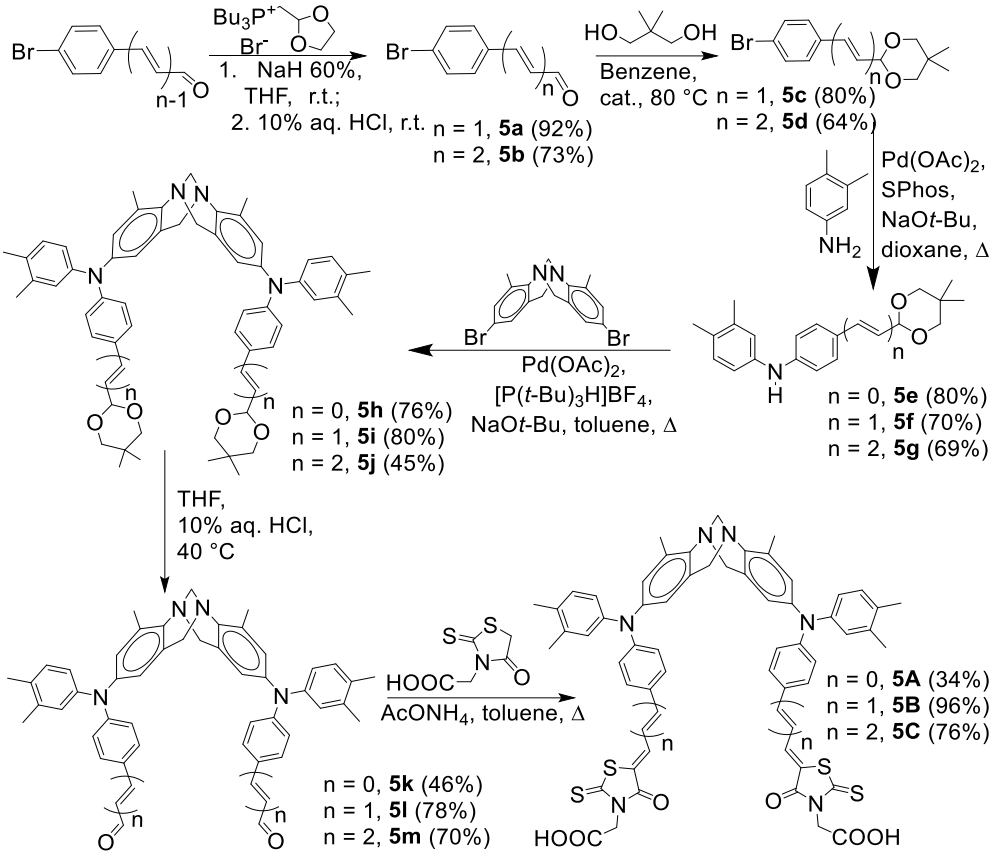

Scheme 3.6. Synthesis of di-anchoring dyes based on TB scaffold **5A**–**C**

These new dyes were prepared in moderate to high yields, and their chemical structures were confirmed by ^{1}H and ^{13}C NMR spectroscopy.

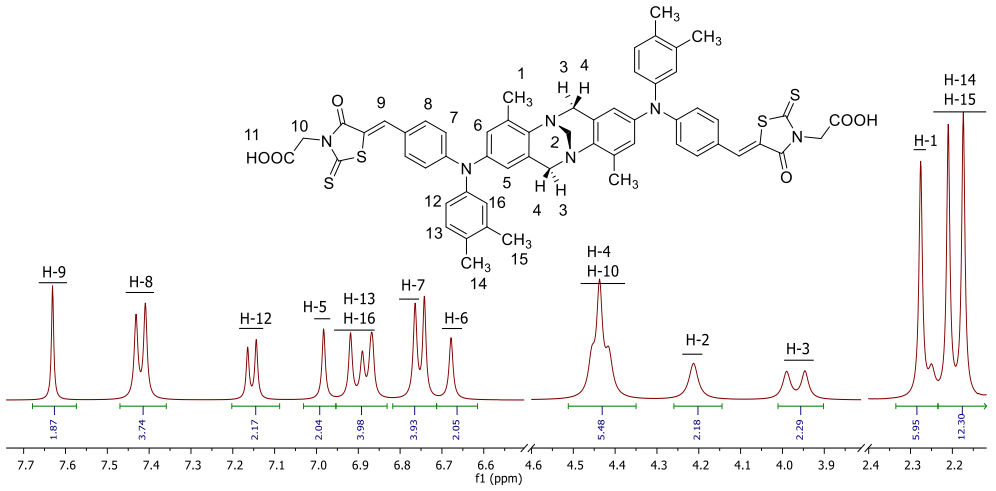

Figure 3.38. ^{1}H NMR spectrum (400MHz, $(CD_3)_2SO$) of compound **5A**

The pattern of signals in the interval of 3.75–4.50 ppm in the ^{1}H NMR spectrum is essential for proving the presence of the TB core. Each ^{1}H NMR spectrum of **5A**–**C** shows two doublets near each margin of the mentioned interval, and these two doublets that signify the *endo/exo* protons in bridging methylene part (Ar-CH_2-N) are magnetically nonequivalent due to the rigid structure of the TB. For example, in ^{1}H NMR spectrum of compound **5A** (Figure 3.38), the bridging methylene protons (Ar-CH_2-N) show two doublets at 4.44 and 3.97 ppm, *exo* and *endo* hydrogens respectively, but in this case, *exo* doublet overlaps with a signal of protons in H-10 position. As a contrasting example of this, the signals of two protons of the other bridging methylene carbon (N-CH_2-N) can be observed as a singlet at *ca.* 4.20 ppm in this spectrum.

Dyes **5D**, **5E,** and **5F** (Figure 3.37) that are possessing one anchoring group were synthesized for comparison. Firstly, compound **5n** was prepared according to the reported procedure [220]. Then, the diphenylamine bearing the protected aldehyde group has been synthesized and equipped with 3-iodotoluene by using the palladium-catalyzed Buchwald-Hartwig C–N cross-coupling reactions to form the intermediate aldehyde **5o**. The Knoevenagel condensation of the obtained aldehyde with rhodanine-3-acetic acid in glacial acetic acid gave dye **5D**. In parallel, Horner-Wittig condensation of aldehyde **5o** with 1.1 equivalents of tributyl(1,3-dioxalan-2-ylmethyl)phosphonium bromide gave aldehyde **5p** in 78% yield. Another vinylogation and subsequent Knoevenagel condensation produced dyes **5E** and **5F** (Scheme 3.7).

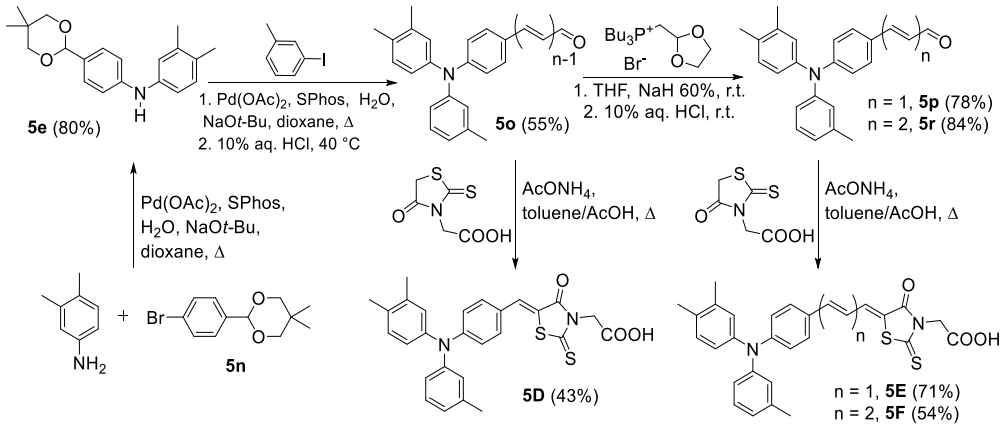

Scheme 3.7. Synthesis of mono-anchoring dyes **5D**–**F**

3.5.2. Optical properties

In order to gain an insight about the impact of the number of polymethine chains and chain length on the optical properties of investigated dyes, UV-vis and FL studies were performed with di-anchoring dyes **5A–C** and their mono-anchoring analogues **5D**–**3F**.

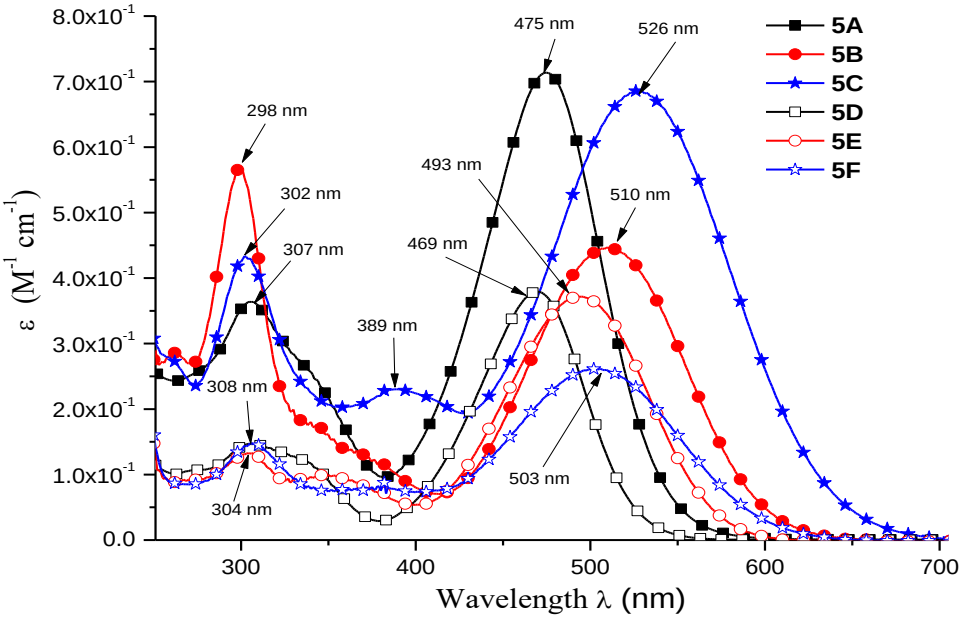

Figure 3.39. UV-vis spectra of the investigated dyes **5A**–**F** in DMSO solutions (c = 10^{-4} M)

As shown in Figure 3.39, the absorption spectra of both, di-anchoring organic dyes based on TB scaffold **5A**, **5B**, **5C**, and mono-anchoring dyes **5D–F** display two distinct absorption bands at around 270–350 nm and 400–670 nm, respectively. The absorption bands in the UV region show peaks at longer wavelengths that correspond to the π–π* electron transitions of the conjugate system. Interestingly, the sensitizers **5C** and its mono analogue **5F** exhibit weak but clear additional absorption band at around 380 nm. This is a consequence of largest extended conjugation that was made possible by two additional methine units in the present series of dyes. The strong absorption bands in the visible region can be assigned to an intramolecular charge transfer (ICT) between the triphenylamine-based donor and the electron accepting rhodanine-3-acetic acid moiety, providing efficient charge separation in the excited state. The comparison of the absorption spectra of π-extended dyes **5B**, **5C** and **5E**, **5F** with those of their lower homologues **5A** and **5D**, clearly demonstrates that the extension of the polymethine chain results in 10–35 nm bathochromic shift of the absorption band compared to that of the lower homologues. Next, the comparison of the optical properties of di-anchoring dyes **5A–C** with those of their mono-anchoring analogues **5D–F** clearly demonstrates two effects. First, the organic dyes based on TB scaffold, with the exception of **5B**, exhibit approximately twice higher extinction coefficients (Table 3.10) compared to those of the references mono-anchoring dyes. The molar extinction coefficient of the charge transfer transition in these dyes indicates a good ability for light harvesting. Second, only a negligible bathochromic shift (6 nm) was observed for the di-anchoring dye **5A** in comparison with mono-anchoring sensitizer **5D**. This indicates that there is no interaction at the ground state between the two chromophores in this di-anchoring dye. However, the comparison of

the ICT absorption bands of **5B** and **5C** with references **5E** and **5F** clearly indicates this interaction. Probably, this is a consequence of the extended polymethine chains that should ensure flexibility of these units and inspire the interaction between two chromophores in TB-based dyes.

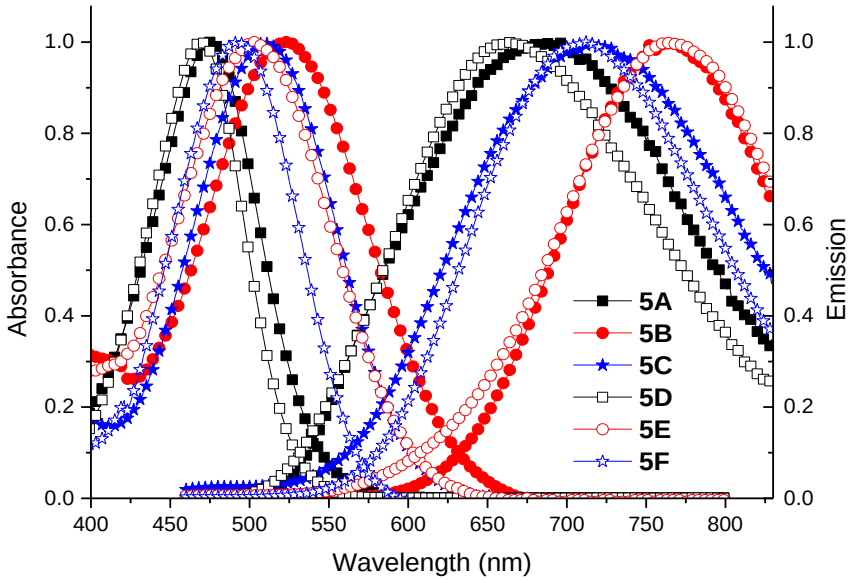

Figure 3.40. Emission and absorption spectra of the dyes **5A**–**F** in DMSO solution

Figure 3.40 shows the emission and absorption spectra in the visible region of the dyes in DMSO solution. The excitation wavelength for emission was the maximum absorption in the visible region. It can be seen that the maximum emission wavelengths in DMSO solution follow the order **5D** < **5E** < **5F** and **5A** < **5B** < **5C**. In addition, relatively large Stokes shifts of designing molecules were observed between the absorption and emission spectral maxima. Moreover, the Stokes shifts were calculated to lie within the range of 193–276 nm, meaning an enhanced geometrical difference between the ground and excited state geometry and thus a good molecular flexibility of the excited state (Table 3.10). The Stokes shifts follow the trend **5C** > **5B** > **5A** and **5F** > **5E** > **5D**. In this respect, it is easy to postulate that the largest Stokes shifts found in **5C** and its mono-analogue **5F** are due to their hexadiene moieties between donor and acceptor that confirms a great flexibility of these dyes.

The absorption maxima of the investigated dyes on the TiO_2 layer are broader and slightly blue shifted compared to the results obtained in DMSO solutions, indicating that the energy levels of the sensitizer molecules have somewhat changed due to the interaction with TiO_2 (Figure 3.41, Table 3.10). Upon increasing the number of double bonds from n = 0 to 2, progressive blue shifts are observed for each additional methine unit, leading to the biggest shift of 30 nm for the V-shaped dye **5C** (from 526 to 496 nm) and 14 nm for its reference rod-shaped dye **5F** (from 503 to 489 nm). It shows that H-aggregates form on the TiO_2 surface. The absorption spectrum

of mono-anchoring dye **5D** (n = 0) on TiO_2 film shows no difference in comparison with that in DMSO solution, implying that there are no evident aggregations. It can be attributed to the size of the molecule. This phenomenon indicates that **5D** may show the highest open-circuit photovoltage value among these six dyes, which is in favor of a better photovoltaic performance.

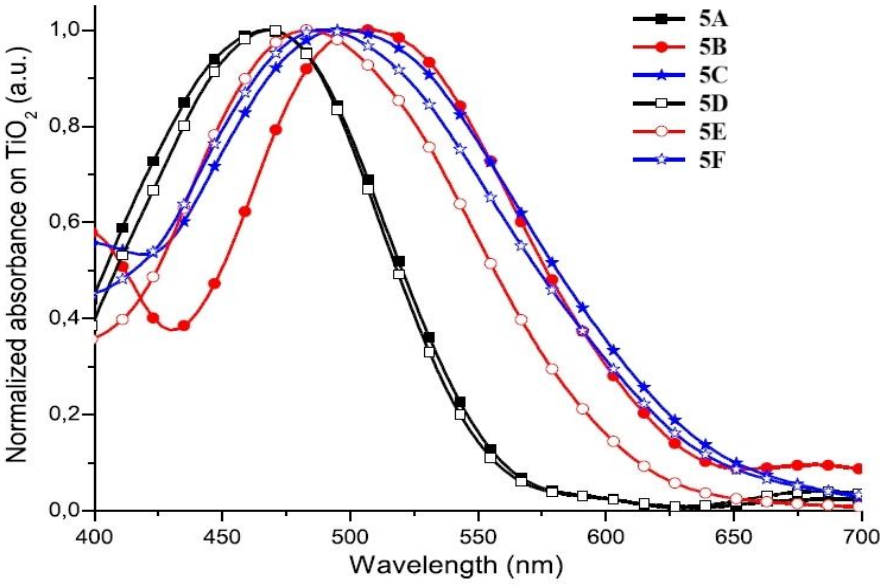

Figure 3.41. Normalized absorption of dyes **5A**–**F** anchored on TiO_2 film

Table 3.10 Optical properties of dyes **3A**–**F**

Dye	λ_{abs}^{sol} (nm) [a]	ε (M^{-1} cm^{-1})	λ_{max} on TiO_2 (nm)	λ_{em} (nm)[a]	Stokes shift[b] (nm)	λ_{int} (nm)[c]
5A	307, 475	36 382, 71 369	468	694	219	528
5B	298, 510	56 510, 44 680	506	712	202	555
5C	302, 389, 526	43 360, 23 040, 68 550	496	786	263	626
5D	307, 469	14 679, 37 956	469	679	208	520
5E	304, 493	13 270, 37 190	483	724	231	559
5F	308, 503	14 740, 26 190	489	789	286	610

[a]Absorption spectra were measured in DMSO solution. [b]Stokes shift = $\lambda_{em(solution)} - \lambda_{abs(solution)}$. [c]λ intersection obtained from the cross point of normalized absorption and emission spectra in DMSO solution.

3.5.3. Photoelectrical properties

In order to evaluate the thermodynamic allowed electron transfer processes from the excited dye molecule to the conduction band of TiO_2, cyclic voltammetry (CV) measurements were performed (Table 3.11, Figure 3.42). The cyclic voltammograms of all synthesized compounds show quasi-reversible oxidation and reduction couples. The zero-zero excitation energy ($E_{0\text{-}0}$) values were estimated from the cross-point of the normalized UV absorption and photoluminescence spectra [204]. Adding an additional electron-accepting group in **5A**, **5B**, and **5C** decreases the LUMO level by 0.09, 0.34, and 0.18 eV respectively, in comparison with their mono analogues **5D**, **5E**, and **5F**. The LUMO energy levels for the dyes lie above the conduction band edge of TiO_2 (-4.0 eV) [159, 221], ensuring favorable electron injection from the excited state of the sensitizers to the conduction band of the semiconductor. The HOMO levels of V-shaped dyes **5A**, **5B**, and **5C** (-5.62, -5.58, and -5.51 eV) are more positive than that of their counterparts **5D** (-5.70 eV), **5E** (-5.64 eV), and **5F** (-5.59 eV). Apparently, the HOMO levels of all dyes were more negative than the iodide/triiodide potential (-4.97 eV; -0.54 V *vs* SHE) [222], which implied that the thermodynamic driving force for the regeneration of the oxidized dyes is sufficient.

When considering the use of an organic material for optoelectronic applications, it is important to have an understanding of its solid-state ionization potential. This understanding can help in identifying suitable organic transport and inorganic electrode materials. The ionization potential (I_p) was measured by the electron photoemission in the air method (Figure 3.43)[1], and the results are presented in Table 3.11; the measurement error is evaluated as ±0.03 eV.

Table 3.11 Photoelectrical properties of dyes

Dye	$E_{0\text{-}0}$ (eV) [b]	$E_g^{opt\text{-}film}$ (eV) [c]	E_{HOMO} (eV)[a]	E_{LUMO} (eV) [a]	I_p (eV) [d]	EA (eV) [e]
5A	2.35	2.07	-5.62	-3.36	5.48	-3.41
5B	2.23	1.80	-5.58	-3.76	5.54	-3.74
5C	1.98	1.68	-5.51	-3.65	5.45	-3.77
5D	2.38	2.07	-5.70	-3.27	5.43	-3.36
5E	2.22	1.84	-5.64	-3.42	5.38	-3.54
5F	2.03	1.73	-5.59	-3.47	5.45	-3.72

The CV measurements were carried out at a glassy carbon electrode in tetrahydrofuran solutions containing 0.1 M tetrabutylammonium hexafluorophosphate as an electrolyte and $Ag/AgNO_3$ as the reference electrode. Each measurement was calibrated with ferrocene (Fc). Potentials measured vs Fc+/Fc. [a] Conversion factors: ferrocene in THF vs SCE 0.56 [162], SCE vs SHE: 0.244 [163], SHE vs. vacuum: 4.43 [164]. [b] $E_{0\text{-}0} = 1240/\lambda$ intersection. [c] Optical band gap ($E_g^{opt\text{-}film}$) estimated from the edge of electronic absorption spectra from thin film. [d] Ionization potential (I_p) was measured by the photoemission in the air method from films. [e] Electron affinity (EA) calculated from the equation $EA = I_p - E_g^{opt\text{-}film}$.

[1] Measurements of ionization potential were performed at the Department of Solid State Electronics, Vilnius University, by Dr. V. Jankauskas, E. Kamarauskas.

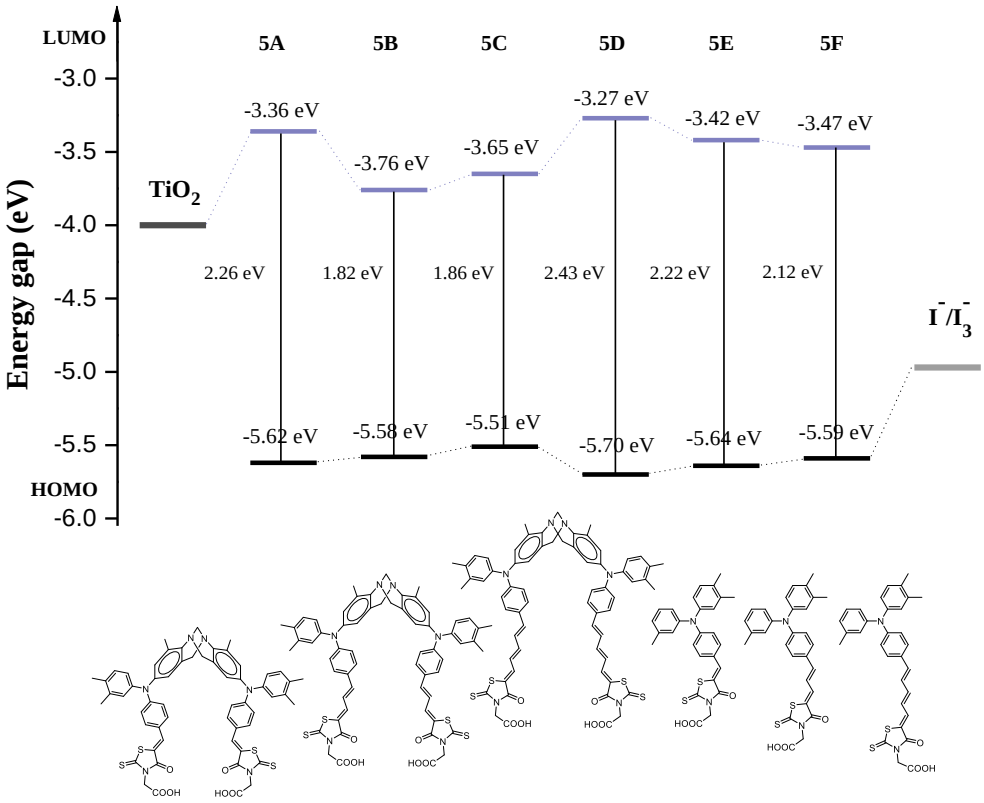

Figure 3.42. Schematic energy level diagram for a DSSC based on dyes attached to a nanocrystalline TiO_2 film deposited on conducting FTO glass

In general, I_p measurements indicate that all investigated sensitizers have very similar energy levels that are in the range of 5.38–5.54 eV. From the data presented in Table 3.11 and Figure 3.43, it can be stated that I_p values of the dyes **5A** and **5C** based on TB scaffold and possessing di-anchoring system are the same or really close to their rod-shaped mono-analogues **5D** and **5F**. The ionization potential of **5B** was determined to be 5.54 eV. It has the highest I_p value of all investigated dyes and the biggest difference of 0.16 eV with his mono counterpart **5E** (5.38 eV). The measured I_p values are slightly lower than the HOMO levels found in the CV experiments. The difference may result from different measurement techniques and conditions (solution in CV and a solid film in the photoemission method). From the ionization potential and optical band gap ($E_g^{opt\text{-}film}$) estimated from the edge of electronic absorption spectra from the thin films, the electron affinity (EA) was calculated (Table 3.11). The expansion of the methine component contributes to the higher EA value of the investigated dyes.

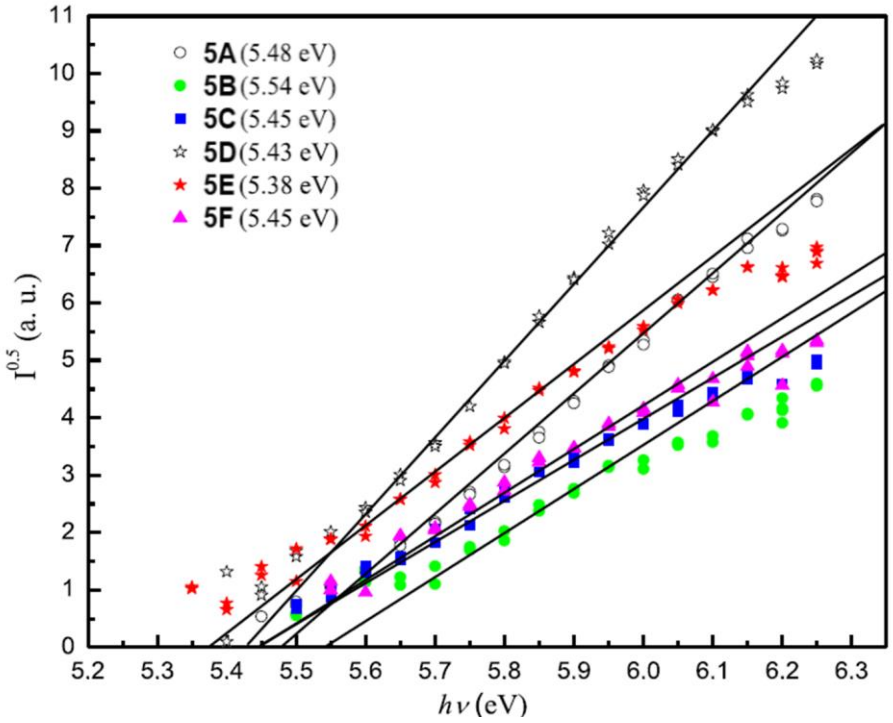

Figure 3.43. Photoemission in the air spectra of the investigated dyes

3.5.4. Quantum chemistry calculations

It is known [7, 12, 218] that Tröger's base has a V-shaped twisted configuration with large dihedral angle (80–104°). It displays the huge rigidity and steric hindrance, which can restrict internal rotation. Moreover, all the protons on the poly[n]enic backbones are in *trans*-geometry, as the TB scaffold-based metal-free sensitizers dye molecules were formed by Horner-Wittig condensation, which leads to excellent *E*-geometry selectivity [223]. In addition, according to the literature [224, 225], the synthesis of rhodanine dyes results in the thermodynamically more stable *Z*-geometry isomers. Taking into account the above mentioned arguments, a computational study of TB-based di-anchoring dyes have been undertaken. Two possible rotamers were studied for each of the TB-based dyes. One – "*closed*" form (Figure 3.44 a) is of the minimal energy and employs intramolecular association between two carboxylic acid fragments. In the other "*open*" form (Figure 3.44 b), the substituted diphenylamine fragments were rotated 180° around N-C bond prior to the optimization, in order to obtain an association-free rotamer. These geometries were optimized at the B3LYP/def2-SVP level of Density Functional Theory. In the more stable one ("*closed*" form), the rhodanine ring is slightly twisted with respect to the phenyl group at the triphenylamine and determine the possible internal hydrogen bonding between carboxylic acid moieties, prohibiting effective utilization of both anchoring

groups. The less stable conformer ("*open*" form) is a planar from rhodanine-acceptor to triphenylamine-donor. Optimized geometries of the "*closed*" and "*open*" forms are given in Table 3.12. Two rotamers differ by 14.9–16.4 kcal/mol for different dyes; hence, the association is favorable at room temperature.

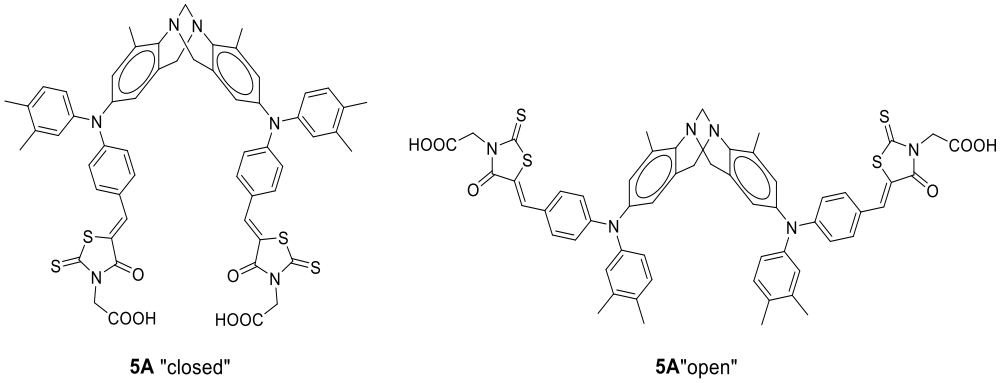

Figure 3.44. Possible geometry-rotamers of TB-based dye **5A**: (a) "closed", (b) "open"

HOMO and LUMO orbital plots are shown in Table 3.12. It can be seen that HOMO orbitals are delocalized over the whole molecule with the slight shift towards triphenylamine fragments. LUMO orbitals are shifted towards rhodanine fragment. This shows partial charge-transfer character of the HOMO/LUMO transition.

Table 3.12 Optimized structures and frontier molecular orbitals of di-anchoring dyes **5A**–**C**

Dye	HOMO	LUMO
5A "closed"	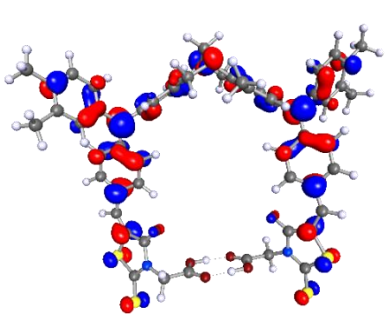	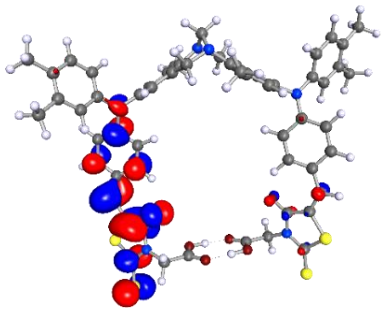
5A "open"	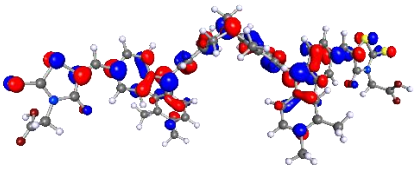	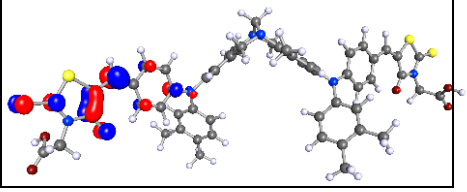

5B “closed”	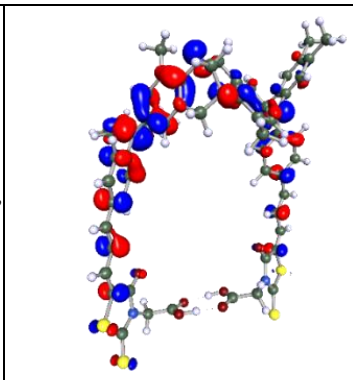	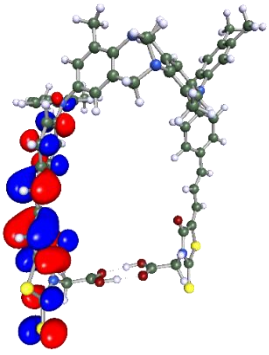
5B “open”	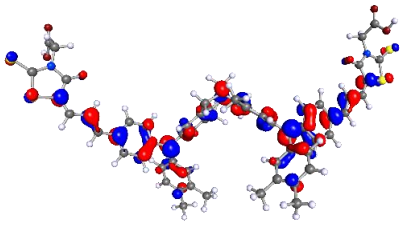	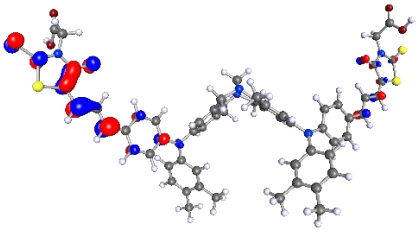
5C “closed”	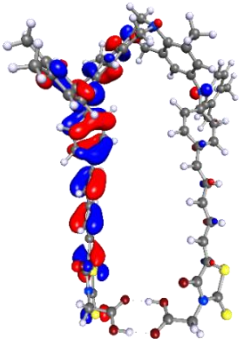	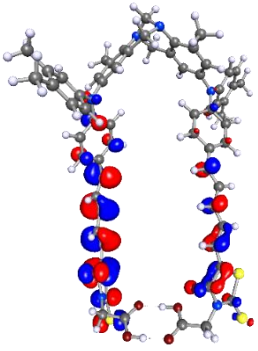
5C “open”	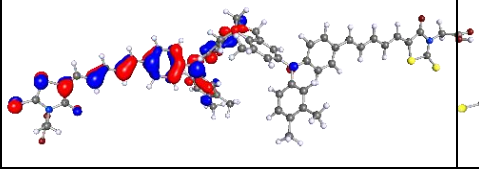	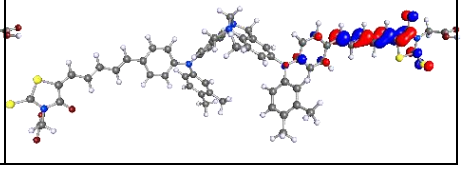

3.5.5. Photovoltaic performance in dye-sensitized solar cells

The photovoltaic performance of the investigated dyes (**5A**–**F**) was evaluated in DSSCs based on iodide-triiodide electrolyte without any added co-adsorbent or co-sensitizer. Figure 3.45 shows *J-V* characteristics of these DSSCs, and the photovoltaic parameters are summarized in Table 3.13. The cells based on the dye **5C** and its counterpart **5F** with the longest methine chains showed broader IPCEs (400–700 nm) but lower values (around 7%) compared to the other dyes (400–600 nm; 12–40%), resulting in lower J_{sc} values (1.44 and 1.12 mA/cm^2).

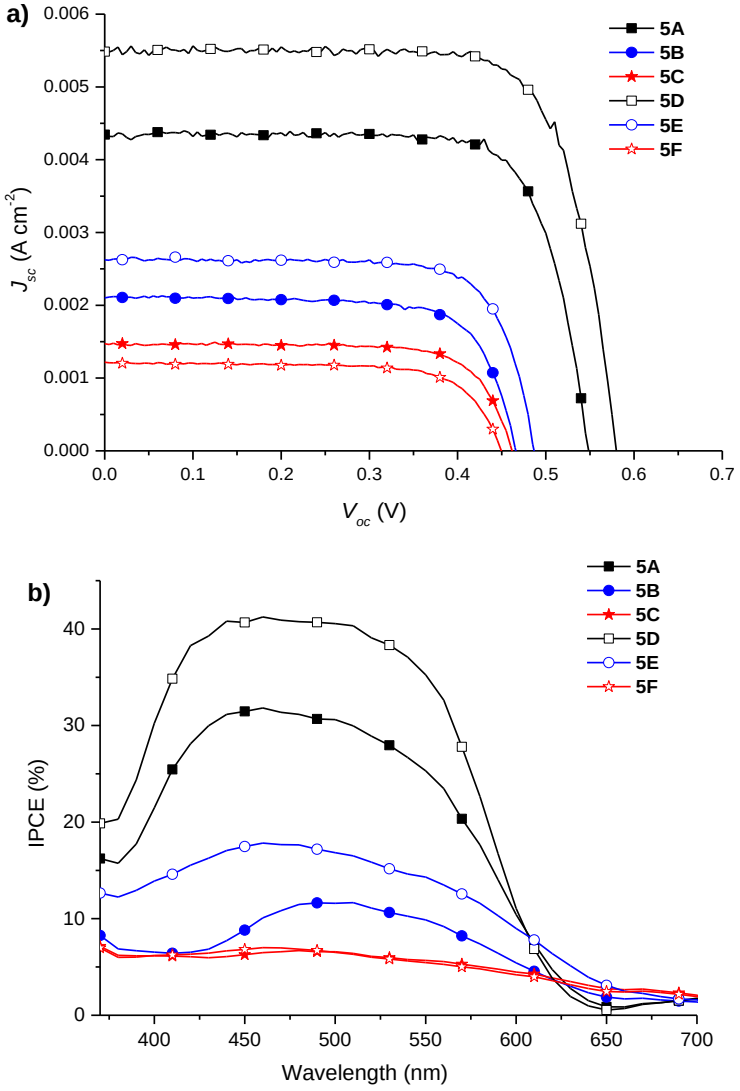

Figure 3.45. (a) *J-V* characteristics of the DSSCs based on dyes **5A**–**F**. (b) IPCE spectra of **5A**–**F** dye-sensitized devices

The cells fabricated with the di-anchoring dyes, except of **5C**, showed slightly lower V_{oc} values to those with the mono-anchoring dyes. It is obvious that J_{sc}-V_{oc} values decreased together with the increasing number of double bonds (n = 0 > n = 1 > n = 2) between the donor and acceptor/anchoring group. As it can be assumed from the analyzed optical properties, the best results were obtained by using dye **5D**, showing an overall conversion efficiency (η) of 2.36% (J_{sc} = 5.42 mA cm^{-2}, V_{oc} = 582 mV, FF = 0.75). It is obvious that the reduced tendency of dye aggregate formation is the main factor influencing better DSSC characteristics. Interestingly, the additional acceptor-anchor units in sensitizers **5A**, **5B** did not have a positive effect on the device performance; overall, DSSC efficiencies are noticeably lower compared with mono-anchoring dyes **5D**, **5E**.

Table 3.13 Photovoltaic performance of DSSCs based on the different dyes under 100 mW·cm^{-2} AM1.5 G illumination

Dyes	V_{oc} (mV)	J_{sc} (mA/cm^2)	FF (%)	η (%)
5A	548±3	4.30±0.06	75.9±1.7	1.79±0.05
5B	468±6	1.99±0.11	73.1±0.9	0.68±0.04
5C	460±0	1.44±0.04	74.9±0.2	0.50±0.02
5D	582±3	5.42±0.15	75.3±1.5	2.36±0.05
5E	482±3	2.52±0.13	75.2±0.7	0.91±0.06
5F	448±3	1.12±0.10	72.1±0.3	0.36±0.03
D35	775±10	11.17±0.05	73.5±1.2	6.35±0.03
N719	740±0	13.30±0.36	72.9±1.1	7.17±0.07

To conclude this chapter, a set of novel metal-free di-anchoring organic dyes based on a Tröger's base scaffold (**5A**, **5B**, **5C**) have been designed and synthesized. These compounds are possessing triphenylamine donor and rhodanine-3-acetic acid as acceptor/anchoring group linked by the poly[n]enic (from n = 0 to 2) chain. The influence of the polymethine chain length and number of the anchoring groups on the photophysical, electrochemical, and photovoltaic properties of these V-shape sensitizers has been investigated, and it was found that the extended polymethine chains ensure flexibility of these units and inspire the interaction between two chromophores, hence promoting aggregate formation in these Tröger's base-based dyes. Therefore, the best result of DSSCs, showing an overall conversion efficiency of 2.36%, was obtained by using dye **5D** that is possessing the shortest polymethine chain length and one anchoring group. Evidently, if further research is aiming to create efficient TB derivatives of similar design, the solution for chain flexibility and intra-anchoring needs to be found, and one of such ways is the enhancement of polymethine backbones by bulky structural moieties, which should prevent aggregate formation in di-anchoring organic dyes based on Tröger's base scaffold.

3.6. Improved sensitizers for dye-sensitized solar cells based on Tröger's base scaffold

Seeking to improve the molecular design of previously investigated sensitizers further, while avoiding the drawbacks of flexible polymethine chain and intra-anchoring of acceptor groups it causes, an alternative interlinking conjugated fragment needs to be found. Such fragment should be rigid, hence solving the problem of flexibility and possibly providing some structural bulk, hence restricting the access of acceptor groups reaching each other by bestowed sterical hindrance. These structural modifications should solve the problem of aggregate formation, while still providing the advantages of two anchoring groups and improved binding to titanium dioxide layer and possibly a higher efficiency of electron injection.

As promising candidates for such fragments could be thiophene units for their rigidity and beneficial molecular properties, they bestow to bianchoring sensitizers, surpassing that of the regular phenyl group or some other spacers [226]; a more sophisticated spacer option could be phenyl-branched hydrazone fragment, providing both a longer conjugated system and an additional structural bulk.

In this chapter, novel sensitizer compounds of improved molecular design, of both A-π-D-π-A and D-π-A type, are synthesized and analyzed, providing further insight into a topic of double-anchored dyes.

3.6.1. Synthesis of novel dyes based on Tröger's base scaffold

New structurally improved bianchoring organic sensitizers, containing spacer fragments of either thiophene or phenyl-branched hydrazone, based on TB scaffold and, likewise, their mono-anchoring counterparts, were synthesized.

Both thiophene spacer possessing compounds, bianchoring dye **6f** and its counterpart **6i**, were synthesized in a six-step reaction route as described in Scheme 3.8. Both routes have the same intermediate compounds **6a**–**c**, and synthetic pathway starts to differ as **6c** is being attached to either Tröger's base or smaller system of a single aromatic ring and proceeds by two more synthetic steps further modifying them towards obtaining final compounds **6f** and **6i** respectively.

Initially, compound **6a** was obtained from 3,4-dimethyl-*N*-phenylaniline by bromination reaction with *N*-bromosuccinimide in DMF. This compound underwent the Suzuki coupling reaction with (5-formylthiophen-2-yl)boronic acid, resulting in aldehyde compound **6b**, which was further modified by blocking its active group by *p*-toluenesulfonic acid catalyzed reaction with 2,2-dimethyl-1,3-propanediol, affording product **6c** with the yield of 68%. The obtained corresponding diphenylamine **6c** underwent reaction with either 2,8-dibromo-4,10-dimethyl-6*H*,12*H*-5,11-methanodibenzo[*b*,*f*][1,5]diazocine (brominated Tröger's base derivative) [40] or 3-iodotoluene, in the presence of palladium(II) acetate, tri-*tert*-butylphosphonium tetrafluoroborate, and sodium *tert*-butoxide, to provide intermediates **6d** and **6g**, respectively. After deprotection, the obtained penultimate aldehydes **6e** and **6h** were obtained, and they were condensed with rhodanine-3-acetic acid, resulting in thiophene spacer possessing sensitizers **6f** and **6i**.

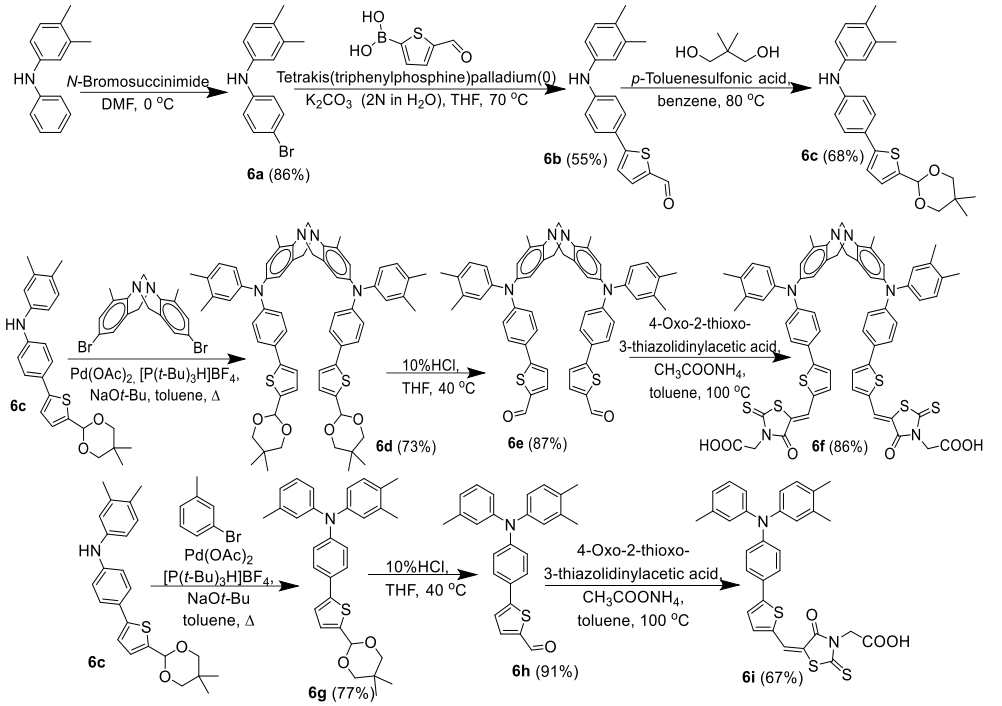

Scheme 3.8. Synthesis of new sensitizers containing thiophene spacer

Sensitizers, having a phenyl-branched hydrazone spacers, were synthesized (Scheme 3.9) by modifying already investigated intermediate aldehydes **5k** and **5o**. Their reaction with phenylhydrazine resulted in phenylhydrazones **6j** and **6n**, which were used in arylation reactions with **5n** (2-(4-bromophenyl)-5,5-dimethyl-1,3-dioxane) to obtain hydrazones with protected aldehyde functional groups **6k** and **6o**, respectively. After deprotection, the penultimate aldehyde compounds **6l** and **6p** were obtained. Finally, the condensation of the aldehydes **6l** and **6p** with rhodanine-3-acetic acid yielded sensitizers **6m** and **6r**.

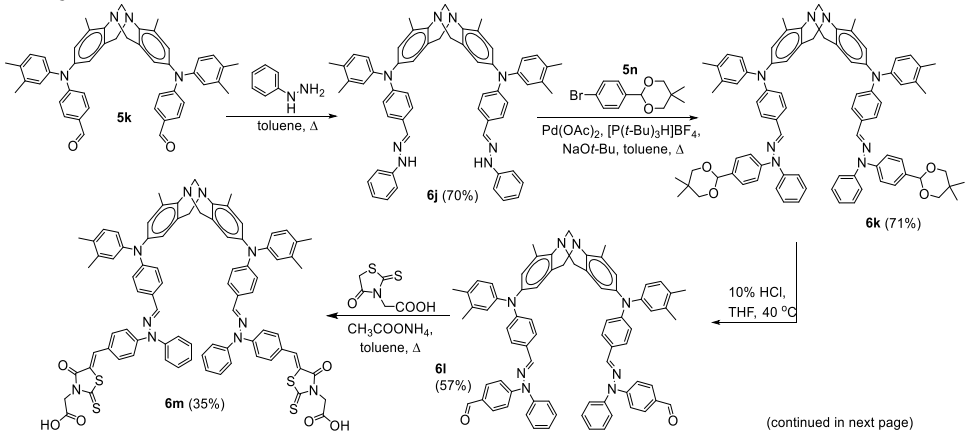

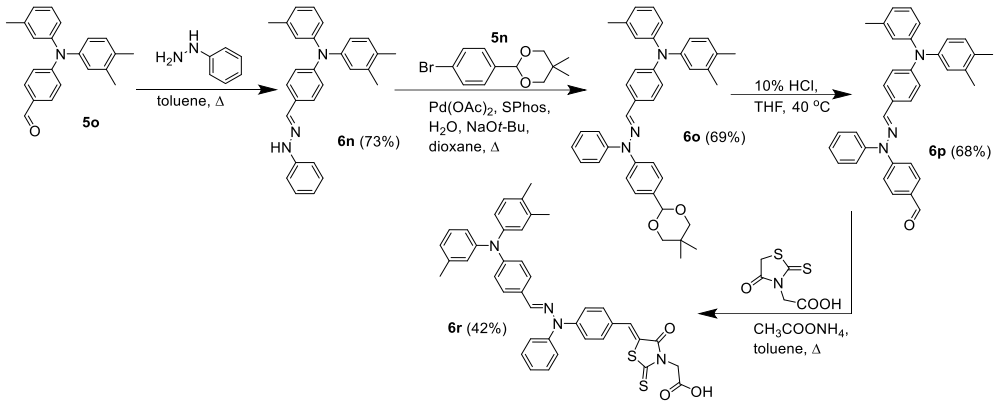

Scheme 3.9. Synthesis of new sensitizers with hydrazone spacer

^{1}H and ^{13}C NMR as well as elemental analysis data confirmed the structure of newly synthesized dyes **6f**, **6i**, **6m**, and **6r**. The signal pattern of ^{1}H NMR spectrum in the region between 3.7 and 4.5 ppm allows identifying the presence of the TB core, as the pattern of the protonic signals of **6f**, **6i**, **6m**, and **6r** shows two doublets (although sometimes overlapped with other signals) near each margin of the mentioned interval. These two doublets signify the *endo/exo* protons of *methanodiazocine* bridge (part Ar-CH_2-N), as they are magnetically nonequivalent due to the structural rigidity of the Tröger's base. As it is observed in ^{1}H NMR spectrum of compound **6m** (Figure 3.46), the protons of methylene bridge show two doublets at 3.89 and 4.38 ppm, *endo* and *exo* hydrogens, respectively, but in this case, *exo* doublet overlaps with a signal of protons in H-21 position. As a contrasting example of this, the signals of two protons located in the center of the outer corner of TB core, attached to bridging methylene carbon (N-CH_2-N), are not hindered structurally and can be observed as a singlet at 4.20 ppm in this spectrum.

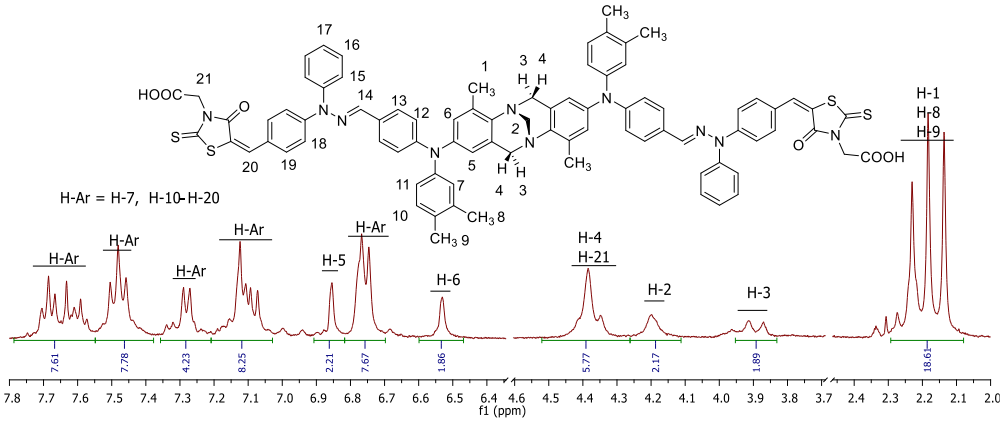

Figure 3.46. ^{1}H NMR spectrum (400MHz, $(CD_3)_2SO$) of compound **6m**

3.6.2. Optical properties

In order to examine and evaluate the impact of the thiophene and hydrazone spacers introduced into the molecular design and the optical properties of new dyes, the UV-vis measurements of di-anchoring dyes **6f** and **6m** and their mono-anchoring analogues **6i** and **6r** were performed.

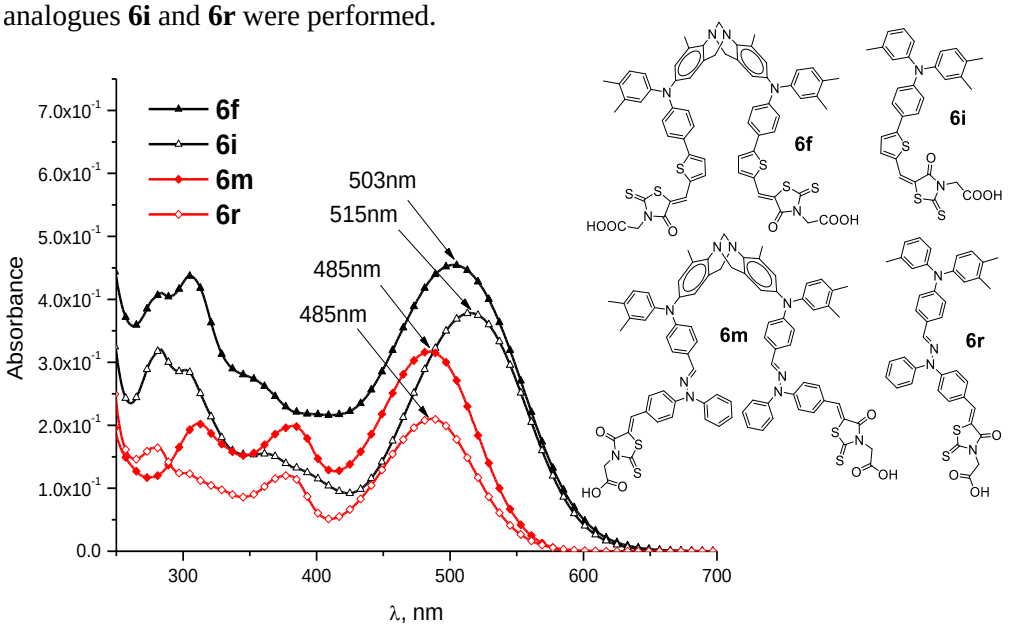

Figure 3.47. UV-vis spectra of dyes **6f**, **6i**, **6m**, and **6r** in DMSO solutions ($c = 10^{-4}$ M)

As shown in Figure 3.47, the absorption spectra of both, bianchoring organic dyes based on TB scaffold, **6f** and **6m**, and mono-anchoring dyes, **6i** and **6r**, display two distinct absorption bands at around 270–340 nm and 400–650 nm, respectively. The bands in the UV region demonstrate higher absorption at longer wavelengths, corresponding to the π–π* electron transitions of the conjugated system. Interestingly, the sensitizers **6m** and its mono-anchoring counterpart **6r** exhibit weak but clear additional absorption band at around 385 nm, likely due to phenyl groups branching out of hydrazone unit that is present in these dyes. The strong absorption bands in the visible region can be attributed to an intramolecular charge transfer (ICT) between the triphenylamine-based donor and the electron accepting rhodanine-3-acetic acid moiety, providing efficient charge separation at the excited state. The comparison in between the absorption spectra of dyes **6f**, **6i**, **6m**, and **6r** clearly demonstrates that the extension by thiophene unit results in 18 and 30 nm (in bi- and mono- sensitizers, respectively) of bathochromic shift of the absorption band compared to that of the hydrazone homologues. Next, the comparison of the optical properties of di-anchoring dyes **6f** and **6m** with those of their mono-anchoring analogues, **6i** and **6r**, clearly demonstrates that the organic dyes based on a TB scaffold exhibit significantly higher extinction coefficients compared to that of the counterpart mono-anchoring sensitizers. Moreover, the molar extinction coefficient of the charge transfer transition in these dyes indicates a good ability for light harvesting, especially noticeable in

thiophene sensitizers. However, the comparison of the ICT absorption bands of **6f** and **6i** clearly indicates a hypsochromic shift of 12 nm, hinting of an interaction at the ground state between the two chromophores in this di-anchoring dye, leading to conclusion that thiophene unit does not prevent the intra-anchoring of two sides of the molecule. Luckily, no such shift was observed in dye **6m** in comparison to its mono-anchoring sensitizer **6r**. This indicates that phenyl-branched hydrazone unit provides the expected properties and prevents the interaction between the two chromophores in this di-anchoring dye.

To conclude this chapter, two methods to improve the molecules of previously investigated dyes structurally by introducing thiophene and hydrazone fragments were offered and tested, and their synthetic pathway was discovered, resulting in sensitizers **6f**, **6i**, **6m**, and **6r**. It was found that even though a thiophene fragment bestowed the compounds with light absorption properties surpassing that provided by hydrazone unit, it still does not offer sufficient structural stiffness to prevent the interaction between the two chromophores of bianchoring sensitizer. However, phenyl-branched hydrazone unit successfully provided both the rigid structure and structural bulk, hampering these unfavorable interactions. These dyes are promising candidates for the DSSC applications.

3.7. Light emitting materials containing tetraphenylethenyl fragments and Tröger's base core

One of the most important and widely investigated topics of optoelectronics is organic light emitting diodes. Thanks to the research efforts contributed by the scientists, OLEDs with various emission colors in high efficiencies have been fabricated and utilized in full-color flat panel displays and solid-state white lighting [227]. For the improvement of these devices, a development of new efficient materials possessing desirable properties is essential. Whereas many luminophors exhibit strong photoluminescence (PL) in dilute solutions, their light emissions are often weakened or even completely quenched in concentrated solutions or in the solid state [228]. As the luminogenic molecules are located in the immediate vicinity under these circumstances, the aromatic rings of the neighboring fluorophors, especially those with disc-like shapes, experience strong π–π stacking interactions, which promote the formation of species that are detrimental to the light emission. The excited states of the aggregates often decay via nonradiative relaxation pathways, which are notoriously known as aggregation-caused quenching (ACQ) of light emission in the condensed phase [229]. The ACQ effect has prevented many potentially effective luminophors from finding their use in devices due to their drastically decreased efficiency in a solid form.

A phenomenon of aggregation-induced emission (AIE), that is exactly opposite to the ACQ effect, was as well discovered, where instead of quenching, aggregate formation boosted the Φ_F values, turning them from faint fluorophores to strong emitters [230]. Amongst various luminogens, tetraphenylethene (TPE) possesses, a simple molecular structure shows a splendid AIE effect [231]. Its four phenyl groups

are twisted out of the central alkene plane by ~50°, such propeller-like conformation effectively prevents direct π–π stacking interactions that tend to induce nonradiative recombination and red-shift as observed in normal crystals. TPE is a very attractive and useful molecule as it can be facilely introduced to many ACQ chromophores, generating new luminogens with AIE or aggregation-enhanced emission (AEE) characteristics and high emission efficiency in the aggregated state for the fabrication of efficient non-doped OLEDs [229].

In order to further inhibit the direct π–π stacking, an angle-oriented TB core could be incorporated into the molecular structure of luminophors, hence potentially resulting efficient luminogenic molecules. It is as well an interesting approach towards the investigation and better understanding of the structure–property relationship, as it could be compared to the previously investigated TB derivatives, especially compounds containing triphenylethenyl fragment and, therefore, having some structural similarities like compound **2b**.

This chapter is dedicated to the synthesis and investigation of luminogenic Tröger's base derivatives, containing tetraphenylethene moieties and possessing AIE properties.

3.7.1. Synthesis of novel Tröger's base compounds

Novel TB compounds containing TPE moieties, chosen for the investigation in this chapter, were synthesized by obtaining suitable Tröger's base derivative and expanding it with either two or four TPE moieties by employing Suzuki–Miyaura cross-coupling or Buchwald–Hartwig amination reactions.

Firstly, the compound 4,10-dimethyl-N^2,N^2,N^8,N^8-tetrakis(4-(1,2,2-triphenylvinyl)phenyl)-6*H*,12*H*-5,11-methanodibenzo[*b*,*f*][1,5]diazocine-2,8-diamine (**7a**), as the most structurally related to previously investigated compound **2b**, was synthesized from amino-substituted TB derivative **4b** and brominated TPE derivative via Buchwald–Hartwig amination reaction (Scheme 3.10).

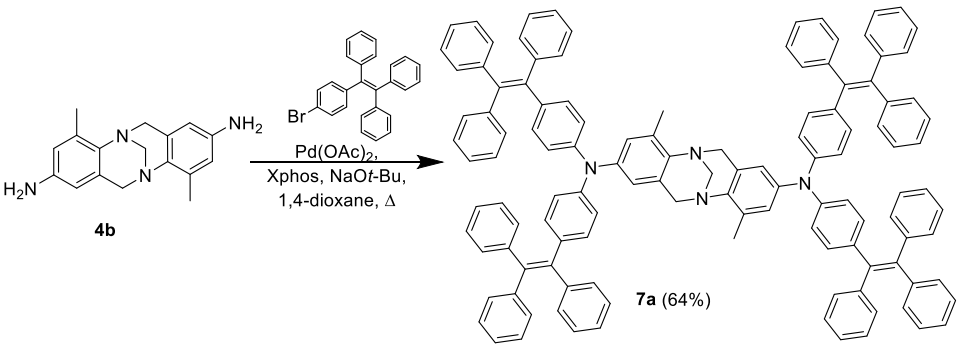

Scheme 3.10. Synthesis of compound **7a**

Secondly, the plan to investigate compounds having two TPE fragments connected directly to TB with no interlinking nitrogen was created. These compounds, namely 4,10-dimethyl-2,8-bis(4-(1,2,2-triphenylvinyl)phenyl)-6*H*,12*H*-5,11-

methanodibenzo[*b*,*f*][1,5]diazocine (**7c**) and 2,8-dimethyl-4,10-bis(4-(1,2,2-triphenylvinyl)phenyl)-6*H*,12*H*-5,11-methanodibenzo[*b*,*f*][1,5]diazocine (**7e**), were synthesized by obtaining intermediate boronic group possessing TB derivatives **7b** and **7d** via metalation with *n*-butyllithium, and their further reaction with 1-(4-bromophenyl)-1,2,2-triphenylethylene via Suzuki-Miyaura cross-coupling (Scheme 3.11).

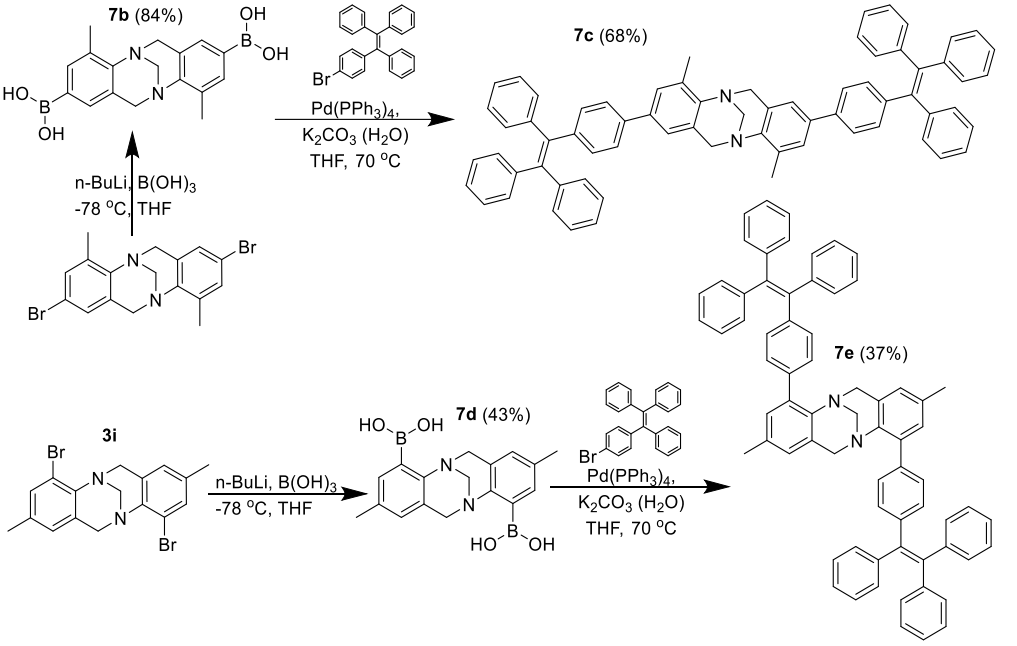

Scheme 3.11. Synthesis of compounds **7b**–**e**

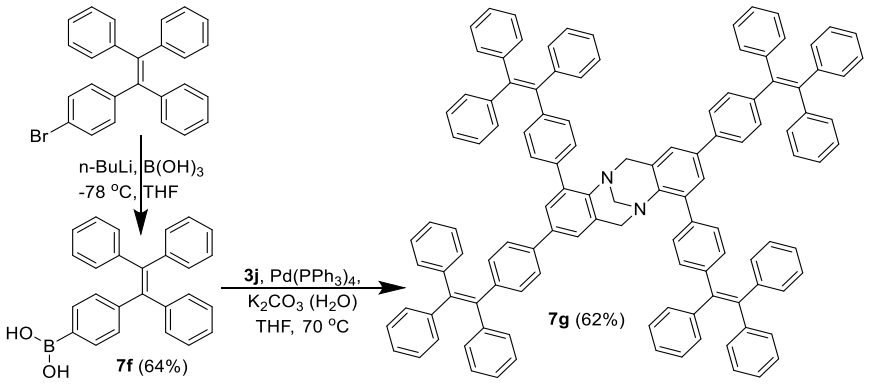

Scheme 3.12. Synthesis of compounds **7f**–**g**

Compound 2,4,8,10-tetrakis(4-(1,2,2-triphenylvinyl)phenyl)-6*H*,12*H*-5,11-methanodibenzo[*b*,*f*][1,5]diazocine (**7g**), containing four TPE moieties, was

synthesized by obtaining intermediate boronic group possessing TPE derivative **7f** and attaching it to bromine-substituted TB core **3j** by employing Suzuki-Miyaura cross-coupling reaction (Scheme 3.12). This method was chosen due to the propensity to undergo protodeboronation that is frequently observable in boronic compounds that are involved in metal-catalysed coupling reactions; hence, a reaction employing TB derivative with four boronic groups would likely be susceptible to such undesirable outcome, as a single event of protodeboronation, occurring in any of the four sites, would be detrimental for the synthesis.

The structures of synthesized compounds were confirmed by NMR ^{1}H and ^{13}C spectroscopy as well as elemental analysis. Signal pattern of compounds **7a**, **7c**, **7e**, and **7g** in the 3.35–4.65 ppm in a range of ^{1}H NMR spectrum is essential for the identification of *methanodiazocine* bridge, proving the presence of the TB core (Figure 3.48). ^{1}H NMR spectra of these compounds show two doublets at 3.38 ppm and 3.97 ppm, *endo* and *exo* protons, respectively, signifying that the protons in bridging methylene part (Ar-CH_2-N) are magnetically nonequivalent due to the rigid structure of the TB. As a contrasting example, the signals of two protons of the other bridging methylene carbon (N-CH_2-N) are detected as a singlet at 4.22 ppm. Other typical proton signals of aromatic part of the core unit can be observed at 6.53 and 6.88 ppm.

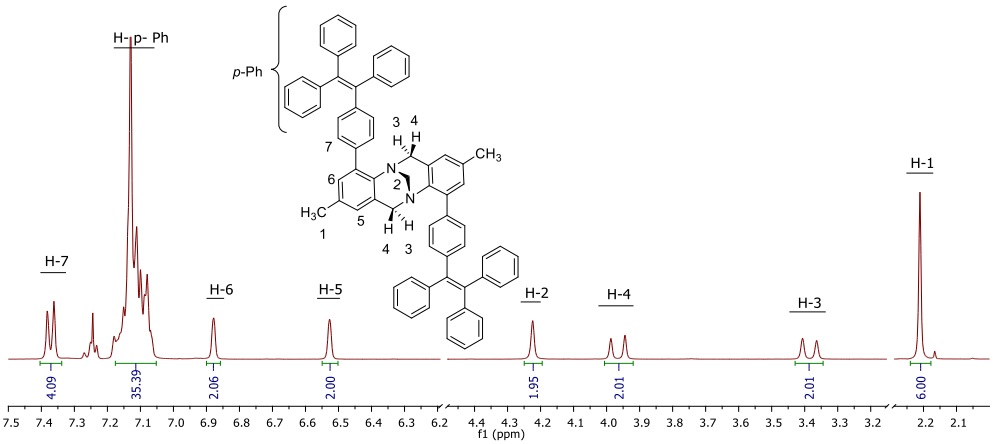

Figure 3.48. ^{1}H NMR spectrum (400MHz, $CDCl_3$) of compound **7e**

3.7.2. Thermal and optical properties

DSC measurements of compounds **7a**, **7c**, **7e**, and **7g** were performed, and they reveal that the investigated TB derivatives **7c** and **7g** are fully amorphous (Figure 3.49), while compounds **7a** and **7e** exist both in crystalline and amorphous state (Table 3.14), as during the first heating, the melting of the crystals (T_m) was observed in their samples. No crystallization takes place during cooling or second heating scans of compound **7a**, and only glass transition (T_g) is registered during the second heating (Figure 3.49).

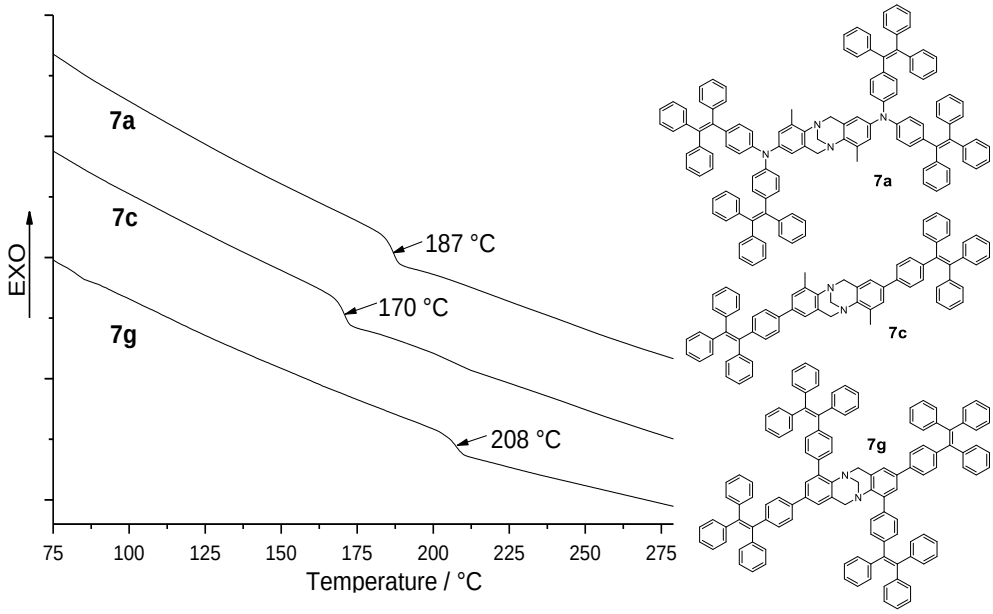

Figure 3.49. DSC curves of **7a**, **7c**, and **7g** indicating T_g. Heating rate 10 K/min; second run

These properties can be compared to that of compound **2b** due to their structural resemblance, but as the additional phenyl group is introduced into each branch (triphenylethenyl moieties in compound **2b**, as compared to tetraphenylethene in **7a**), the fully amorphous **2b** (Figure 3.10 b) is getting more crystalline as **7a**. A more interesting case is compound **7e**, demonstrating the glass transition, crystallization, and melting of crystals in both runs (Figure 3.50). These two states could be explained by the increased planarity of the compound as TPE fragments are branching off from the TB core to the sides of it, not being effectively oriented along the axes of V-shaped core.

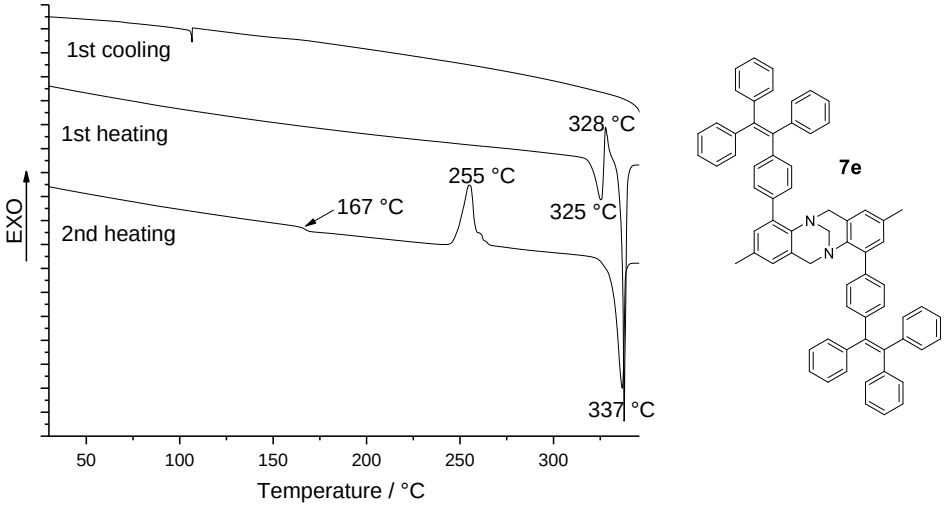

Figure 3.50. DSC curves of compound **7e**. Heating rate 10 K/min

Thermogravimetric analysis of compounds **7a**, **7c**, **7e**, and **7g** reveals high decomposition temperatures (Figure 3.51, Table 3.14). In general, all the compounds within the series have demonstrated superior thermal stability with initial destruction temperatures (corresponding to 5% weight loss) exceeding 400 °C, confirming that their thermal stability will not be a limiting factor for the practical application in optoelectronic devices.

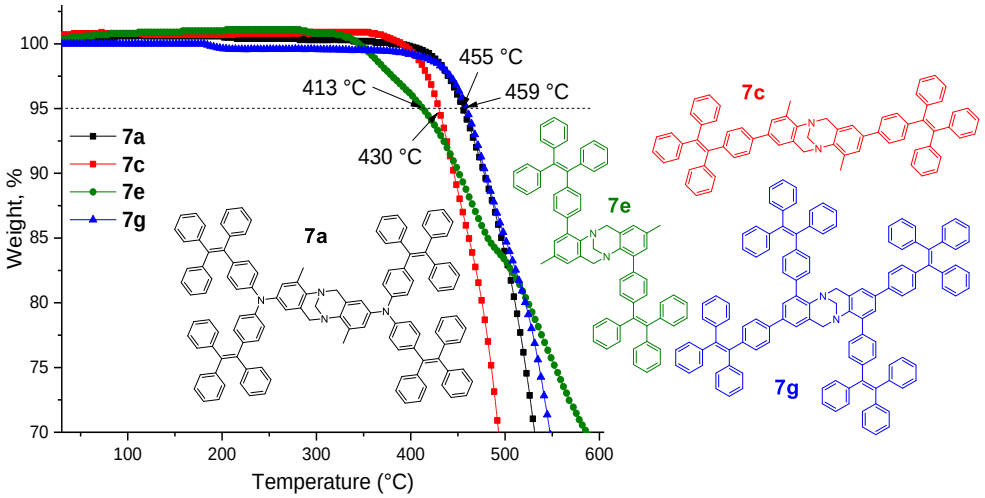

Figure 3.51. TGA curves for compounds **7a**, **7c**, **7e**, and **7g**

UV–VIS absorption spectra of Tröger`s base derivatives **7a**, **7c**, **7e**, and **7g** in the THF solution (Figure 3.52) were obtained, and the emission spectra of **7c**, **7e**, and **7g** were measured in THF and neat film (Figure 3.53, Table 3.14).

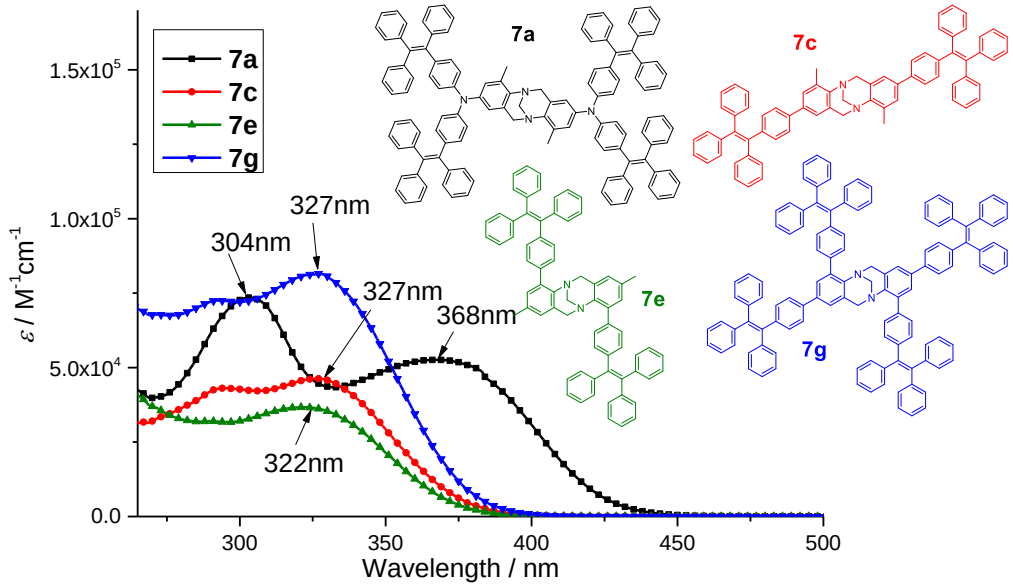

Figure 3.52. UV-VIS spectra of compounds **7a**, **7c**, **7e**, and **7g** in THF solutions (c=10^{-4} M)

Table 3.14 Thermal and optical properties of TB derivatives

Comp.	T_m [°C]	T_g [°C] [b]	T_{dec} [°C] [c]	λ_{max}^{abs} [nm] [d]	ε [$M^{-1}cm^{-1}$]	THF solution		Neat film	
						λ_F (nm) [e]	Φ_F (%) [f]	λ_F (nm) [e]	Φ_F (%) [f]
7a	229[a]	187	455	304;368	73518;52599	511	0.03	526	4.2
7c	-	170	430	327	46275	507	0.06	497	27.84
7e	338	325	413	322	36693	509	0.07	494	17.05
7g	-	208	459	327	81514	507	0.19	500	22.15

[a] Melting point was only detected during the first heating 10 K/min. [b] Determined by DSC: scan rate, 10 K/min; N_2 atmosphere; second run. [c] Onset of decomposition determined by TGA: heating rate, 10 K/min; N_2 atmosphere. [d] UV-Vis spectra were measured in 10^{-4} M THF solution. [e] Fluorescence maxima in THF solution, neat film. [f] Fluorescence quantum yield in THF solution, neat film.

UV-VIS absorption spectra shows that a compound **7a** have two absorption maximums, peaking at 304 nm and 368 nm, having the most red-shifted maximum in this group of compounds, possibly showing the interaction of TPE fragments, surpassing that of the other compounds. The first maximum, observable at 304 nm, could correspond to *n*-σ* electron transitions in the proximity of nitrogen atoms, to which TPE fragments are attached. Compound **7e** have its absorption maximum at 322 nm, indicating a 5 nm hypsochromic shift compared to compounds **7c** and **7g**, a phenomena that could be explained by possible interaction and steric hindrance between TPE fragment and *endo*- hydrogens of the TB core unit. Interestingly, the absorption of **7g** look like a sum of absorptions of **7c** and **7e**, by both wave length and absorption intensity, showing no bathochromic shift whatsoever, suggesting that these fragments do not interact as a single conjugated π-system.

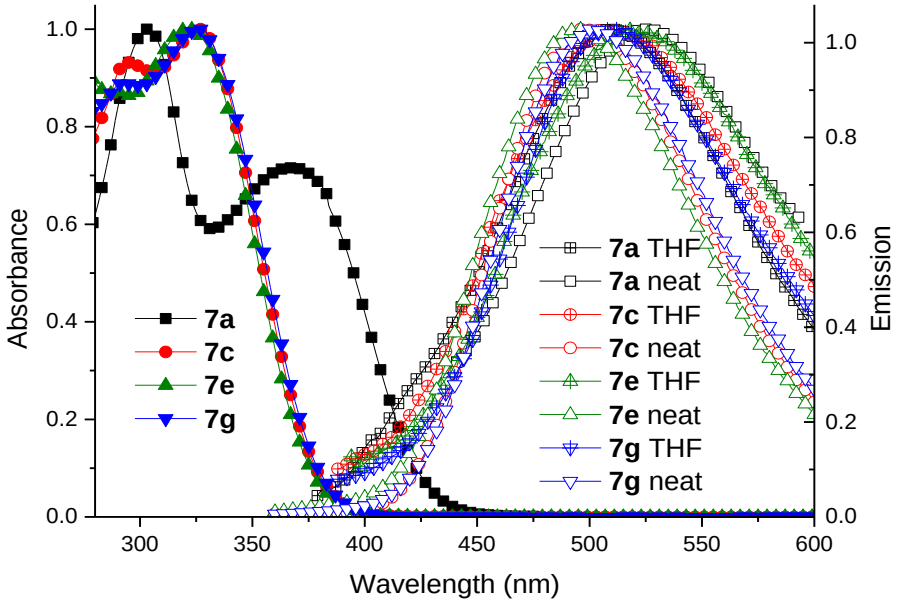

Figure 3.53. Emission of neat layers, solution, and absorption spectra of **7a**, **7c**, **7e**, and **7g**

The emission spectra and quantum yields of compounds **7c**, **7e**, and **7g** demonstrate the typical effect of AIE, while emitting poorly in dilute solutions, emission greatly increases in a solid state (Table 3.14). This phenomenon is as well observed in compound **7a**, but it did not exhibit good light emission in either solution or film. There should be noted that the largest difference between emission maximums in solution and solid state is observed in **7e**, indicating the formation of aggregates and, subsequently, decreased quantum efficiency. This can be attributed to the structure of **7e**, having its TPE fragments attached to the sides, not the ends, of V-shaped TB core: those fragments are oriented in the fashion resembling parallel lines heading to the opposite directions out from the core unit, avoiding core-caused orientation not making a significant angle with each other. Compound **7c** have its TPE fragments interlinked into the core unit in a way they are oriented nearly perpendicularly towards each other: a molecular design that results in the highest solid-state quantum efficiency in a group. Compound **7g** have its two pairs of TPEs attached in both ways, and its quantum efficiency is close to that of the arithmetical average between the previous two molecules, suggesting that it suffers the drawbacks of **7e**, hence making two additional TPE fragments (in comparison with **7c**) more of a disadvantage than an improvement.

3.7.3. Photoelectrical properties

The ionization potential of compounds **7a**, **7c**, **7e**, and **7g** was measured by the PESA method (Figure 3.54, Table 3.15) [1].

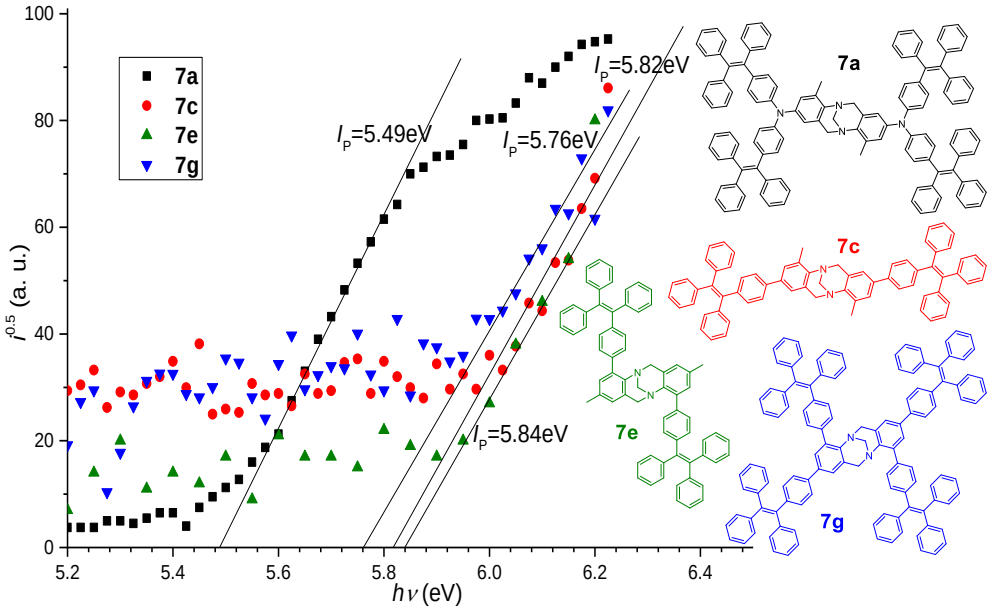

Figure 3.54. Photoemission in the air spectra of Tröger's base derivatives **7a**, **7c**, **7e**, and **7g**

[1] Measurements of ionization potential were performed at the Department of Solid State Electronics, Vilnius University, by Dr. V. Jankauskas, E. Kamarauskas.

Table 3.15 Energy level data for compounds **7a**, **7c**, **7e**, and **7g** [a]

Compound	E_g^{opt} (eV) [b]	E_{HOMO} (eV)[c]	E_{LUMO} (eV)[d]	I_p (eV)[e]
7a	2.77	-4.90	-2.13	5.49
7c	3.12	-5.57	-2.45	5.82
7e	3.14	-5.36	-2.22	5.84
7g	3.11	-5.47	-2.36	5.76

[a] The CV measurements were carried out at a glassy carbon electrode in dichloromethane solutions containing 0.1 M tetrabutylammonium hexafluorophosphate as an electrolyte and Pt wire as the reference electrode. Each measurement was calibrated with ferrocene (Fc). Potentials measured vs Fc^+/Fc. [b] The optical band gaps E_g^{opt} estimated from the edges of electronic absorption spectra in solution. [c] Conversion factors: ferrocene in DCM vs SCE 0.46 [143], SCE vs SHE: 0.244 [166], SHE vs. vacuum: 4.43 [167]. [d] E_{LUMO} calculated from the equation $E_{LUMO} = E_{HOMO} - E_g^{otp}$. [e] Solid state ionization potential (I_p) was measured by the photoemission in the air method from films.

I_p value of 5.49 eV for **7a** is comparable with 5.45 eV of compound **2b**, as having four additional unsubstituted phenyl groups (tetraphenylethenyl branches compared to triphenylethenyl ones) increase the ionization potential by 0.04 eV. The ionization potentials of compounds **7c**, **7e**, and **7g** are comparatively high, having their values of 5.82 eV, 5.84 eV, and 5.76 eV, respectively. This can be attributed to the absence of donor group substituents, interlinking nitrogen atoms, binding TPE fragments together, or conjugated π-system that is not sufficiently large.

The ground-state oxidation potentials of compounds **7a**, **7c**, **7e**, and **7g** were measured employing the cyclic voltammetry technique (Table 3.15). All measured derivatives undergo reversible oxidation in their CV scans, indicating the electrochemical stability of the compounds. The observed CV results in the solution correlate reasonably with the ionization potential measurement data that was obtained from films, indicating limited intermolecular interaction in the solid state.

To conclude this chapter, four novel Tröger's base compounds possessing TPE side arms were synthesized and investigated. These compounds are thermally stable, soluble, and possess AIE properties, allowing them to be used in forming solid-state layer in devices. The quantum efficiency values of these compounds were not as high as expected, but the research results revealed some structure-properties relations that allow further improvement and optimization in the molecular design of future compounds. It was discovered as well that the highest quantum efficiency were obtained by molecules where TPE moieties are attached to the TB core in 2,8-position, hence allowing to be oriented angle-wise towards each other. Other molecular designs resulted in decreased quantum efficiency, even when the number of attached TPE fragments was doubled. These findings suggest the conclusion that the TB core (preferably being substituted to 2,8- positions) could be useful in the synthesis of functional luminogenic molecules that are possessing AIE properties.

4. EXPERIMENTAL PART

4.1. Instrumentation

Measurements

^{1}H NMR spectra were recorded at 400 MHz on a Bruker Avance III spectrometer with a 5 mm double resonance broad band BBO z-gradient room temperature probe and at 700 MHz on a Bruker Avance III spectrometer equipped with a 5mm TCI 1H-13C/15N/D z-gradient cryoprobe. ^{13}C NMR spectra were collected by using the same instruments at 100 and 176 MHz, respectively. The chemical shifts, expressed in ppm, were relative to tetramethylsilane (TMS). The compounds were dissolved in deuterated solvents as indicated for each compound. All the experiments were performed at 25 °C.

The course of the reaction products was monitored by TLC on ALUGRAM SIL G/UV254 plates and developed with I_2 or UV light. Silica gel (grade 62, 60–200 mesh, 150 Å, Aldrich) was used for column chromatography.

The elemental analysis was performed with an Exeter Analytical CE-440 Elemental.

IR-spectroscopy was performed on Perkin Elmer Spectrum BX II FT-IR System, using KBr pellets. The fluorescence emission and excitation spectra were recorded with a Hitachi MPF-4 luminescence spectrometer. All the data are given as shifts in ν (cm^{-1}).

The melting points were determined in capillary tubes by using Electrothermal MEL-TEMP capillary melting point apparatus.

Differential scanning calorimetry (DSC) was performed on a Q10 calorimeter (TA Instruments) at a scan rate of 10 K min^{-1} in the nitrogen atmosphere. The glass transition temperatures for the investigated compounds were determined during the second heating scan.

Thermogravimetric analysis (TGA) was performed on a Q50 thermogravimetric analyzer (TA Instruments) at a scan rate of 10 K min^{-1} in the nitrogen atmosphere.

The absorption spectra of the dilute THF solutions were recorded on a UV–VIS-NIR spectrophotometer Lambda 950 (Perkin Elmer). The microcells with an internal width of 1 mm were used.

X-ray crystallography measurements were made in the Department of Polymer Chemistry and Technology, KTU, on a Rigaku XtaLAB mini diffractometer by using graphite monochromated Mo-Ka radiation. The data were collected and processed by using CrystalClear (Rigaku). All calculations were performed by using the CrystalStructure 4.0 crystallographic software package, except for refinement, which was performed by using SHELXL-97.

Cyclic voltammetry (CV) measurements were carried out by a three-electrode assembly cell from Bio-Logic SAS potentiostat-galvanostat. The measurements were carried out at a glassy carbon electrode in dichlormethane solutions containing 0.1 M tetrabutylammonium hexafluorophosphate as an electrolyte, Pt as the reference, and counter electrodes at a scan rate of 50 mV s^{-1}. Each measurement was calibrated with ferrocene (Fc). The oxidation potential was obtained as an average value between anodic and cathodic potentials: $E_{1/2}^{red/ox} = 1/2(E_{pc} + E_{pa})$.

The fluorescence of the investigated compounds in dilute toluene solutions was measured by using an Edinburgh Instruments Fluorescence Spectrometer FLS920. The fluorescence quantum yields (Φ_F) of the solutions were estimated by using the integrated sphere method [232].

The fluorescence and phosphorescence of compounds **3f–3h** were measured in the Institute of Applied Research, Vilnius University. The fluorescence of the investigated compounds in dilute THF solutions, PS, and neat films were measured by using excitation at 350 nm from a Xe lamp (FWHM<10 meV), using a back-thinned CCD spectrometer PMA-11 (*Hamamatsu*). The samples of dilute solutions were prepared by dissolving investigated materials in a spectral grade THF at 1×10^{-6} M concentration. The PS films with the dispersed compounds with 0.1 wt % concentration were prepared by mixing the dissolved compounds and PS in the THF solutions at appropriate ratios and casting the solutions on quartz substrates under the ambient conditions. For phosphorescence measurements, Zeonex (polyolefin) polymer and spectral grade chlorobenzene as a solvent with dispersed compounds of 1 % w.t. in wet-cast films under ambient conditions were used. The neat films of the compounds were cast from 1×10^{-3} M THF solutions under ambient conditions. The fluorescence quantum yields (Φ_F) of the solutions, PS, and neat films were estimated by using the integrated sphere method with integrating sphere (*Sphere Optics*) coupled to the CCD spectrometer via optical fiber using 350 nm excitation wavelength. Quinine sulfate in 0.1 M H_2SO_4 with Φ_F 0.53 ± 0.023 was used as a reference. Fluorescence transients were measured by using a time-correlated single photon counting system PicoHarp 300 (*PicoQuant*) utilizing a semiconductor diode (repetition rate 1 MHz, pulse duration 70 ps, emission wavelength 350 nm) as an excitation source. Radiative (τ_r) and nonradiative (τ_{nr}) decay time constants were calculated by using the following relations: $\tau_r = \tau_F/\Phi_F$, $\tau_{nr} = \tau_F/(1-\Phi_F)$, where the term τ_{nr} takes into account all the possible nonradiative decay pathways. Phosphorescence measurements of 1% w.t. Zeonex (polyolefin) films were performed by using nanosecond (τ = 7 ns) Ekspla NT 242 laser with 350 nm excitation (laser fluence 200 μJ) and Andor Sr-303i-A iCCD camera at 5×10^{-5} mbar vacuum by closed-cycle helium cryostat (293 K) with 1 ms delay time after the excitation.

Photoelectrical measurements

The solid state ionization potential (I_p) of layers of the synthesized compounds was measured by the electron photoemission in the air method at the Department of Solid State Electronics, Vilnius University. The samples for the ionization energy measurement were prepared by dissolving materials in THF, and these solutions were coated on Al plates that were pre-coated with ~0.5 μm thick methylmethacrylate and methacrylic acid copolymer adhesive layer. The thickness of the transporting material layer was 0.5–1 μm. Usually, the photoemission experiments are carried out in a vacuum, and high vacuum is one of the main requirements for these measurements. If the vacuum is not high enough, the sample surface oxidation and gas adsorption are influencing the measurement results. In this case, however, the organic materials that were investigated were stable enough to oxygen, and the measurements could be carried out in the air. The samples were illuminated with monochromatic light from

the quartz monochromator with deuterium lamp. The power of the incident light beam was $(2–5)\cdot10^{-8}$ W. The negative voltage of –300 V was supplied to the sample substrate. The counter-electrode with the 4.5×15 mm^2 slit for illumination was placed at 8 mm distance from the sample surface. The counter-electrode was connected to the input of the BK2-16 type electrometer, working in the open input regime, for the photocurrent measurement. The 10^{-15} –10^{-12} A strong photocurrent was flowing in the circuit under illumination. The photocurrent I is strongly dependent on the incident light photon energy hν. The $I^{0.5} = f(h\nu)$ dependence was plotted. Usually, the dependence of the photocurrent on incident light quanta energy is well described by a linear relationship between $I^{0.5}$ and $h\nu$ near the threshold [233, 234]. The linear part of this dependence was extrapolated to the hν axis, and I_p value was determined as the photon energy at the interception point.

The hole drift mobility was measured by xerographic time of flight technique (XTOF) [235, 236] at the Department of Solid State Electronics, Vilnius University. The samples for the hole mobility measurements were prepared by spin-coating the solutions of the synthesized compounds or compositions of synthesized compounds with bisphenol-Z polycarbonate (PC-Z) (Iupilon Z-200 from Mitsubishi Gas Chemical Co.) in weight ratio 1:1 on the polyester films with conductive Al layer. The layer thickness was in the range 5–11 μm. The electric field was created by positive corona charging. The charge carriers were generated at the layer surface by illumination with pulses of nitrogen laser (pulse duration was 2 ns, wavelength 337 nm). The layer surface potential decreases as a result of pulse illumination that was up to 1–5% of initial potential before the illumination. The capacitance probe that was connected to the wide frequency band electrometer measured the speed of the surface potential decrease dU/dt. The transit time t_t was determined by the kink on the curve of the dU/dt transient in double logarithmic scale. The drift mobility was calculated by the formula $\mu = d^2/U_0 t_t$, where d is the layer thickness, U_0 is the surface potential at the moment of illumination.

Perovskite Device Fabrication and Measurements

The method that was used for the measurement of TB derivatives **2a–c**, performed in the Department of Physics, Clarendon Laboratory, University of Oxford. FTO-coated glass sheets (TEC 7, 7Ω/sheet, Pilkington) were etched with zinc powder and 2M HCl to obtain the required electrode pattern. The sheets were washed with 2% Hellmanex in water, deionized water, acetone, ethanol, and iso-propanol. The last traces of organic residues were removed by oxygen plasma cleaning for 10 min. The FTO sheets were subsequently coated with a TiO_2 compact layer with 40 mM Aquarius $TiCl_4$ solution at 70 °C for 60 min, then washed with DI-water and ethanol. The coated FTO substrate was heated at 500 °C for 30 min. C_{60} self-assembled monolayer (SAM) (10 mg/ml in 1,2-dichlorobenzene) was coated on TiO_2 compact layer at 3000 rpm for 30 sec. C_{60}-SAM between the perovskite and the TiO_2 contact is needed to shift the perovskite valence band to lower binding energies [237]. 38wt% perovskite precursor solutions were made by 3 molar of CH_3NH_3I (MAI) and 1 molar of $PbCl_2$ dissolving in dimethylformamide (dehydrate DMF). The Perovskite precursor solution was coated onto the TiO_2/C_{60} by a consecutive two-step spin-

coating process at 1300 rpm for 25 sec and 3000 rpm for 10 sec under low humidity (15–20% at 20 °C) condition with a dry compressed air parching in dry box. The perovskite films were quickly dried by the compressed air blowing for 30 sec for drying the film surface. The perovskite films were drying at 20–25 °C for 15 min and then 70 °C for 15 min on the hot plate. The dried films were annealing at 100 °C for 90 min, then ramp up to 120 °C for 10 min in the box oven without controlling humidity. 32 mg HTMs containing TB core (**2a–c**) was solved in 800 µl cholobenzene with additives of 9 µl *tert*- butylpyridine, 22 µl lithium bis(trifluoromethylsulfonyl)imide salt in acetonitrile (170 mg ml^{-1}) and 17 µl and 8.8 µl Co[t-BuPyPz]$_3$[TFSI]$_3$ in acetonitrile (40 mg ml^{-1}). The HTM solution was coated on the perovskite with spin-coating at 4000 rpm for 30 sec. film 96 mg 2,2(7,7(-tetrakis-(*N*,*N*-di-pmethoxyphenylamine)9,9(-spirobifluorene))) (spiro-OMeTAD) as a reference was solved in 1 ml cholobenzene with additives of 15 µl tert-butylpyridine and 35 µl lithium bis(trifluoromethylsulfonyl)imide salt in acetonitrile (170 mg ml^{-1}). Ag metal contact layer was deposited as the counter electrode on the HTM layer by thermal evaporation. The spiro-OMeTAD solution was coated on the perovskite with spin-coating at 2000 rpm for 45 sec. 50–80 nm Au metal contact layer was deposited as the counter electrode on the HTM layer by thermal evaporation.

The cell performance was evaluated by the current–voltage (*J*-*V*) measurements under simulated solar light (AAB ABET technologies Sun 2000 solar simulator) with its light intensity, 100 mW cm^{-2} (AM 1.5), calibrated against a standard amorphous-silicon PV cell (NREL-calibrated KG5 filtered silicon reference cell). The *J*-*V* curves were measured by short circuit (0.1V) to forward bias (-1.4V) and forward bias (-1.4V) to short circuit (0.1V). The cell aperture area of light incidence was set to 0.0913 cm^2 photoactive area.

The method used for the measurement of TB derivatives **3g** and **3h** was performed in the Department of Physics, Clarendon Laboratory, University of Oxford. FTO-coated glass sheets (TEC 15, 15Ω/sheet, Pilkington) were etched with zinc powder and 2M HCl to obtain the required electrode pattern. The sheets were washed with 2% Hellmanex in water, deionized water, acetone, ethanol, and iso-propanol. The last traces of organic residues were removed by oxygen plasma cleaning for 10 min. The FTO sheets were subsequently coated with a SnO_2 compact layer with 40 mM aqueous $SnCl_4 \cdot 5H_2O$ solution at 70 °C for 60 min, then washed with DI-water and ethanol. The coated FTO substrate was heated at 180 °C for 60 min. C_{60} (10 mg/ml in 1,2-dichlorobenzene) was coated on SnO_2 compact layer at 2000 rpm for 40 sec. C_{60} between the perovskite and the TiO_2 contact is needed to shift the perovskite valence band to lower binding energies [237]. 1.2 M perovskite precursor solutions were made by using formamidinium iodide, CsI, PbI_2, and $PbBr_2$, dissolved in anhydrous DMF, to obtain a stoichiometric solution with desired composition, i.e., $FA_{0.83}CsI_{0.17}PbI_{2.55}Br_{0.45}$. 70 µl of HI and 30 µl of HBr were added into 1 ml of perovskite solution. After the addition of acids, the solution was stirred for 40 h. Perovskite precursor solution was coated onto the SnO_2/C_{60} by a consecutive two-step spin-coating process at 1300 rpm for 20 sec and 3000 rpm for 20 sec under low humidity (7–12% at 20 °C) condition with a dry compressed air parching in dry box.

The perovskite films were quickly treated with the compressed air blowing for 30 sec to dry the film surface. The perovskite films were dried at 20–25 °C for 15 min and then at 70 °C for 15 min on the hotplate. The dried films were annealed at 180 °C for 90 min in the box oven without controlling humidity. 40 mg of **3g** or **3h** was dissolved in 1 ml of cholobenzene. 30 µl *tert*-butylpyridine, 10 µl lithium bis(trifluoromethylsulfonyl)imide salt in acetonitrile (510 mg ml^{-1}), and 17 µl or 20 µl Co[*t*-BuPyPz]$_3$[TFSI]$_3$ in acetonitrile (50 mg ml^{-1}) were added. The HTM solution was coated on the perovskite with spin-coating at 3500 rpm for 30 sec. 87 mg spiro-OMeTAD as a reference was solved in 1 ml cholobenzene with additives of 30 µl *tert*-butylpyridine and 10 µl lithium bis(trifluoromethylsulfonyl)imide salt in acetonitrile (510 mg ml^{-1}). The spiro-OMeTAD solution was coated on the perovskite with spin-coating at 2500 rpm for 45 sec. 50–80 nm Ag metal contact layer was deposited as the counter electrode on the HTM layer by thermal evaporation.

The cell performance was evaluated by the current–voltage (J-V) measurements under simulated solar light (AAB ABET technologies Sun 2000 solar simulator) with its light intensity, 100.6 ± 0.6 mW cm^{-2} (AM 1.5), calibrated against a standard amorphous-silicon PV cell (NREL-calibrated KG5 filtered silicon reference cell). The mismatch factor was estimated to be M=1.035405, and the lamp intensity changes to account for this mismatch. The J-V curves were measured by short circuit (0 V) to forward bias (1.4 V) and forward bias (1.4 V) to short circuit (0 V) in 15 mV s^{-1} scan rate. The cell aperture area of light incidence was set to 0.0913 cm^2 photoactive area by employing an opaque mask. The "stabilized power output" of the devices versus time was measured under load near the maximum power point at the same conditions. The external quantum efficiency (EQE) was measured by using Fourier transform photocurrent spectroscopy. The EQE was measured in short-circuit (J_{sc}) configuration following a 1.4 V prebias for 20s, using a simulated airmass (AM) 1.5 100 mW cm^{-2} sun light as illumination source.

The method used for measurement of TB derivatives **3l**, **4c**, **4d**, and **4e**, performed in the Institute of Chemical Sciences and Engineering, École Polytechnique Fédérale de Lausanne. Fluorine doped tin oxide (FTO) glass (Nippon Sheet Glass) was sequentially cleaned in deionized water, acetone, and isopropanol by using sonication for 15 min, followed by a 15 min UV-ozone treatment. The spray pyrolysis method was applied for the fabrication of TiO_2 blocking layer. A solution containing 0.9 ml of titanium diisopropoxide bis(acetylacetonate) (TAA) (Sigma-Aldrich) in 15 ml of ethanol was sprayed at 450 °C. The mesoporous TiO_2 layer was prepared by spin-coated 40 µl of a solution made of 1 g of commercially available TiO_2 paste (Dyesol 30NRD) in 6 ml of ethanol at 2000 rpm (the acceleration is 1000 rpm/s) for 20 s followed by 500 °C of heat treatment for 30 min. Then, a SnO_2 layer was deposited on the top of UV-ozone treated mesoporous TiO_2 layer by spin-coating 30 µl of the precursor solution containing 12 µl $SnCl_4$ (Acros) dissolved in 988 µl of water at 3000 rpm (the acceleration is 1000 rpm/s) for 30 s, followed by sintering at 190 °C for 1 h. Before the deposition of the perovskite layer, the samples needed another 15 min UV-ozone treatment. The triple cation perovskite layer was prepared based on 1.3 M of $[(FAPbI_3)_{0.87}(MAPbBr_3)_{0.13}]_{0.92}(CsPbI_3)_{0.08}$, containing 178.94 mg

of FAI, 17.41 mg of MABr, 57.06 mg of $PbBr_2$, 27.02 mg of CsI, and 548.60 mg of PbI_2 into 0.78 ml of DMF and 0.22 ml of DMSO (molar ratio of PbI_2: MAI is 1.05: 1). Then, 50 µl of perovskite solution were spin coated at 2000 rpm for 12 s (acceleration 200 rpm/s), followed by 5000 rpm for 30 s (acceleration 3000 rpm/s). 15 s before the end of the process, 110 µl of chlorobenzene were dropped. The sample was annealed at 100 °C for 1 h in the glovebox. For depositing the HTM, 20 mM of the material was dissolved in chlorobenzene. *Tert*-butylpyridine (TBP), tris(2-(1H-pyrazol-1-yl)-4-*tert*-butylpyridine) cobalt(III) (FK209) solution, and tris(bis(trifluoromethylsulfon-yl)imide) (Li-TFSI) solution were applied as dopants (330 mol%, 50 mol%, and 3 mol% respectively). The solution was spin-coated at 4000 rpm for 30 s. Finally, 70 nm of gold was thermal evaporated on the HTM as an electrode.

The morphology of the sample was analyzed by a high-resolution scanning electron microscopy (SEM, ZEISS Merlin). Photoluminescence (PL) spectra were acquired by using a Perkin LS-55 fluorescence spectrometer excited at 600 nm. Photocurrent-photovoltage (*J–V*) curves were measured by using a Keithley 2400 source-measurement-unit under AM1.5G, 100 mW cm^{-2} illumination and certified by a Class AAA, 450 W solar simulator (ORIEL, 94023A). The active area is 0.16 cm^2, and the scan rate is 100 mV s^{-1}. Incident photon-to-electron conversion efficiency (IPCE) spectra was recorded with a Newport 150 W xenon lamp coupled to an Oriel Cornerstone 260 motorized 1/4 m monochromator as the light source, and a 2936-R Power Meter to measure the short-circuit current.

Fabrication and characterization of dye sensitized solar cells

TiO_2 photo-electrodes were prepared on fluorine-doped tin oxide (FTO) glass, which initially was cleaned in an ultrasonic bath with detergent, water, acetone, and ethanol for 30 min respectively. Then, a screen printing technique was used to prepare mesoporous TiO_2 films with an area of 5 × 5 mm^2. The film consists of one transparent layer (8 µm), which was printed with colloidal TiO_2 paste (Dyenamo GPS-30TS) and one 4 µm light-scattering layer (Dyenamo paste DN-GPS-22OS). Before printing the second layer, the film was dried at 125 °C for 6 min. Afterwards, the electrodes were sintered in an oven (Nabertherm Controller P320) in an air atmosphere using a temperature gradient program with four levels at 180 °C (15 min), 320 °C (15 min), 390 °C (15 min), and 500 °C (30 min). Prior to the dye-sensitization, the electrodes were post treated with 40 mM $TiCl_4$ solution for 30 min, followed by heating at 500 °C for 30 min. At a temperature of 90 °C, the electrodes were immersed in a dye bath for 18 h containing either **5D** (0.5 mM), **5E** (0.5 mM), **5F** (0.5 mM) in DCM and **5A** (0.5 mM), **5B** (0.5 mM), **5C** (0.5 mM) in DCM:MeOH (4:1 v/v), or N719 (0.3 mM) and D35 (0.2 mM) in *tert*-butanol: acetonitrile (1:1 v/v). Any non-attached dye was removed with solvent used for the dye bath. The counter electrodes were prepared by depositing 10 µL of a H_2PtCl_6 solution in ethanol (5 mM) to FTO glass substrates followed by heating in the air at 400 °C for 30 min. The solar cells were assembled by sandwiching the photoelectrode and the counter electrode by using a 25 µm thick thermoplastic Surlyn frame. An electrolyte solution was injected through a hole predrilled in the counter electrode by vacuum back filling, and the cell was sealed

with thermoplastic Surlyn cover and a microscope glass coverslip. The electrolyte consists of LiI (0.1 M), I_2 (0.05 M), 1-butyl-3-methylimidazolium iodide (BMII, 0.6 M), and 4-*tert*-butylpyridine (TBP, 0.5 M) in acetonitrile. Three solar cells were made with every dye.

Current-voltage (IV) characteristics were determined by using a combination of a source measurement unit (Keithley 2400) and a solar simulator (Newport, model 91160). The solar simulator provided light with AM 1.5 G spectral distribution and was calibrated to an intensity of 100 mW cm^{-2} by using a certified reference solar cell (Fraunhofer ISE). On the top of the DSC, a black metal mask with an aperture of 5 × 5 mm^2 was applied. Incident photon-to-current conversion efficiency (IPCE) spectra were measured with a computer-controlled setup comprising a xenon light source (Spectral Products ASB-XE-175), a monochromator (Spectral Products CM110), and a Keithley multimeter (model 2700). The IPCE spectra were calibrated by using a certified reference solar cell (Fraunhofer ISE).

Computational Details

The theoretical calculations were performed by using TURBOMOLE version 7.0 software [238]. The molecular structure of the investigated compounds was optimized by using Becke's three parameter functional, B3LYP [239, 240], and the def2-SVP [241, 242] basis set in vacuum. The optimized structures and the molecular orbitals were visualized with TmoleX version 4.1 software [243].

4.2. Materials

All chemicals were purchased from Aldrich or TCI Europe and used as received without further purification. Diatomaceous earth (Celite® 500 fine, Sigma-Aldrich) was used for filtering where mentioned.

Bis(4-methoxyphenyl)amine [154], 4-methoxy-*N*-(4-methoxyphenyl)-3-methylaniline [144], and 4-methoxy-*N*-(*p*-tolyl)aniline [155] were synthesized according to the procedures reported earlier. 2,2-Bis(4-methoxyphenyl)acetaldehyde and 2,2-bis(4-methylphenyl)acetaldehyde were synthesized according to the published procedure [244]. The intermediate compounds **3a-e** were synthesized according to the modified procedures reported in the literature [245–247]. The brominated TB cores **3i** and **3j** were prepared by the reported method [248]. 2,8-Dinitro-4,10-dimethyl-6*H*,12*H*-5,11-methanodibenzo[1,5]-diazocine (**4a**) and 2,8-diamino-4,10-dimethyl-6*H*,12*H*-5,11-methanodibenzo[1,5]-diazocine (**4b**) were synthesized according to the procedure reported earlier [44]. 2-(4-Bromophenyl)-5,5-dimethyl-1,3-dioxane (**5n**) [220] was synthesized according to the earlier reported procedure. Boronic acid TB derivative **7b** was synthesized based on the literature [71]. 1,2,2-Triphenylethenyl-(4′-phenylene) boronic acid (**7f**) was synthesized according to the literature [249].

2,8-Dibromo-4,10-dimethyl-6H,12H-5,11-methanodibenzo[b,f]- diazocine (**1'**)

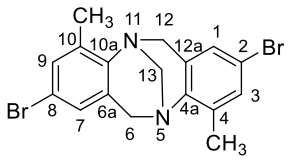

TFA (50 ml) was slowly poured into a stirring mixture of the 4-bromo-2-methylaniline (4.65 g, 25 mmol) and 37% formaldehyde aqueous solution (3.72 ml, 50 mmol), the temperature was slowly raised to 60 °C, and stirring was continued for 2h. TFA was removed under reduced pressure; the water (25 ml) was added followed by the addition of a saturated aqueous solution of NH_3 (25 ml). The aqueous layer was extracted with ethyl acetate. The organic layer was dried over anhydrous Na_2SO_4, filtered; the solvent was removed under reduced pressure, resulting in slightly yellowish solid, which was used without further purification. Yield: 4.3 g (85%).

^{1}H NMR (400 MHz, $CDCl_3$): δ 7.18 (d, *J* = 1.6 Hz, 2H, H-3, and H-9), 6.90 (d, *J*= 1.6 Hz, 2H, H-1, and H-7), 4.51 (d, *J* = 16.9 Hz, 2H, H-6*exo*, and H-12*exo*), 4.24 (s, 2H, H-13), 3.89 (d, *J* = 17.0 Hz, 2H, H-6*endo*, and H-12*endo*), 2.35 (s, 6H, 2× CH_3).

^{13}C NMR (101 MHz, $CDCl_3$) δ 144.82, 135.34, 131.78 (C-3 and C-9), 129.90, 127.09 (C-1 and C- 7), 116.81, 67.27 (C-13), 54.63 (C- 6 and C-12), 16.79 (2× CH_3).

Anal. calcd. for $C_{17}H_{16}Br_2N_2$: C 50.03, H 3.95, N 6.86; found: C 50.09, H 3.93, N 6.75.

4,10-Dimethyl-N^2,N^2,N^8,N^8-tetraphenyl-6H,12H-5,11-methanodibenzo-[b,f][1,5]diazocine-2,8-diamine (**1a**)

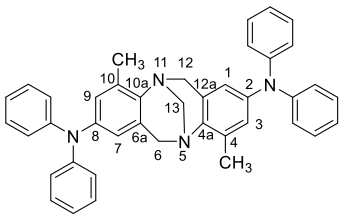

2,8-Dibromo-4,10-dimethyl-6*H*,12*H*-5,11-methanodibenzo[*b*,*f*][1,5]-diazocine (**1'**) (2.03 g, 5 mmol) and diphenylamine (2.539 g, 15 mmol) were dissolved in toluene (11 ml per gram of **1'**) and stirred under argon atmosphere for 30 min; tri-*tert*-butylphosphonium tetrafluoroborate (0.039 g, 0.135 mmol) (0.027 equiv.), palladium (II) acetate (0.0225 g, 0.1 mmol), and sodium *tert*-butoxide (1.4415 g, 15 mmol) were added, and the mixture was heated at reflux for 5 hours. After the termination of the reaction (TLC: acetone/ *n*-hexane, 3:22, v/v), the mixture was diluted with THF and filtered through Celite. The solvent was partially removed until ~30 ml of mixture remained; ~4 ml of acetone was added, and the mixture slowly evaporated further until the crystallization started. The mixture was left to cool down; the crystals were filtered and washed with acetone, resulting in 2.38 g of crystals. The product was further purified by recrystallization from THF and acetone mixture (10:1) to give fine white crystals (67%, 1.95 g). M.p. 158 °C.

^{1}H NMR (400 MHz, $CDCl_3$) δ 7.28–7.20 (m, 8H, Ar), 7.06 (d, *J* = 7.6 Hz, 8H, Ar), 7.00 (t, *J* = 7.3 Hz, 4H, *p*-Ph), 6.85 (d, *J* = 2.2 Hz, 2H, H-3, and H-9), 6.55 (d, *J* = 2.3 Hz, 2H, H-1, and H-7), 4.48 (d, *J* = 16.9 Hz, 2H, H-6*exo*, and H-12*exo*), 4.32 (s, 2H, H-13), 3.89 (d, *J* = 17.0 Hz, 2H, H-6*endo*, and H-12*endo*), 2.29 (s, 6H, 2× CH_3).

^{13}C NMR (101 MHz, $CDCl_3$): δ 147.97, 143.28, 141.54, 133.99, 129.13, 128.89, 125.33, 123.78, 122.25, 120.23, 67.64 (C-13), 54.94 (C-6 and C-12), 17.08 (2× CH_3).

Anal. calcd. for $C_{41}H_{36}N_4$: C 84.21, H 6.21, N 9.58; found: C 84.33, H 6.08, N 9.59.

N^2,N^2,N^8,N^8-tetrakis(4-methoxyphenyl)-4,10-dimethyl-6H,12H-5,11-methanodibenzo[b,f][1,5]diazocine-2,8-diamine (**1b**)

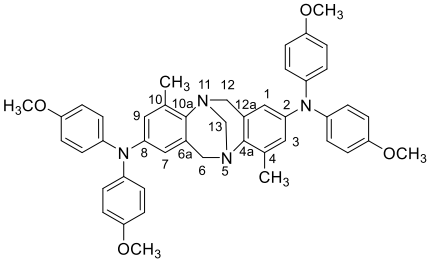

2,8-Dibromo-4,10-dimethyl-6*H*,12*H*-5,11-methanodibenzo[*b*,*f*][1,5]-diazocine (**1'**) (0.325 g, 0.8 mmol) and bis(4-methoxyphenyl)amine (0.55 g, 2.4 mmol) were dissolved in toluene (5 ml) and stirred under argon atmosphere for 30 min.; tri-*tert*-butylphosphonium tetrafluoroborate (0.0063 g, 0.0216 mmol), palladium (II) acetate (0.0036 g, 0.016 mmol), and sodium *tert*-butoxide (0.23 g, 2.4 mmol) were added, and the mixture was heated at reflux for 6 hours. After the termination of the reaction (TLC: acetone/ *n*-hexane, 3:22, v/v), the mixture was diluted with THF and filtered through Celite. The water was added, and the mixture was extracted with ethyl acetate. The organic layer was dried over anhydrous Na_2SO_4, filtered, and the solvent was removed under reduced pressure. The material was purified by column chromatography (acetone/*n*-hexane 1:20) to give slightly grayish solid (73%, 0.41 g).

^{1}H NMR (400 MHz, $CDCl_3$) δ 6.98 (d, *J* = 8.8 Hz, 8H, Ar), 6.79 (d, *J* = 8.8 Hz, 8H, Ar), 6.67 (s, 2H, H-3, and H-9), 6.34 (d, *J* = 1.5 Hz, 2H, H-1, and H-7), 4.44 (d, *J* = 16.5 Hz, 2H, H-6*exo*, and H-12*exo*), 4.31 (s, 2H, H-13), 3.80 (m, 14H, 4× OCH_3, H-6*endo*, and H-12*endo*), 2.24 (s, 6H, 2× TB-CH_3).

^{13}C NMR (101 MHz, $CDCl_3$) δ 155.52, 144.77, 143.09, 141.24, 133.60, 128.77, 126.20, 122.08, 116.50, 114.62, 67.95, 55.48, 55.02, 17.18.

Anal. calcd. for $C_{45}H_{44}N_4O_4$: C 76.68, H 6.29, N 7.95; found: C 76.71, H 6.28, N 7.88.

N^2,*N^8*-bis(4-methoxy-3-methylphenyl)-*N^2*,*N^8*-bis(4-methoxyphenyl)-4,10-dimethyl-6*H*,12*H*-5,11-methanodibenzo[*b*,*f*][1,5]diazocine-2,8-diamine (**1c**)

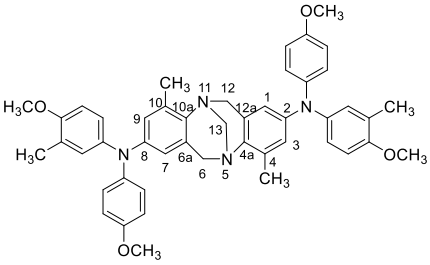

2,8-Dibromo-4,10-dimethyl-6*H*,12*H*-5,11-methanodibenzo[*b*,*f*][1,5]-diazocine (**1'**) (1.015 g, 2.5 mmol) and 4-methoxy-*N*-(4-methoxyphenyl)-3-methylaniline (1.824 g, 7.5 mmol) were dissolved in toluene (14 ml) and stirred under argon atmosphere for 30 min; tri-*tert*-butylphosphonium tetrafluoroborate (0.020 g, 0.07 mmol), palladium (II) acetate (0.012 g, 0.05 mmol), and sodium *tert*-butoxide (0.721 g, 7.5 mmol) were added, and the mixture was heated at reflux for 6 hours. After the termination of the reaction (TLC: acetone/ *n*-hexane, 3:22, v/v), the mixture was diluted with THF and filtered through Celite. The organic layer was dried over anhydrous Na_2SO_4, filtered, and the solvent was removed under reduced pressure. The material was purified by column chromatography (THF/*n*-hexane 1:16). The material (1.13 g, 62%) still had some impurities, and it was noticed that it tends to crystallize. A recrystallization form THF and acetone mixture (10:1) was performed, but minor impurities remained. The material was further purified by

column chromatography (acetone /*n*-hexane 2:23) to give 480 mg of pure material as white solid; moreover, 280 mg of pure material were recovered from the part that crystallized within the column by washing removed silica gel with hot THF, overall resulting in 0.76 g of pure product (41%).
^{1}H NMR (400 MHz, $CDCl_3$) δ 7.07–6.95 (m, 4H, Ar), 6.94–6.77 (m, 8H, Ar), 6.77–6.65 (m, 4H, Ar), 6.37 (d, *J* = 2.3 Hz, 2H, H-1, and H-7), 4.44 (d, *J* = 16.9 Hz, 2H, H-6*exo*, and H-12*exo*), 4.30 (s, 2H, H-13), 3.88–3.75 (m, 14H, 4× OCH_3, H-6*endo*, and H-12*endo*), 2.25 (s, 6H, 2× TB-CH_3), 2.17 (s, 6H, 2× Ph-CH_3).
^{13}C NMR (101 MHz, $CDCl_3$) δ 155.22, 153.85, 144.60, 141.57, 140.79, 139.58, 133.51, 128.67, 127.87, 127.53, 125.94, 123.46, 121.98, 116.57, 114.50, 110.59, 68.01, 55.53, 55.48, 55.12, 17.13, 16.34.
Anal. calcd. for $C_{47}H_{48}N_4O_4$: C 77.02, H 6.60, N 7.64; found: C 76.92, H 6.63, N 7.56.

N^2,N^8-bis(4-methoxyphenyl)-4,10-dimethyl-N^2,N^8-di-p-tolyl-6H,12H-5,11-methanodibenzo[b,f][1,5]diazocine-2,8-diamine (**1d**)

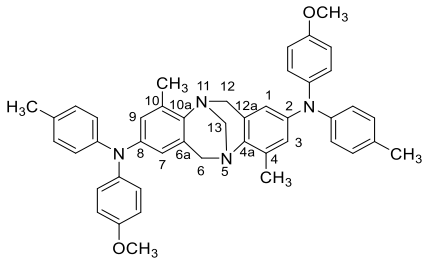

2,8-Dibromo-4,10-dimethyl-6*H*,12*H*-5,11-methanodibenzo[*b*,*f*][1,5]-diazocine (**1'**) (1.015 g, 2.5 mmol) and 4-methoxy-*N*-(*p*-tolyl)aniline (1.6 g, 7.5 mmol) were dissolved in toluene (14 ml) and stirred under argon atmosphere for 30 min, tri-*tert*-butylphosphonium tetrafluoroborate (0.020 g, 0.07 mmol), palladium (II) acetate (0.012 g, 0.05 mmol), and sodium *tert*-butoxide (0.721 g, 7.5 mmol) were added, and the mixture was heated at reflux for 5 hours. After the termination of the reaction (TLC: acetone/ *n*-hexane, 3:22, v/v), the mixture was diluted with THF and filtered through Celite. Some crystals were observed; thus, the solvent was removed until ~20 ml of mixture remained; ~1 ml of methanol was slowly added, and the mixture slowly evaporated further until the crystallization intensified. The mixture was left to cool down; the crystals were filtered and washed with ethanol. The material was further purified by column chromatography (THF/*n*-hexane 2:23) to give slightly grayish solid (62%, 1.05 g).
^{1}H NMR (400 MHz, $CDCl_3$) δ 7.08–6.76 (m, 16H, Ar), 6.73 (s, 2H, H-3, and H-9), 6.41 (s, 2H, H-1, and H-7), 4.44 (d, *J* = 15.3 Hz, 2H, H-6*exo*, and H-12*exo*), 4.31 (s, 2H, H-13), 3.90–3.73 (m, 8H, 4× OCH_3, H-6*endo*, and H-12*endo*), 2.38–2.18 (m, 12H, 4× CH_3).
^{13}C NMR (101 MHz, $CDCl_3$) δ 155.80, 145.69, 142.85, 141.02, 135.37, 133.67, 131.56, 130.73, 129.75, 129.60, 126.84, 123.45, 123.19, 114.66, 68.02, 55.47, 54.95, 20.76, 17.15.
Anal. calcd. for $C_{45}H_{44}N_4O_2$: C 80.33, H 6.59, N 8.33; found: C 80.31, H 6.62, N 8.19.

4,10-Dimethyl-N^2,N^2,N^8,N^8-tetrakis(4-((E)-2-phenylprop-1-en-1-yl)phenyl)-6H,12H-5,11-methanodibenzo[b,f][1,5]diazocine-2,8-diamine (**2a**)

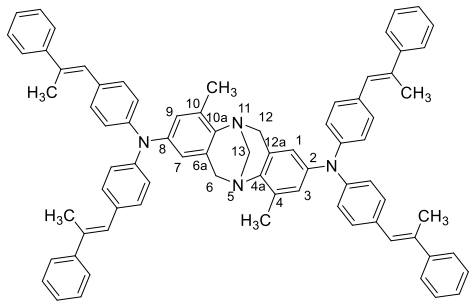

4,10-Dimethyl-N^2,N^2,N^8,N^8-tetraphenyl-6*H*,12*H*-5,11-methanodibenzo-[*b*,*f*][1,5]diazocine-2,8-diamine (**1a**) (0.702 g, 1.20 mmol) and (+/-)-camphor-10-sulfonic acid (0.753 g, 3.24 mmol) were dissolved in toluene (3.5 ml + volume of the Dean-Stark trap) and stirred at 80 °C for 15 min. 2-Phenylpropionaldehyde (1.288 g, 9.60 mmol) was added, and the reaction mixture was refluxed 18 hours by using Dean-Stark trap (TLC THF/ *n*-hexane, 1:24, v/v). After the termination of the reaction, the solution was mixed with water and extracted with ethyl acetate. The organic layer was dried over anhydrous Na_2SO_4, filtered; the solvent was removed under reduced pressure, and the residue purified by column chromatography (acetone/*n*-hexane 1:35 and ethyl acetate/toluene/*n*-hexane 1:19:30, *v*/*v*) to give bright yellow powder (39%, 0.49 g).

^{1}H NMR (700 MHz, $CDCl_3$) δ 7.53–7.46 (m, 6H, Ar), 7.40–7.17 (m, 22H, Ar), 7.10–7.02 (m, 6H, Ar), 6.98 (d, *J* = 8.5 Hz, 2H, Ar), 6.91–6.86 (m, 2H, Ar), 6.82–6.71 (m, 6H, Ar), 4.49 (d, *J* = 17.0 Hz, 2H, H-6*exo*, and H-12*exo*), 4.32 (s, 2H, H-13), 3.91 (d, *J* = 17.0 Hz, 2H, H-6*endo*, and H-12*endo*), 2.39–2.22 (m, 18H, 6× CH_3).

^{13}C NMR (176 MHz, $CDCl_3$) δ 146.09, 144.31, 142.53, 136.26, 134.15, 132.39, 130.04, 129.93, 129.57, 128.53, 128.31, 128.25, 128.08, 127.33, 127.31, 126.98, 126.95, 126.83, 125.95, 125.65, 123.21, 67.97, 54.96, 17.74, 17.72.

Anal. calcd. for $C_{77}H_{68}N_4$: C 88.13, H 6.53, N 5.34; found: C 88.27, H 6.32, N 5.41.

N^2,N^2,N^8,N^8-Tetrakis(4-(2,2-diphenylvinyl)phenyl)-4,10-dimethyl-6H,12H-5,11-methanodibenzo[b,f][1,5]diazocine-2,8-diamine (**2b**)

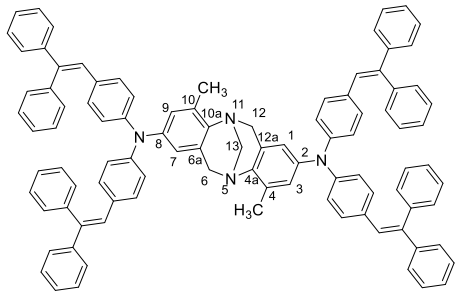

4,10-Dimethyl-N^2,N^2,N^8,N^8-tetraphenyl-6*H*,12*H*-5,11-methanodibenzo-[*b*,*f*][1,5]diazocine-2,8-diamine **(1a)** (0.503 g, 0.86 mmol) and (+/-)-camphor-10-sulfonic acid (0.539 g, 2.32 mmol) were dissolved in toluene (2.5 ml + volume of the Dean-Stark trap) and stirred at 80 °C for 15 min. Diphenylacetaldehyde (1.013 g, 5.16 mmol) was added, and the reaction mixture was refluxed for 40 hours by using Dean-Stark trap (TLC: THF/*n*-hexane, 3:22, v/v). After the termination of the reaction, the solution was mixed with water and extracted with ethyl acetate. The organic layer was dried over anhydrous Na_2SO_4, filtered; the solvent was removed under reduced pressure, and the residue purified by column chromatography (THF/*n*-hexane 3:22, *v*/*v*) to give bright yellow powder (42%, 0.47 g).

^{1}H NMR (700 MHz, $CDCl_3$) δ 7.43–7.13 (m, 40H, Ar), 6.95–6.78 (m, 12H, Ar), 6.78–6.65 (m, 10H, Ar), 6.43 (s, 2H, H-1, and H-7), 4.38 (d, *J* = 17.0 Hz, 2H, H-6*exo*, and

H-12*exo*), 4.21 (s, 2H, H-13), 3.79 (d, *J* = 17.0 Hz, 2H, H-6*endo*, and H-12*endo*), 2.22 (s, 6H, 2× CH_3).
^{13}C NMR (176 MHz, $CDCl_3$) δ 146.14, 143.53, 142.45, 142.00, 140.77, 140.69, 134.00, 131.27, 130.27, 128.86, 128.73, 128.17, 127.56, 127.33, 127.21, 125.78, 122.71, 120.80, 67.97, 54.80, 16.97.
Anal. calcd. for $C_{97}H_{76}N_4$: C 89.78, H 5.90, N 4.32; found: C 89.95, H 5.93, N 4.12.

N^2,N^2,N^8,N^8-Tetrakis(4-(2,2-bis(4-methoxyphenyl)vinyl)phenyl)-4,10-dimethyl-6H,12H-5,11-methanodibenzo[b,f][1,5]diazocine-2,8-diamine (**2c**)

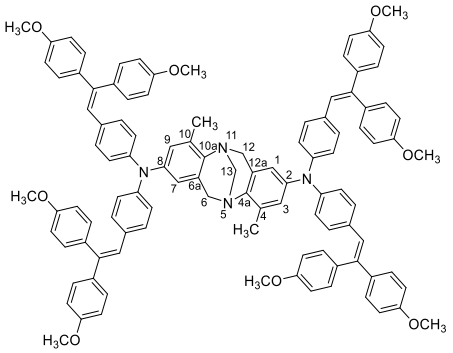

4,10-Dimethyl-N^2,N^2,N^8,N^8-tetraphenyl-6*H*,12*H*-5,11-methanodibenzo-[*b*,*f*][1,5]diazocine-2,8-diamine (**1a**) (1.11 g, 1.90 mmol) and (+/-)-camphor-10-sulfonic acid (1.54 g, 6.65 mmol) were dissolved in toluene (2.5 ml + volume of the Dean-Stark trap) and stirred at 80 °C for 15 min. Bis(4-methoxyphenyl)acetaldehyde (2.922 g, 11.40 mmol) was added, and the reaction mixture was refluxed for 20 hours by using Dean-Stark trap (TLC acetone: *n*-hexane, 2:23, v/v). After the termination of the reaction, the solution was mixed with water and extracted with ethyl acetate. The organic layer was dried over anhydrous Na_2SO_4, filtered; the solvent was removed under reduced pressure, and the residue purified by column chromatography (acetone/*n*-hexane 1/16 and acetone/toluene/*n*-hexane 3/10/12, *v*/*v*) to give bright yellow powder (41%, 1.21 g).
^{1}H NMR (700 MHz, $CDCl_3$) δ 7.32–7.26 (m, 2H, Ar), 7.25–7.21 (m, 4H, Ar), 7.19–7.08 (m, 8H, Ar), 7.07–6.72 (m, 38H, Ar), 6.71–6.62 (m, 4H, Ar), 4.43 (d, *J* = 9.3 Hz, 2H, H-6*exo*, and H-12*exo*), 4.25 (s, 2H, H-13), 3.90–3.70 (m, 26H, 8× OCH_3, H-6*endo*, and H-12*endo*), 2.26 (s, 6H, 2× CH_3).
^{13}C NMR (176 MHz, $CDCl_3$) δ 159.02, 158.86, 158.10, 140.01, 139.66, 136.59, 132.99, 131.54, 131.47, 131.42, 130.62, 130.20, 130.04, 128.64, 128.61, 128.57, 125.69, 114.11, 114.07, 113.63, 113.53, 113.41, 55.31, 55.19, 55.14, 29.69, 17.04.
Anal. calcd. for $C_{105}H_{92}N_4O_8$: C 82.00, H 6.03, N 3.64; found: C 81.88, H 6.05, N 3.73.

N^4,$N^{4'}$-di-p-tolyl-(1,1'-biphenyl)-4,4'-diamine (**3a**)

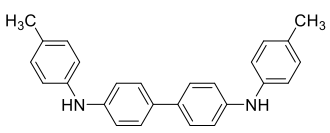

2-Dicyclohexylphosphino-2′,6′-dimethoxybiphenyl (SPhos) (0.099 g, 0.240 mmol) and palladium (II) acetate (0.018 g, 0.080 mmol) were dissolved in anhydrous dioxane (16.3 ml, 5 ml per gram of 4,4'-diiodobiphenyl) and stirred under argon atmosphere at 80 °C for 10 min. 4,4'-Diiodobiphenyl (3.248 g, 8 mmol), *p*-toluidine (1.757 g, 16.4 mmol) and sodium *tert*-butoxide (2.153 g, 22.40 mmol) were added, and the mixture was heated at reflux for an hour. After the termination of the reaction, the mixture was diluted with THF and filtered through Celite. The solvent was

removed, the residue was dissolved in hot THF, and *n*-hexane was added. The mixture was left to cool down, and the formed solid was filtered and washed with *n*-hexane to give fine white crystals (75%, 2.2 g), m.p. 232 °C.
^{1}H NMR (400 MHz, DMSO+$CDCl_3$) δ 7.38 (d, *J* = 6.8 Hz, 4H, Ar), 7.21–6.75 (m, 12H, Ar), 2.23 (s, 6H, 2× CH_3). NH protonic signals are not observed.
^{13}C NMR (101 MHz, DMSO+$CDCl_3$) δ 140.37, 139.77, 129.80, 129.13, 126.73, 126.60, 117.92, 116.79, 20.77.
Anal. calcd. for $C_{26}H_{24}N_2$: C 85.68, H 6.64, N 7.69; found: C 85.86, H 6.52, N 7.62.

N^4,$N^{4'}$-bis(4-methoxyphenyl)-(1,1'-biphenyl)-4,4'-diamine (**3b**)

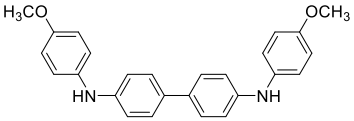

2-Dicyclohexylphosphino-2′,4′,6′-triisopropylbiphenyl (XPhos) (0.229 g, 0.480 mmol) and palladium (II) acetate (0.036 g, 0.160 mmol) were dissolved in anhydrous dioxane (32.8 ml, 6.5 ml per gram of 4,4'-dibromobiphenyl) and stirred under argon atmosphere at 80 °C for 10 min. 4,4'-Dibromobiphenyl (4.992 g, 16 mmol), *p*-anisidine (4.040 g, 32.8 mmol), and sodium *tert*-butoxide (4.305 g, 44.80 mmol) were added, and the mixture was heated at reflux for 3 hours. After the termination of the reaction, the mixture was diluted with THF and filtered through Celite passivated with 2% triethylamine solution in THF. The solvent was removed, the residue dissolved in hot THF, and ethyl acetate was added. The mixture was left to cool down, and the formed solid was filtered and washed with *n*-hexane to give fine white crystals (72%, 4.54 g), m.p. 227 °C.
^{1}H NMR (400 MHz, DMSO+$CDCl_3$) δ 7.75 (s, 2H, NH), 7.36 (d, *J* = 8.3 Hz, 4H, Ar), 7.14–6.89 (m, 8H, Ar), 6.89–6.73 (m, 4H, Ar), 3.72 (s, 6H, 2× OCH_3).
^{13}C NMR (101 MHz, DMSO+$CDCl_3$) δ 154.17, 143.99, 136.67, 131.07, 126.71, 120.60, 115.77, 114.80, 55.57.
Anal. calcd. for $C_{26}H_{24}N_2O_2$: C 78.76, H 6.10, N 7.07; found: C 78.97, H 5.93, N 7.02.

N^4-(4-methoxyphenyl)-N^4,$N^{4'}$-diphenyl-(1,1'-biphenyl)-4,4'-diamine (**3c**)

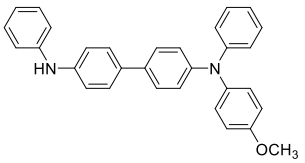

2-Dicyclohexylphosphino-2′,6′-dimethoxybiphenyl (SPhos) (0.055 g, 0.135 mmol) and palladium (II) acetate (0.010 g, 0.045 mmol) were dissolved in anhydrous dioxane (9 ml, 3 ml per gram of *N*,*N*-diphenylbenzidine) under argon atmosphere and stirred at 80 °C for 5 min, *N*,*N*-diphenylbenzidine (3.028 g, 9 mmol), 4-iodoanisole (2.106 g, 9 mmol), and sodium *tert*-butoxide (1.211 g, 12.6 mmol) were added, and the mixture was heated at reflux for 3 hours. After the termination of the reaction, the solution was mixed with water and extracted with ethyl acetate. The organic layer was dried over anhydrous Na_2SO_4, filtered; the solvent was removed, and the residue purified by column chromatography (THF/*n*-hexane 1/24, *v*/*v*) to give slightly gray solid product (45%, 1.78 g).
^{1}H NMR (400 MHz, $CDCl_3$) δ 7.40 (d, *J* = 8.1 Hz, 4H, Ar), 7.25–7.18 (m, 4H, Ar), 7.14–6.91 (m, 12H, Ar), 6.90–6.77 (m, 2H, Ar), 3.80 (s, 3H, OCH_3). NH protonic signals are not observed.

^{13}C NMR (101 MHz, $CDCl_3$) δ 156.24, 147.06, 140.65, 127.36, 127.15, 123.08, 122.85, 114.80, 55.50.
Anal. calcd. for $C_{31}H_{26}N_2O$: C 84.13, H 5.92, N 6.33; found: C 84.41, H 6.10, N 6.45.

N^4,N^4,$N^{4'}$-tri-p-tolyl-(1,1'-biphenyl)-4,4'-diamine (**3d**)

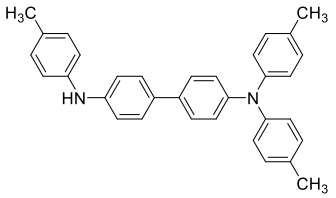

2-Dicyclohexylphosphino-2′,6′-dimethoxybiphenyl (SPhos) (0.046 g, 0.111 mmol) and palladium (II) acetate (0.008 g, 0.037 mmol) were dissolved in anhydrous dioxane (15 ml, 5.5 ml per gram of **3a**) under argon atmosphere and stirred at 80 °C for 5 min; N^4,$N^{4'}$-di-*p*-tolyl-[1,1'-biphenyl]-4,4'-diamine (**3a**) (2.697 g, 7.4 mmol), 4-iodtoluene (1.613 g, 7.4 mmol), and sodium *tert*-butoxide (1.00 g, 10.36 mmol) were added, and the mixture was heated at reflux for 5 hours. After the termination of the reaction, the mixture was diluted with THF and filtered through Celite; the solvent was removed, and the residue was purified by column chromatography (acetone/*n*-hexane 1/24, *v*/*v*) to give light gray powder (38%, 1.27 g).
^{1}H NMR (400 MHz, $CDCl_3$) δ 7.39 (d, *J* = 8.6 Hz, 4H, Ar), 7.13–6.90 (m, 16H, 8H, Ar), 2.30 (s, 18H, 6× CH_3). NH protonic signals are not observed.
^{13}C NMR (101 MHz, $CDCl_3$) δ 145.33, 141.25, 136.64, 133.93, 132.43, 129.94, 129.88, 127.07, 124.87, 124.55, 123.20, 122.94, 119.59, 20.83.
Anal. calcd. for $C_{33}H_{30}N_2$: C 87.19, H 6.65, N 6.16; found: C 87.02, H 6.90, N 6.08.

N^4,N^4,$N^{4'}$-tris(4-methoxyphenyl)-(1,1'-biphenyl)-4,4'-diamine (**3e**)

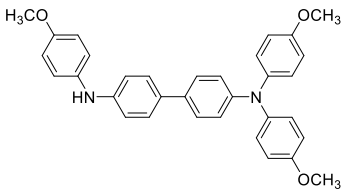

2-Dicyclohexylphosphino-2′,6′-dimethoxybiphenyl (SPhos) (0.068 g, 0.165 mmol) and palladium (II) acetate (0.012 g, 0.055 mmol) were dissolved in anhydrous dioxane (35 ml, 8 ml per gram of **3b**) under argon atmosphere and stirred at 80 °C for 5 min; N^4,$N^{4'}$-bis(4-methoxyphenyl)-[1,1'-biphenyl]-4,4'-diamine (**3b**), (4.361 g, 11 mmol), 4-iodoanisole (2.574 g, 11 mmol), and sodium *tert*-butoxide (1.480 g, 15.4 mmol) were added, and the mixture was heated at reflux for 3 hours. After the termination of the reaction, the mixture was diluted with THF and filtered through Celite passivated with 2% triethylamine solution in THF; the solvent was removed, and the residue was purified by the column chromatography (THF/*n*-hexane 1/30, *v*/*v*) (silica gel in column was passivated with 2% triethylamine solution in THF beforehand) to give light gray powder (41%, 2.27 g).
^{1}H NMR (400 MHz, $CDCl_3$) δ 7.49–7.30 (m, 4H, Ar), 7.07 (d, *J* = 8.5 Hz, 6H, Ar), 6.97 (d, *J* = 7.6 Hz, 4H, Ar), 6.90–6.79 (m, 6H, Ar), 3.79 (s, 9H, 3× OCH_3). NH protonic signals are not observed.
^{13}C NMR (101 MHz, $CDCl_3$) δ 155.71, 147.36, 141.14, 126.85, 126.80, 126.37, 121.23, 114.76, 114.68, 55.61, 55.52.
Anal. calcd. for $C_{33}H_{30}N_2O_3$: C 78.86, H 6.02, N 5.57; found: C 78.59, H 6.15, N 5.46.

N^4,$N^{4'}$-(4,10-dimethyl-6H,12H-5,11-methanodibenzo[b,f][1,5]diazocine-2,8-diyl)bis-$N^{4'}$-(4-methoxyphenyl)-N^4,$N^{4'}$-diphenyl-(1,1'-biphenyl)-4,4'-diamine (**3f**)

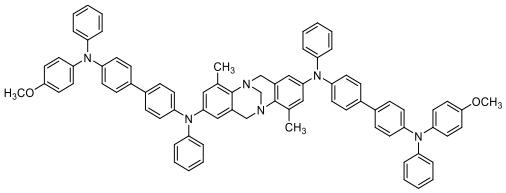

2,8-Dibromo-4,10-dimethyl-6*H*,12*H*-5,11-methanodibenzo[*b*,*f*][1,5]diazocine (0.2842 g, 0.7 mmol) and N^4-(4-methoxyphenyl)-N^4,$N^{4'}$-diphenyl-[1,1'-biphenyl]-4,4'-diamine (**3c**) (0.929 g, 2.1 mmol) were dissolved in anhydrous toluene (6 ml) and stirred under argon atmosphere for 30min. Tri-*tert*-butylphosphonium tetrafluoroborate (0.006 g, 0.019 mmol) and palladium (II) acetate (0.003 g, 0.014 mmol) were added, and the mixture was stirred for another 10 minutes. Finally, sodium *tert*-butoxide (0.202 g, 2.100 mmol) was added, and the mixture was heated at reflux for 6 hours. After the termination of the reaction, the mixture was diluted with THF and filtered through Celite; the solvent was removed, and the residue was purified by column chromatography (THF/toluene/*n*-hexane 1:19:30, *v*/*v*) to give light gray powder (61%, 0.483 g).

^{1}H NMR (400 MHz, $CDCl_3$) δ 7.40 (d, *J* = 8.1 Hz, 8H, Ar), 7.25–7.18 (m, 8H, Ar), 7.14–6.91 (m, 24H, Ar), 6.90–6.77 (m, 6H, Ar), 6.55 (d, *J* = 2.2 Hz, 2H, H-1, and H-7), 4.47 (d, *J* = 16.9 Hz, 2H, H-6*exo*, and H-12*exo*), 4.31 (s, 2H, H-13), 3.87 (d, *J* = 17.1 Hz, 2H, H-6*endo*, and H-12*endo*), 3.80 (s, 6H, 2× OCH_3), 2.27 (s, 6H, 2× CH_3).

^{13}C NMR (101 MHz, $CDCl_3$) δ 156.23, 148.02, 147.83, 147.05, 146.71, 140.64, 134.05, 133.91, 129.19, 129.12, 127.35, 127.16, 127.14, 125.34, 123.99, 123.82, 123.07, 122.84, 122.45, 122.00, 120.21, 114.80, 55.50, 54.94, 29.72, 17.11.

Anal. calcd. for $C_{79}H_{66}N_6O_2$: C 83.86, H 5.88, N 7.43; found: C 83.94, H 6.07, N 7.13.

N^4,$N^{4'}$-(4,10-dimethyl-6H,12H-5,11-methanodibenzo[b,f][1,5]diazocine-2,8-diyl)bis(N^4,$N^{4'}$,$N^{4'}$-tri-p-tolyl-[1,1'-biphenyl]-4,4'-diamine) (**3g**)

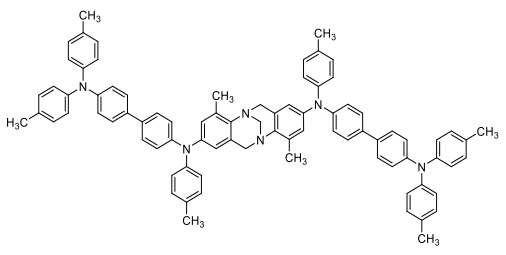

2,8-Dibromo-4,10-dimethyl-6*H*,12*H*-5,11-methanodibenzo[*b*,*f*][1,5]diazocine (0.365 g, 0.90 mmol) and N^4,N^4,$N^{4'}$-tri-*p*-tolyl-[1,1'-biphenyl]-4,4'-diamine (**3d**) (1.228 g, 2.70 mmol) were dissolved in anhydrous toluene (8 ml) and stirred under argon atmosphere for 30 min. Tri-*tert*-butylphosphonium tetrafluoroborate (0.007 g, 0.024 mmol) and palladium (II) acetate (0.004 g, 0.018 mmol) were added, and the mixture was stirred for another 10 minutes. Finally, sodium *tert*-butoxide (0.259 g, 2.70 mmol) was added, and the mixture was heated at reflux for 6 hours. After the termination of the reaction, the mixture was diluted with THF and filtered through Celite; the solvent was removed, and the residue was purified by column chromatography (ethyl acetate/toluene/*n*-hexane 1:30:19, *v*/*v*) to give light gray powder (43%, 0.441 g).

^{1}H NMR (400 MHz, $CDCl_3$) δ 7.39 (d, *J* = 8.6 Hz, 8H, Ar), 7.13–6.90 (m, 32H, 8H, Ar), 6.83 (s, 2H, H-3, and H-9), 6.53 (d, *J* = 2.0 Hz, 2H, H-1, and H-7), 4.46 (d, *J* =

15.2 Hz, 2H, H-6*exo*, and H-12*exo*), 4.31 (s, 2H, H-13), 3.87 (d, *J* = 16.8 Hz, 2H, H-6*endo*, and H-12*endo*), 2.31 (s, 18H, 6× CH_3), 2.27 (s, 6H, 2× TB-CH_3).
^{13}C NMR (101 MHz, $CDCl_3$) δ 147.06, 145.31, 145.13, 134.08, 134.03, 133.92, 133.85, 132.62, 132.42, 129.93, 129.86, 129.82, 127.09, 127.06, 124.86, 124.54, 123.17, 122.93, 65.71, 54.93, 20.87, 20.83, 17.13.
Anal. calcd. for $C_{83}H_{74}N_6$: C 86.27, H 6.46, N 7.27; found: C 86.19, H 6.76, N 7.05.

N^4,$N^{4'}$-(4,10-dimethyl-6H,12H-5,11-methanodibenzo[b,f][1,5]diazocine-2,8-diyl)bis(N^4,N^4,$N^{4'}$-tris(4-methoxyphenyl)-[1,1'-biphenyl]-4,4'-diamine) (**3h**)

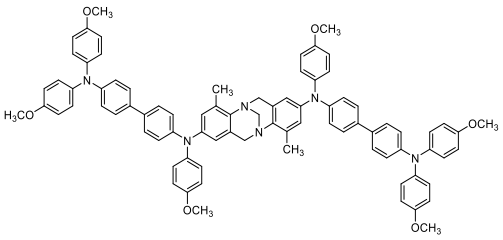

2,8-Dibromo-4,10-dimethyl-6*H*,12*H*-5,11-methanodibenzo[*b*,*f*][1,5]diazocine (0.727 g, 1.78 mmol) and N^4,N^4,$N^{4'}$-tris(4-methoxyphenyl)-[1,1'-biphenyl]-4,4'-diamine (**3e**) (2.237 g, 4.45 mmol) were dissolved in anhydrous toluene (15 ml) and stirred under argon atmosphere for 30 min. Tri-*tert*-butylphosphonium tetrafluoroborate (0.014 g, 0.048 mmol) and palladium (II) acetate (0.008 g, 0.036 mmol) were added, and the mixture was stirred for another 10 minutes. Finally, sodium *tert*-butoxide (0.428 g, 4.45 mmol) was added, and the mixture was heated at reflux for 6 hours. After the termination of the reaction, the mixture was diluted with THF and filtered through Celite passivated with 2% triethylamine solution in THF; the solvent was removed, and the residue was purified by column chromatography (ethyl acetate/toluene/*n*-hexane 1:5:6 followed by ethyl acetate/toluene 1:24, *v*/*v*) (silica gel in the column was passivated with 2% triethylamine solution in THF beforehand) to give light gray powder (34%, 0.733 g).
^{1}H NMR (400 MHz, $CDCl_3$) δ 7.42–7.29 (m, 8H, Ar), 7.12–6.89 (m, 20H, Ar), 6.88–6.69 (m, 14H, Ar), 6.49 (d, *J* = 2.2 Hz, 2H, H-1, and H-7), 4.46 (d, *J* = 16.5 Hz, 2H, H-6*exo*, and H-12*exo*), 4.30 (s, 2H, H-13), 3.85 (d, *J* = 16.9 Hz, 2H, H-6*endo*, and H-12*endo*), 3.79 (d, *J* = 1.6 Hz, 18H, 6× OCH_3), 2.26 (s, 6H, 2× CH_3).
^{13}C NMR (101 MHz, $CDCl_3$) δ 156.06, 155.74, 147.54, 146.97, 141.04, 140.70, 133.84, 132.87, 132.84, 131.13, 128.35, 127.26, 126.94, 126.42, 126.03, 124.13, 122.39, 121.27, 121.04, 119.01, 114.74, 114.67, 108.78, 67.74, 55.51, 55.48, 54.99, 17.14.
Anal. calcd. for $C_{83}H_{74}N_6O_6$: C 79.65, H 5.96, N 6.72; found: C 79.74, H 6.21, N 6.47.

4,10-dibromo-2,8-dimethyl-6H,12H-5,11-methanodibenzo[b,f][1,5]diazocine (**3i**)

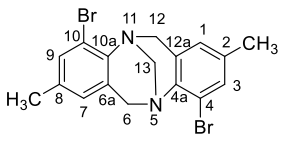

2-Bromo-4-methylaniline (3.721 g, 20 mmol) were mixed with paraformaldehyde (1.261 g, 42 mmol) and added portionwise to trifluoroacetic acid that was cooled to -15 °C (40 ml). After the addition was complete, the mixture was allowed to slowly reach r.t. and stir for 34 h in the dark. Then, the reaction mixture was slowly poured on ice with ammonia solution (97 ml, 25%). The mixture was extracted with dichloromethane (3×180 ml), washed with

water and brine. The organic layer was dried over anhydrous Na_2SO_4, filtered; the solvent was removed under reduced pressure, resulting in white solid (91%, 3.7 g).
^{1}H NMR (400 MHz, DMSO) δ 7.30 (s, 2H, H-3, and H-9), 6.86 (s, 2H, H-1, and H-7), 4.49 (d, *J* = 17.2 Hz, 2H, H-6*exo*, and H-12*exo*), 4.25 (s, 2H, H-13), 4.12 (d, *J* = 17.3 Hz, 2H, H-6*endo*, and H-12*endo*), 2.16 (s, 6H, 2× CH_3).
^{13}C NMR (101 MHz, DMSO) δ 142.34, 135.48, 131.85, 131.12, 127.44, 119.27, 67.33, 55.41, 20.41.
Anal. calcd. for $C_{17}H_{16}Br_2N_2$: C 50.03, H 3.95, N 6.86; found: C 49.87, H 4.10, N 6.77.

2,4,8,10-tetrabromo-6H,12H-5,11-methanodibenzo[b,f][1,5]diazocine (**3j**)

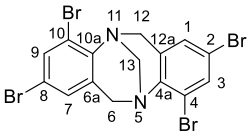

2-Bromo-4-methylaniline (3.10 g, 12.36 mmol) were mixed with paraformaldehyde (0.78 g, 26 mmol) and added portionwise to trifluoroacetic acid that was cooled to -15 °C (25 ml). After the addition was complete, the mixture was allowed to slowly reach r.t. and stir for 34 h in the dark. Then, the reaction mixture was slowly poured on ice with ammonia solution (60 ml, 25%) while mixing.

The precipitate was filtered off and washed well with water, resulting in product as white powder (90%, 3 g).
^{1}H NMR (400 MHz, $CDCl_3$) δ 7.60 (d, *J* = 2.0 Hz, 2H, H-3, and H-9), 7.10 (d, *J* = 2.0 Hz, 2H, H-1, and H-7), 4.55 (d, *J* = 17.6 Hz, 2H, H-6*exo*, and H-12*exo*), 4.35–4.20 (m, 4H, H-13, H-6*endo*, and H-12*endo*).
^{13}C NMR (101 MHz, $CDCl_3$) δ 143.64, 133.97, 132.10, 129.13, 120.68, 117.68, 67.40, 55.00.
Anal. calcd. for $C_{15}H_{10}Br_4N_2$: C 33.50, H 1.87, N 5.21; found: C 33.75, H 1.63, N 5.13.

N^4,$N^{4'}$-(2,8-dimethyl-6H,12H-5,11-methanodibenzo[b,f][1,5]diazocine-4,10-diyl)bis(N^4,$N^{4'}$,$N^{4'}$-tris(4-methoxyphenyl)-[1,1'-biphenyl]-4,4'-diamine) (**3k**)

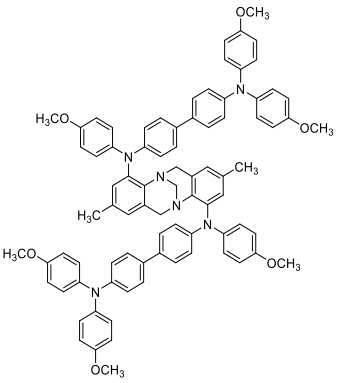

4,10-dibromo-2,8-dimethyl-6*H*,12*H*-5,11-methanodibenzo[*b*,*f*][1,5]diazocine (**3i)** (0.408 g, 1 mmol) and N^4,N^4,$N^{4'}$-tris(4-methoxyphenyl)-[1,1'-biphenyl]-4,4'-diamine (**3e**) (1.257 g, 2.5 mmol) were dissolved in anhydrous toluene (10 ml) and stirred under argon atmosphere for 30 min. Tri-*tert*-butylphosphonium tetrafluoroborate (0.008 g, 0.028 mmol) and palladium (II) acetate (0.005 g, 0.02 mmol) were added, and the mixture was stirred for another 10 minutes. Finally, sodium *tert*-butoxide (0.24 g, 2.5 mmol) was added, and the mixture was heated at reflux for 6 hours. After the termination of the reaction, the mixture was diluted with THF and filtered through Celite passivated with 2% triethylamine solution in THF; the solvent was removed under reduced

pressure. The residue was purified by column chromatography (ethyl acetate/toluene/*n*-hexane 1:5:6 followed by DCM/*n*-hexane 1:3, *v*/*v*) (silica gel in the column was passivated with 2% triethylamine solution in THF beforehand) to give white powder (32%, 0.39 g).

^{1}H NMR (400 MHz, $CDCl_3$) δ 7.43–7.29 (m, 8H, Ar), 7.12–6.88 (m, 20H, Ar), 6.88–6.72 (m, 14H, Ar), 6.54 (s, 2H, Ar), 4.16 (d, *J* = 5.7 Hz, 2H, CH_2), 3.85–3.73 (m, 20H, CH_2, 6× OCH_3), 3.67 (s, 2H, CH_2), 2.16 (s, 6H, 2× CH_3).

^{13}C NMR (101 MHz, $CDCl_3$) δ 157.14, 155.69, 155.25, 149.47, 147.54, 147.37, 146.84, 143.59, 141.14, 140.98, 133.20, 132.72, 132.70, 127.69, 126.86, 126.66, 126.42, 126.34, 124.89, 124.20, 121.25, 120.35, 114.67, 114.21, 67.22, 55.52, 55.49, 55.41, 20.81.

Anal. calcd. for $C_{83}H_{74}N_6O_6$: C 79.65, H 5.96, N 7.67; found: C 79.87, H 5.85, N 7.62.

N^2,N^4,N^8,N^{10}-tetrakis(4'-(bis(4-methoxyphenyl)amino)-[1,1'-biphenyl]-4-yl)-N^2,N^4,N^8,N^{10}-tetrakis(4-methoxyphenyl)-6H,12H-5,11-methanodibenzo[b,f][1,5]diazocine-2,4,8,10-tetraamine (**3l**)

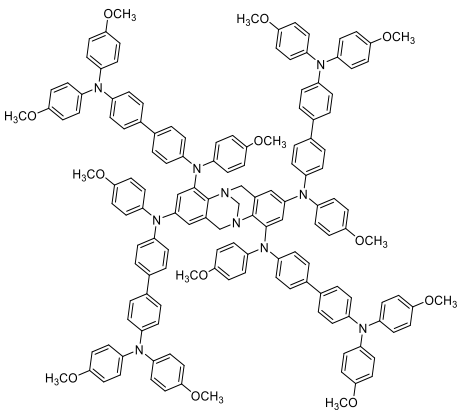

2,4,8,10-tetrabromo-6*H*,12*H*-5,11-methanodibenzo[*b*,*f*][1,5]diazocine (**3j**) (0.7 g, 1.3 mmol) and N^4,N^4,$N^{4'}$-tris(4-methoxyphenyl)-[1,1'-biphenyl]-4,4'-diamine (**3e**) (3.4 g, 6.76 mmol) were dissolved in anhydrous toluene (22 ml) and stirred under argon atmosphere for 30 min. Tri-*tert*-butylphosphonium tetrafluoroborate (0.021 g, 0.07 mmol) and palladium (II) acetate (0.012 g, 0.052 mmol) were added, and the mixture was stirred for another 10 minutes. Finally, sodium *tert*-butoxide (0.65 g, 6.76 mmol) was added, and the mixture was heated at reflux for 7 hours. After the termination of the reaction, the mixture was diluted with THF and filtered through Celite passivated with 2% triethylamine solution in THF; the solvent was removed under reduced pressure; the residue was purified by column chromatography (ethyl acetate/toluene/*n*-hexane 1:3:3, *v*/*v*) (silica gel in the column was passivated with 2% triethylamine solution in THF beforehand) to give grayish solid (43%, 1.25 g). The product was further purified by column chromatography (THF/toluene 3:14 followed by THF/DCM/*n*-hexane 1:6:9, *v*/*v*) (silica gel in the column was passivated with 2% triethylamine solution in THF beforehand) to give lightly grayish powder (17%, 0.5 g).

^{1}H NMR (400 MHz, $CDCl_3$) δ 7.36–7.26 (m, 16H, Ar), 7.13–6.69 (m, 66H, Ar), 6.40 (s, 2H, Ar), 4.06 (s, 2H, -CH_2-), 3.82–3.62 (m, 40H, 2× -CH_2-, 12× OCH_3).

^{13}C NMR (101 MHz, $CDCl_3$) δ 155.69, 155.66, 147.51, 147.36, 144.11, 141.13, 141.09, 140.26, 136.08, 135.63, 134.01, 133.14, 132.87, 130.38, 126.99, 126.91, 126.85, 126.65, 126.31, 124.80, 123.91, 122.15, 121.28, 121.24, 114.75, 114.67, 114.24, 68.00, 55.49, 55.47, 55.44.

Anal. calcd. for $C_{147}H_{126}N_{10}O_{12}$: C 79.36, H 5.71, N 6.30; found: C 79.46, H 5.70, N 6.22.

2,8-Dinitro-4,10-dimethyl-6H,12H-5,11-methanodibenzo[1,5]-diazocine (**4a**)

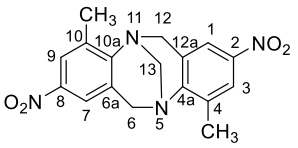

2-methyl-4-nitroaniline (5 g, 32.86 mmol) and paraformaldehyde (2.07 g, 69.01 mmol) were dissolved in trifluoroacetic acid (66 ml) resulting in a black colored reaction mixture, which was stirred for 48 h and poured into 165 ml H_2O, afterwards yielding an intensively yellow precipitate. NaOH (6N) solution was added to this suspension until pH 9 was reached; the precipitate was filtered off and suspended in 120 ml of refluxing acetone for 20 min. The mixture was cooled down, stored at –20 °C for 16 h, and the yellow colored product was filtered off. Yield: 4.50 g (80%).

^{1}H NMR (400 MHz, DMSO-*d*$_6$) δ 7.96 (s, 2H, H-3, H-9), 7.81 (s, 2H, H-1, H-7), 4.68 (d, 2H, H-6*exo*, H-12*exo*, *J* = 17.0 Hz), 4.36 (s, 2H, H-13), 4.30 (d, 2H, H-6*endo*, H-12*endo*, *J* = 17.0 Hz), 2.47 (s, 6H, 2× CH_3).

^{13}C NMR (101 MHz, DMSO-*d*$_6$) δ 153.0, 142.7, 134.5, 129.3, 123.4, 120.3, 66.1, 54.0, 16.8.

Anal. calcd. for $C_{17}H_{16}N_4O_4$: C 60.00, H 4.74, N 16.46; found: C 59.89, H 4.91, N 16.42.

2,8-Diamino-4,10-dimethyl-6H,12H-5,11-methanodibenzo[1,5]-diazocine (**4b**)

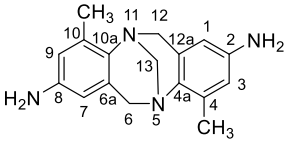

2,8-Dinitro-4,10-dimethyl-6*H*,12*H*-5,11-methanodibenzo[1,5]-diazocine (**4a**) (4.08 g, 12 mmol) and iron powder (9.05 g, 0.16 mol) were suspended in a mixture of 18.2 ml acetic acid and 184.5 ml ethanol. The reaction mixture was refluxed for 12 h, poured into water; the excessive iron was filtered off, and the aqueous layer extracted with dichloromethane (5 times). The combined organic layers were washed with sat. $NaHCO_3$ solution and dried over Na_2SO_4. The crude product was pure according to TLC; thus, it was used in the next step without further purification. Yield: 2.84 g (84%).

^{1}H NMR (400 MHz, $CDCl_3$) δ 6.26 (s, 2H, H-3, H-9, *J* = 1.6 Hz), 5.94 (s, 2H, H-1, H-7, *J* = 1.6 Hz), 4.55 (s, 4H, 2× NH_2), 4.26 (d, 2H, H-6*exo*, H-12*exo*, *J* = 16.5 Hz), 4.06 (s, 2H, H-13), 3.62 (d, 2H, H-6*endo*, H-12*endo*, *J* = 16.5 Hz), 2.18 (s, 6H, 2× CH_3).

^{13}C NMR (101 MHz, $CDCl_3$) δ 144.1, 135.4, 132.2, 128.4, 114.9, 108.8, 67.9, 54.9, 16.7.

Anal. calcd. for $C_{17}H_{20}N_4$: C 72.83, H 7.19, N 19.98; found: C 72.63, H 7.36, N 20.01.

N^2,N^2,N^8,N^8-tetrakis(2,2-diphenylvinyl)-4,10-dimethyl-6H,12H-5,11-methanodibenzo[b,f][1,5]diazocine-2,8-diamine (**4c**)

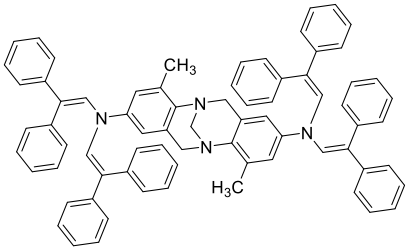

2,8-Diamino-4,10-dimethyl-6*H*,12*H*-5,11-methanodibenzo[1,5]-diazocine **(4b)** (0.294 g, 1.05 mmol) and (±)-camphor-10-sulfonic acid (0.366 g, 1.58 mmol) were dissolved in THF (1.5 ml + volume of the Dean-Stark trap), and 2,2-diphenyl-acetaldehyde (1.082 g, 5.51 mmol) was added, and the reaction mixture was refluxed by using Dean-Stark trap with some anhydrous Na_2SO_4 in it for 3 hours (TLC acetone/ *n*-hexane, 3:22, v/v). After the termination of the reaction, the solution was mixed with water and extracted with ethyl acetate. The organic layer was dried over anhydrous Na_2SO_4, filtered; the solvent was removed, and the residue was dissolved in acetone. The solvent was partially removed until ~10 ml of mixture remained, ~2 ml of methanol was added, and the mixture was slowly evaporated further until the crystallization started. The mixture was left to cool down; the crystals were filtered and washed with methanol to give fine yellow crystals (61%, 0.64 g).

^{1}H NMR (400 MHz, $CDCl_3$) δ 7.34–7.17 (m, 12H, Ar), 7.15–6.93 (m, 20H, Ar), 6.80 (s, 2H, Ar), 6.51 (s, 2H, Ar), 6.47–6.34 (m, 8H, Ar), 5.77 (s, 4H, N-C<u>H</u>=C), 4.52 (d, *J* = 17.0 Hz, 2H, H-6*exo*, and H-12*exo*), 4.27 (s, 2H, H-13), 3.91 (d, *J* = 17.0 Hz, 2H, H-6*endo*, and H-12*endo*), 2.34 (s, 6H, 2× CH_3).

^{13}C NMR (101 MHz, $CDCl_3$) δ 141.67, 141.39, 141.00, 140.10, 134.23, 131.41, 129.64, 129.12, 129.05, 128.56, 127.72, 127.10, 126.71, 118.13, 112.75, 68.03, 55.49, 17.35.

Anal. calcd. for $C_{73}H_{60}N_4$: C 88.27, H 6.09, N 5.64; found: C 88.34, H 6.19, N 5.47.

N^2,N^2,N^8,N^8-tetrakis(2,2-di-p-tolylvinyl)-4,10-dimethyl-6H,12H-5,11-methanodibenzo[b,f][1,5]diazocine-2,8-diamine (**4d**)

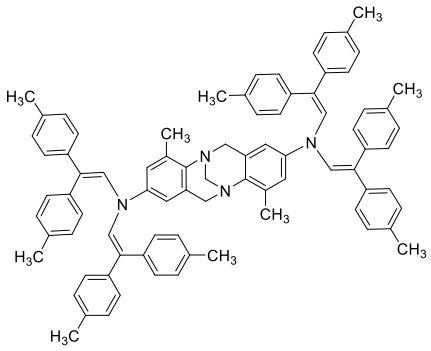

2,8-Diamino-4,10-dimethyl-6*H*,12*H*-5,11-methanodibenzo[1,5]-diazocine **(4b)** (0.28 g, 1 mmol) and (±)-camphor-10-sulfonic acid (0.35 g, 1.5 mmol) were dissolved in THF (1. ml + volume of the Dean-Stark trap); bis(4-methylphenyl)acetaldehyde (1.346 g, 6 mmol) was added, and the reaction mixture was refluxed by using Dean-Stark trap with some anhydrous Na_2SO_4 in it for 15 hours (TLC acetone/ *n*-hexane, 3:22, v/v). After the termination of the reaction, the solution was mixed with water and extracted with ethyl acetate. The organic layer was dried over anhydrous Na_2SO_4, filtered; the solvent was removed, and the residue was dissolved in acetone, concentrated, and precipitated into methanol. The filtered solid product was purified by column chromatography (THF/*n*-hexane 2:23, *v*/*v*) to give bright yellow powder (38%, 0.42 g).

^{1}H NMR (400 MHz, $CDCl_3$) δ 7.09 (d, *J* = 7.9 Hz, 8H, Ar), 6.97–6.86 (m, 16H, Ar), 6.83 (d, *J* = 2.2 Hz, 2H, Ar), 6.55 (d, *J* = 2.2 Hz, 2H, Ar), 6.37 (d, *J* = 8.0 Hz, 8H, Ar),

5.72 (s, 4H, N-C<u>H</u>=C), 4.56 (d, *J* = 17.1 Hz, 2H, H-6*exo*, and H-12*exo*), 4.32 (s, 2H, H-13), 3.97 (d, *J* = 17.1 Hz, 2H, H-6*endo*, and H-12*endo*), 2.42 (s, 12H, 4× CH_3), 2.35 (s, 6H, 2× TB-CH_3), 2.27 (s, 12H, 4× CH_3).
^{13}C NMR (101 MHz, $CDCl_3$) δ 142.04, 140.64, 138.95, 137.23, 136.78, 136.29, 134.23, 130.90, 129.50, 129.05, 128.30, 128.02, 127.68, 117.87, 112.49, 67.90, 55.30, 29.74, 21.29, 21.08, 17.18.
Anal. calcd. for $C_{81}H_{76}N_4$: C 88.00, H 6.93, N 5.07; found: C 87.93, H 6.90, N 5.17.

N^2,N^2,N^8,N^8-tetrakis(2,2-bis(4-methoxyphenyl)vinyl)-4,10-dimethyl-6H,12H-5,11-methanodibenzo[b,f][1,5]diazocine-2,8-diamine (**4e**)

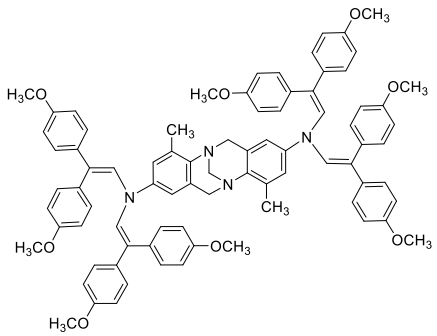

2,8-Diamino-4,10-dimethyl-6*H*,12*H*-5,11-methanodibenzo[1,5]-diazocine **(4b)** (0.280 g, 1 mmol) and (±)-camphor-10-sulfonic acid (0.349 g, 1.5 mmol) were dissolved in THF (1.8 ml + volume of the Dean-Stark trap); bis(4-methoxyphenyl)acetaldehyde (1.2815 g, 5 mmol) was added, and the reaction mixture was refluxed by using Dean-Stark trap with some anhydrous Na_2SO_4 in it for 4 hours (TLC acetone/ *n*-hexane, 3:22, v/v). After the termination of the reaction, the solution was mixed with water and extracted with ethyl acetate. The organic layer was dried over anhydrous Na_2SO_4, filtered; the solvent was removed, and the residue was dissolved in acetone. The solvent was partially removed until ~10 ml of mixture remained, ~2 ml of methanol was added, and the mixture was slowly evaporated further until the crystallization started. The mixture was left to cool down; the crystals were filtered and washed with methanol to give fine yellow crystals (45%, 0.55 g).
^{1}H NMR (400 MHz, DMSO) δ 6.96–6.78 (m, 16H, Ar), 6.71 (s, 2H, Ar), 6.61 (d, *J* = 8.8 Hz, 8H, Ar), 6.50 (s, 2H, Ar), 6.32 (d, *J* = 8.7 Hz, 8H, Ar), 5.56 (s, 4H, N-C<u>H</u>=C), 4.44 (d, *J* = 17.4 Hz, 2H, H-6*exo*, and H-12*exo*), 4.20 (s, 2H, H-13), 3.97 (d, *J* = 17.0 Hz, 2H, H-6*endo*, and H-12*endo*), 3.81 (s, 12H, 4× OCH_3), 3.67 (s, 12H, 4× OCH_3), 2.28 (s, 6H, 2× CH_3).
^{13}C NMR (101 MHz, DMSO) δ 159.16, 159.16, 158.81, 141.69, 141.69, 140.89, 140.89, 136.85, 136.61, 134.18, 134.18, 134.14, 132.47, 132.47, 130.59, 129.92, 129.85, 128.73, 126.76, 126.73, 123.75, 120.62, 117.22, 114.44, 114.44, 113.48, 113.48, 112.29, 65.68, 58.70, 55.73, 55.73, 55.48, 55.48, 17.28.
Anal. calcd. for $C_{81}H_{76}N_4O_8$: C 78.87, H 6.21, N 4.54; found: C 79.06, H 6.19, N 4.39.

E-3-(4-Bromophenyl)-2-propenal (**5a**)

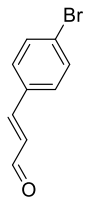

4-bromobenzaldehyde (2 g, 10.8 mmol) and tributyl(1,3-dioxalan-2-ylmethyl)phosphonium bromide (4.39 g, 11.89 mmol) were dissolved in anhydrous THF (30 ml) under argon gas atmosphere; NaH (60% dispersed in mineral oil, 1.30 g, 32.5 mmol) was added in portions, and the resulting turbid solution was stirred at room temperature for 12 h. After the completion of the reaction (TLC 3:1:21 v/v ethyl acetate/toluene/*n*-hexane), the excess

NaH was quenched by using 10% aq. HCl solution under cooling, and the reaction mixture was brought to acidic pH. The reaction mixture was stirred further at room temperature for 1 hour. The mixture was poured into distilled water and extracted with ethyl acetate. The organic layer was dried over anhydrous Na_2SO_4, filtered off, and the solvent evaporated under reduced pressure. The product was purified by column chromatography (ethyl acetate/toluene/*n*-hexane 3:1:21, v/v), resulting in light yellow crystals (92%, 2.1 g).

^{1}H NMR (400 MHz, $CDCl_3$) δ 9.71 (d, *J* = 7.6 Hz, 1H, CHO), 7.60–7.54 (m, 2H, Ar), 7.49–7.37 (m, 3H, CH, Ar), 6.71 (dd, *J* = 16.0, 7.6 Hz, 1H, CH).

^{13}C NMR (101 MHz, $CDCl_3$) δ 193.46, 151.19, 132.86, 132.39, 129.79, 128.98, 125.70.

Anal. calcd. for C_9H_7BrO: C 51.22, H 3.34; found: C 51.23, H 3.22.

(2E,4E)-5-(4-bromophenyl)penta-2,4-dienal (**5b**)

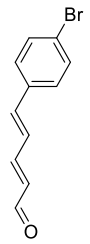

E-3-(4-Bromophenyl)-2-propenal (**5a)** (0.31 g, 1.48 mmol) and tributyl(1,3-dioxalan-2-ylmethyl)phosphonium bromide (0.60 g, 1.63 mmol) were dissolved in anhydrous THF (3.5 ml) under argon gas atmosphere; NaH (60% dispersed in mineral oil, 0.178 g, 4.44 mmol) was added in portions, and the resulting turbid solution was refluxed for 5 h. After the completion of the reaction (TLC ethyl acetate/toluene/*n*-hexane 3:1:2, v/v), the excess NaH was quenched by using 10% aq. HCl solution under cooling, and the reaction mixture was brought to acidic pH. The reaction mixture was stirred further at room temperature for 1 hour. The mixture was poured into distilled water and extracted with ethyl acetate. The organic layer was dried over anhydrous Na_2SO_4, filtered off, and the solvent evaporated under reduced pressure. The crude product was purified by column chromatography (ethyl acetate/toluene/*n*-hexane 3:1:21, v/v), resulting in light yellow crystals (73%, 0.26 g). The obtained data of product are in good agreement with the reported data [250].

^{1}H NMR (400 MHz, $CDCl_3$) δ 9.64 (d, *J* = 7.9 Hz, 1H, CHO), 7.53 (d, *J* = 8.5 Hz, 2H, Ar), 7.38 (d, *J* = 8.5 Hz, 2H, Ar), 7.32–7.20 (m, 1H, CH), 7.07–6.91 (m, 2H, CH), 6.30 (dd, *J* = 15.2, 7.9 Hz, 1H, CH).

^{13}C NMR (101 MHz, $CDCl_3$) δ 193.57, 151.54, 140.91, 134.50, 132.17, 132.07, 128.91, 126.81, 123.79.

Anal. calcd. for $C_{11}H_9BrO$: C 55.72, H 3.83; found: C 55.69, H 3.80.

(E)-2-(4-bromostyryl)-5,5-dimethyl-1,3-dioxane (**5c**)

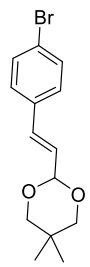

E-3-(4-Bromophenyl)-2-propenal (**5a)** (1.79 g, 8.49 mmol), 2-dimethyl-1,3-propanediol (1.06 g, 10.19 mmol), and *p*-toluenesulfonic acid monohydrate (0.17 g, 0.93 mmol) were dissolved in benzene (17 ml) and stirred at 80 °C for 3.5 h. After cooling to room temperature, the reaction was quenched by adding distilled water and was extracted with ethyl acetate. The organic layer was dried over anhydrous Na_2SO_4, filtered, and the solvent evaporated. The product was purified by column chromatography (ethyl acetate/toluene/ *n*-hexane 3:1:21, v/v) resulting in whitish crystals (80%, 2.0 g).

^{1}H NMR (400 MHz, $CDCl_3$) δ 7.43 (d, *J* = 8.5 Hz, 2H, Ar), 7.26 (d, *J* = 8.5 Hz, 2H, Ar), 6.72 (d, *J* = 16.2 Hz, 1H, CH), 6.21 (dd, *J* = 16.2, 4.7 Hz, 1H, CH), 5.02 (d, *J* = 4.2 Hz, 1H, O-CH-O), 3.69 (d, *J* = 11.2 Hz, 2H, O-CH_2-C), 3.55 (d, *J* = 10.8 Hz, 2H, O-CH_2-C), 1.24 (s, 3H, CH_3), 0.76 (s, 3H, CH_3).
^{13}C NMR (101 MHz, $CDCl_3$) δ 135.08, 132.19, 131.70, 128.36, 126.39, 122.03, 100.57, 30.24, 23.01, 21.93.
Anal. calcd. for $C_{14}H_{17}BrO_2$: C 56.58, H 5.77; found: C 56.60, H 5.74.

2-((1E,3E)-4-(4-bromophenyl)buta-1,3-dien-1-yl)-5,5-dimethyl-1,3-dioxane (**5d**)

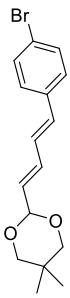

(2*E*,4*E*)-5-(4-Bromophenyl)penta-2,4-dienal (**5b**) (1.84 g, 7.76 mmol), 2-dimethyl-1,3-propanediol (0.97 g, 9.31 mmol), and *p*-toluenesulfonic acid monohydrate (0.16 g, 0.85 mmol) were dissolved in benzene (16 ml), and the mixture was stirred at 80 °C for 3 h. After cooling to room temperature, the reaction was quenched by adding distilled water and was extracted with ethyl acetate. The organic layer was dried over anhydrous Na_2SO_4, filtered, and the solvent evaporated. The product was purified by column chromatography (ethyl acetate/toluene/*n*-hexane 3:1:21, v/v) obtaining yellow crystals (64%, 1.6 g).

^{1}H NMR (400 MHz, $CDCl_3$) δ 7.43 (d, *J* = 8.4 Hz, 2H, Ar), 7.25 (d, *J* = 7.6 Hz, 2H, Ar), 6.81–6.68 (m, 1H, CH), 6.62–6.48 (m, 2H, CH), 5.83 (dd, *J* = 15.3, 4.6 Hz, 1H, CH), 4.96 (d, *J* = 4.6 Hz, 1H, O-CH-O), 3.68 (d, *J* = 11.1 Hz, 2H, O-CH_2-C), 3.53 (d, *J* = 10.8 Hz, 2H, O-CH_2-C), 1.23 (s, 3H, CH_3), 0.76 (s, 3H, CH_3).
^{13}C NMR (101 MHz, $CDCl_3$) δ 135.91, 133.23, 133.15, 131.74, 129.86, 128.47, 128.02, 121.59, 100.37, 30.22, 22.99, 21.93.
Anal. calcd. for $C_{16}H_{19}BrO_2$: C 59.45, H 5.93; found: C 59.41, H 5.89.

N-(4-(5,5-dimethyl-1,3-dioxan-2-yl)phenyl)-3,4-dimethylaniline (**5e**)

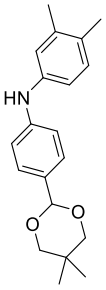

The mixture of dioxane (35 ml) and water (0.03 ml) was purged with argon for 20 minutes. $Pd(OAc)_2$ (0.02 g, 0.09 mmol) and SPhos (0.11 g, 0.27 mmol) were added, and the mixture was heated to 80 °C for 2 min. 2-(4-Bromophenyl)-5,5-dimethyl-1,3-dioxane (**5n**) (5 g, 18.44 mmol), 3,4-dimethylaniline (2.68 g, 22.13 mmol), and NaO*t*-Bu (2.48 g, 25.81 mmol) were added, and the solution was refluxed for 30 min under Ar atmosphere. After the termination of the reaction, the mixture was filtered through Celite, the distilled water was added, and the mixture was extracted with ethyl acetate. The organic layer was dried over anhydrous Na_2SO_4, filtered, and the solvent evaporated under reduced pressure. The crude product was purified by column chromatography (ethyl acetate/toluene/ *n*-hexane 0.5:14.5:10, v/v) and was further purified by the crystallization from 2-propanol to obtain the product as white crystals (80%, 4.62 g).
^{1}H NMR (400 MHz, $CDCl_3$) δ 7.36 (d, *J* = 8.5 Hz, 2H, Ar), 7.03–6.95 (m, 3H, Ar), 6.87 (d, *J* = 2.2 Hz, 1H, Ar), 6.82 (dd, *J* = 8.0, 2.4 Hz, 1H, Ar), 5.60 (s, 1H, NH), 5.32

(s, 1H, O-CH-O), 3.75 (d, *J* = 11.2 Hz, 2H, O-CH_2-C), 3.63 (d, *J* = 10.6 Hz, 2H, O-CH_2-C), 2.20 (s, 6H, 2× Ar-C$\underline{H}_3$), 1.29 (s, 3H, C-CH_3), 0.78 (s, 3H, C-CH_3).
^{13}C NMR (101 MHz, $CDCl_3$) δ 144.52, 140.53, 137.54, 130.47, 130.36, 129.76, 127.25, 120.33, 116.65, 116.33, 101.92, 30.22, 23.11, 21.94, 19.96, 19.02.
Anal. calcd. for $C_{20}H_{25}NO_2$: C 77.14, H 8.09, N 4.50; found: C 77.03, H 8.00, N 4.52.

(E)-N-(4-(2-(5,5-dimethyl-1,3-dioxan-2-yl)vinyl)phenyl)-3,4-dimethylaniline (**5f**)

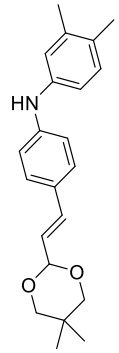

The mixture of dioxane (15 ml) and water (0.02 ml) was purged with argon for 20 minutes. $Pd(OAc)_2$ (0.007 g, 0.03 mmol) and SPhos (0.04 g, 0.10 mmol) were added, and the mixture was heated to 80 °C for 2 min. (*E*)-2-(4-bromostyryl)-5,5-dimethyl-1,3-dioxane (**5c**) (2.02 g, 6.81 mmol), 3,4-dimethylaniline (1.00 g, 8.17 mmol), and NaO*t*-Bu (0.92 g, 9.53 mmol) were added, and the solution was stirred at reflux for 30 min under Ar atmosphere. After the termination of the reaction, the mixture was filtered through Celite, the distilled water was added, and the mixture was extracted with ethyl acetate. The organic layer was dried over anhydrous Na_2SO_4, filtered, and the solvent evaporated under reduced pressure. The product was purified by column chromatography (ethyl acetate/toluene/ *n*-hexane 3:1:21, v/v) and further purified by the crystallization from 2-propanol, resulting in pale yellow crystals (70%, 1.60 g).
^{1}H NMR (400 MHz, $CDCl_3$) δ 7.27 (d, *J* = 8.6 Hz, 2H, Ar), 7.04 (d, *J* = 8.0 Hz, 1H, Ar), 6.94–6.84 (m, 4H, Ar), 6.70 (d, *J* = 16.1 Hz, 1H, Ar), 6.08 (dd, *J* = 16.1, 5.1 Hz, 1H, Ar), 5.65 (s, 1H, NH), 5.02 (d, *J* = 4.9 Hz, 1H, O-CH-O), 3.69 (d, *J* = 11.2 Hz, 2H, O-CH_2-C), 3.56 (d, *J* = 10.9 Hz, 2H, O-CH_2-C), 2.22 (s, 3H, Ar-C$\underline{H}_3$), 2.21 (s, 3H, Ar-C$\underline{H}_3$), 1.25 (s, 3H, C-CH_3), 0.76 (s, 3H, C-CH_3).
^{13}C NMR (101 MHz, $CDCl_3$) δ 144.20, 139.90, 137.63, 133.37, 130.37, 130.21, 128.05, 127.90, 122.34, 120.95, 116.89, 116.06, 101.47, 30.23, 23.05, 21.99, 20.00, 19.08.
Anal. calcd. for $C_{22}H_{27}NO_2$: C 78.30, H 8.06, N 4.15; found: C 78.28, H 8.06, N 4.05.

N-(4-((1E,3E)-4-(5,5-dimethyl-1,3-dioxan-2-yl)buta-1,3-dien-1-yl)phenyl)-3,4-dimethylaniline (**5g**)

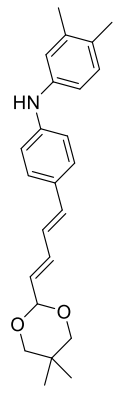

The mixture of dioxane (10 ml) and water (0.01 ml) was purged with argon for 20 minutes. $Pd(OAc)_2$ (0.005 g, 0.02 mmol) and SPhos (0.03 g, 0.07 mmol) were added, and the mixture was heated to 80 °C for 2 min.

2-((1*E*,3*E*)-4-(4-Bromophenyl)buta-1,3-dien-1-yl)-5,5-dimethyl-1,3-dioxane (**5d**) (1.58 g, 4.90 mmol), 3,4-dimethylaniline (0.71 g, 5.89 mmol), and NaO*t*-Bu (0.66 g, 6.87 mmol) were added, and the solution was refluxed for 1 h under Ar atmosphere. After the termination of the reaction, the mixture was filtered through Celite, the distilled water was added, and the mixture was extracted with ethyl acetate. The organic layer was dried over anhydrous Na_2SO_4, filtered, and the solvent evaporated under reduced pressure. The product was purified by column chromatography (ethyl acetate/toluene/ *n*-hexane 3:1:21, v/v) and further

purified by the crystallization from 2-propanol, resulting in yellow crystals (69%, 1.23 g).

^{1}H NMR (400 MHz, $CDCl_3$) δ 7.28 (d, *J* = 8.6 Hz, 2H, Ar), 7.04 (d, *J* = 8.0 Hz, 1H, Ar), 6.93 (d, *J* = 8.6 Hz, 2H, Ar), 6.91–6.82 (m, 2H, Ar), 6.68–6.49 (m, 3H, Ar), 5.77 (dd, *J* = 15.2, 4.9 Hz, 1H, Ar), 5.67(s, 1H, NH), 4.95 (d, *J* = 5.1 Hz, 1H, O-CH-O),), 3.67 (d, *J* = 11.1 Hz, 2H, O-CH_2-C), 3.53 (d, *J* = 10.9 Hz, 2H, O-CH_2-C), 2.22 (s, 3H, Ar-C$\underline{H}_3$), 2.21 (s, 3H, Ar-C$\underline{H}_3$), 1.23 (s, 3H, C-CH_3), 0.75 (s, 3H, C-CH_3).

^{13}C NMR (101 MHz, $CDCl_3$) δ 143.84, 139.87, 137.60, 134.42, 134.19, 130.34, 130.13, 128.84, 127.73, 127.35, 124.80, 120.71, 116.67, 116.30, 100.85, 30.17, 22.98, 21.93, 19.95, 19.03.

Anal. calcd. for $C_{24}H_{29}NO_2$: C 79.30, H 8.04, N 3.85; found: C 79.20, H 8.08, N 3.86.

N^2,N^8-bis(4-(5,5-dimethyl-1,3-dioxan-2-yl)phenyl)-N^2,N^8-bis(3,4-dimethylphenyl)-4,10-dimethyl-6H,12H-5,11-methanodibenzo[b,f][1,5]diazocine-2,8-diamine (**5h**)

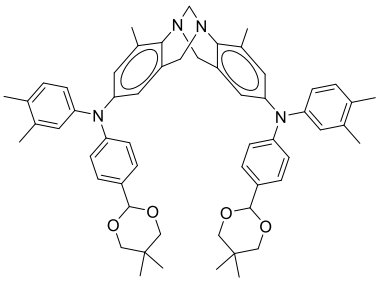

A mixture of *N*-(4-(5,5-dimethyl-1,3-dioxan-2-yl)phenyl)-3,4-dimethylaniline (**5e**) (2.18 g, 7.00 mmol), 2,8-dibromo-4,10-dimethyl-6*H*,12*H*-5,11-methanodibenzo[*b*,*f*][1,5]diazocine (**1'**) (1.14 g, 2.80 mmol), and anhydrous toluene (20 ml) was purged with argon for 30 minutes. $Pd(OAc)_2$ (0.012 g, 0.05 mmol), $[P(t\text{-}Bu)_3H]BF_4$ (0.023 g, 0.07 mmol), and NaO*t*-Bu (0.81 g, 8.39 mmol) were added, and the mixture was heated at reflux for 2.5 h under Ar atmosphere. After the termination of the reaction, the mixture was filtered through Celite, the distilled water was added, and the mixture was extracted with ethyl acetate. The organic layer was dried over anhydrous Na_2SO_4, filtered, and the solvent evaporated under reduced pressure. The product was purified by column chromatography (ethyl acetate/toluene/ *n*-hexane 3:1:21, v/v), resulting in yellow solid (76%, 1.8 g).

^{1}H NMR (400 MHz, $CDCl_3$) δ 7.32 (d, *J* = 8.5 Hz, 4H, Ar), 6.98 (d, *J* = 8.5 Hz, 6H, Ar), 6.86–6.74 (m, 6H, Ar), 6.48–6.44 (m, 2H, Ar), 5.33 (s, 2H, O-CH-O), 4.40 (d, *J* = 17.0 Hz, 2H, H-6*exo*, and H-12*exo*), 4.27 (s, 2H, H-13), 3.82 (d, *J* = 17.0 Hz, 2H, H-6*endo*, and H-12*endo*), 3.76 (d, *J* = 11.1 Hz, 4H, O-CH_2-C), 3.63 (d, *J* = 10.9 Hz, 4H, O-CH_2-C), 2.24 (s, 6H, Ar-C$\underline{H}_3$), 2.21 (s, 6H, Ar-C$\underline{H}_3$), 2.15 (s, 6H, Ar-C$\underline{H}_3$), 1.30 (s, 6H, C-CH_3), 0.79 (s, 6H, C-CH_3).

^{13}C NMR (101 MHz, $CDCl_3$) δ 148.98, 145.48, 143.42, 141.19, 137.49, 133.78, 131.61, 131.33, 130.34, 129.07, 128.83, 128.27, 126.94, 126.11, 124.74, 122.93, 122.43, 119.66, 101.93, 77.77, 67.70, 54.99, 30.25, 23.13, 21.94, 19.87, 19.18, 17.03.

Anal. calcd. for $C_{57}H_{64}N_4O_4$: C 78.77, H 7.42, N 6.45; found: C 78.78, H 7.39, N 6.45.

N^2,N^8-bis(4-((E)-2-(5,5-dimethyl-1,3-dioxan-2-yl)vinyl)phenyl)-N^2,N^8-bis(3,4-dimethylphenyl)-4,10-dimethyl-6H,12H-5,11-methanodibenzo[b,f][1,5]diazocine-2,8-diamine (**5i**)

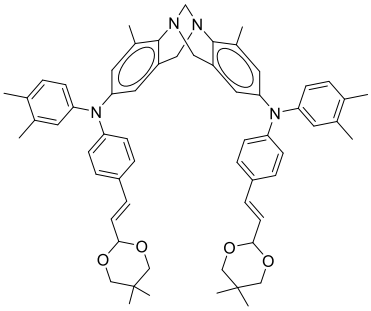

A mixture of (*E*)-*N*-(4-(2-(5,5-dimethyl-1,3-dioxan-2-yl)vinyl)phenyl)-3,4-dimethylaniline (**5f**) (1.57 g, 4.67 mmol), 2,8-dibromo-4,10-dimethyl-6*H*,12*H*-5,11-methanodibenzo[*b*,*f*][1,5]diazocine (0.76 g, 1.87 mmol), and anhydrous toluene (34 ml) was purged with argon for 30 minutes. $Pd(OAc)_2$ (0.008 g, 0.04 mmol), $[P(t\text{-}Bu)_3H]BF_4$ (0.015 g, 0.05 mmol), and NaO*t*-Bu (0.54 g, 5.60 mmol) were added, and the mixture was heated at reflux for 1 h under Ar atmosphere. After the termination of the reaction, the mixture was filtered through Celite, the distilled water was added, and the mixture was extracted with ethyl acetate. The organic layer was dried over anhydrous Na_2SO_4, filtered, and the solvent evaporated under reduced pressure. The product was purified by column chromatography (ethyl acetate/toluene/ *n*-hexane 3:1:21, v/v), resulting in light yellow crystals (80%, 1.37 g).

^{1}H NMR (400 MHz, $CDCl_3$) δ 7.28–7.12 (m, 9H, Ar), 7.02 (d, *J* = 8.1 Hz, 2H, Ar), 6.90–6.78 (m, 5H, Ar), 6.69 (d, *J* = 16.1 Hz, 2H, CH), 6.49 (d, *J* = 2.3 Hz, 2H, Ar), 6.07 (dd, *J* = 16.1, 4.9 Hz, 2H, CH), 5.01 (d, *J* = 4.7 Hz, 2H, O-CH-O), 4.44 (d, *J* = 17.0 Hz, 2H, H-6*exo*, and H-12*exo*), 4.28 (s, 2H, H-13), 3.85 (d, *J* = 17.0 Hz, 2H, H-6*endo*, and H-12*endo*), 3.69 (d, *J* = 11.1 Hz, 4H, O-CH_2-C), 3.55 (d, *J* = 10.9 Hz, 4H O-CH_2-C), 2.25 (s, 6H, Ar-C$\underline{H}_3$), 2.22 (s, 6H, Ar-C$\underline{H}_3$), 2.17 (s, 6H, Ar-C$\underline{H}_3$), 1.24 (s, 6H, C-CH_3), 0.76 (s, 6H, C-CH_3).

^{13}C NMR (101 MHz, $CDCl_3$) δ 148.32, 145.08, 143.01, 141.50, 137.63, 133.90, 133.06, 131.86, 130.41, 128.88, 128.81, 127.54, 126.60, 125.23, 123.11, 122.92, 121.62, 120.16, 101.24, 67.57, 54.87, 30.18, 22.99, 21.94, 19.88, 19.20, 17.03.

Anal. calcd. for $C_{61}H_{68}N_4O_4$: C 79.53, H 7.44, N 6.08; found: C 79.53, H 7.40, N 6.05.

N^2,N^8-bis(4-((1E,3E)-4-(5,5-dimethyl-1,3-dioxan-2-yl)buta-1,3-dien-1-yl)phenyl)-N^2,N^8-bis(3,4-dimethylphenyl)-4,10-dimethyl-6H,12H-5,11-methanodibenzo[b,f][1,5]diazocine-2,8-diamine (**5j**)

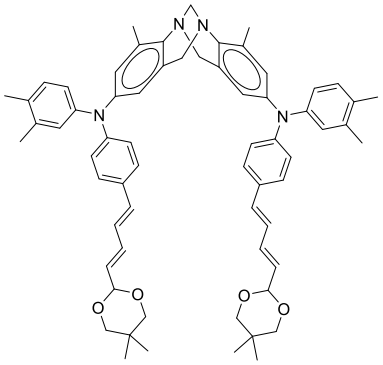

A mixture of *N*-(4-((1*E*,3*E*)-4-(5,5-dimethyl-1,3-dioxan-2-yl)buta-1,3-dien-1-yl)phenyl)-3,4-dimethylaniline (**5g**) (1.20 g, 3.30 mmol), 2,8-dibromo-4,10-dimethyl-6*H*,12*H*-5,11-methanodibenzo[*b*,*f*][1,5]diazocine (**1'**) (0.54 g, 1.32 mmol), and anhydrous toluene (30 ml) was purged with argon for 30 minutes. $Pd(OAc)_2$ (0.006 g, 0.03 mmol), $[P(t\text{-}Bu)_3H]BF_4$ (0.011 g, 0.03 mmol), and NaO*t*-Bu (0.38 g, 3.96 mmol) were added, and the mixture was heated at reflux for 3.5 h under Ar atmosphere. After the termination of the reaction, the mixture was filtered through Celite, the distilled water

was added, and the mixture was extracted with ethyl acetate. The organic layer was dried over anhydrous Na_2SO_4, filtered, and the solvent evaporated under reduced pressure. The crude product was purified by column chromatography (acetone/*n*-hexane 3:22, v/v), yielding product as yellow solid (45%, 1.4 g).

^{1}H NMR (400 MHz, $CDCl_3$): δ = 7.25 (d, *J* = 8.6 Hz, 4H, Ar), 7.05 (d, *J* = 8.1 Hz, 2H, Ar), 6.96–6.30 (m, 11H, Ar), 6.71–6.49 (m, 7H, Ar), 5.79 (dd, *J* = 15.0, 4.9 Hz, 2H, CH), 4.98 (d, *J* = 4.9 Hz, 2H, O-CH-O), 4.52 (d, *J* = 16.8 Hz, 2H, H-6*exo*, and H-12*exo*), 4.38 (s, 2H, H-13), 3.90 (d, *J* = 17.0 Hz, 2H, H-6*endo*, and H-12*endo*), 3.70 (d, *J* = 10.7 Hz, 4H, O-CH_2-C), 3.56 (d, *J* = 11.0 Hz, 4H, O-CH_2-C), 2.30 (s, 6H, Ar-C$\underline{H}_3$), 2.26 (s, 6H, Ar-C$\underline{H}_3$), 2.20 (s, 6H, Ar-C$\underline{H}_3$), 1.26 (s, 6H, C-CH_3), 0.78 (s, 6H, C-CH_3).

^{13}C NMR (101 MHz, $CDCl_3$): δ = 147.92, 144.96, 137.75, 134.23, 134.11, 133.98, 130.50, 127.81, 127.35, 126.62, 125.70, 125.05, 122.95, 122.25, 100.82, 54.84, 30.22, 23.02, 21.97, 19.93, 19.25, 17.14.

Anal. calcd. for $C_{65}H_{72}N_4O_4$: C 80.21, H 7.46, N 5.76; found: C 80.15, H 7.43, N 5.71.

4,4'-((4,10-dimethyl-6H,12H-5,11-methanodibenzo[b,f][1,5]diazocine-2,8-diyl)bis((3,4-dimethylphenyl)azanediyl))dibenzaldehyde (**5k**)

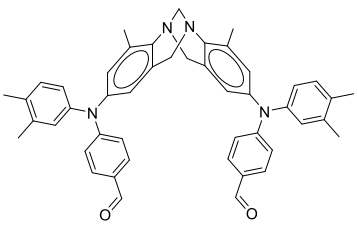

The protected aldehyde compound **5h** (1.74 g, 2 mmol) was dissolved in THF (10 ml), 12% aq. HCl solution (4 ml) was added, and the mixture was stirred at 40 °C for 1 hour. The reaction mixture was poured into the saturated $NaHCO_3$ solution and extracted with ethyl acetate. The organic layer was dried over anhydrous Na_2SO_4, filtered, and the solvent evaporated under reduced pressure. The crude product was purified by column chromatography (acetone/*n*-hexane 1:4, v/v), resulting in yellow crystals (46%, 0.66 g).

^{1}H NMR (400 MHz, $CDCl_3$) δ 9.76 (s, 2H, CHO), 7.61 (d, *J* = 8.8 Hz, 4H, Ar), 7.11 (d, *J* = 8.0 Hz, 2H, Ar), 6.98–6.78 (m, 10H, Ar), 6.61 (d, *J* = 2.1 Hz, 2H, Ar), 4.50 (d, *J* = 17.0 Hz, 2H, H-6*exo*, and H-12*exo*), 4.29 (s, 2H, H-13), 3.90 (d, *J* = 17.1 Hz, 2H, H-6*endo*, and H-12*endo*), 2.32 (s, 6H, 2× CH_3), 2.26 (s, 6H, 2× CH_3), 2.22 (s, 6H, 2× CH_3).

^{13}C NMR (101 MHz, $CDCl_3$) δ 190.32, 153.90, 143.49, 143.46, 141.46, 138.30, 134.71, 134.24, 131.32, 130.94, 129.39, 128.08, 128.02, 126.98, 124.40, 122.16, 117.78, 67.44, 54.78, 26.93, 19.91, 19.36, 17.11.

Anal. calcd. for $C_{47}H_{44}N_4O_2$: C 81.00, H 6.36, N 8.04; found: C 81.02, H 6.36, N 8.00.

(2E,2'E)-3,3'-(((4,10-dimethyl-6H,12H-5,11-methanodibenzo[b,f][1,5]diazocine-2,8-diyl)bis((3,4-dimethylphenyl)azanediyl))bis(4,1-phenylene))diacrylaldehyde (**5l**)

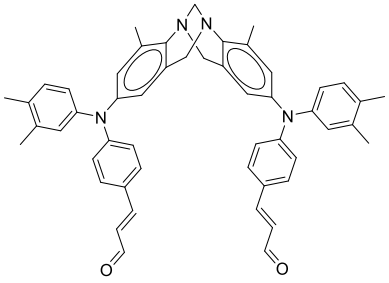

The protected aldehyde compound **5i** (1.37 g, 1.5 mmol) was dissolved in THF (8 ml), 12% aq. HCl solution (3 ml) was added, and the mixture was stirred at 40 °C for 1 hour. The reaction mixture was poured into the saturated $NaHCO_3$ solution and extracted with ethyl acetate. The organic layer was dried over anhydrous Na_2SO_4, filtered, and the solvent evaporated under reduced pressure. The crude product was purified by column chromatography (acetone/*n*-hexane 1:4, v/v), yielding product as yellow crystals (78%, 0.86 g).

^{1}H NMR (400 MHz, $CDCl_3$) δ 9.61 (d, *J* = 7.8 Hz, 2H, CHO), 7.40–7.32 (m, 6H, Ar), 7.09 (d, *J* = 8.1 Hz, 2H, Ar), 6.96–6.92 (m, 2H, Ar), 6.90–6.84 (m, 8H, Ar), 6.60–6.50 (m, 4H, CH), 4.49 (d, *J* = 17.0 Hz, 2H, H-6*exo*, and H-12*exo*), 4.29 (s, 2H, H-13), 3.89 (d, *J* = 17.1 Hz, 2H, H-6*endo*, and H-12*endo*), 2.30 (s, 6H, 2× CH_3), 2.26 (s, 6H, 2× CH_3), 2.21 (s, 6H, 2× CH_3).

^{13}C NMR (101 MHz, $CDCl_3$) δ 193.78, 153.01, 151.36, 143.88, 142.83, 141.86, 138.11, 134.45, 133.59, 130.76, 129.82, 129.21, 127.57, 126.42, 125.34, 125.30, 123.94, 121.53, 119.31, 67.45, 54.77, 19.91, 19.32, 17.09.

Anal. calcd. for $C_{51}H_{48}N_4O_2$: C 81.79, H 6.46, N 7.48; found: C 87.78, H 6.45, N 7.50.

(2E,2'E,4E,4'E)-5,5'-(((4,10-dimethyl-6H,12H-5,11-methanodibenzo[b,f][1,5]diazocine-2,8-diyl)bis((3,4-dimethylphenyl)azanediyl))bis(4,1-phenylene))bis(penta-2,4-dienal) (**5m**)

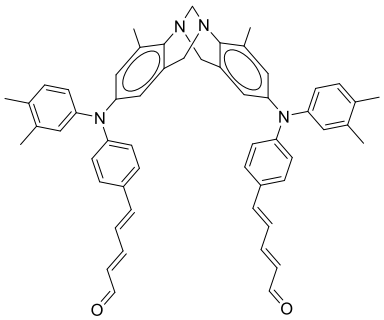

The protected aldehyde compound **5j** (1.38 g, 1.42 mmol) was dissolved in THF (8 ml), 12% aq. HCl solution (3 ml) was added, and the mixture was stirred at 40 °C for 1 hour. The reaction mixture was poured into the saturated $NaHCO_3$ solution and extracted with ethyl acetate. The organic layer was dried over anhydrous Na_2SO_4, filtered, and the solvent evaporated under reduced pressure. The crude product was purified by column chromatography (THF/*n*-hexane 1:4, v/v), yielding product as orange crystals (70%, 0.8 g).

^{1}H NMR (400 MHz, $CDCl_3$) δ 9.57 (d, *J* = 8.0 Hz, 2H, CHO), 7.34–7.18 (m, 5H, Ar), 7.06 (d, *J* = 8.1 Hz, 2H, Ar), 6.95–6.79 (m, 15H, Ar), 6.55 (d, *J* = 2.1 Hz, 2H, CH), 6.20 (dd, *J* = 15.1, 8.0 Hz, 2H, CH), 4.47 (d, *J* = 17.0 Hz, 2H, H-6*exo*, and H-12*exo*), 4.29 (s, 2H, H-13), 3.87 (d, *J* = 16.7 Hz, 2H, H-6*endo*, and H-12*endo*), 2.28 (s, 6H, 2× CH_3), 2.25 (s, 6H, 2× CH_3), 2.20 (s, 6H, 2× CH_3).

^{13}C NMR (101 MHz, $CDCl_3$) δ 193.57, 153.00, 149.94, 144.38, 142.56, 142.38, 137.94, 134.27, 132.96, 130.66, 130.04, 129.11, 128.61, 127.62, 127.21, 125.94, 123.57, 123.37, 120.96, 120.47, 114.15, 67.55, 54.88, 19.90, 19.28, 17.08.

Anal. calcd. for $C_{55}H_{52}N_4O_2$: C 82.47, H 6.54, N 6.99; found: C 82.45, H 6.56, N 7.01.

2,2'-((5Z,5'Z)-((((4,10-dimethyl-6H,12H-5,11-methanodibenzo[b,f][1,5]diazocine-2,8-diyl)bis((3,4-dimethylphenyl)azanediyl))bis(4,1-phenylene))bis(methanylylidene))bis(4-oxo-2-thioxothiazolidin-3-yl-5-ylidene))diacetic acid (**5A**)

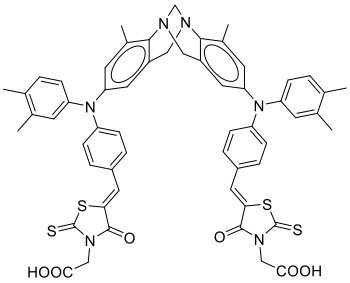

Aldehyde compound **5k** (0.73 g, 1.05 mmol), rhodanine-3-acetic acid (0.48 g, 2.52 mmol), and $AcONH_4$ (0.05 g, 0.63 mmol) were refluxed in anhydrous toluene (3 ml) for 12 h. After the termination of the reaction, the distilled water was added, and the mixture was extracted with ethyl acetate. The organic layer was dried over anhydrous Na_2SO_4, filtered, and the solvent evaporated under reduced pressure. The crude product was purified by column chromatography (acetone/*n*-hexane 7:18, acetone/*n*-hexane 2:3 and methanol/toluene 3:22, v/v) to obtain dye **5A** as a red solid (34%, 0.37 g), m.p. > 400 °C.

^{1}H NMR (400 MHz, DMSO-d_6) δ 7.63 (s, 2H, Ar), 7.42 (d, J = 8.9 Hz, 4H, Ar), 7.15 (d, J = 8.2 Hz, 2H, Ar), 7.00–6.83 (m, 6H, Ar), 6.75 (d, J = 8.9 Hz, 4H, Ar), 6.70–6.62 (m, 2H, Ar), 4.48–4.37 (m, 6H, H-6*exo*, and H-12*exo*, N-C$\underline{H_2}$-COOH), 4.21 (s, 2H, H-13), 3.97 (d, J = 17.6 Hz, 2H, H-6*endo*, and H-12*endo*), 2.28 (s, 6H, 2× CH_3), 2.21 (s, 6H, 2× CH_3), 2.17 (s, 6H, 2× CH_3).

^{13}C NMR (101 MHz, DMSO-d_6) 207.04, 193.22, 167.40, 167.33, 150.97, 143.68, 143.50, 141.12, 138.54, 134.81, 134.42, 133.40, 133.08, 131.45, 130.09, 128.14, 126.79, 124.77, 124.10, 122.39, 118.51, 117.73, 67.49, 54.50, 47.63, 31.16, 19.92, 19.38, 17.26.

IR (KBr, cm^{-1}): v = 3394 (OH); 3016 (aromatic CH); 2950, 2916, 2883 (aliphatic CH); 1698 (2×C=O); 1575 (C=C); 1505 (C-C); 1324 (C=S); 1200, 1181 (C-N).

Anal. calcd. for $C_{57}H_{50}N_6O_6S_4$: C 65.62, H 4.83, N 8.06; found: C 65.60, H 4.85, N 8.06.

2,2'-((5Z,5'Z)-((2E,2'E)-((((5R)-4,10-dimethyl-6H,12H-5,11-methanodibenzo[b,f][1,5]diazocine-2,8-diyl)bis((3,4-dimethylphenyl)azanediyl))bis(4,1-phenylene))bis(prop-2-en-3-yl-1-ylidene))bis(4-oxo-2-thioxothiazolidin-3-yl-5-ylidene))diacetic acid (**5B**)

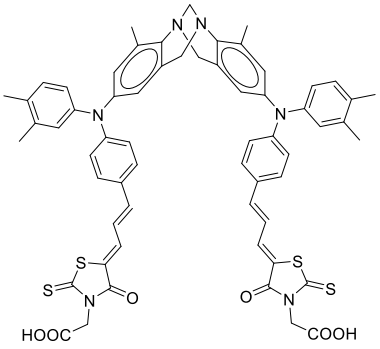

A mixture of aldehyde compound **5l** (0.29 g, 0.38 mmol), rhodanine-3-acetic acid (0.18 g, 0.93 mmol), and $AcONH_4$ (0.01 g, 0.11 mmol) was refluxed in anhydrous toluene (8 ml) for 12 h. At the end of the reaction, the mixture was cooled to room temperature. Dark red crystals, formed upon standing, were filtered off and washed with water (50 ml), toluene (50 ml), and finally with diethyl ether (25 ml) to give dye **5B** (96%, 0.41 g), m.p. 232–234 °C.

^{1}H NMR (400 MHz, DMSO-d_6) δ 7.62–7.39 (m, 3H, Ar), 7.36–6.97 (m, 10H, Ar), 6.95–6.55 (m, 11H, Ar), 4.65 (s, 2H, N-C$\underline{H_2}$-COOH), 4.54 (s, 2H, N-C$\underline{H_2}$-COOH), 4.40 (d, *J* = 17.0 Hz, 2H, H-6*exo*, and H-12*exo*), 4.19 (s, 2H, H-13), 3.94 (d, *J* = 17.5 Hz, 2H, H-6*endo*, and H-12*endo*), 2.25 (s, 6H, 2× CH_3), 2.20 (s, 6H, 2× CH_3), 2.16 (s, 6H, 2× CH_3).

^{13}C NMR (101 MHz, DMSO-d_6) δ 203.31, 192.94, 174.26, 167.86, 167.80, 166.11, 152.26, 151.52, 150.49, 146.89, 144.09, 143.13, 143.02, 138.31, 137.82, 135.66, 131.32, 129.92, 129.37, 128.68, 127.65, 125.79, 119.60, 45.49, 36.41, 21.52, 19.92, 19.35, 17.26.

IR (KBr, cm^{-1}): *v* = 3430 (OH); 3033 (aromatic CH); 2966, 2922, 2850 (aliphatic CH); 1735 (2×C=O); 1600, 1563 (C=C); 1505 (C-C); 1327 (C=S); 1192, 1162 (C-N).

Anal. calcd. for $C_{61}H_{54}N_6O_6S_4$: C 66.89, H 4.97, N 7.67; found: C 66.89, H 4.95, N 7.67.

2,2'-((5Z,5'Z)-((2E,2'E,4E,4'E)-(((4,10-dimethyl-6H,12H-5,11-methanodibenzo[b,f][1,5]diazocine-2,8-diyl)bis((3,4-dimethylphenyl)azanediyl))bis(4,1-phenylene))bis(penta-2,4-dien-5-yl-1-ylidene))bis(4-oxo-2-thioxothiazolidin-3-yl-5-ylidene))diacetic acid (**5C**)

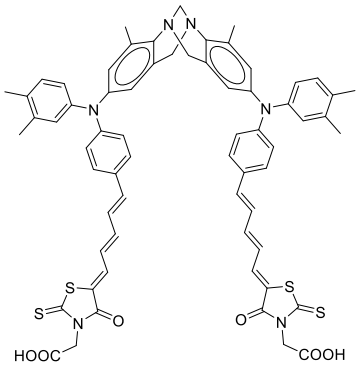

A mixture of aldehyde compound **5m** (0.25 g, 0.31 mmol), rhodanine-3-acetic acid (0.14 g, 0.74 mmol), and $AcONH_4$ (0.01 g, 0.10 mmol) was refluxed in anhydrous toluene (8 ml) for 12 h. At the end of the reaction, the mixture was cooled to room temperature. Dark violet crystals, formed upon standing, were filtered off and washed with water (50 ml), methanol (50 ml), and finally diethyl ether (25 ml), yielding dye **5C** (76%, 0.27 g), m.p. > 400 °C.

^{1}H NMR (400 MHz, DMSO-d_6) δ 7.51 (d, *J* = 11.9 Hz, 2H, Ar), 7.35 (d, *J* = 8.5 Hz, 4H, Ar), 7.28–7.12 (m, 8H, Ar), 7.09 (d, *J* = 8.2 Hz, 2H, Ar), 6.93–6.64 (m, 8H, Ar), 6.56 (s, 2H, Ar), 6.51–6.39 (m, 2H, Ar), 4.61 (s, 4H, N-C$\underline{H_2}$-COOH), 4.38 (d, *J* = 17.0 Hz, 2H, H-6*exo*, and H-12*exo*), 4.18 (s, 2H, H-13), 3.90 (d, *J* = 17.4 Hz, 2H, H-6*endo*, and H-12*endo*), 2.23 (s, 6H, 2× CH_3), 2.18 (s, 6H, 2× CH_3), 2.13 (s, 6H, 2× CH_3).

^{13}C NMR (101 MHz, DMSO-d_6) δ 192.51, 174.28, 167.77, 166.05, 149.46, 147.93, 144.46, 142.66, 142.07, 140.42, 138.14, 137.75, 134.68, 134.43, 133.17, 131.23, 129.81, 129.37, 129.08, 128.67, 127.37, 126.19, 125.81, 121.45, 120.33, 54.53, 45.89, 21.52, 19.92, 19.31, 17.25.

IR (KBr, cm^{-1}): *v* = 3433 (OH); 3033 (aromatic CH); 2946, 2916 (aliphatic CH); 1698 (2×C=O); 1600, 1545 (C=C); 1502 (C-C); 1309 (C=S); 1197, 1154 (C-N).

Anal. calcd. for $C_{65}H_{58}N_6O_6S_4$: C 68.04, H 5.10, N 7.32; found: C 68.00, H 5.12, N 7.34.

2-(4-bromophenyl)-5,5-dimethyl-1,3-dioxane (**5n**)

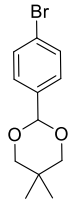

4-Bromobenzaldehyde (6.18 g, 7.76 mmol), 2,2-dimethyl-1,3-propanediol (4.18 g, 40.11 mmol), and *p*-toluenesulfonic acid monohydrate (0.70 g, 3.67 mmol) were dissolved in benzene (55 ml) and stirred at 80 °C for 3 h. After the reaction, its mixture was poured into distilled water (150 ml), and the product was extracted with ethyl acetate. The solvent was removed under reduced pressure, resulting in white crystalline solid (86%, 7.8 g) that matches the described in literature and was sufficiently clean (based on TLC) to be used without further purification.

^{1}H NMR (400 MHz, $CDCl_3$) δ 7.50 (d, *J* = 8.5 Hz, 2H, Ar), 7.38 (d, *J* = 8.4 Hz, 2H, Ar), 5.34 (s, 1H, O-CH-O), 3.76 (d, *J* = 11.2 Hz, 2H, O-C$\underline{H_2}$-C), 3.63 (d, *J* = 10.6 Hz, 2H, O-C$\underline{H_2}$-C), 1.27 (s, 3H, CH_3), 0.79 (s, 3H, CH_3).

^{13}C NMR (101 MHz, $CDCl_3$) δ 137.57, 131.41, 127.95, 122.88, 100.94, 30.23, 23.03, 21.88.

Anal. calcd. for $C_{12}H_{15}BrO_2$: C 53.16, H 5.58; found: C 53.21, H 5.78.

4-((3,4-dimethylphenyl)(m-tolyl)amino)benzaldehyde (**5o**)

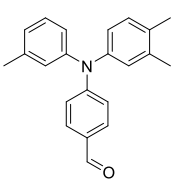

A mixture of dioxane (10 ml) and water (0.01 ml) was purged with argon for 20 minutes. $Pd(OAc)_2$ (0.009 g, 0.03 mmol), SPhos (0.04 g, 0.09 mmol) were added, and the mixture was heated to 80 °C for 2 min. *N*-(4-(5,5-dimethyl-1,3-dioxan-2-yl)phenyl)-3,4-dimethylaniline (**5e**) (2 g, 6.42 mmol), 3-iodotoluene (1 ml, 7.71 mmol), and NaO*t*-Bu (0.86 g, 8.99 mmol) were added, and the solution was refluxed for 2 h under Ar atmosphere. After the termination of the reaction, the mixture was filtered through Celite, the distilled water was added, and the mixture was extracted with ethyl acetate. The organic layer was dried over anhydrous Na_2SO_4, filtered, and the solvent evaporated under reduced pressure. The crude product was purified by column chromatography (THF/*n*-hexane 0.5:24.5, v/v) yielding product as light brown oil. Subsequently, it was dissolved in THF (15 ml), 12% aq. HCl solution (7 ml) was added, and the mixture was stirred at 40 °C for 1 hour. The reaction mixture was poured into the saturated $NaHCO_3$ solution and extracted with ethyl acetate. The organic layer was dried over anhydrous Na_2SO_4, filtered, and the solvent evaporated under reduced pressure, resulting in yellow solid (55%, 1.04 g).

^{1}H NMR (400 MHz, $CDCl_3$) δ 9.77 (s, 1H, CHO), 7.64 (d, *J* = 8.8 Hz, 2H, Ar), 7.26–7.18 (m, 1H, Ar), 7.10 (d, *J* = 8.1 Hz, 1H, Ar), 7.01–6.85 (m, 7H, Ar), 2.30 (s, 3H, CH_3), 2.26 (s, 3H, CH_3), 2.21 (s, 3H, CH_3).

^{13}C NMR (101 MHz, $CDCl_3$) δ 190.41, 153.77, 146.08, 143.70, 139.65, 138.21, 133.99, 131.31, 130.86, 129.46, 128.43, 127.86, 126.87, 125.91, 124.20, 123.40, 118.52, 21.40, 19.89, 19.33.

Anal. calcd. for $C_{22}H_{21}NO$: C 83.78, H 6.71, N 4.44; found: C 83.73, H 6.76, N 4.45.

(E)-3-(4-((3,4-dimethylphenyl)(m-tolyl)amino)phenyl)acrylaldehyde (**5p**)

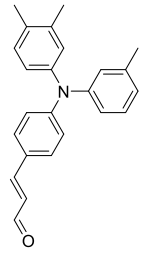

4-((3,4-dimethylphenyl)(*m*-tolyl)amino)benzaldehyde (**5o**) (0.60 g, 1.91 mmol) and tributyl(1,3-dioxalan-2-ylmethyl)phosphonium bromide (0.78 g, 2.10 mmol) were dissolved in anhydrous THF (7 ml) under argon gas atmosphere; NaH (60% dispersed in mineral oil, 0.23 g, 5.73 mmol) was added in portions, and the resulting turbid solution was stirred at room temperature for 3 h. After the completion of the reaction (TLC ethyl acetate/toluene/*n*-hexane 3:1:21, v/v), the excess NaH was quenched by using 10% aq. HCl solution under cooling, and the reaction mixture was brought to acidic pH. The reaction mixture was stirred further at room temperature for 1 hour. The mixture was poured into the distilled water and extracted with ethyl acetate. The organic layer was dried over anhydrous Na_2SO_4, filtered off, and the solvent evaporated under reduced pressure. The product was purified by column chromatography (ethyl acetate/toluene/*n*-hexane 3:1:21, v/v), yielding a yellow solid (78%, 0.51 g).

^{1}H NMR (400 MHz, $CDCl_3$) δ 9.64 (d, *J* = 7.8 Hz, 1H, CHO), 7.43–7.36 (m, 3H, Ar), 7.31–7.25 (m, 1H, Ar), 7.25–7.16 (m, 2H, Ar), 7.12 (d, *J* = 8.0 Hz, 1H, Ar), 7.02–6.88 (m, 5H, Ar), 6.60 (dd, *J* = 15.8, 7.8 Hz, 1H, CH), 2.32 (s, 3H, CH_3), 2.28 (s, 3H, CH_3), 2.23 (s, 3H, CH_3).

^{13}C NMR (101 MHz, $CDCl_3$) δ 193.82, 153.03, 151.24, 146.51, 144.12, 139.48, 138.07, 133.39, 130.74, 129.85, 129.32, 127.45, 126.25, 125.80, 125.53, 125.22, 123.79, 122.79, 120.13, 21.44, 19.93, 19.33.

Anal. calcd. for $C_{24}H_{23}NO$: C 84.42, H 6.79, N 4.10; found: C 84.38, H 6.76, N 4.10.

(2E,4E)-5-(4-((3,4-dimethylphenyl)(m-tolyl)amino)phenyl)penta-2,4-dienal (**5r**)

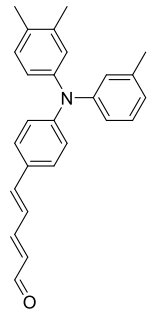

(*E*)-3-(4-((3,4-dimethylphenyl)(*m*-tolyl)amino)phenyl)acrylaldehyde (**5p**) (0.62 g, 1.81 mmol) and (tributyl(1,3-dioxalan-2-ylmethyl)phosphonium bromide (0.74 g, 1.99 mmol) were dissolved in anhydrous THF (6 ml) under argon gas atmosphere; NaH (60% dispersed in mineral oil, 0.22 g, 5.45 mmol) was added in portions, and the resulting turbid solution was stirred at room temperature for 1 h. After the completion of the reaction (TLC 3:1:21 v/v ethyl acetate/toluene/*n*-hexane), the excess NaH was quenched by using 10% aq. HCl solution under cooling, and the reaction mixture was brought to acidic pH. The reaction mixture was stirred further more at room temperature for 1 hour. The mixture was poured into distilled water and extracted with ethyl acetate. The organic layer was dried over anhydrous Na_2SO_4, filtered off, and the solvent evaporated under reduced pressure. The product was purified by column chromatography (ethyl acetate/toluene/ *n*-hexane 3:1:21, v/v), yielding a yellow solid. Yield: 0.56 g (84%).

^{1}H NMR (400 MHz, $CDCl_3$) δ 9.57 (d, *J* = 8.0 Hz, 1H, CHO), 7.32 (d, *J* = 8.6 Hz, 2H, Ar), 7.28–7.12 (m, 4H, Ar), 7.06 (d, *J* = 8.0 Hz, 1H, Ar), 6.98–6.80 (m, 7H, Ar), 6.20 (dd, *J* = 15.1, 8.0 Hz, 1H, CH), 2.27 (s, 3H, CH_3), 2.24 (s, 3H, CH_3), 2.19 (s, 3H, CH_3).

^{13}C NMR (101 MHz, $CDCl_3$) δ 193.70, 153.15, 149.80, 146.93, 144.53, 142.62, 139.32, 137.92, 132.84, 130.64, 130.10, 129.21, 128.64, 127.98, 127.12, 125.76, 124.65, 123.53, 123.44, 122.32, 121.13, 21.45, 19.93, 19.30.
Anal. calcd. for $C_{26}H_{25}NO$: C 84.98, H 6.86, N 3.81; found: C 84.94, H 6.88, N 3.84.

2-(5-(4-((3,4-dimethylphenyl)(m-tolyl)amino)benzylidene)-4-oxo-2-thioxothiazolidin-3-yl)acetic acid (**5D**)

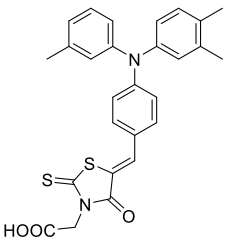

A mixture of 4-((3,4-dimethylphenyl)(*m*-tolyl)amino)benzaldehyde (**5o**) (0.47 g, 1.50 mmol), rhodanine-3-acetic acid (0.34 g, 1.80 mmol), and $AcONH_4$ (0.03 g, 0.45 mmol) was refluxed in anhydrous toluene (2 ml) for 12 h. After the termination of the reaction, the distilled water was added, and the mixture was extracted with ethyl acetate. The organic layer was dried over anhydrous Na_2SO_4, filtered, and the solvent evaporated under reduced pressure. The crude product was purified by column chromatography (acetone/*n*-hexane 7:18, acetone/*n*-hexane 2:3, and methanol/toluene 3:22, v/v) yielding dye **5D** as a red solid (43%, 0.31 g), m.p. 193–195 °C.
^{1}H NMR (400 MHz, DMSO-d_6) δ 7.65 (s, 1H, Ar), 7.47 (d, J = 9.0 Hz, 2H, Ar), 7.32–7.22 (m, 1H, Ar), 7.18 (d, J = 8.1 Hz, 1H, Ar), 7.06–6.88 (m, 5H, Ar), 6.85 (d, J = 8.9 Hz, 2H, Ar), 4.47 (s, 2H, N-C$\underline{H_2}$-COOH), 2.26 (s, 3H, CH_3), 2.22 (s, 3H, CH_3), 2.18 (s, 3H, CH_3).
^{13}C NMR (101 MHz, DMSO-d_6) δ 193.31, 167.36, 150.71, 146.04, 143.64, 139.83, 138.54, 134.31, 133.31, 133.06, 131.40, 130.15, 128.01, 126.81, 126.35, 124.58, 124.54, 123.53, 119.19, 118.10, 67.49, 47.74, 21.40, 19.91, 19.37.
IR (KBr, cm^{-1}): v = 3423 (OH); 3033 (aromatic CH); 2919, 2850 (aliphatic CH); 1711 (2×C=O); 1574 (C=C); 1506 (C-C); 1320, 1308 (C=S); 1200, 1180 (C-N).
Anal. calcd. for $C_{27}H_{24}N_2O_3S_2$: C 66.37, H 4.95, N 5.73; found: C 66.35, H 4.94, N 5.74.

2-((Z)-5-((E)-3-(4-((3,4-dimethylphenyl)(m-tolyl)amino)phenyl)allylidene)-4-oxo-2-thioxothiazolidin-3-yl)acetic acid (**5E**)

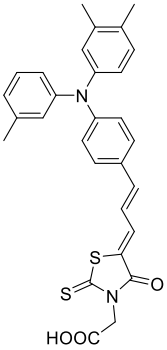

A mixture of (*E*)-3-(4-((3,4-dimethylphenyl)(*m*-tolyl)amino)phenyl)acrylaldehyde (**5p**) (0.22 g, 0.66 mmol), rhodanine-3-acetic acid (0.15 g, 0.79 mmol), and $AcONH_4$ (0.02 g, 0.19 mmol) was refluxed in glacial acetic acid (2 ml) for 2.5 h. After the termination of the reaction, the distilled water was added, and the mixture was extracted with ethyl acetate. The organic layer was dried over anhydrous Na_2SO_4, filtered, and the solvent evaporated under reduced pressure. The crude product was purified by column chromatography (methanol/toluene 2:23, v/v) yielding dye **5E** as a red solid (71%, 0.27 g), m.p. 239–240 °C.
^{1}H NMR (400 MHz, DMSO-d_6) δ 7.57–7.42 (m, 3H, Ar), 7.31–7.08 (m, 3H, Ar), 6.97–6.76 (m, 8H, Ar), 4.39 (s, 2H, N-C$\underline{H_2}$-COOH), 2.23 (s, 3H, CH_3), 2.20 (s, 3H, CH_3), 2.16 (s, 3H, CH_3).

^{13}C NMR (101 MHz, DMSO-d_6) δ 192.94, 166.60, 149.96, 146.72, 145.61, 144.29, 138.27, 134.08, 133.42, 131.23, 130.02, 129.94, 129.37, 128.67, 128.35, 127.41, 125.96, 125.78, 123.90, 122.70, 122.26, 121.29, 120.43, 48.22, 21.42, 19.91, 19.32.
IR (KBr): ν = 3412 (OH); 3033 (aromatic CH); 2918, 2850 (aliphatic CH); 1704 (2×C=O); 1600, 1565 (C=C); 1498 (C-C); 1316, 1300 (C=S); 1197, 1160 (C-N).
Anal. calcd. for $C_{29}H_{26}N_2O_3S_2$: C 67.68, H 5.09, N 5.44; found: C 67.65, H 5.10, N 5.47.

2-((Z)-5-((2E,4E)-5-(4-((3,4-dimethylphenyl)(m-tolyl)amino)phenyl)penta-2,4-dien-1-ylidene)-4-oxo-2-thioxothiazolidin-3-yl)acetic acid (**5F**)

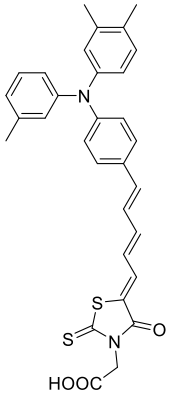

A mixture of (2*E*,4*E*)-5-(4-((3,4-dimethylphenyl)(*m*-tolyl)amino)phenyl)penta-2,4-dienal (**5r**) (0.25 g, 0.69 mmol), rhodanine-3-acetic acid (0.16 g, 0.83 mmol), and $AcONH_4$ (0.02 g, 0.20 mmol) was refluxed in glacial acetic acid (2.5 ml) for 45 min. The crude product was purified by column chromatography (methanol/toluene 2:23, v/v) resulting in dye **5F** as a red solid (54%, 0.20 g), m.p. 199–200 °C.
^{1}H NMR (700 MHz, DMSO-d_6) δ 7.48–7.39 (m, 3H, Ar), 7.23–7.10 (m, 4H, Ar), 7.08–7.00 (m, 1H, Ar), 6.94–6.78 (m, 7H, Ar), 6.50–6.43 (m, 1H, CH), 4.38 (s, 2H, N-C$\underline{H_2}$-COOH), 2.23 (s, 3H, CH_3), 2.20 (s, 3H, CH_3), 2.16 (s, 3H, CH_3).
^{13}C NMR (176 MHz, DMSO-d_6) δ 192.55, 166.50, 149.05, 147.03, 146.92, 144.58, 139.69, 139.44, 138.19, 131.20, 129.89, 129.37, 128.98, 128.68, 127.26, 126.59, 125.79, 125.59, 125.38, 125.01, 123.74, 122.74, 122.33, 121.14, 48.20, 21.52, 21.45, 19.93, 19.30.
IR (KBr): ν = 3423 (OH); 3033 (aromatic CH); 2916, 2866 (aliphatic CH); 1703 (2×C=O); 1600, 1566, 1545 (C=C); 1503 (C-C); 1314 (C=S); 1197, 1154 (C-N).
Anal. calcd. for $C_{31}H_{28}N_2O_3S_2$: C 68.86, H 5.22, N 5.18; found: C 68.85, H 5.23, N 5.15.

3,4-dimethyl-N-phenylaniline (**6'**)

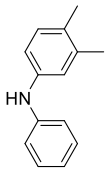

A mixture of dioxane (52 ml) and water (0.03 ml) was purged with argon for 20 minutes. $Pd(OAc)_2$ (0.045 g, 0.2 mmol), XPhos (0.286 g, 0.6 mmol) were added, and the mixture was heated to 80 °C for 2 min. 3,4-dimethyl-*N*-phenylaniline (4.85 g, 40 mmol), bromobenzene (7.1 ml, 52 mmol), and NaO*t*-Bu (5.38 g, 56 mmol) were added, and the solution was refluxed for 2 h under Ar atmosphere. After the termination of the reaction, the mixture was filtered through Celite, the distilled water was added, and the mixture was extracted with ethyl acetate. The organic layer was dried over anhydrous Na_2SO_4, filtered, and the solvent removed under reduced pressure. The crude product was purified by column chromatography (THF/*n*-hexane 0.5:24.5, v/v) yielding white solid (85%, 6.7 g).
^{1}H NMR (400 MHz, $CDCl_3$): 7.21 (t, 2H, J = 7.8 Hz, Ar), 7.02–6.97 (m, 3H, Ar), 6.86–6.81 (m, 3H, Ar), 5.51 (s, 1H, NH), 2.20 (s, 3H, CH_3), 2.19 (s, 3H, CH_3).

^{13}C NMR (101 MHz, $CDCl_3$): 144.1, 140.7, 137.7, 130.5, 129.8, 129.4, 120.4, 120.3, 116.9, 116.3, 20.1, 19.2.
Anal. calcd. for $C_{14}H_{15}N$: C 85.24, H 7.66, N 7.1; found: C 85.29, H 7.66, N 7.05.

N-(4-bromophenyl)-3,4-dimethylaniline (**6a**)

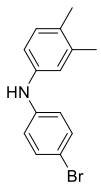

3,4-dimethyl-*N*-phenylaniline (**6'**) (5.6 g, 28.4 mmol) was dissolved in DMF (48 ml), cooled down to 0 °C in the ice bath, and *N*-bromosuccinimide (5.05 g, 28.4 mmol) was dissolved in 24 ml and added dropwise to the mixture while cooling. The stirring mixture was allowed to reach r.t. and was kept stirring for 1 hour. Afterwards, the water was added, and the extraction was done with ethyl acetate. The organic layer was dried over anhydrous Na_2SO_4, filtered, and the solvent evaporated. The crude product was purified by column chromatography (THF/*n*-hexane 1:24, v/v) yielding yellowish solid (85%, 6.7 g).
^{1}H NMR (400 MHz, $CDCl_3$) δ 7.54 (d, *J* = 8.5 Hz, 2H, Ar), 7.09 (d, *J* = 8.0 Hz, 1H, Ar), 7.03–6.88 (m, 4H, Ar), 5.81 (s, 1H, NH), 2.25 (s, 3H, CH_3), 2.24 (s, 3H, CH_3).
^{13}C NMR (101 MHz, $CDCl_3$) δ 140.78, 138.99, 137.89, 131.25, 130.50, 127.69, 124.26, 122.22, 121.82, 115.82, 19.96, 19.11.
Anal. calcd. for $C_{14}H_{14}BrN$: C 60.89, H 5.11, N 5.07; found: C 61.1, H 4.92, N 4.89.

5-(4-((3,4-dimethylphenyl)amino)phenyl)thiophene-2-carbaldehyde (**6b**)

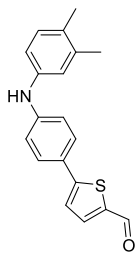

A solution of *N*-(4-bromophenyl)-3,4-dimethylaniline (**6a**) (2 g, 7.25 mmol) and 5-formyl-2-thiopheneboronic acid (2.52 g, 16.17 mmol) in THF (18 ml) was mixed with argon-purged 2N aqueous K_2CO_3 solution (7 ml) and was stirred under argon atmosphere. After 20 min, $Pd(PPh_3)_4$ (0.838 g, 0.725 mmol) was added, and the solution was refluxed for 12 hours. The solution was allowed to cool to room temperature, the water was added, and the organic layer was extracted with ethyl acetate. The organic layer was dried over anhydrous Na_2SO_4, filtered, and the solvent was removed under reduced pressure. The crude product was purified by column chromatography (acetone/*n*-hexane 1:24, v/v) yielding a yellow solid (55%, 1.23 g).
^{1}H NMR (400 MHz, $CDCl_3$) δ 9.84 (s, 1H, CHO), 7.69 (d, *J* = 3.9 Hz, 1H, Ar), 7.54 (d, *J* = 8.5 Hz, 2H, Ar), 7.27 (d, *J* = 4.0 Hz, 1H, Ar), 7.09 (d, *J* = 8.0 Hz, 1H, Ar), 7.03–6.88 (m, 4H, Ar), 5.81 (s, 1H, NH), 2.25 (s, 3H, CH_3), 2.24 (s, 3H, CH_3).
^{13}C NMR (101 MHz, $CDCl_3$) δ 182.58, 155.26, 145.82, 140.78, 138.99, 137.89, 137.82, 131.25, 130.50, 127.69, 124.26, 122.22, 121.82, 117.81, 115.82, 19.96, 19.11.
Anal. calcd. for $C_{19}H_{17}NOS$: C 74.24, H 5.57, N 4.56; found: C 74.47, H 5.73, N 4.32.

N-(4-(5-(5,5-dimethyl-1,3-dioxan-2-yl)thiophen-2-yl)phenyl)-3,4-dimethylaniline (**6c**)

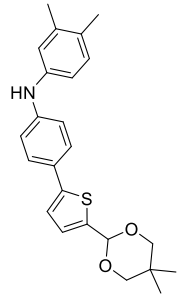

5-(4-((3,4-dimethylphenyl)amino)phenyl)thiophene-2-carbaldehyde (**6b**) (1.23 g, 4 mmol), 2-dimethyl-1,3-propanediol (0.5 g, 4.8 mmol), and *p*-toluenesulfonic acid monohydrate (0.084 g, 0.44 mmol) were dissolved in benzene (8 ml), and the mixture was stirred at 80 °C for 3 h. After cooling to room temperature, the reaction was quenched by adding distilled water and then was extracted with ethyl acetate. The organic layer was dried over anhydrous Na_2SO_4, filtered, and the solvent evaporated. The product was purified by column chromatography (acetone/*n*-hexane 1:24, v/v) obtaining yellow solid (68%, 1.07 g).

^{1}H NMR (400 MHz, $CDCl_3$) δ 7.45 (d, *J* = 8.4 Hz, 2H, Ar), 7.14–6.74 (m, 7H, Ar), 5.80–5.47 (m, 2H, O-CH-O, NH), 3.70 (dd, *J* = 49.5, 10.9 Hz, 4H, O-C$\underline{H_2}$-C), 2.23 (d, *J* = 4.2 Hz, 6H, Ar-CH_3), 1.29 (s, 3H, C-CH_3), 0.80 (s, 3H, C-CH_3).

^{13}C NMR (101 MHz, $CDCl_3$) δ 145.12, 143.78, 140.02, 139.01, 137.66, 130.41, 130.17, 126.99, 125.94, 120.95, 120.85, 116.80, 116.59, 98.45, 77.58, 30.24, 23.02, 21.87, 19.97, 19.05.

Anal. calcd. for $C_{24}H_{27}NO_2S$: C 73.25, H 6.92, N 3.56; found: C 73.29, H 6.68, N 3.6.

N^2,N^8-bis(4-(5-(5,5-dimethyl-1,3-dioxan-2-yl)thiophen-2-yl)phenyl)-N^2,N^8-bis(3,4-dimethylphenyl)-4,10-dimethyl-6H,12H-5,11-methanodibenzo[b,f][1,5]diazocine-2,8-diamine (**6d**)

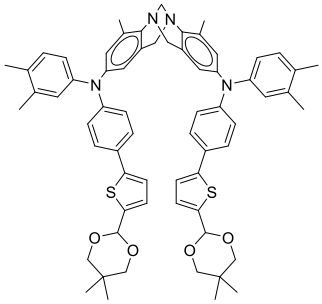

A mixture of *N*-(4-(5-(5,5-dimethyl-1,3-dioxan-2-yl)thiophen-2-yl)phenyl)-3,4-dimethylaniline (**6c**) (0.72 g, 1.83 mmol), 2,8-dibromo-4,10-dimethyl-6*H*,12*H*-5,11-methanodibenzo[*b*,*f*][1,5]diazocine (**1'**) (0.298 g, 0.73 mmol), and anhydrous toluene (6 ml) was purged with argon for 30 minutes. $Pd(OAc)_2$ (0.004 g, 0.016 mmol), $[P(t\text{-}Bu)_3H]BF_4$ (0.0057 g, 0.02 mmol), and NaO*t*-Bu (0.175 g, 1.83 mmol) were added, and the mixture was heated at reflux for 5 h under Ar atmosphere. After the termination of the reaction, the water was added, and the mixture was extracted with ethyl acetate. The organic layer was dried over anhydrous Na_2SO_4, filtered, and the solvent evaporated under reduced pressure. The product was purified by column chromatography (ethyl acetate/toluene/*n*-hexane 2:5:18, v/v), resulting in orange solid (73%, 0.55 g).

^{1}H NMR (400 MHz, $CDCl_3$) δ 7.40 (d, *J* = 8.5 Hz, 4H, Ar), 7.09–6.80 (m, 16H, Ar), 6.53 (d, *J* = 1.6 Hz, 2H, Ar), 5.62 (s, 2H, O-CH-O), 4.70–4.15 (m, 4H, H-13, H-6*exo*, and H-12*exo*), 3.91 (d, *J* = 16.7 Hz, 2H, H-6*endo*, and H-12*endo*), 3.70 (dd, *J* = 49.2, 11.0 Hz, 8H, O-C$\underline{H_2}$-C), 2.31 (s, 6H, Ar-CH_3), 2.23 (s, 6H, Ar-CH_3), 2.19 (s, 6H, Ar-CH_3), 1.29 (s, 6H, C-CH_3), 0.80 (s, 6H, C-CH_3).

^{13}C NMR (101 MHz, $CDCl_3$) δ 144.73, 144.32, 141.77, 139.54, 139.50, 137.84, 137.83, 134.04, 130.58, 129.05, 128.24, 126.75, 126.60, 125.97, 125.32, 123.10, 123.05, 121.48, 121.46, 98.41, 77.58, 57.64, 54.78, 30.24, 23.01, 21.86, 21.47, 19.91, 19.22.

Anal. calcd. for $C_{65}H_{68}N_4O_4S_2$: C 75.55, H 6.63, N 5.42; found: C 75.52, H 6.84, N 5.4.

5,5'-(((4,10-dimethyl-6H,12H-5,11-methanodibenzo[b,f][1,5]diazocine-2,8-diyl)bis((3,4-dimethylphenyl)azanediyl))bis(4,1-phenylene))bis(thiophene-2-carbaldehyde) (**6e**)

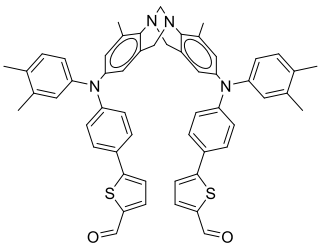

Protected aldehyde compound **6d** (0.56 g, 0.55 mmol) was dissolved in THF (5 ml), 12% aq. HCl solution (2 ml) was added, and the mixture was stirred at 40 °C for 1 hour. The reaction mixture was poured into the saturated $NaHCO_3$ solution and extracted with ethyl acetate. The organic layer was dried over anhydrous Na_2SO_4, filtered, and the solvent was removed under reduced pressure. The crude product was purified by column chromatography (acetone/*n*-hexane 2:23, v/v), resulting in yellow solid (87%, 0.412 g).

^{1}H NMR (400 MHz, $CDCl_3$) δ 9.83 (s, 2H, CHO), 7.69 (d, *J* = 3.9 Hz, 2H, Ar), 7.46 (d, *J* = 8.7 Hz, 4H, Ar), 7.26 (d, *J* = 4.2 Hz, 2H, Ar), 7.07 (d, *J* = 8.0 Hz, 2H, Ar), 6.99–6.80 (m, 10H, Ar), 6.56 (s, 2H, Ar), 4.48 (d, *J* = 17.0 Hz, 2H, H-6*exo*, and H-12*exo*), 4.29 (s, 2H, H-13), 3.88 (d, *J* = 17.0 Hz, 2H, H-6*endo*, and H-12*endo*), 2.29 (s, 6H, 2× CH_3), 2.25 (s, 6H, 2× CH_3), 2.20 (s, 6H, 2× CH_3).

^{13}C NMR (101 MHz, $CDCl_3$) δ 182.59, 154.98, 149.73, 144.46, 142.45, 142.33, 140.97, 137.96, 134.31, 132.87, 130.68, 129.14, 127.12, 125.93, 125.32, 124.86, 123.48, 122.50, 120.94, 120.78, 67.57, 54.91, 19.92, 19.28, 17.10.

Anal. calcd. for $C_{55}H_{48}N_4O_2S_2$: C 76.71, H 5.62, N 6.51; found: C 76.76, H 5.76, N 6.21.

2,2'-((((((4,10-dimethyl-6H,12H-5,11-methanodibenzo[b,f][1,5]diazocine-2,8-diyl)bis((3,4-dimethylphenyl)azanediyl))bis(4,1-phenylene))bis(thiophene-5,2-diyl))bis(methanylylidene))bis(4-oxo-2-thioxothiazolidin-3-yl-5-ylidene))diacetic acid (**6f**)

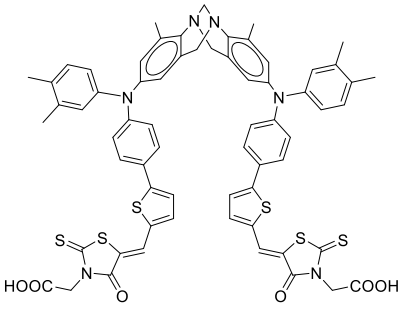

A mixture of aldehyde compound **6e** (0.198 g, 0.23 mmol), rhodanine-3-acetic acid (0.132 g, 0.69 mmol), and $AcONH_4$ (0.011 g, 0.14 mmol) was refluxed in anhydrous toluene (1.5 ml) for 10 h. After the termination of the reaction, the distilled water was added, and the mixture was extracted with ethyl acetate. The organic layer was dried over anhydrous Na_2SO_4, filtered, and the solvent was removed under reduced pressure. The crude product was purified by column chromatography (acetone/*n*-hexane 6:19, and methanol/toluene 2:23, v/v) to obtain dye **6f** as a red solid (86%, 0.24 g).

^{1}H NMR (400 MHz, DMSO) δ 7.72 (s, 2H, Ar), 7.50 (d, *J* = 5.2 Hz, 6H, Ar), 7.26–6.65 (m, 14H, Ar), 6.56 (s, 2H, Ar), 4.53 (s, 4H, N-C$\underline{H_2}$-COOH), 4.38 (d, *J* = 17.0 Hz,

2H, H-6*exo*, and H-12*exo*), 4.20 (s, *J* = 21.6 Hz, 2H, H-13), 3.90 (d, *J* = 16.1 Hz, 2H, H-6*endo*, and H-12*endo*), 2.22 (s, 6H, 2× CH_3), 2.18 (s, 6H, 2× CH_3), 2.13 (s, 6H, 2× CH_3).

^{13}C NMR (101 MHz, DMSO) δ 189.65, 189.59, 153.00, 151.80, 143.89, 142.73, 140.95, 140.52, 140.25, 139.35, 138.20, 137.13, 135.54, 134.83, 134.48, 133.03, 131.22, 130.77, 129.89, 128.16, 127.33, 124.82, 124.80, 122.88, 121.25, 118.10, 117.65, 113.53, 110.72, 95.50, 31.18, 22.51, 19.92, 19.31, 17.25.

Anal. calcd. for $C_{65}H_{54}N_6O_6S_6$: C 64.65, H 4.51, N 6.96; found: C 64.77, H 4.43, N 6.76.

N-(4-(5-(5,5-dimethyl-1,3-dioxan-2-yl)thiophen-2-yl)phenyl)-3,4-dimethyl-N-(m-tolyl)aniline (**6g**)

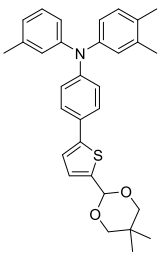

A mixture of dioxane (2.5 ml) and water (0.01 ml) was purged with argon for 20 minutes. $Pd(OAc)_2$ (0.001 g, 0.05 mmol), XPhos (0.286 g, 0.6 mmol) were added, and the mixture was heated to 80 °C for 2 min. *N*-(4-(5-(5,5-dimethyl-1,3-dioxan-2-yl)thiophen-2-yl)phenyl)-3,4-dimethylaniline (**6c**) (0.3 g, 0.75 mmol), 3-iodotoluene (0.22 g, 1 mmol), and NaO*t*-Bu (0.1 g, 1 mmol) were added, and the solution was refluxed for 2 h under Ar atmosphere. After the termination of the reaction, the distilled water was added, and the mixture was extracted with ethyl acetate. The organic layer was dried over anhydrous Na_2SO_4, filtered, and the solvent evaporated under reduced pressure. The crude product was purified by column chromatography (acetone/*n*-hexane 1:24, v/v) yielding yellow solid (77%, 0.28 g).

^{1}H NMR (400 MHz, $CDCl_3$) δ 7.41 (d, *J* = 8.6 Hz, 1H, Ar), 7.19–6.77 (m, 12H, Ar), 5.62 (s, 1H, O-CH-O), 3.70 (dd, *J* = 49.3, 10.9 Hz, 4H, O-C$\underline{H_2}$-C), 2.26 (s, 3H, Ar-CH_3), 2.23 (s, 3H, Ar-CH_3), 2.18 (s, 3H, Ar-CH_3), 1.29 (s, 3H, C-CH_3), 0.80 (s, 3H, C-CH_3).

^{13}C NMR (101 MHz, $CDCl_3$) δ 147.62, 145.19, 144.85, 139.40, 139.07, 137.68, 131.92, 130.47, 129.01, 127.63, 127.15, 126.59, 126.55, 125.95, 124.87, 123.64, 122.90, 122.77, 121.46, 121.39, 98.43, 77.58, 30.24, 23.02, 21.87, 21.44, 19.88, 19.20.

Anal. calcd. for $C_{31}H_{33}NO_2S$: C 76.98, H 6.88, N 2.9; found: C 76.81, H 6.68, N 3.06.

5-(4-((3,4-dimethylphenyl)(m-tolyl)amino)phenyl)thiophene-2-carbaldehyde (**6h**)

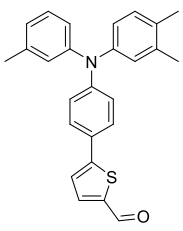

N-(4-(5-(5,5-dimethyl-1,3-dioxan-2-yl)thiophen-2-yl)phenyl)-3,4-dimethyl-*N*-(*m*-tolyl)aniline (**6g**) was dissolved in THF (5 ml), 12% aq. HCl solution (2 ml) was added, and the mixture was stirred at 40 °C for 1 hour. The reaction mixture was poured into the saturated $NaHCO_3$ solution and extracted with ethyl acetate. The organic layer was dried over anhydrous Na_2SO_4, filtered, and the solvent evaporated under reduced pressure resulting in yellow solid (91%, 0.2 g).

^{1}H NMR (400 MHz, $CDCl_3$) δ 9.84 (s, 1H, CHO), 7.69 (d, *J* = 3.9 Hz, 1H, Ar), 7.48 (d, *J* = 8.6 Hz, 2H, Ar), 7.19–6.81 (m, 10H, Ar), 2.28 (s, 3H, CH_3), 2.25 (s, 3H, CH_3),

2.20 (s, 3H, CH_3).
^{13}C NMR (101 MHz, $CDCl_3$) δ 182.60, 154.93, 149.59, 147.01, 144.60, 141.07, 139.32, 137.91, 137.82, 132.75, 130.64, 129.20, 127.06, 126.59, 125.63, 125.29, 124.54, 123.37, 122.62, 122.18, 121.51, 98.43, 23.02, 21.87, 21.44.
Anal. calcd. for $C_{26}H_{23}NOS$: C 78.56, H 5.83, N 3.52; found: C 78.51, H 5.75, N 3.56.

2-(5-((5-(4-((3,4-dimethylphenyl)(m-tolyl)amino)phenyl)thiophen-2-yl)methylene)-4-oxo-2-thioxothiazolidin-3-yl)acetic acid (**6i**)

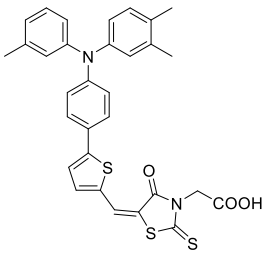

A mixture of 5-(4-((3,4-dimethylphenyl)(*m*-tolyl)amino)phenyl)thiophene-2-carbaldehyde (**6h**) (0.1 g, 0.26 mmol), rhodanine-3-acetic acid (0.12 g, 0.625 mmol), and $AcONH_4$ (0.012 g, 0.156 mmol) was refluxed in anhydrous toluene (0.8 ml) for 7 h. After the termination of the reaction, the distilled water was added, and the mixture was extracted with ethyl acetate. The organic layer was dried over anhydrous Na_2SO_4, filtered, and the solvent was removed under reduced pressure. The crude product was purified by column chromatography (methanol/toluene 2:23, v/v) yielding dye **6i** as a red solid (67%, 0.1 g).
^{1}H NMR (400 MHz, DMSO) δ 8.12 (s, 1H, Ar), 7.79 (d, *J* = 3.3 Hz, 1H, Ar), 7.71–7.51 (m, 3H, Ar), 7.22 (t, *J* = 7.6 Hz, 1H, Ar), 7.13 (d, *J* = 8.0 Hz, 1H, Ar), 7.05–6.72 (m, 7H, Ar), 4.71 (s, 2H, N-C$\underline{H_2}$-COOH), 2.24 (s, 3H, CH_3), 2.21 (s, 3H, CH_3), 2.17 (s, 3H, CH_3).
^{13}C NMR (101 MHz, DMSO) δ 192.27, 167.78, 166.45, 153.36, 149.24, 146.95, 144.50, 139.50, 138.97, 138.25, 135.52, 133.17, 131.23, 129.93, 127.48, 127.22, 125.62, 125.26, 125.12, 124.92, 123.71, 122.37, 121.35, 118.02, 45.69, 21.45, 19.94, 19.32.
Anal. calcd. for $C_{31}H_{26}N_2O_3S_3$: C 65.24, H 4.59, N 4.91; found: C 65.27, H 4.56, N 5.01.

N^2,N^8-bis(3,4-dimethylphenyl)-4,10-dimethyl-N^2,N^8-bis(4-((E)-(2-phenylhydrazono)methyl)phenyl)-6H,12H-5,11-methanodibenzo[b,f][1,5]diazocine-2,8-diamine (**6j**)

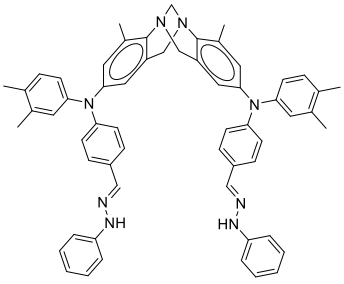

Compound 4,4'-((4,10-dimethyl-6*H*,12*H*-5,11-methanodibenzo[*b*,*f*][1,5]diazocine-2,8-diyl)bis((3,4-dimethylphenyl)azanediyl))dibenzaldehyde (**5k**) (2.29 g, 3.73 mmol) was dissolved in toluene (20 ml), phenylhydrazine (0.92 ml, 9.33 mmol) was added, and the mixture was refluxed until the arylaldehyde **5k** disappeared (TLC acetone/*n*-hexane 1:4, v/v). After the reaction was complete, the solvents were removed under reduced pressure, the reaction mass dissolved in hot toluene, double amount of 2-propanol was added and allowed to cool down while inducing crystallization. The yellow crystals of the product (70%, 2.289 g) were filtered off and washed with 2-propanol.

^{1}H NMR (400 MHz, $CDCl_3$) δ 7.59 (s, 2H, Ar), 7.45 (d, *J* = 8.7 Hz, 4H, Ar), 7.32–7.13 (m, 4H, Ar), 7.12–6.68 (m, 18H, Ar), 6.53 (d, *J* = 2.2 Hz, 2H, Ar), 4.46 (d, *J* = 17.0 Hz, 2H, H-6*exo*, and H-12*exo*), 4.32 (s, 2H, H-13), 3.87 (d, *J* = 17.0 Hz, 2H, H-6*endo*, and H-12*endo*), 2.32–2.11 (m, 18H, 6× CH_3).
^{13}C NMR (101 MHz, $CDCl_3$) δ 146.17, 144.96, 144.94, 143.56, 140.76, 138.98, 136.32, 135.26, 134.91, 132.00, 131.10, 130.21, 129.24, 128.92, 124.92, 123.80, 123.19, 121.92, 121.29, 121.19, 112.11, 66.21, 56.22, 20.17, 19.25, 17.43.
Anal. calcd. for $C_{59}H_{56}N_8$: C 80.79, H 6.44, N 12.77; found: C 80.84, H 6.62, N 12.54.

N^2,N^8-bis(4-((E)-(2-(4-(5,5-dimethyl-1,3-dioxan-2-yl)phenyl)-2-phenylhydrazono)methyl)phenyl)-N^2,N^8-bis(3,4-dimethylphenyl)-4,10-dimethyl-6H,12H-5,11-methanodibenzo[b,f][1,5]diazocine-2,8-diamine (**6k**)

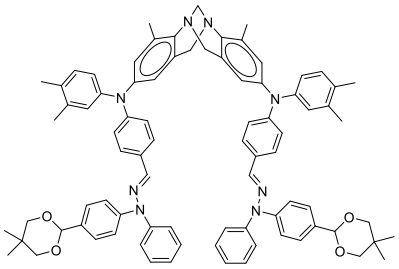

A mixture of N^2,N^8-bis(3,4-dimethylphenyl)-4,10-dimethyl-N^2,N^8-bis(4-((*E*)-(2-phenylhydrazono)methyl)phenyl)-6*H*,12*H*-5,11-methanodibenzo[*b*,*f*][1,5]diazocine-2,8-diamine (**6j**) (0.878 g, 1 mmol), 2-(4-bromophenyl)-5,5-dimethyl-1,3-dioxane (**5n)** (0.814 g, 3 mmol), and anhydrous toluene (10 ml) was purged with argon for 30 minutes. $Pd(OAc)_2$ (0.005 g, 0.02 mmol), $[P(t\text{-}Bu)_3H]BF_4$ (0.008 g, 0.027 mmol), and NaO*t*-Bu (0.29 g, 3 mmol) were added, and the mixture was heated at reflux for 1.5 h (TLC THF/*n*-hexane 1:4, v/v) under Ar atmosphere. After the termination of the reaction, the mixture was filtered through Celite, the distilled water was added, and the mixture was extracted with ethyl acetate. The organic layer was dried over anhydrous Na_2SO_4, filtered, and the solvent evaporated under reduced pressure. The product was purified by column chromatography (THF/*n*-hexane 1:4, v/v), resulting in yellow resin (71%, 0.89 g).
^{1}H NMR (400 MHz, $CDCl_3$) δ 7.73–7.39 (m, 14H, Ar), 7.29–7.09 (m, 10H, Ar), 7.04 (d, *J* = 8.1 Hz, 2H, Ar), 6.99–6.76 (m, 10H, Ar), 6.52 (d, *J* = 1.9 Hz, 2H, Ar), 5.61 (s, 2H, O-CH-O), 4.45 (d, *J* = 17.0 Hz, 2H, H-6*exo*, and H-12*exo*), 4.29 (s, 2H, H-13), 3.95–3.54 (m, 10H, H-6*endo*, and H-12*endo*, O-CH_2-C), 2.31–2.15 (m, 18H, 6× Ar-CH_3), 1.29 (s, 6H, C-CH_3), 0.80 (s, 6H, C-CH_3).
^{13}C NMR (101 MHz, $CDCl_3$) δ 149.43, 144.59, 144.20, 143.12, 141.94, 140.41, 140.08, 138.06, 134.07, 133.71, 133.69, 132.96, 130.78, 130.34, 129.33, 128.59, 127.80, 126.28, 125.44, 125.38, 124.83, 124.45, 123.35, 123.23, 102.92, 76.47, 66.21, 56.22, 30.46, 21.99, 20.17, 19.25, 17.43.
Anal. calcd. for $C_{83}H_{84}N_8O_4$: C 80.79, H 6.44, N 12.77; found: C 80.73, H 6.35, N 12.92.

4,4'-(((1E,1'E)-(((4,10-dimethyl-6H,12H-5,11-methanodibenzo[b,f][1,5]diazocine-2,8-diyl)bis((3,4-dimethylphenyl)azanediyl))bis(4,1-phenylene))bis(methanylylidene))bis(1-phenylhydrazin-1-yl-2-ylidene))dibenzaldehyde (**6l**)

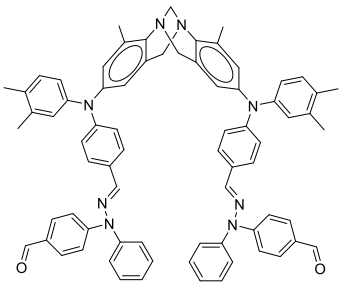

Protected aldehyde compound **6k** (0.88 g, 0.7 mmol) was dissolved in THF (5 ml), 12% aq. HCl solution (1.5 ml) was added, and the mixture was stirred at 40 °C for 2 h. The reaction mixture was poured into saturated $NaHCO_3$ solution and extracted with ethyl acetate. The organic layer was dried over anhydrous Na_2SO_4, filtered, and the solvent evaporated under reduced pressure. The crude product was purified by column chromatography (THF/*n*-hexane 7:18, v/v), resulting in yellow resin (46%, 0.66 g).

^{1}H NMR (400 MHz, $CDCl_3$) δ 9.80 (s, 2H, Ar), 7.77–7.39 (m, 14H, Ar), 7.29–7.09 (m, 10H, Ar), 7.04 (d, *J* = 8.1 Hz, 2H, Ar), 6.99–6.76 (m, 10H, Ar), 6.52 (d, *J* = 1.9 Hz, 2H, Ar), 4.45 (d, *J* = 17.0 Hz, 2H, H-6*exo*, and H-12*exo*), 4.29 (s, 2H, H-13), 3.86 (d, *J* = 17.0 Hz, 2H, H-6*endo*, and H-12*endo*), 2.31–2.15 (m, 18H, 6× CH_3).^{13}C NMR (101 MHz, $CDCl_3$) δ 190.29, 149.86, 145.30, 144.94, 143.56, 142.58, 140.76, 140.69, 138.98, 135.26, 134.91, 134.45, 132.11, 131.10, 130.21, 129.82, 129.31, 127.13, 124.92, 123.80, 123.19, 122.71, 121.92, 121.64, 121.61, 66.21, 56.22, 20.17, 19.25, 17.43.

Anal. calcd. for $C_{73}H_{64}N_8O_2$: C 80.78, H 5.94, N 10.32; found: C 80.99, H 5.92, N 10.27.

2,2'-((5Z,5'Z)-(((((1E,1'E)-(((4,10-dimethyl-6H,12H-5,11-methanodibenzo[b,f][1,5]diazocine-2,8-diyl)bis((3,4-dimethylphenyl)azanediyl))bis(4,1-phenylene))bis(methanylylidene))bis(1-phenylhydrazin-1-yl-2-ylidene))bis(4,1-phenylene))bis(methanylylidene))bis(4-oxo-2-thioxothiazolidin-3-yl-5-ylidene))diacetic acid (**6m**)

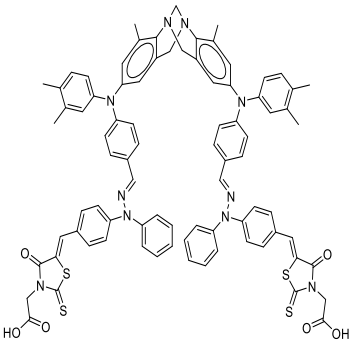

A mixture of aldehyde compound **6l** (0.408 g, 0.376 mmol), rhodanine-3-acetic acid (0.180 g, 0.94 mmol), and $AcONH_4$ (0.009 g, 0.11 mmol) was refluxed in anhydrous toluene (5 ml) for 2.5 h. After the termination of the reaction, the distilled solvent was removed under reduced pressure, and the product was purified by column chromatography (methanol/toluene 3:22, v/v) to obtain dye **6m** as a red solid (35%, 0.190 g).

^{1}H NMR (400 MHz, DMSO) δ 7.76–7.38 (m, 16H, Ar), 7.37–7.24 (m, 4H, Ar), 7.20–7.03 (m, 8H, Ar), 6.92–6.68 (m, 10H, Ar), 6.53 (s, 2H, Ar), 4.49–4.31 (m, 6H, H-6*exo*, and H-12*exo*, N-C$\underline{H_2}$-COOH), 4.20 (s, 2H, H-13), 3.89 (d, *J* = 17.4 Hz, 2H, H-6*endo*, and H-12*endo*), 2.27–2.06 (m, 18H, 6× CH_3).

^{13}C NMR (101 MHz, DMSO-d_6) 193.31, 167.41, 149.16, 148.95, 143.12, 141.94, 140.41, 140.09, 138.95, 138.06, 135.28, 134.07, 133.71, 132.96, 131.79, 130.78, 130.35, 129.83, 129.33, 128.26, 127.80, 126.29, 125.38, 124.96, 124.82, 124.46, 123.36, 123.23, 120.29, 66.21, 57.60, 47.55, 25.60, 20.37, 19.94, 19.28.

Anal. calcd. for $C_{83}H_{70}N_{10}O_6S_4$: C 69.63, H 4.93, N 9.78; found: C 69.50, H 5.15, N 9.50.

3,4-dimethyl-N-(4-((2-phenylhydrazono)methyl)phenyl)-N-(m-tolyl)aniline (**6n**)

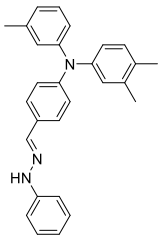

4-((3,4-dimethylphenyl)(*m*-tolyl)amino)benzaldehyde (**5o**) (1.214 g, 3.84 mmol) was dissolved in toluene (10 ml), phenylhydrazine (0.46 ml, 4.62 mmol) was added, and the mixture was refluxed until the arylaldehyde **5o** disappeared (TLC acetone/*n*-hexane 1:5, v/v). After the reaction was complete, the solvents were removed under reduced pressure, the reaction mass dissolved in hot 2-propanol and allowed to cool down while inducing crystallization. The mixture was left overnight in the refrigerator, the formed crystals were filtered off and washed with 2-propanol, resulting in light yellow crystalline product (70%, 1.05 g).

^{1}H NMR (400 MHz, $CDCl_3$) δ 7.75–7.46 (m, 7H, Ar), 7.34–7.06 (m, 7H, Ar), 6.91–6.74 (m, 7H, Ar), 5.62 (s, 2H, O-CH-O), 3.70 (dd, *J* = 49.3, 10.9 Hz, 4H, O-C$\underline{H_2}$-C), 2.21 (s, 3H, CH_3), 2.19 (s, 3H CH_3), 2.14 (s, 3H CH_3), 1.29 (s, 6H, C-CH_3), 0.80 (s, 6H, C-CH_3).

^{13}C NMR (101 MHz, $CDCl_3$) δ 146.66, 145.17, 144.96, 144.94, 139.93, 138.98, 136.32, 135.26, 132.00, 130.21, 129.24, 129.08, 128.92, 126.41, 123.19, 122.19, 121.92, 121.29, 121.19, 120.69, 112.11, 21.39, 20.17, 19.25.

Anal. calcd. for $C_{28}H_{27}N_3$: C 82.93, H 6.71, N 10.36; found: C 83.09, H 6.68, N 10.23.

N-(4-((2-(4-(5,5-dimethyl-1,3-dioxan-2-yl)phenyl)-2-phenylhydrazono)methyl)phenyl)-3,4-dimethyl-N-(m-tolyl)aniline (**6o**)

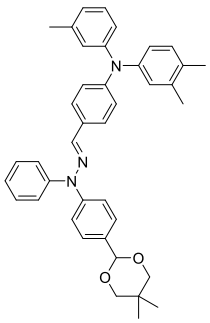

A mixture of 3,4-dimethyl-*N*-(4-((2-phenylhydrazono)methyl)phenyl)-*N*-(*m*-tolyl)aniline (**6n**) (0.69 g, 1.7 mmol), 2-(4-bromophenyl)-5,5-dimethyl-1,3-dioxane (**5n**) (0.692 g, 2.55 mmol), and anhydrous toluene (10 ml) was purged with argon for 30 minutes. $Pd(OAc)_2$ (0.004 g, 0.02 mmol), [P(*t*-Bu)$_3$H]BF_4 (0.014 g, 0.046 mmol), and NaO*t*-Bu (0.245 g, 2.55 mmol) were added, and the mixture was heated at reflux for 0.5 h under Ar atmosphere. After the termination of the reaction, the mixture was filtered through Celite, and the solvent evaporated under reduced pressure. The crude product was purified by column chromatography (acetone/*n*-hexane 3:22, v/v), yielding a product as yellow resin (72%, 0.72 g).

^{1}H NMR (400 MHz, $CDCl_3$) δ 7.75–7.46 (m, 7H, Ar), 7.34–7.06 (m, 7H, Ar), 6.91–6.74 (m, 7H, Ar), 5.62 (s, 2H, O-CH-O), 3.70 (dd, *J* = 49.3, 10.9 Hz, 4H, O-C$\underline{H_2}$-C), 2.21 (s, 3H, CH_3), 2.19 (s, 3H CH_3), 2.14 (s, 3H CH_3), 1.29 (s, 6H, C-CH_3), 0.80 (s, 6H, C-CH_3).

^{13}C NMR (101 MHz, $CDCl_3$) δ 149.86, 148.43, 145.30, 144.94, 142.28, 140.69, 139.93, 138.98, 136.02, 135.26, 132.11, 130.21, 129.30, 129.08, 127.13, 126.41, 126.27, 123.19, 122.71, 122.19, 121.95, 121.92, 121.64, 120.69, 103.32, 76.47, 30.46, 21.99, 21.39, 20.17, 19.25.

Anal. calcd. for $C_{40}H_{41}N_3O_2$: C 80.64, H 6.94, N 7.05; found: C 80.75, H 6.92, N 6.99.

4-(2-(4-((3,4-dimethylphenyl)(m-tolyl)amino)benzylidene)-1-phenylhydrazinyl)benzaldehyde (**6p**)

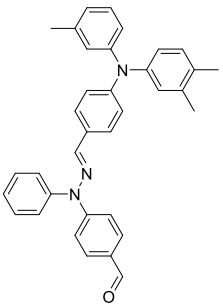

N-(4-((2-(4-(5,5-dimethyl-1,3-dioxan-2-yl)phenyl)-2-phenylhydrazono)methyl)phenyl-3,4-dimethyl-*N*-(*m*-tolyl)aniline (**6o**) (1.72 g, 1.2 mmol) was dissolved in THF (6 ml), 12% aq. HCl solution (2 ml) was added, and the mixture was stirred at 40 °C for 1 hour. The reaction mixture was poured into the saturated $NaHCO_3$ solution and extracted with ethyl acetate. The organic layer was dried over anhydrous Na_2SO_4, filtered, and the solvent evaporated under reduced pressure. The crude product was purified by column chromatography (acetone/*n*-hexane 1:24, v/v) yielding product as yellow solid (68%, 0.614 g).

^{1}H NMR (400 MHz, $CDCl_3$) δ 9.82 (s, 1H, CHO), 7.74–7.46 (m, 7H, Ar), 7.34–7.06 (m, 7H, Ar), 6.91–6.74 (m, 7H, Ar), 2.23 (s, 3H, CH_3), 2.21 (s, 3H CH_3), 2.17 (s, 3H CH_3).

^{13}C NMR (101 MHz, $CDCl_3$) δ 190.19, 154.86, 148.43, 145.30, 144.94, 142.58, 140.69, 139.93, 138.98, 135.26, 134.45, 132.11, 130.21, 129.82, 129.30, 129.08, 127.13, 126.41, 123.19, 122.71, 122.19, 121.92, 121.64, 121.61, 120.69, 21.39, 20.17, 19.25.

Anal. calcd. for $C_{35}H_{31}N_3O$: C 82.48, H 6.13, N 8.25; found: C 82.68, H 6.17, N 8.08.

2-(5-((Z)-4-(2-((E)-4-((3,4-dimethylphenyl)(m-tolyl)amino)benzylidene)-1-phenylhydrazinyl)benzylidene)-4-oxo-2-thioxothiazolidin-3-yl)acetic acid (**6r**)

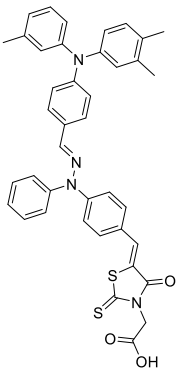

A mixture of 4-(2-(4-((3,4-dimethylphenyl)(*m*-tolyl)amino)benzylidene)-1-phenylhydrazinyl)benzaldehyde (**6p**) (0.614 g, 1.2 mmol), rhodanine-3-acetic acid (0.277 g, 1.45 mmol), and $AcONH_4$ (0.028 g, 0.36 mmol) was refluxed in anhydrous toluene (10 ml) for 1.5 h. After the termination of the reaction, the distilled solvent was removed under reduced pressure, and the product was purified by column chromatography (methanol/toluene 2:23, v/v) to obtain dye **6r** as a red solid (73%, 0.596 g).

^{1}H NMR (400 MHz, DMSO) δ 7.74–7.46 (m, 8H, Ar), 7.31 (d, *J* = 7.3 Hz, 2H, Ar), 7.22–7.06 (m, 5H, Ar), 6.91–6.74 (m, 7H, Ar), 4.41 (s, 2H, N-C$\underline{H_2}$-COOH), 2.21 (s, 3H, CH_3), 2.19 (s, 3H CH_3), 2.14 (s, 3H CH_3).

^{13}C NMR (101 MHz, DMSO) δ 193.31, 167.41, 149.16, 148.95, 147.26, 144.80, 139.34, 138.82, 138.31, 138.10, 133.28, 133.00, 132.77, 131.77, 131.14, 129.86, 128.25, 128.16, 126.97, 125.19, 124.94, 124.66, 123.43, 121.92, 121.68, 118.27, 115.22, 67.49, 48.30, 25.60, 21.46, 19.94, 19.28.

Anal. calcd. for $C_{40}H_{34}N_4O_3S_2$: C 70.36, H 5.02, N 8.2; found: C 70.52, H 5.04, N 8.13.

4,10-dimethyl-N_2,N_2,N_8,N_8-tetrakis(4-(1,2,2-triphenylvinyl)phenyl)-6H,12H-5,11-methanodibenzo[b,f][1,5]diazocine-2,8-diamine (**7a**)

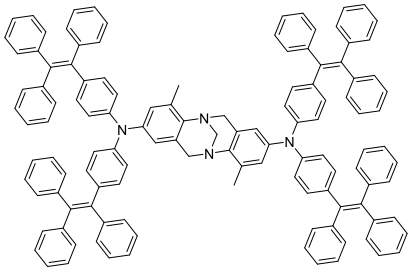

A mixture of dioxane (5 ml) and water (0.02 ml) was purged with argon for 20 minutes. $Pd(OAc)_2$ (0.001 g, 0.08 mmol), XPhos (0.011 g, 0.024 mmol) were added, and the mixture was heated to 80 °C for 2 min. 2,8-Diamino-4,10-dimethyl-6*H*,12*H*-5,11-methanodibenzo[1,5]-diazocine **(4b)** (0.112 g, 0.40 mmol), 1-(4-bromophenyl)-1,2,2-triphenylethylene (0.823 g, 2 mmol), and NaO*t*-Bu (0.215 g, 2.24 mmol) were added, and the solution was refluxed for 3 h under Ar atmosphere. After the termination of the reaction, the mixture was diluted with THF (30 ml) and filtered through Celite, the distilled water was added, and the mixture was extracted with ethyl acetate. The organic layer was dried over anhydrous Na_2SO_4, filtered, and the solvent evaporated under reduced pressure. The crude product was purified by column chromatography (THF/*n*-hexane 2:23, v/v), but started to crystallize during the process. The compound was further purified via crystallization from THF-acetone mixture. Bright yellow crystals were obtained (64%, 0.41 g).

^{1}H NMR (400 MHz, DMSO) δ 7.62–7.42 (m, 4H, Ar), 7.13–6.82 (m, 56H, Ar), 6.82–6.41 (m, 18H, Ar), 6.30 (s, 2H, Ar), 4.32 (d, *J* = 16.9 Hz, 2H, H-6*exo*, and H-12*exo*), 4.07 (s, 2H, H-13), 3.68 (d, *J* = 16.9 Hz, 2H, H-6*endo*, and H-12*endo*), 2.22 (s, 6H, 2× CH_3).

^{13}C NMR (101 MHz, DMSO) δ 145.75, 143.98, 143.63, 143.42, 143.20, 140.66, 140.32, 137.37, 132.78, 132.29, 131.57, 130.68, 128.92, 127.88, 127.79, 126.62, 126.46, 122.62, 120.62, 117.11, 67.54, 62.20, 55.04, 23.83.

Anal. calcd. for $C_{121}H_{92}N_4$: C 90.71, H 5.79, N 3.5; found: C 90.78, H 5.69, N 3.53.

(4,10-dimethyl-6H,12H-5,11-methanodibenzo[b,f][1,5]diazocine-2,8-diyl)diboronic acid (**7b**)

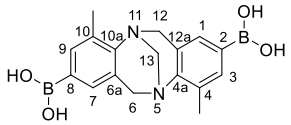

A solution of **1'** (2.49 g, 6.1 mmol) in THF (25 ml) and under argon atmosphere was cooled to -78 °C. At this temperature, n-BuLi (9.09 ml of a 1.6 M solution in *n*-hexane, 14.64 mmol) was added dropwise within 5 min. After stirring for 5 min, trimethylborate (2.04 ml, 18.3 mmol) was added instantly. The reaction mixture was allowed to warm to r.t. and stirred for another 15 min. H_2O (37.5 ml) was added, and after the extraction with CH_2Cl_2, the aqueous solution was extracted with EtOAc and dried over Na_2SO. The concentration under reduced pressure yielded a product **7b** as white solid (84%).

^{1}H NMR (400 MHz, DMSO) δ 7.74 (s, 4 H, OH), 7.44 (s, 2 H, H-3, H-9), 7.19 (s, 2 H, H-1, H-7), 4.51 (d, J= 17.0 Hz, 2 H, H-6*exo*, H-12*exo*), 4.24 (s, 2 H, H-13), 3.93 (d, J = 17.0 Hz, 2 H, H-6*endo*, H-12*endo*), 2.33 (s, 6 H, 2× CH_3).

^{13}C NMR (101 MHz, DMSO) δ 148.1, 135.0, 131.1, 131.0, 129.0, 127.2, 67.5, 54.9, 17.3.

Anal. calcd. for $C_{17}H_{20}B_2N_2O_4$: C 60.41, H 5.96, N 8.29; found: C 60.23, H 5.84, N 8.58.

4,10-dimethyl-2,8-bis(4-(1,2,2-triphenylvinyl)phenyl)-6H,12H-5,11-methanodibenzo[b,f][1,5]diazocine (**7c**)

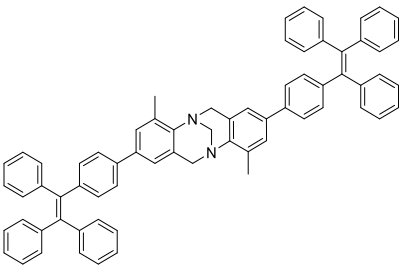

A solution of (4,10-dimethyl-6*H*,12*H*-5,11-methanodibenzo[*b*,*f*][1,5]diazocine-2,8-diyl)diboronic acid (**7b**) (0.338 g, 1 mmol) and 1-(4-bromophenyl)-1,2,2-triphenylethylene (1.03 g, 2.5 mmol) in THF (3 ml) was mixed with argon-purged 2N aqueous K_2CO_3 solution (1 ml) and stirred under argon atmosphere. After 20 min, $Pd(PPh_3)_4$ (0.116 g, 0.1 mmol) was added, and the solution was refluxed for 6 hours. The solution was allowed to cool to room temperature, the water was added, and the organic layer was extracted with ethyl acetate. The organic layer was dried over anhydrous Na_2SO_4, filtered, and the solvent was removed under reduced pressure. The crude product was purified by column chromatography (ethyl acetate/toluene/ *n*-hexane 1:9:15, v/v), resulting in white solid (78%, 0.71 g).

^{1}H NMR (400 MHz, $CDCl_3$) δ 7.25–7.19 (m, 6H, Ar), 7.13–6.98 (m, 34H, Ar), 6.94 (d, *J* = 1.0 Hz, 2H, Ar), 4.61 (d, *J* = 16.8 Hz, 2H, H-6*exo*, and H-12*exo*), 4.35 (s, 2H, H-13), 4.03 (d, *J* = 16.9 Hz, 2H, H-6*endo*, and H-12*endo*), 2.43 (s, 6H, 2× CH_3).

^{13}C NMR (101 MHz, $CDCl_3$) δ 145.35, 143.82, 143.77, 143.74, 142.33, 141.01, 140.61, 138.61, 136.13, 133.10, 131.68, 131.44, 131.37, 131.34, 128.24, 127.73, 127.67, 127.64, 127.55, 126.46, 126.43, 125.90, 122.87, 67.76, 55.29, 17.30.

Anal. calcd. for $C_{69}H_{54}N_2$: C 90.95, H 5.97, N 3.07; found: C 90.93, H 5.89, N 3.18.

(2,8-dimethyl-6H,12H-5,11-methanodibenzo[b,f][1,5]diazocine-4,10-diyl)diboronic acid (**7d**)

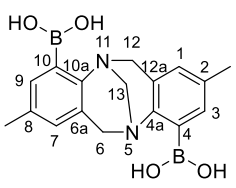

A solution of 4,10-dibromo-2,8-dimethyl-6*H*,12*H*-5,11-methanodibenzo[*b*,*f*][1,5]diazocine (**3i**) (3.469 g, 8.5 mmol) in THF (52 ml) and under argon atmosphere was cooled to -78 °C. At this temperature, n-BuLi (12.75 ml of a 1.6 M solution in *n*-hexane, 20.4 mmol) was added dropwise within 5 min. After stirring for 15 min, trimethylborate (2.84 ml, 25.5 mmol) was added instantly. The reaction mixture was allowed to warm to r.t. and stirred for another 15 minutes. The water (52 ml) was added; then, the mixture was extracted with DCM, the aqueous layer was acidified with 6 M HCl. After filtration, the filter residue was washed with distilled water repeatedly and dried, yielding white solid (43%, 1.23 g).

^{1}H NMR (400 MHz, $CDCl_3$) δ 8.53 (s, 4H, Ar), 7.46 (s, 2H, Ar), 6.78 (d, *J* = 5.2 Hz, 2H, Ar), 4.69 (d, *J* = 16.8 Hz, 2H, H-6*exo*, and H-12*exo*), 4.42 (s, 2H, H-13), 3.92 (d, *J* = 16.9 Hz, 2H, H-6*endo*, and H-12*endo*), 2.19 (s, 6H, 2× CH_3).

^{13}C NMR (101 MHz, $CDCl_3$) δ 154.73, 140.16, 138.41, 134.46, 132.59, 131.34, 70.36, 63.53, 25.63.
Anal. calcd. for $C_{17}H_{20}B_2N_2O_4$: C 60.41, H 5.96, N 8.29; found: C 60.3, H 6.15, N 8.06.

2,8-dimethyl-4,10-bis(4-(1,2,2-triphenylvinyl)phenyl)-6H,12H-5,11-methanodibenzo[b,f][1,5]diazocine (**7e**)

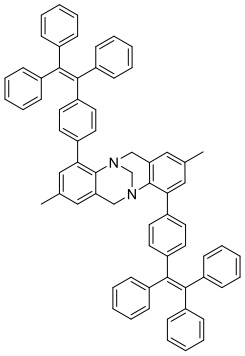

A solution of (2,8-dimethyl-6*H*,12*H*-5,11-methanodibenzo[*b*,*f*][1,5]diazocine-4,10-diyl)diboronic acid (**7d**) (0.338 g, 1 mmol) and 1-(4-bromophenyl)-1,2,2-triphenylethylene (1.03 g, 2.5 mmol) in THF (3 ml) was mixed with argon-purged 2N aqueous K_2CO_3 solution (1 ml) and stirred under argon atmosphere. After 20 min, $Pd(PPh_3)_4$ (0.022 g, 0.1 mmol) was added, and the solution was refluxed for 6 hours. The solution was allowed to cool to room temperature, the water was added, and the organic layer was extracted with ethyl acetate. The organic layer was dried over anhydrous Na_2SO_4, filtered, and the solvent was removed under reduced pressure. The crude product was purified by column chromatography (THF/*n*-hexane 3:22, v/v and toluene) yielding a grayish solid (37%, 0.335 g).
^{1}H NMR (400 MHz, $CDCl_3$) δ 7.37 (d, *J* = 8.1 Hz, 4H, Ar), 7.17–7.03 (m, 34H, Ar), 6.88 (s, 2H, Ar), 6.53 (s, 2H, Ar), 4.22 (s, 2H, H-13), 3.97 (d, *J* = 17.1 Hz, 2H, C-CH_2-N), 3.39 (d, *J* = 17.1 Hz, 2H, C-CH_2-N), 2.21 (s, *J* = 17.9 Hz, 6H, 2× CH_3).
^{13}C NMR (101 MHz, $CDCl_3$) δ 144.09, 143.68, 143.56, 142.58, 142.29, 141.13, 141.08, 138.13, 136.03, 132.99, 131.51, 131.39, 131.06, 129.47, 129.06, 128.75, 128.46, 128.25, 127.70, 127.66, 126.57, 126.49, 126.34, 125.33, 67.60, 55.13, 20.83.
Anal. calcd. for $C_{69}H_{54}N_2$: C 90.95, H 5.97, N 3.07; found: C 91.12, H 5.95, N 2.93.

(4-(1,2,2-triphenylvinyl)phenyl)boronic acid (**7f**)

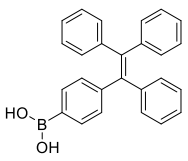

1-(4-bromophenyl)-1,2,2-triphenylethylene (4.525 g, 11 mmol) was dissolved in argon-purged THF (110 ml) and cooled to -78 °C under argon atmosphere. At this temperature, *n*-BuLi (13.75 ml of a 1.6 M solution in n-hexane, 22 mmol) was slowly added dropwise. After that mixture was stirred for 2 h at −78 °C, trimethyl borate (6.13 ml, 55 mmol) was injected. After 2 h, the mixture was allowed to reach the room temperature. HCl (3 M, 55 ml) aq. solution was added, and the mixture was stirred for another 3 h. The mixture was extracted with DCM three times, and the collected organic layers were combined, washed with brine twice, dried over anhydrous sodium sulfate, filtered, and the solvent was removed under reduced pressure. The crude product was purified by column chromatography (THF/n-hexane 1:4, v/v) yielding white solid (64%, 2.63 g).
^{1}H NMR (400 MHz, $CDCl_3$) δ 7.15–6.91 (m, 15H, Ar), 6.88 (d, *J* = 8.6 Hz, 2H, Ar), 6.55 (d, *J* = 8.6 Hz, 2H, Ar).

^{13}C NMR (101 MHz, $CDCl_3$) δ 154.01, 144.01, 143.91, 143.90, 140.44, 140.21, 136.39, 132.75, 131.39, 131.36, 131.34, 127.73, 127.63, 126.40, 126.28, 114.61.
Anal. calcd. for $C_{26}H_{21}BO_2$: C 83, H 5.63, N 5.63; found: C 82.85, H 5.87, N 5.61.

2,4,8,10-tetrakis(4-(1,2,2-triphenylvinyl)phenyl)-6H,12H-5,11-methanodibenzo[b,f][1,5]diazocine (**7g**)

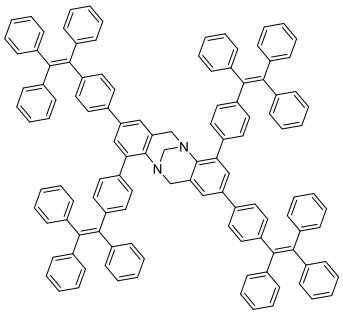

A solution of 2,4,8,10-tetrabromo-6*H*,12*H*-5,11-methanodibenzo[*b*,*f*][1,5]diazocine (**3j)** (0.29 g, 0.5 mmol) and (4-(1,2,2-triphenylvinyl)phenyl)boronic acid (**7f**) (1.317 g, 3.5 mmol) in THF (3 ml) was mixed with argon-purged 2N aqueous K_2CO_3 solution (1 ml) and stirred under argon atmosphere. After 20 min, $Pd(PPh_3)_4$ (0.022 g, 0.1 mmol) was added, and the solution was refluxed for 20 hours. The solution was allowed to cool to room temperature, the water was added, and the organic layer was extracted with ethyl acetate. The organic layer was dried over anhydrous Na_2SO_4, filtered, and the solvent was removed under reduced pressure. The product was purified by column chromatography (ethyl acetate/toluene/ *n*-hexane 2:5:18, v/v), resulting in white solid (62%, 0.48 g).
^{1}H NMR (400 MHz, $CDCl_3$) δ 7.40 (d, *J* = 8.2 Hz, 4H, Ar), 7.28–7.18 (m, 8H, Ar), 7.18–6.95 (m, 66H, Ar), 6.89 (d, *J* = 1.6 Hz, 2H, Ar), 4.29 (s, 2H, H-13), 4.06 (d, *J* = 17.1 Hz, 2H, C-CH_2-N), 3.48 (d, *J* = 17.2 Hz, 2H, C-CH_2-N).
^{13}C NMR (101 MHz, $CDCl_3$) δ 144.37, 144.07, 143.76, 143.68, 143.63, 143.49, 142.57, 142.47, 141.19, 141.06, 140.53, 138.38, 137.92, 136.56, 136.09, 131.76, 131.50, 131.44, 131.36, 131.16, 128.91, 128.79, 127.74, 127.67, 127.64, 127.29, 126.47, 126.41, 125.83, 124.44, 55.30, 51.97.
Anal. calcd. for $C_{119}H_{86}N_2$: C 92.57, H 5.61, N 1.81; found: C 92.61, H 5.5, N 1.89.

5. MAIN RESULTS AND CONCLUSIONS

1) Small-molecular HTMs containing triphenylamine fragments conjoined by Tröger's base core, varying in substituents on outer phenyl rings, were synthesized. Their structural, thermal, optical, and photophysical properties were investigated. It has been found that:
   a) TB derivatives are thermally stable, destruction temperature for each of them exceeds 370 °C;
   b) Measured values of ionization potential (5.25–5.34 eV) and charge drift mobility ($1.2 \cdot 10^{-5}$–$3.3 \cdot 10^{-4}$ cm^2/Vs) of compounds **1b**–**d** demonstrate their potential for optoelectronic applications.
2) HTMs containing Tröger's base core and phenylethenyl side-branches were obtained via aldehyde condensation, and their investigation has revealed that:
   a) Structural expansion by phenylethenyl moieties provides TB derivatives with amorphousness, expanded conjugated π-system, lowered ionization potential (5.27–5.45 V), and high hole drift mobility (0.002–0.011 cm^2/Vs) values;
   b) Power conversion efficiency (PCE) of perovskite solar cells with synthesized HTMs reaching 11.09% (with compound **2c**, vs 15.34% with spiro-OMeTAD) indicates the potential applicability of these compounds in optoelectronic devices.
3) Synthesis of hole-transporting TPD derivatives containing Tröger's base core was performed, and the investigation of their properties has revealed that:
   a) TB core provides orientation for *p*-substituted TPD fragments angle-wise towards each other, producing stable, fully amorphous HTMs with comparatively high charge mobility (up to 0.036 cm^2/Vs);
   b) Fabrication of perovskite solar cells with synthesized materials as HTMs allowed to reach the maximum power conversion efficiency of 14.6% with methoxy substituted compound **3h** (vs 16.1% with spiro-OMeTAD) and PCE of 17.91% with **3l** (vs 19.22% with spiro-OMeTAD), proving that this class of TB-linked molecules can function effectively as HTM in the device.
4) HTMs containing Tröger's base core and enamine-linked diphenyl branches were synthesized and studied. It has been found that:
   a) Synthetic pathway via enamine condensation affords hole-transporting TB derivatives while completely eliminating the need to use palladium catalysts and corresponding ligands, inert atmosphere conditions, and excessive purification from palladium residue, consequently, making this approach attractive from an industrial perspective;
   b) Synthesized hole-transporting materials are thermally stable and have a relatively high hole-drift mobility ($3.35 \cdot 10^{-4}$ cm^2/Vs in **4e**), making these compounds attractive for various applications in optoelectronics;
   c) Compounds were tested in perovskite solar cells with particularly good results, the highest maximum power conversion efficiency being 18.62% (with methoxy substituted compound **4e**, vs 19.22% with spiro-OMeTAD)

under reverse scan, comparable to the efficiency of spiro-OMeTAD, and even outperforming it by 1.6 times in a dopant-free device.

5) Sensitizers based on Tröger's base scaffold and two acceptor/anchoring groups of rhodanine-3-acetic acid, linked by the poly[n]enic (n = 0–2) chain, were designed and synthesized. Their "half" counterparts, having one anchoring group, were synthesized as well, allowing study and comparison of these dyes, thus leading to such conclusions:
   a) UV-vis absorption spectra show the red-shifting between absorption maximums of single- and corresponding double-anchored dyes, and this difference is increasing with each fragment in poly[n]enic (n = 0–2) chain, suggesting flexibility-caused interaction of anchoring groups within double-acceptor dyes;
   b) Testing sensitizers in DSSCs has shown that flexibility provided by extended polymethine chains and, consequently, the interaction in-between two chromophores is promoting aggregate formation and impairing device performance. The best results were obtained in short-chained, mono-anchored dye **5D**.
6) TB sensitizers of improved molecular design were designed and synthesized. These compounds contain either thiophene or phenyl-branched hydrazone spacers, as a replacement for flexible polymethine chains, and the study of their properties has revealed that:
   a) As shown by UV-vis absorption spectra, thiophene fragment offers the compounds light absorption superior to that of hydrazone dyes, but it still does not provide sufficient structural stiffness to prevent inner interactions (shifting maximums by 12 nm);
   b) No observable absorption shift in hydrazone di-anchoring dye **6m** in comparison to its mono-anchoring counterpart **6r** indicates that phenyl-branched hydrazone unit provides the desired properties and prevents the intra-anchoring of chromophores.
7) Novel Tröger's base compounds with TPE side-arms were synthesized and investigated. These compounds are thermally stable, solution processable and possess aggregation induced emission (AIE) properties, showing their potential use in forming pristine solid-state layers in light emitting devices.

6. SANTRAUKA

Įvadas

Dėl technologinės pažangos įvairūs įrenginiai tampa neatsiejama mūsų kasdienio gyvenimo dalimi, todėl kyla naujų jiems gaminti skirtų medžiagų poreikis. Pastaraisiais metais vis daugiau dėmesio skiriama organinėms medžiagoms, skirtoms naudoti elektronikos ir optoelektronikos srityse. Organinių junginių naudojimas prietaisuose turi nemažai privalumų: tokie prietaisai ar jų dalys gali būti pigesni, lengvesni, reikalauja mažiau energijos gamybai, taip pat leidžia spręsti brangiųjų cheminių elementų naudojimo problemą – šiuos junginius dažniausiai sudaro lengvai prieinami cheminiai elementai: anglis, vandenilis, azotas, deguonis ir kt. Šie organiniai junginiai naudojami įvairiose srityse, tokiose kaip organiniai šviesos diodai (OLED technologija), fotovoltiniai elementai, elektrofotografija, lauko tranzistoriai ir kt. [1].

Efektyvūs optoelektroniniai prietaisai taip pat gali padėti spręsti didėjančio energijos poreikio problemą, kylančią dėl augančio žmonių skaičiaus ir intensyvesnio įvairių technologijų naudojimo. Prognozuojama, kad iki 2040 m. energijos suvartojimas padidės 56 % [2]. Šią problemą galima spręsti užtikrinant pigią ir patogią prieigą prie atsinaujinančiosios energijos šaltinių, tokių kaip saulės energija, ir mažinant neefektyvių prietaisų išeikvojamą energiją. Saulės energijos naudojimas ypač patrauklus, nes tai yra pirminis ir tiesioginis energijos šaltinis, iš kurio kyla dauguma kitų naudojamų atsinaujinančiųjų šaltinių. O saulės elementai tiesiogiai paverčia saulės šviesos energiją elektra – forma, kuria ją patogu perduoti, kaupti ir naudoti. Saulės elementų rinkoje vis dar dominuoja išvystyta neorganinių junginių (dažniausiai silicio) pagrindu veikiančių prietaisų technologija, tačiau organiniai ir hibridiniai saulės elementai išsikovoja vis didesnę jos dalį dėl siūlomų alternatyvų, pasižyminčių mažesne kaina, lankstumu, lengvumu ir gamybos technologija, nereikalaujančia brangiųjų cheminių elementų ir tiek daug energijos [3]. Populiariausi iš šių prietaisų yra dažikliais įjautrinti saulės elementai bei perovskitiniai saulės elementai – sparčiai besivystanti technologija, jau pasiekusi 23,2 % energijos konversijos efektyvumo rodiklį [4].

Sprendžiant didėjančio energijos poreikio problemą, svariai prisidėtų energiją taupančių technologijų kūrimas ir diegimas. Labai svarbi niša tokioms inovacijoms yra apšvietimas, nes dirbtinis apšvietimas – pagrindinė elektros energijos suvartojimo priežastis visame pasaulyje (energija, sunaudojama apšvietimui, sudaro 15 proc. visos sunaudojamos energijos) [5, 6]. Šviesos diodai (LED) ir jų organiniai analogai (OLED) pasižymi aukštu energijos konversijos į šviesą koeficientu, leidžiančiu kelis kartus sumažinti energijos poreikį tokio paties apšvietimo stipriui gauti. OLED taip pat pasižymi organinės elektronikos teikiamais privalumais, tokiais kaip lengvumas ir lankstumas, leidžiančiais gaminti plonus, didelio ploto įrenginius, lakštus ir skydus. Pagrindinės organinių junginių funkcijos visuose šiuose optoelektroniniuose įrenginiuose yra krūvio pernaša, šviesos emisija ir krūvio generavimas. Dėl to dideliu efektyvumu ir pageidaujamomis savybėmis pasižyminčių naujų medžiagų kūrimas yra neatsiejamas nuo didelio efektyvumo įrenginių kūrimo ir gamybos.

Triogerio bazė (TB) yra V formos C_2 simetrija pasižyminti chiralinė molekulė, sudaryta iš biciklinio alifatinio metandiazocino fragmento, sujungiančio du aromatinius žiedus, kurių plokštumos orientuojamos beveik statmenai viena kitai. Tokia standi V formos molekulinė struktūra leidžia šią molekulę naudoti kaip struktūrinį karkasą ir orientuoti prie jo prijungtus pakaitus (pvz., konjuguotąsias π-sistemas) kampu vienas kito atžvilgiu. Buvo pastebėta, kad Triogerio bazės alifatinis fragmentas suteikia ir elektroninę sąveiką tarp juo sujungtų trifenilamino fragmentų ir tokiu būdu pagerina skylių pernašą, nors π-ryšiai tarp šių fragmentų ir nesusidaro [7]. Dėl šių priežasčių Triogerio bazė yra patraukli kaip unikalus nanometrinių matmenų karkasas neįprastam molekuliniam dizainui, leidžiantis junginiui suteikti norimų, bet nedažnai pasitaikančių savybių. Nors Triogerio bazė jau yra palyginti nemenkai ištirta ir buvo pritaikyta įvairiose srityse, tokiose kaip supramolekulinė chemija, molekulinis atpažinimas, biologiniai žymekliai, ligandų sintezė (ypač asimetrinei katalizei), sąveika su DNR ar net potencialios vaistinės medžiagos, – šios molekulės taikymas optoelektronikai nebuvo plačiai tirtas ar aprašytas – ši niša vis dar atvira tolesniems tyrimams ir atradimams. Dėl išvardytų priežasčių šiame darbe pristatoma naujų funkcinių Triogerio bazės junginių, skirtų optoelektroniniams prietaisams – krūvį generuojančių dažiklių saulės celėms, kietosios būsenos spinduolių organiniams šviesos diodams ir skyles pernešančių puslaidininkių perovskitiniams saulės elementams, – sintezė ir tyrimas.

Šio darbo tikslas – susintetinti ir ištirti V formos Triogerio bazės darinius, skirtus krūviui generuoti, krūvininkų pernašai ir šviesos emisijai.

Disertacijos tikslui pasiekti išsikelti šie **uždaviniai**:

1. Susintetinti ir ištirti mažamolekulius skyles pernešančius puslaidininkius, turinčius trifenilamino fragmentus, sujungtus Triogerio bazės karkasu.
2. Susintetinti ir ištirti puslaidininkius, sudarytus iš fotolaidžių TPD (*N*,*N*'-di(3-metilfenil)-*N*,*N*'-difenilbenzidinas) tipo grupių, sujungtų Triogerio bazės fragmentu.
3. Susintetinti ir ištirti skyles pernešančius puslaidininkius, turinčius Triogerio bazės fragmentą ir per enamino grupes prijungtus šoninius pakaitus.
4. Susintetinti ir ištirti dažiklius, turinčius Triogerio bazės molekulinį karkasą.
5. Susintetinti ir ištirti spinduolius, turinčius tetrafenileteno pakaitų ir Triogerio bazės fragmentą.

Darbo mokslinis naujumas

Susintetinta serija naujų skyles pernešančių puslaidininkių, turinčių Triogerio bazės fragmentą, ir ištirta šoninių pakaitų įtaka šių junginių terminėms ir fotoelektrinėms savybėms. Nustatyta, kad susintetinti Triogerio bazės junginiai, turintys trifenilamino fragmentų su metil- ir metoksipakaitais, yra puslaidininkiai, pasižymintys skylių pernaša, palankiomis fizinėmis savybėmis, stabilumu, dauguma jų amorfiniai ir lengvai tirpūs, todėl gali būti naudojami optoelektronikoje. Be to, šių junginių sintezė ir tyrimas suteikė naudingos informacijos ir leido padaryti įžvalgas, reikalingas Triogerio bazės junginių molekuliniam dizainui tobulinti.

Susintetinti ir ištirti nauji V formos skyles pernešantys junginiai, turintys Triogerio bazės fragmentą ir trifenilamino grupių su feniletenilo pakaitais. TB karkasas gerokai padidina skyles pernešančių medžiagų stiklėjimo temperatūrą (tai ypač pastebima lyginant su Triogerio bazės struktūros neturinčiais analogais), o feniletenilo fragmentai suteikia struktūrinį tūrį, mažina kristališkumą ir svariai prisideda prie konjuguotosios molekulių π-sistemos dydžio. Šie puslaidininkiai buvo ištirti ir išbandyti perovskitiniuose saulės elementuose. Patvirtinta, kad juos perspektyvu naudoti organiniams ir hibridiniams optoelektroniniams įrenginiams, nes su jais gali būti dirbama atmosferos sąlygomis, jie yra termiškai stabilūs, nereikalauja atkaitinimo aukštoje temperatūroje ir turi palyginti didelį krūvininkų judrį (iki 0,011 $cm^2 V^{-1} s^{-1}$).

Susintetinti ir ištirti nauji skyles pernešantys junginiai, turintys TPD tipo grupių, sujungtų Triogerio bazės fragmentu. Šis molekulinis karkasas kampu orientuoja TPD fragmentus vieną kito atžvilgiu ir trukdo kristalizacijos procesams. Dėl to susintetinti junginiai yra visiškai amorfiniai, o TPD fragmentų *para*-padėtyse esantys pakaitai užtikrina didelį krūvininkų judrį. Šiuos puslaidininkius perspektyvu naudoti organiniuose ir hibridiniuose optoelektroniniuose įrenginiuose dėl jų stabilumo, amorfiškumo, aukštos stiklėjimo temperatūros, gero tirpumo ir palyginti didelio krūvininkų judrio (iki 0,036 $cm^2 V^{-1} s^{-1}$), kuris Triogerio bazės karkasu nesujungtų TPD analogų su metil- ir metoksigrupėmis judrį viršija daugiau nei šimtą kartų. Susintetintas medžiagas testuojant perovskitiniuose saulės elementuose įrodyta, kad ši junginių klasė gali būti veiksmingai naudojama kaip skyles pernešantys puslaidininkiai.

Taikant patogų ir efektyvų sintezės metodą susintetinti nauji V formos skyles pernešantys puslaidininkiai, turintys Triogerio bazės fragmentą ir per enamino grupes prijungtus difenilo šoninius pakaitus. Šių medžiagų sintezė nereikalauja paladžio katalizatorių, atitinkamų ligandų ir inertinių dujų atmosferos, o paladžio liekanų reakcijos mišinyje nebuvimas leidžia lengvai išgryninti medžiagą, išvengiant chromatografinio gryninimo. Šios skyles pernešančios medžiagos yra termiškai stabilios, tirpios organiniuose tirpikliuose ir turi gana didelį krūvininkų judrį, todėl jos yra patrauklios naudoti optoelektronikoje. Išbandant šiuos junginius perovskitiniuose saulės elementuose, geriausia šios grupės medžiaga leido gauti labai didelį efektyvumą. Pagal jį šie junginiai konkuravo su efektyvumo standartu laikomu junginiu *spiro*-OMeTAD ir netgi jį viršijo 1,6 karto, matuojant saulės elementų, pagamintų nenaudojant priedų, efektyvumą.

Suprojektuota ir susintetinta serija naujų organinių dažiklių, turinčių Triogerio bazės karkasą su trifenilamino donorinėmis grupėmis, „inkaro“ funkciją atliekančių akceptorinių rodanino-3-acto rūgšties grupių ir šias grupes su karkasu jungiančių poli[n]eninių (n = 0–2) grandinėlių. Atliktas polietino grandinės ilgio ir inkarinių grupių skaičiaus įtakos šių dažiklių fotofizikinėms, elektrocheminėms ir fotovoltinėms savybėms tyrimas ir bandymai dažikliais įjautrintose saulės celėse parodė, kad ilgėjant grandinėms didėja jų lankstumas, o tai leidžia pasireikšti tarpusavio sąveikai tarp dviejų prie jų prijungtų chromoforų, tokiu būdu susidaro agregatai ir mažėja dažiklių bei juos naudojant pagamintų įrenginių efektyvumas. Šie atradimai paskatino polimetino grandinėles pakeisti standžiais erdvinės struktūros

jungiamaisiais fragmentais, kurie galėtų užkirsti kelią agregatų susidarymui tarp inkarinių grupių šiuose Triogerio bazės dažikliuose. Buvo suprojektuoti ir gauti nauji dažikliai su tiofeno bei fenilhidrazono jungiamaisiais fragmentais, atlikti jų savybių tyrimai. Nustatyta, kad, fenilhidrazono jungiamasis fragmentas užkerta kelią inkarinių grupių sąveikai, t. y. minėti agregatai nesusidaro. Šiuos dažiklius būtų galima taikyti saulės celėse.

Susintetinti ir ištirti nauji tetrafenileteno pakaitų turintys Triogerio bazės junginiai. Šie junginiai yra termiškai stabilūs, tirpūs ir pasižymi agregacijos indukuota emisija, leidžiančia naudoti kietosios būsenos grynosios medžiagos sluoksnius šviesą spinduliuojančiuose įrenginiuose. Nors šių junginių kvantinio efektyvumo vertės nebuvo tokios didelės, kaip tikėtasi, tyrimas atskleidė kai kuriuos struktūros ir savybių santykių dėsningumus, leidžiančius toliau tobulinti Triogerio bazės spinduolių molekulinį dizainą.

Pagrindiniai ginamieji disertacijos teiginiai:

1. Susintetintos naujos mažamolekulės skyles pernešančios medžiagos, turinčios trifenilamino fragmentų, sujungtų Triogerio bazės karkasu, ir skirtingų pakaitų prie išorinių fenilo grupių, yra termiškai stabilios, tirpios ir turi palyginti didelį krūvininkų judrį ($1{,}2\cdot10^{-5}$–$3{,}3\cdot10^{-4}$ cm^2/Vs), todėl jas perspektyvu naudoti optoelektroniniuose įrenginiuose.
2. Puslaidininkiai, turintys Triogerio bazės karkasą ir feniletenilo šonines šakas, yra termiškai stabilūs, tirpūs ir pasižymi dideliu teigiamu krūvininkų judriu (iki 0,011 cm^2/Vs). Dėl šių priežasčių šie puslaidininkiai yra tinkami naudoti perovskitinėse saulės celėse.
3. TB fragmentas suteikia juo sujungtiems *para*-padėtyje pakaitą turintiems TPD fragmentams orientaciją beveik statmenai vienas kitam. Taip gaunamos stabilios, visiškai amorfinės medžiagos, turinčios palyginti didelį krūvininkų judrį (iki 0,036 cm^2/Vs). Ši Triogerio bazės junginių grupė gali efektyviai funkcionuoti kaip skylių pernašos medžiaga perovskitiniuose saulės elementuose.
4. Triogerio bazės molekulinio karkaso sintezė ir modifikavimas leidžia lengvai ir nenaudojant brangių paladžio katalizatorių gauti efektyvias skyles pernešančias medžiagas su TB fragmentu ir enamino šoniniais pakaitais, kurios savo efektyvumu saulės celėse gali aplenkti efektyvumo standartu laikomą junginį *spiro*-OMeTAD.
5. Triogerio bazę galima naudoti kaip karkasą naujiems kietosios būsenos spinduoliams, turintiems agregacijos indukuotos šviesos emisijos savybes, ir dažikliams, skirtiems saulės elementams, projektuoti.

1. Skyles pernešantys organiniai puslaidininkiai, turintys Triogerio bazės fragmentą

Elektroniniai ir optoelektroniniai prietaisai, naudojantys organinius junginius, tokie kaip organiniai šviesos diodai, fotovoltiniai įrenginiai ir lauko tranzistoriai, veikia juose vykstant krūvio pernašai, todėl krūvininkus pernešantys junginiai yra neatsiejama jų dalis [136]. Dėl šios priežasties didelio našumo krūvininkų pernašą atliekančių medžiagų kūrimas yra labai svarbus efektyvių prietaisų gamybai [137, 138]. Organinės elektronikos, kaip pigesnės technologijos, potencialui išnaudoti taip pat svarbu pasitelkti paprastus apdorojimo būdus, pvz., įrenginio sluoksnių liejimo iš tirpalų metodą, pageidautina, naudojant paprastas, pigias, lengvai išgryninamas medžiagas [139, 140]. Mažamolekulės skyles gabenančios medžiagos turi daug išskirtinių privalumų, palyginti su polimerais, tokių kaip struktūrinis įvairiapusiškumas, tiksliai nusakoma molekulinė masė ir santykinai lengvas valymas chromatografijos, kristalizacijos arba vakuuminio sublimavimo būdu [141, 142]. Deja, nemažai šių puslaidininkių turi žemą stiklėjimo temperatūrą (T_g) [139, 140, 143], todėl gali pereiti iš stikliškosios būsenos į kristalinę ar skystąją. Dėl šios priežasties gali susilpnėti prietaiso savybės [144, 145].

V formos Triogerio bazės struktūra leidžia ją naudoti kaip karkasą ir suteikti prie jos prijungtoms konjuguotosioms π-sistemoms kampo orientaciją. Naujausi tyrimai taip pat atskleidė, kad TB karkaso standumas ir dėl jo dvigubo funkcionalizavimo gaunama didesnė molekulinė masė sumažina kristalizaciją, todėl Triogerio bazės dariniai pasižymi amorfiškumu ir kur kas aukštesne stiklėjimo temperatūra [134, 146, 147]. Šie rezultatai skatina sintetinti ir tirti naujus organinius puslaidininkius, turinčius TB fragmentą.

1.1. Mažamolekulių skyles pernešančių medžiagų, turinčių Triogerio bazės karkasu susietų trifenilamino grupių, sintezė

Nauji Triogerio bazės junginiai **1a–1d** buvo susintetinti (1) vykdant paladžiu katalizuojamą C–N prijungimo reakciją, kurioje dalyvavo iš 4-brom-2-metilanilino [40] gautas bromintas Triogerio bazės analogas (**1'**) ir atitinkamas difenilaminas (difenilaminas, di(4-metoksifenil)aminas [154], 4-metoksi-*N*-(4-metoksifenil)-3-metilanilinas [144], 4-metoksi-*N*-(p-tolil)anilinas [155]). TB darinių **1a–1d** struktūra buvo patvirtinta ^{1}H ir ^{13}C BMR spektrais ir elementinės analizės metodu.

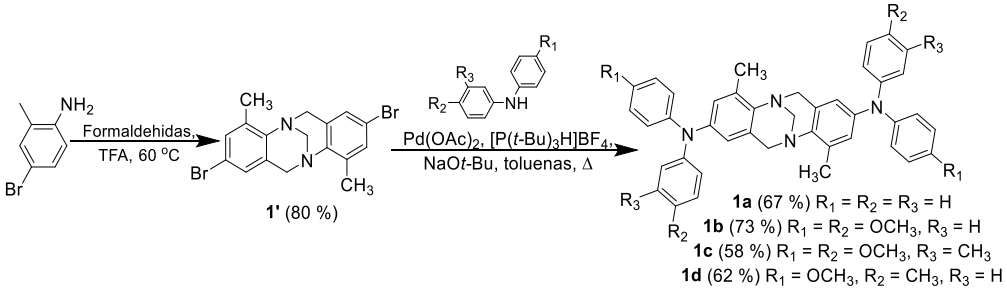

1 schema. Naujų junginių **1a–1d**, turinčių Triogerio bazės fragmentą, sintezė

1.2. Terminės ir optinės savybės

Kad skyles pernešančios medžiagos būtų sėkmingai naudojamos įrenginiuose, reikia suformuoti homogeniškus ir termiškai stabilius sluoksnius. Terminės susintetintų junginių savybės, leidžiančios nusakyti jų kristališkumą ir stiklėjimo temperatūrą, buvo ištirtos diferencinės skenuojamosios kalorimetrijos (DSC) būdu (1 lent.). Visiškai kristalinis yra tik junginys **1a**, visi kiti junginiai turi amorfinę būseną ir antrojo jų kaitinimo ar aušinimo ciklo metu fiksuojama tik stiklėjimo temperatūra, o kristalai nesusidaro.

1 lentelė. Triogerio bazės darinių **1a–1d** terminės savybės

Junginys	T_m [°C][a]	T_g [°C][b]	T_{dec} [°C][c]
1a	158	–	371
1b	–	115	378
1c	162	114	370
1d	–	123	387

[a] Lydymosi temperatūra užfiksuota tik pirmojo kaitinimo metu, 10 K/min. [b] Nustatyta taikant DSC: kaitinimo greitis 10 K/min; N_2 atmosfera; antrasis kaitinimas. [c] Skilimo pradžia nustatyta TGA metodu: kaitinimo greitis 10 K/min; N_2 atmosfera.

Termogravimetrinė analizė atskleidė aukštą skilimo temperatūrą (1 lent.), rodančią labai gerą tiriamų junginių terminį stabilumą.

Junginių **1a–1d** UV-VIS absorbcijos spektrai, išmatuoti iš tetrahidrofurano tirpalų (c = 10^{-4} mol/l, d = 1 mm) (1 pav.), rodo absorbciją artimoje UV zonoje (210 nm), kuri atitinka n-σ^* elektronų judėjimą prie centrinių azoto atomų, o didesnio bangos ilgio (300 nm) absorbcija atitinka konjuguotosios sistemos π–π^* elektronų perėjimus. Jokio absorbcijos maksimumo (303 nm) batochrominio poslinkio nepastebima, nes konjuguotosios π-sistemos dydis yra toks pats, tačiau šiek tiek skiriasi absorbcijos intensyvumas, priklausomai nuo prijungtų pakaitų.

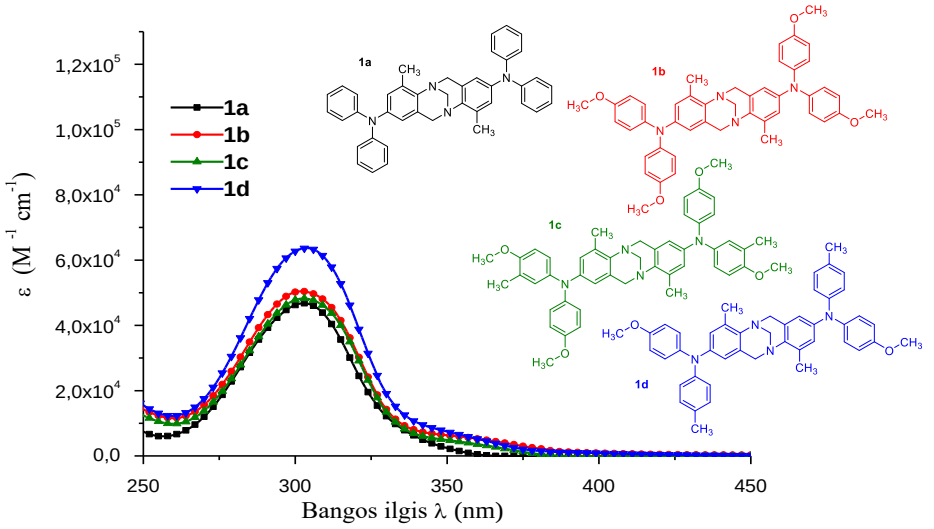

1 pav. Junginių **1a–1d** $1 \cdot 10^{-4}$ M THF tirpaluose absorbcijos spektrai

1.3. Fotoelektrinės savybės

Junginių jonizacijos potencialas (I_p) esant kietai būsenai yra svarbus parametras, nulemiantis organinių skyles pernešančių medžiagų panaudojimą. Šis veiksnys gali padėti parinkti optoelektroniniame įrenginyje kartu naudoti tinkamus organinius puslaidininkius ir neorganines elektrodams naudojamas medžiagas. Susintetintų molekulių jonizacijos potencialai buvo išmatuoti fotoelektronų spektroskopijos ore (PESA) metodu. Rezultatai pateikti 2 lent. Matavimo paklaida vertinama kaip 0,03 eV.

2 lentelė. Junginių **1a–1d** energijos lygmenų ir krūvininkų judrio duomenys

Junginys	I_p [eV][a]	μ_0 [cm^2/Vs][b]	μ (6,4·10^5 V/cm) [cm^2/Vs][c]
1a	5,60	3,8·10^{-7}[d]	4,5·10^{-6}[d]
1b	5,30	3·10^{-8}	1,3·10^{-4}
1c	5,25	1·10^{-7}	1,2·10^{-5}
1d	5,34	3·10^{-6}	3,3·10^{-4}

[a] Kietosios būsenos junginių jonizacijos potencialas (I_p) buvo matuojamas fotoemisijos ore metodu iš plėvelių. [b] Krūvininkų judrio vertė esant nuliniam lauko stipriui. [c] Krūvininkų judrio vertė, kai lauko stipris yra 6,4·10^5 V. [d] Junginio **1a** judrio vertės išmatuotos iš jo ir PC-Z mišinio (1:1).

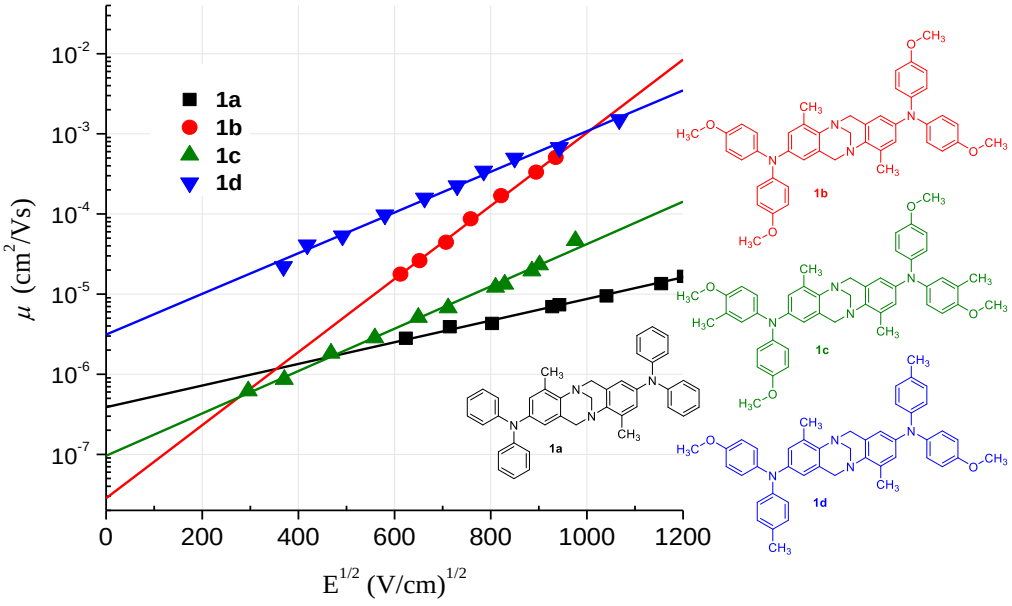

2 pav. Junginių **1a–1d** krūvininkų judrio priklausomybė nuo elektrinio lauko. Junginio **1a** duomenys gauti matuojant iš jo ir PC-Z mišinio (1:1)

Vienas iš pagrindinių parametrų, rodančių, ar medžiaga tinka skylių pernašai, yra krūvininkų judris. Susintetintų Triogerio bazės darinių krūvininkų pernašos

savybės buvo tiriamos kserografiniu lėkio trukmės metodu (XTOF) (2 pav.). Junginių **1a–1d** krūvininkų judrio vertes apibrėžiantys parametrai – dreifinis judris nuliniame elektriniame lauke (μ_0) ir dreifinis judris esant $6{,}4\cdot10^5$ V/cm elektriniam laukui – pateikiami 2 lentelėje. Naudojant junginį **1a** gautos prastos kokybės plėvelės, todėl, siekiant gauti vienodus sluoksnius, buvo panaudotas junginio **1a** ir polikarbonato (PC-Z) mišinys masių santykiu 1:1. Absoliutus junginio **1a** judrio rezultatas buvo mažesnis (apytiksliai viena skaičių eile) dėl nelaidaus polimero.

Junginio **1d** skylių dreifinis judris stipriuose elektriniuose laukuose, matuojant kambario temperatūroje, buvo $3{,}3\cdot10^{-4}$ cm^2 V^{-1} s^{-1}, ir tai yra geriausias rezultatas iš visų trijų grynųjų medžiagų (**1b–1d**). Jis artimas kai kurių literatūroje aprašomų pramoninių puslaidininkių krūvininkų judriui. Junginys **1c** turi mažiausią krūvininkų judrį iš tirtų grynųjų medžiagų. Galima to priežastis – papildomas metilpakaitas *meta*-padėtyje trukdo palankiam molekulių išsidėstymui sluoksnyje.

Apibendrinant šį skyrių galima teigti, kad susintetinti Triogerio bazės junginiai su metil- ir metoksipakaitais turi skyles pernešantiems puslaidininkiams reikalingas savybes, gana palankias fizikines savybes, yra stabilūs, dauguma jų amorfiniai ir lengvai tirpūs. Nors šių junginių krūvininkų judris nuliniame elektriniame lauke (μ_0) nėra pakankamas saulės elementams ir jie negali konkuruoti su tokiomis medžiagomis kaip *spiro*-OMeTAD (μ_0 = $4{,}1\cdot10^{-5}$ cm^2/Vs), tačiau yra kitų sričių (pvz., elektrofotografija), kur šie junginiai gali būti sėkmingai naudojami.

2. Skyles pernešančios medžiagos, turinčios Triogerio bazės karkasą ir feniletenilpakaitus

Šis skyrius skirtas toliau tobulinti organinių puslaidininkių molekuliniam dizainui sintetinant ir tyrinėjant V formos krūvį pernešančias molekules, sudarytas iš Triogerio bazės fragmento ir feniletenilo fragmentų turinčių pakaitų.

2.1. Naujų Triogerio bazės fragmentą turinčių junginių sintezė

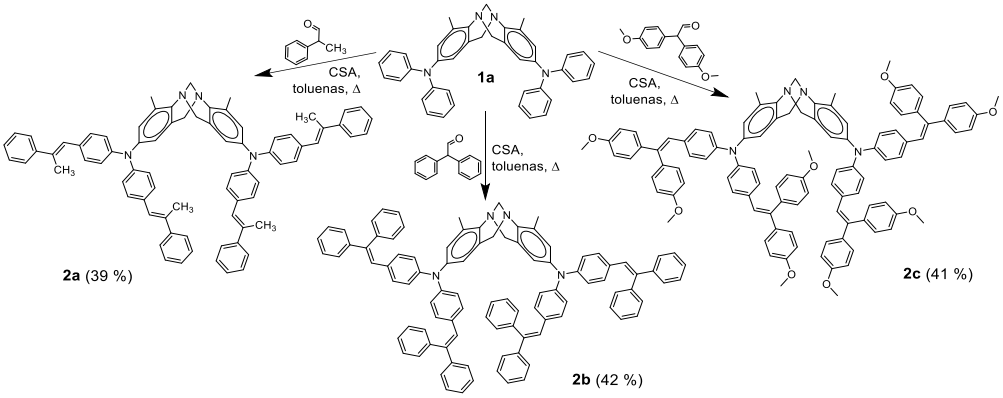

2 schema. Junginių **2a–2c**, turinčių Triogerio bazės fragmentą ir feniletenilo šoninius pakaitus, sintezė

Nauji TB junginiai **2a–2c** buvo susintetinti iš junginio **1a**, vykstant jo kondensacijai su atitinkamu aldehidu (metilfenil-, difenil- arba di(4-metoksi)fenil-

acetaldehidu) tolueno virimo temperatūroje, katalizuojant kamparo-10-sulfonine rūgštimi (CSA) (2 schema). TB darinių **2a–2c** struktūra buvo patvirtinta ^{1}H ir ^{13}C BMR spektrais ir elementine analize.

2.2. Terminės ir optinės savybės

DSC matavimai atskleidė, kad molekulėse atsiradęs struktūrinis tūris ir didelis konformerų skaičius trukdo kristalizacijos procesams tiriamuosiuose junginiuose ir tik vienintelis junginys **2a** dar būna ir kristalinės, o ne tik amorfinės būsenos (3 lent.). Tai ypač pastebima lyginant su stipriomis kristalinėmis savybėmis pasižyminčiu junginiu **1a**. Visi trys junginiai antrojo kaitinimo ir aušinimo ciklo metu pasižymi tik amorfiškumu. Palyginti su analogiškais puslaidininkiais, neturinčiais TB karkaso [160], T_g padidėja nuo 1 °C iki 132 °C junginio **2a** atveju ir padvigubėja junginiuose **2b** ir **2c**.

Termogravimetrinė analizė atskleidė aukštą skilimo temperatūrą (3 lent.). Tai rodo labai gerą tiriamųjų junginių terminį stabilumą.

3 lentelė. Junginių **2a–2c** optinės ir terminės savybės

Jung.	T_g [°C][a]	T_m [°C][b]	T_{dec} [°C][c]	λ_{max}^{abs} [nm][d]	ε [$M^{-1}cm^{-1}$]	λ_{max}^{FL} [nm][e]	Φ_F [%]
2a	132	204	378	353	$8{,}49\cdot10^4$	432	37
2b	152	–	413	393	$9{,}56\cdot10^4$	479	9
2c	146	–	321	377	$7{,}25\cdot10^4$	471	20

[a] Nustatyta pagal DSC: kaitinimo greitis 10 K/min; N_2 atmosfera; antrasis ciklas. [b] Lydymosi temperatūra užfiksuota tik per pirmąjį kaitinimą; junginys sustiklėjo vėsdamas iki kambario temperatūros 10 K/min greičiu. [c] Skilimo temperatūra nustatyta pagal TGA: kaitinimo greitis 10 K/min; N_2 atmosfera. [d] UV-Vis spektrai išmatuoti 10^{-4} M THF tirpale. [e] Fluorescencijos spektrai užrašyti iš 10^{-5} M tolueno tirpalų.

Junginių **2a–2c** UV-Vis absorbcijos spektrai buvo išmatuoti 10^{-4} M tetrahidrofurano tirpaluose ir apibendrinti 3 lentelėje. Junginių **2a–2c** absorbcijos maksimumų batochrominis poslinkis, palyginti su tarpinio junginio **1a** (pvz., **2a** – 49 nm, o **2b** – apie 90 nm), gali būti priskiriamas konjuguotosios π-sistemos išplėtimui feniletenilo fragmentais. Verta paminėti, kad grynuosiuose sluoksniuose be priedų **2a**–**2c** absorbuoja daugiausia UV srityje, trumpesnių nei 450 nm bangų intervale, todėl šie skyles pernešantys puslaidininkiai tinkami kietosios būsenos dažikliais įjautrintiems ir perovskitiniams saulės elementams, nes jie beveik nekonkuruoja su dažiklio sugertimi.

2.3. Fotoelektrinės savybės

Junginių **2a–2c** jonizacijos potencialas buvo išmatuotas fotoelektronų spektroskopijos ore metodu ir rezultatai pateikti 4 lentelėje. Metil- ir fenilpakaitus turinčių junginių **2a** ir **2b** I_p reikšmės labai panašios, o metoksigrupių prijungimas prie junginio **2c** sumažina I_p ~0,2 eV.

Junginių energijos virsmai ir elektronų pernaša tirpaluose, siekiant apskaičiuoti junginių E_{LUMO} ir E_{HOMO}, buvo matuojama taikant ciklinės voltamperometrijos (CV) metodą. Šios vertės neatspindi absoliučios kietosios būsenos arba dujų fazės

jonizacijos energijų, tačiau gali būti naudojamos panašiems junginiams palyginti tarpusavyje.

4 lentelė. Junginių **2a–2c** energijos lygmenų[a] ir skylių judrio duomenys

Junginys	E_g^{opt} [eV][b]	E_{HOMO} [eV][c]	E_{LUMO} [eV][d]	I_p [eV][e]	EA [eV][f]	μ_0 [$cm^2\ V^{-1}\ s^{-1}$][g]	μ [$cm^2\ V^{-1}\ s^{-1}$][h]
2a	3,05	5,38	2,33	5,44	2,39	$1,5\cdot10^{-3}$	0,011
2b	2,82	5,35	2,53	5,45	2,63	$1,3\cdot10^{-4}$	0,005
2c	2,87	5,29	2,42	5,27	2,40	$3,9\cdot10^{-5}$	0,002

[a] CV matavimai atlikti su stiklo elektrodu dichlormetano tirpaluose, naudojant 0,1 M tetrabutilamonio heksafluorfosfatą kaip elektrolitą ir $Ag/AgNO_3$ kaip palyginamąjį elektrodą. Kiekvienas matavimas buvo kalibruotas naudojant feroceną (Fc). Potencialai apskaičiuoti plg. su Fc^+/Fc. [b] Optinės draustinės juostos E_g^{opt} apskaičiuotos iš tirpalų absorbcijos spektrų. [c] Konversijos koeficientai: ferocenas DCM-SCE: 0,46 [162], SCE-SHE: 0,244 [163], SHE-vakuumas: 4,43 [164]. [d] E_{LUMO} apskaičiuota pagal lygtį $E_{LUMO} = I_p - E_g^{otp}$. [e] Kietosios būsenos junginių jonizacijos potencialas (I_p) buvo matuojamas fotoemisijos ore metodu iš plėvelių. [f] Elektronų giminingumas (EA) apskaičiuotas pagal lygtį $EA = E_{HOMO} - E_g^{otp}$. [g] Dreifinio judrio vertė esant nuliniam lauko stipriui. [h] Judrio vertė, kai lauko stipris yra $6,4\cdot10^5$ V cm^{-1}.

Susintetintų Triogerio bazės darinių krūvininkų pernašos savybės buvo ištirtos kserografiniu lėkio trukmės metodu. Junginio **2a** skylių judris stipriuose elektriniuose laukuose buvo 0,011 $cm^2\ V^{-1}\ s^{-1}$, ir tai yra geras rezultatas skyles pernešančiam puslaidininkiui.

2.4. Perovskitiniai saulės elementai

Siekiant ištirti pritaikymo prietaisams galimybes, susintetinti TB junginiai **2a–2c** išbandyti kaip *p*-tipo puslaidininkiai perovskitiniuose saulės elementuose (PSC).

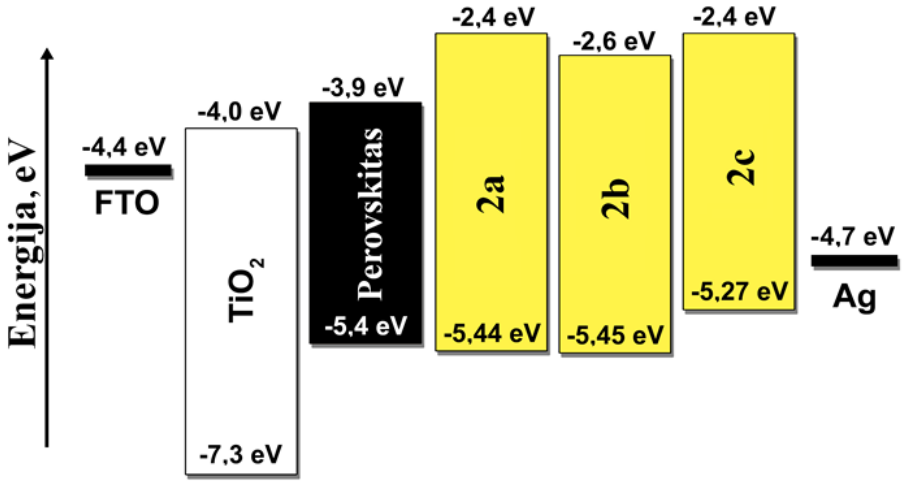

3 pav. Naudojant junginius **2a–2c** pagamintų PSC įrenginių energijos lygmenų diagrama

Eksperimentai buvo atlikti naudojant įrenginius, kurių struktūrą sudaro fluorintas alavo oksidas (FTO), kompaktinis TiO_2, perovskitas, HTM ir Ag (3 pav.).

Šiuose įrenginiuose HTM funkciją atliko junginiai **2a–2c**. Taip pat palyginimui naudotas standartu laikomas *spiro*-OMeTAD (2,2′,7,7′-tetra(N,N-di-p-metoksifenilamino)-9-9′-spirobifluorenas).

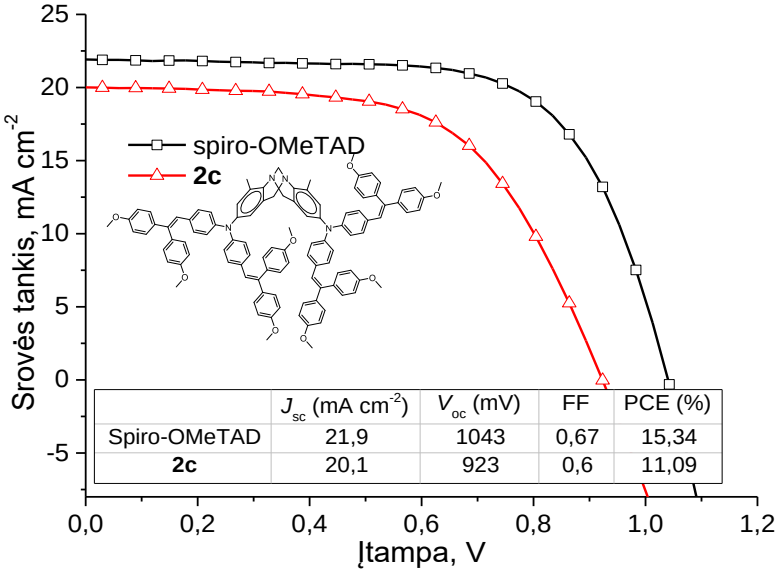

	J_{sc} (mA cm^{-2})	V_{oc} (mV)	FF	PCE (%)
Spiro-OMeTAD	21,9	1043	0,67	15,34
2c	20,1	923	0,6	11,09

4 pav. Geriausiai veikiančių perovskitinių saulės elementų, kuriuose junginiai **2c** ir *spiro*-OMeTAD naudojami kaip skylių pernašos medžiagos, charakteristikos

Didžiausias energijos konversijos efektyvumas, siekiantis 11,09 %, naudojant standartinį AM 1,5 G apšvietimą buvo užregistruotas įrenginyje, kuriame skylių pernašai naudojamas junginys **2c**. Išmatuotas užpildos faktorius (*FF*) buvo 0,6, srovės tankis (J_{sc}) – 20,1 mA cm^{-2} ir atvirosios grandinės įtampa (V_{oc}) – 923 mV (4 pav.). Kita vertus, junginiai **2a** ir **2b** neveikė efektyviai bandomojoje saulės elementų sistemoje dėl perovskito ir HTM energijos lygmenų neatitikimo (3 pav.). Šių medžiagų I_p (siekiantis apie –5,45 eV) viršija suderinamumo su $MAPbI_xCl_{3-x}$ (–5,40 eV) ribą [137].

3. Skyles pernešantys TPD tipo junginiai, sujungti Triogerio bazės fragmentu

3.1. Naujų Triogerio bazės fragmentą turinčių junginių sintezė

Nauji Triogerio bazės fragmentą turintys TPD junginiai **3f–3h** buvo susintetinti naudojant tarpinius bifenilo junginius **3a–3e** (3 schema) ir vykdant Buchwaldo ir Hartwigo prijungimo reakciją.

Iš pradžių bifenilo junginiai **3a–3b** buvo gauti iš 4,4'-dibromobifenilo ir atitinkamo anilino, taikant Buchwaldo ir Hartwigo prijungimo reakciją. **3a**, **3b** ir jų komerciškai prieinamas analogas *N*,*N*-difenilbenzidinas buvo naudojami paladžiu katalizuojamoje prijungimo reakcijoje su atitinkamais arilhalogenidais, siekiant gauti junginius **3c–3e**. Šie junginiai savo ruožtu reagavo su brominta Triogerio baze **1‘**, taip

gauti tiksliniai junginiai **3f–3h**, turintys TPD fragmentų, sujungtų Triogerio bazės molekuliniu karkasu.

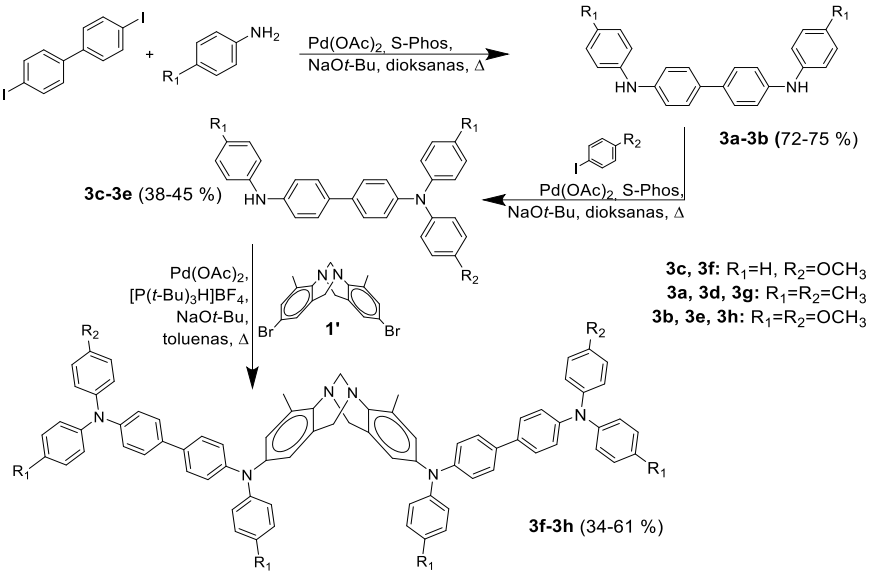

3 schema. Junginių **3a**–**3h**, turinčių TPD tipo fragmentų, sintezė

Atlikus junginių **3f–3h** tyrimus, paaiškėjo, kad perspektyviausias yra darinys **3h**. Tyrimo rezultatai leido daryti prielaidą, jog metoksigrupės, esančios TPD fragmentų galuose, suteikia junginiui palankiausias savybes. Todėl buvo pasiūlytas planas, kaip susintetinti molekules, turinčias du arba keturis metoksigrupių turinčius TPD fragmentus (per reakciją su tarpiniu junginiu **3e**), sujungtus per TB fragmentą kita tvarka. Šis planas buvo įgyvendintas (4 schema).

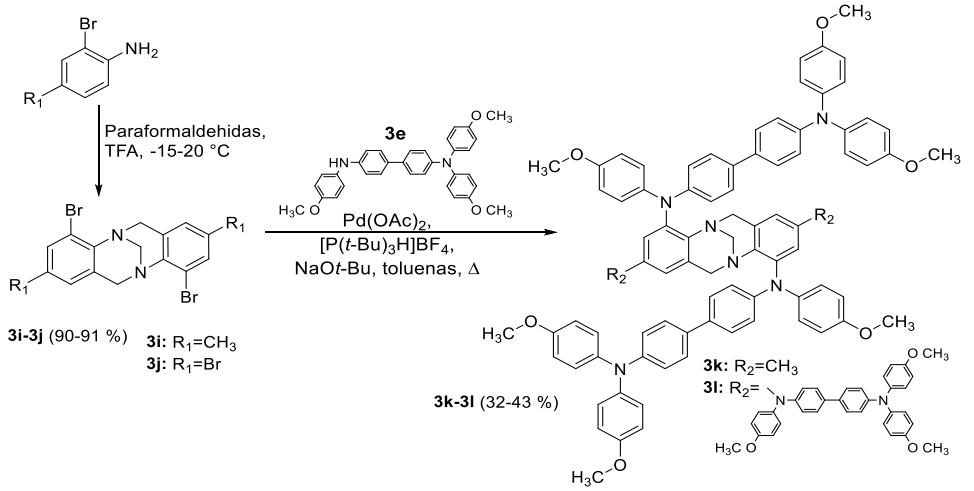

4 schema. Junginių **3i–3l** sintezė

Visų TB junginių struktūra buvo neginčijamai patvirtinta ^{1}H ir ^{13}C BMR spektrais ir elementinės analizės metodu.

3.2. Terminės ir optinės savybės

Neplokščia TB struktūra ir atitinkamai orientuoti TPD tipo fragmentai, nukreipti vienas į kitą kampu, sudaro nesusiglaudžiantį erdvinį tūrį, kuris trukdo kristalizacijos procesams tiriamuose puslaidininkiuose. DSC matavimai parodė, kad visi tiriami Triogerio bazės junginiai **3f–3h** ir **3k–3l** gali būti tik amorfinės būsenos (5 lent.).

Šių junginių termogravimetrinės analizės duomenys atskleidžia aukštą skilimo temperatūrą (5 lent.). Visi serijos junginiai pasižymi puikiu terminiu stabilumu, visų jų skilimo temperatūra (atitinkanti 5 % svorio sumažėjimą) viršija 400 °C. Tai leidžia patvirtinti, kad šie TB dariniai yra termiškai labai stabilūs ir tinkami naudoti praktiškai.

Triogerio bazės darinių **3f–3h** ir **3k–3l** UV-Vis absorbcijos spektrai 10^{-4} M THF tirpale ir emisijos spektrai, išmatuoti iš 10^{-6} M THF tirpalų, yra apibendrinti 5 lentelėje. TB junginys **3l** turi dvigubą skaičių TPD fragmentų, palyginti su kitomis pamatuotomis molekulėmis, ir tai suteikia jam beveik dvigubai didesnį nei kitų junginių sugerties intensyvumą. Vis dėlto nepastebimas joks reikšmingas batochrominis poslinkis – tai rodo, kad dvi gretimos TPD grupės kiekvienoje Triogerio bazės fragmento pusėje nesukuria vientisos konjuguotosios sistemos. Greičiausiai tai lemia nepalankus fragmentų išsidėstymas, pažeidžiantis konjugaciją.

5 lentelė. Triogerio bazės junginių, turinčių TPD fragmentų, terminės ir optinės savybės

Junginys	T_g (°C)	T_{dec} (°C)	λ_{abs} (nm)[a]	ε (l mol^{-1} cm^{-1})[b]	λ_F (nm)[c]	Φ_F (%)[d]
3f	167	454	304	66 391	413	44,5
			354	86 250		
3g	177	451	305	63 454	419	46,8
			356	77 413		
3h	161	419	303	65 804	424	52,1
			355	86 485		
3k	153	409	310	59 758	410	39,33
			352	83 109		
3l	166	420	310	11 647	435	37,26
			354	15 466		

[a] Absorbcijos maksimumai THF tirpale. [b] THF tirpalo absorbcijos molinis ekstinkcijos koeficientas kreivės maksimumo padėtyje. [c] Fluorescencijos maksimumas THF tirpale. [d] Fluorescencijos kvantinis našumas THF tirpale.

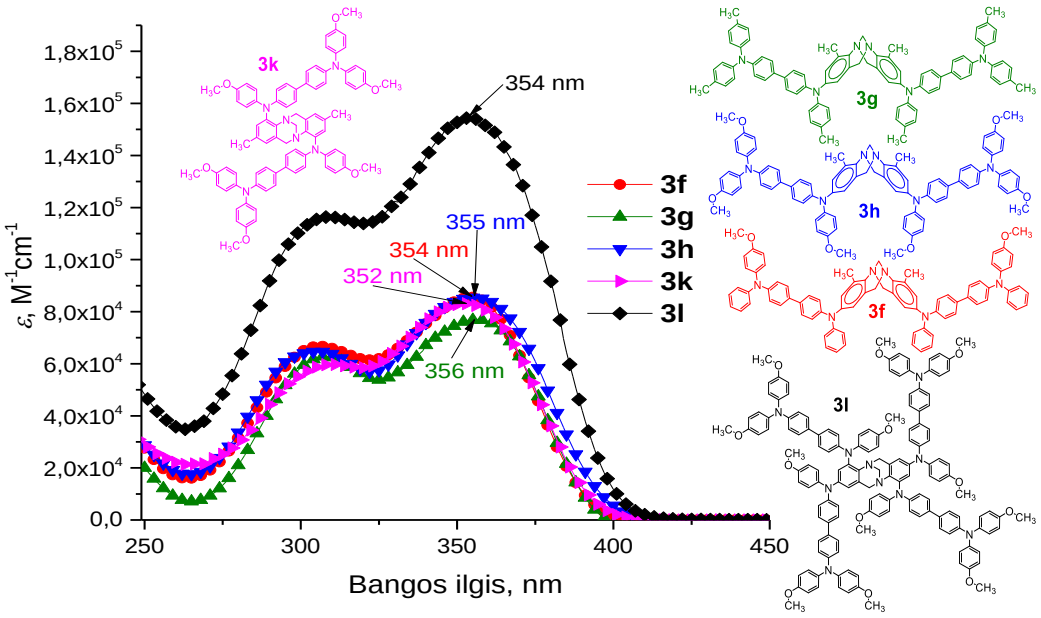

5 pav. Junginių **3f–3h** ir **3k–3l** absorbcijos spektrai $1 \cdot 10^{-4}$ M THF tirpaluose

3.3. Fotoelektrinės savybės

Junginių **3f–3h** ir **3k–3l** jonizacijos potencialas buvo išmatuotas fotoelektronų spektroskopijos ore metodu. Rezultatai pateikti 6 lentelėje. Darinys **3f** turi keturias nepakeistas fenilgrupes ir didžiausią I_p reikšmę (5,31 eV), o metil- arba metoksigrupių pakaitų prijungimas prie galinių fenilų mažina šią vertę: nė vieno iš visiškai pakeistų junginių I_p neviršija 5,25 eV. Tokia jonizacijos potencialo vertė yra palanki junginių naudojimui saulės elementuose.

Junginių **3f–3h** ir **3k–3l** redukcijos ir oksidacijos potencialai buvo išmatuoti ciklinės voltamperometrijos metodu (6 lent.). Gauti rezultatai koreliuoja su jonizacijos potencialo matavimo duomenimis, gautais iš plėvelių. Tai leidžia spręsti apie ribotą molekulinę sąveiką esant kietajai būsenai.

Susintetintų junginių **3f–3h** ir **3k–3l** krūvininkų pernašos savybės buvo ištirtos kserografiniu lėkio trukmės metodu (6 lent.). Geriausias skylių dreifinis judris (0,036 $cm^2 V^{-1} s^{-1}$ stipriuose elektriniuose laukuose) buvo išmatuotas plėvelėse iš metoksigrupių turinčio junginio **3h**. Palyginti su kitomis mažos molekulinės masės skyles pernešančiomis medžiagomis [143, 160, 165–167], susintetinti TB dariniai **3g** ir **3h** pasižymi gana dideliu skylių dreifiniu judriu, kuris atitinkamų metil- ir metoksigrupių turinčių TPD analogų, nesujungtų TB karkasu, rezultatus viršija daugiau nei šimtą kartų [140, 188]. Taip pat pastebėtas įdomus reiškinys – krūvininkų judris nesumažėja, nors įprastai tai įvyksta pakeitus metilgrupes metoksigrupėmis. Galima manyti, jog tai vyksta dėl naudingos tarpmolekulinės metoksigrupių sąveikos, taip pat pastebėtos kituose trifenilamino junginiuose [189–191].

6 lentelė. Junginių **3f–3h** energijos lygmenų[a] ir skylių judrio duomenys (palyginti pateikiami ir *spiro*-OMeTAD duomenys)

Junginys	E_g^{opt} (eV)[b]	E_{HOMO} (eV)[c]	E_{LUMO} (eV)[d]	I_p (eV)[e]	μ_0 ($cm^2 V^{-1} s^{-1}$)[f]	μ_h ($cm^2 V^{-1} s^{-1}$)[g]
3f	3,16	5,24	2,08	5,31	$4 \cdot 10^{-8}$ [h]	$4 \cdot 10^{-6}$[h]
3g	3,15	5,13	1,98	5,25	$1{,}2 \cdot 10^{-4}$	0,004
3h	3,13	5,11	1,98	5,23	$6 \cdot 10^{-5}$	0,036
3k	3,05	5,13	2,08	5,19	_[i]	_[i]
3l	3,01	5,19	2,18	5,24	$1{,}1 \cdot 10^{-5}$	$9{,}4 \cdot 10^{-4}$
Spiro-OMeTAD	–	–	–	5,00	$4{,}1 \cdot 10^{-5}$	$5 \cdot 10^{-4}$

[a] CV matavimai atlikti su stiklo elektrodu dichlormetano tirpaluose, naudojant 0,1 M tetrabutilamonio heksafluorfosfatą kaip elektrolitą ir $Ag/AgNO_3$ kaip palyginamąjį elektrodą. Kiekvienas matavimas buvo kalibruotas naudojant feroceną (Fc). Potencialai apskaičiuoti plg. su Fc^+/Fc. [b] Optinės draustinės juostos E_g^{opt} apskaičiuotos iš tirpalų absorbcijos spektrų. [c] Konversijos koeficientai: ferocenas DCM-SCE: 0,46 [162], SCE-SHE: 0,244 [163], SHE-vakuumas: 4,43 [164]. [d] E_{LUMO} apskaičiuota pagal lygtį $E_{LUMO} = I_p - E_g^{otp}$. [e] Kietosios būsenos junginių jonizacijos potencialas (I_p) buvo matuojamas fotoemisijos ore metodu iš plėvelių. [f] Dreifinio judrio vertė esant nuliniam lauko stipriui. [g] Judrio vertė, kai lauko stipris yra $6{,}4 \cdot 10^5$ V cm^{-1}. [h] Junginio **3f** judrio vertės buvo išmatuotos iš jo ir PC-Z mišinio (1:1). [i] nepavyko gauti matavimams tinkamo sluoksnio.

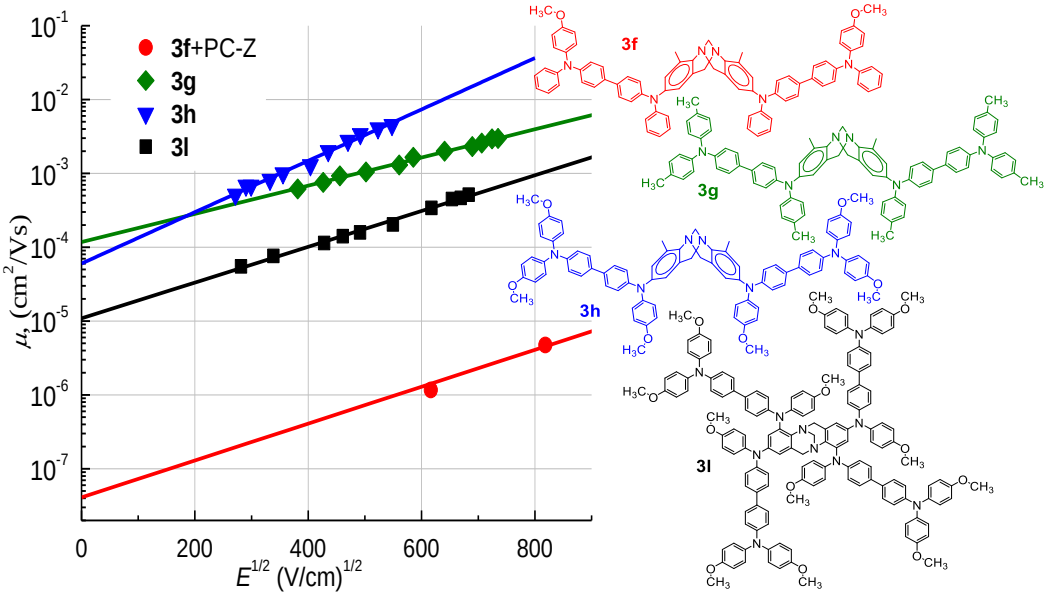

6 pav. Junginių **3f**–**3h** ir **3l** krūvininkų judrio priklausomybė nuo elektrinio lauko. Junginio **3f** duomenys gauti matuojant iš jo ir PC-Z mišinio (1:1)

3.4. Perovskitinių saulės elementų konstravimas

Atsižvelgiant į savybes atrinkti daugiausia žadantys susintetinti TB junginiai **3g** ir **3h** buvo išbandyti perovskitiniuose saulės elementuose kaip organiniai puslaidininkiai. Eksperimentai buvo atlikti naudojant įrenginius, sudarytus iš fluorinto alavo oksido (FTO), kompaktinio SnO_2, C_{60}, perovskito, HTM ir Ag.

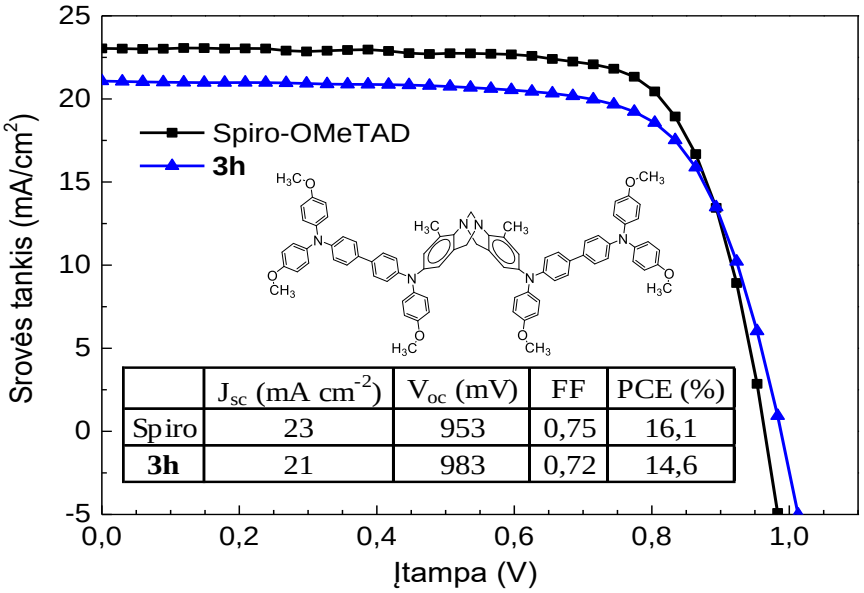

	J_{sc} (mA cm^{-2})	V_{oc} (mV)	FF	PCE (%)
Spiro	23	953	0,75	16,1
3h	21	983	0,72	14,6

7 pav. Geriausiai veikiančių perovskitinių saulės elementų, kuriuose kaip skylių pernašos medžiagos naudojami junginiai **3h** ir *spiro*-OMeTAD, charakteristikos

Prietaisai su metoksigrupių neturinčiu junginiu **3g** pasižymėjo prastesnėmis savybėmis, jų efektyvumas buvo iki 10 %. Efektyviausiuose perovskitiniuose prietaisuose, kuriuose kaip skylių pernašos medžiaga naudotas junginys **3h**, buvo užfiksuotas 14,6 % rezultatas (7 pav.).

Junginys **3l** buvo išbandytas kaip HTM optimizuotos architektūros perovskito saulės elementuose, kuriuos sudaro FTO, TiO_2 blokuojantis sluoksnis, mezoporinis TiO_2, amorfinis SnO_2, perovskitas, HTM ir Au. Juose kaip šviesą sugeriantis sluoksnis buvo naudojamas mišraus perovskito $[(FAPbI_3)_{0,87}(MAPbBr_3)_{0,13}]_{0,92}(CsPbI_3)_{0,08}$ sluoksnis (8 pav.).

Prietaisai, kuriuose naudojamas junginys **3l**, puikiai veikė, jų maksimalus galios konversijos efektyvumas pasiekė 17,91 %. Šis rezultatas yra gana artimas gautam tiriant prietaisus su *spiro*-OMeTAD (geriausio našumo įrenginyje pasiekė 19,22 % PCE).

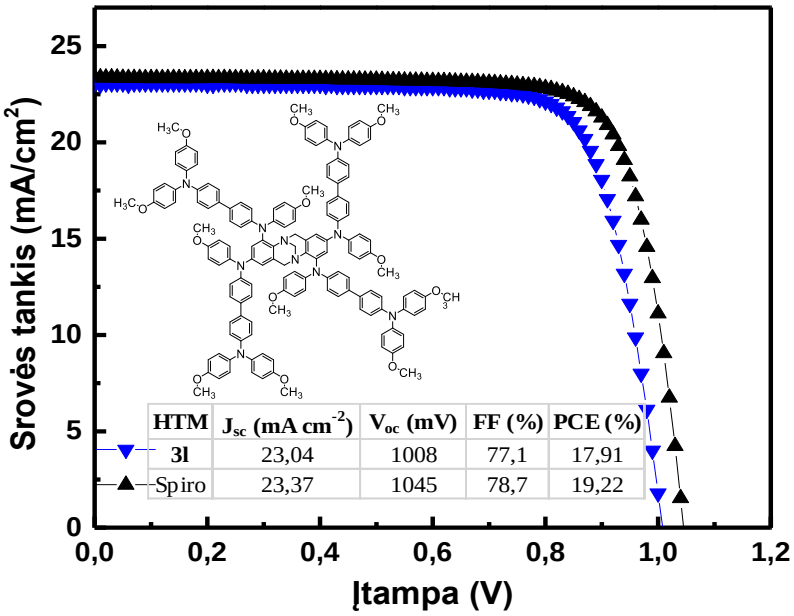

HTM	J_{sc} (mA cm^{-2})	V_{oc} (mV)	FF (%)	PCE (%)
3l	23,04	1008	77,1	17,91
Spiro	23,37	1045	78,7	19,22

8 pav. Geriausiai veikiančių perovskitinių saulės elementų, kuriuose kaip skylių pernašos medžiagos naudojami junginiai **3l** ir *spiro*-OMeTAD, charakteristikos

4. Skyles pernešantys puslaidininkiai, turintys Triogerio bazės fragmentą ir šoninius enamino pakaitus

4.1. Naujų Triogerio bazės fragmentą turinčių junginių sintezė

Nauji enamino pakaitų turintys Triogerio bazės junginiai **4c–4e** buvo susintetinti per tarpinius junginius **4a–4b**, taikant trijų pakopų sintezės metodiką (5 schema).

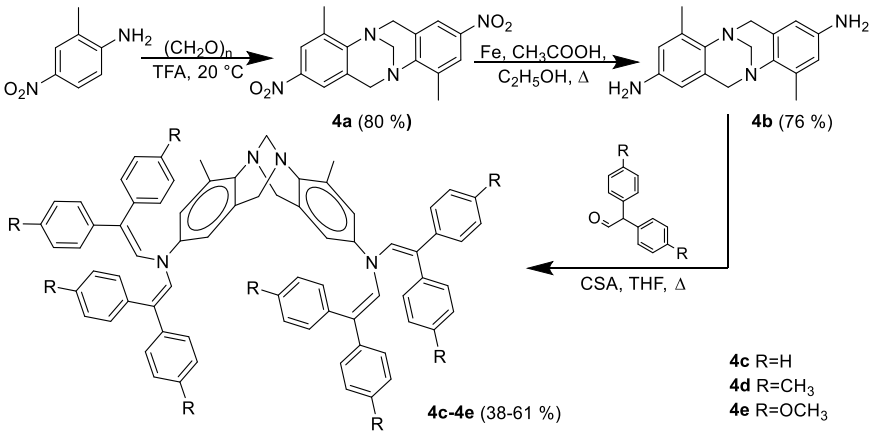

5 schema. Triogerio bazės junginių **4a–4e** sintezė

Iš pradžių reakcijos su paraformaldehidu metu 2-metil-4-nitroanilinas ciklizavosi ir susidarė nitrogrupių turintis Triogerio bazės junginys **4a**. Šis junginys per kitą reakciją buvo redukuotas elementine geležimi. Gautas aminogrupių turintis

TB junginys **4b**. Junginiai **4c**–**4e** buvo susintetinti iš **4b**, vykstant jo kondensacijai su atitinkamu aldehidu (difenil-, di-*p*-tolil- arba di(4-metoksi)fenilacetaldehidu) THF virimo temperatūroje, katalizuojant kamparo-10-sulfonine rūgštimi (CSA) (5 schema). TB darinių **4c**–**4e** struktūra buvo patvirtinta ^{1}H ir ^{13}C BMR spektrais ir elementine analize.

4.2. Terminės ir optinės savybės

DSC matavimai parodė, kad junginiai **4c** ir **4e** turi kristalinę ir amorfinę būsenas: šildant buvo pastebimas kristalų lydymasis (7 lent.). Tiriant medžiagą **4d**, kaip ir visas kitas medžiagas, antrojo kaitinimo ir vėsimo ciklo metu užfiksuota tik stiklėjimo temperatūra, o kristalinimasis nebuvo fiksuojamas.

Termogravimetrinės analizės metodu gauti duomenys rodo didelį junginių terminį stabilumą (7 lent.).

7 lentelė. Triogerio bazės junginių **4c**–**4e**, turinčių enamino pakaitų, terminės ir optinės (palyginti pateikti darinio **4b** duomenys) savybės

Junginys	T_m [°C][a]	T_g [°C][b]	T_{dec} [°C][c]	λ_{max}^{abs} [nm][d]	ε [$M^{-1}cm^{-1}$]
4b				220; 252	25 990;13 834
4c	363	167	399	341	529 280
4d	–	135	315	342	54 850
4e	229	176	396	261; 343	69 145; 55 918

[a] Nustatyta pagal DSC: kaitinimo greitis 10 K/min; N_2 atmosfera; antrasis ciklas. [b] Lydymosi temperatūra fiksuota tik per pirmąjį kaitinimą; junginys sustiklėjo vėsdamas iki kambario temperatūros 10 K/min greičiu. [c] Skilimo riba, nustatoma pagal TGA: kaitinimo greitis 10 K/min; N_2 atmosfera. [d] UV-Vis spektrai buvo išmatuoti iš 10^{-4} M THF tirpalų.

Junginių **4c**–**4e** UV-Vis absorbcijos spektrai, išmatuoti tetrahidrofurano tirpaluose (c = 10^{-4} mol/l, d = 1 mm) (7 lent.), rodo didžiulius batochrominius ir hiperchrominius poslinkius, palyginti su pradiniu diamino junginiu **4b**. Absorbciją 240–290 nm intervale ir jos maksimumą esant 261 nm, matomus junginio **4e** spektre, galėjo lemti n-σ* elektronų perėjimais prie deguonies atomo metoksipakaituose.

4.3. Fotoelektrinės savybės

Junginių **4c**–**4e** jonizacijos potencialas buvo išmatuotas fotoelektronų spektroskopijos ore metodu (8 lent.). Junginys **4e** turi mažiausią I_p (5,25 eV) ir todėl yra perspektyvus naudoti saulės elementuose: jonizacijos potencialas leidžia jį derinti su daugeliu šioje srityje naudojamų šviesą sugeriančių medžiagų.

Junginių **4c**–**4e** krūvininkų pernašos savybės buvo tiriamos kserografiniu lėkio trukmės metodu. Judrio parametrų vertės pateiktos 8 lentelėje. Gautos prastos kokybės **4c** ir **4d** grynųjų medžiagų plėvelės, todėl, siekiant gauti tolygius sluoksnius, buvo naudojamas ir mišinys su polikarbonatu (PC-Z) masės santykiu 1:1. Nepaisant to, **4c** sluoksnio kokybė vis tiek buvo nepakankama krūvininkų judriui įvertinti.

8 lentelė. Junginių **4c–4e** energijos lygmenų[a] ir krūvininkų judrio duomenys

Junginys	E_g^{opt} (eV) [b]	E_{HOMO} (eV)[c]	E_{LUMO} (eV)[d]	I_p (eV)[e]	μ_0, cm^2/Vs[f]	μ (6,4·10^5 V/cm), cm^2/Vs[g]
4c	2,80	4,98	2,18	5,54	_[h]	_[h]
4d	2,80	4,84	2,04	5,44	4·10^{-6}[i]	1,5·10^{-5}[i], ~10^{-3}[h], [j]
4e	2,80	4,87	2,07	5,25	2,1·10^{-4}	3,35·10^{-4}

[a] CV matavimai atlikti su stiklo elektrodu dichlormetano tirpaluose, naudojant 0,1 M tetrabutilamonio heksafluorfosfatą kaip elektrolitą ir $Ag/AgNO_3$ kaip palyginamąjį elektrodą. Kiekvienas matavimas buvo kalibruotas naudojant feroceną (Fc). Potencialai apskaičiuoti plg. su Fc^+/Fc. [b] Optinės draustinės juostos E_g^{opt} apskaičiuotos iš tirpalų absorbcijos spektrų. [c] Konversijos koeficientai: ferocenas DCM-SCE: 0,46 [162], SCE-SHE: 0,244 [163], SHE-vakuumas: 4,43 [164]. [d] E_{LUMO} apskaičiuota pagal lygtį $E_{LUMO} = I_p - E_g^{otp}$. [e] Kietosios būsenos junginių jonizacijos potencialas (I_p) buvo matuojamas fotoemisijos ore metodu iš plėvelių. [f] Dreifinio judrio vertė esant nuliniam lauko stipriui. [g] Judrio vertė, kai lauko stipris yra 6,4·10^5 V cm^{-1}. [h] Nepavyko gauti matavimams tinkamo sluoksnio. [i] Junginio **4d** judrio vertės buvo išmatuotos iš jo ir PC-Z mišinio (1:1). [j] Rezultatai gauti taikant tik integravimo metodą.

4.4. Junginių išbandymas perovskitiniuose saulės elementuose

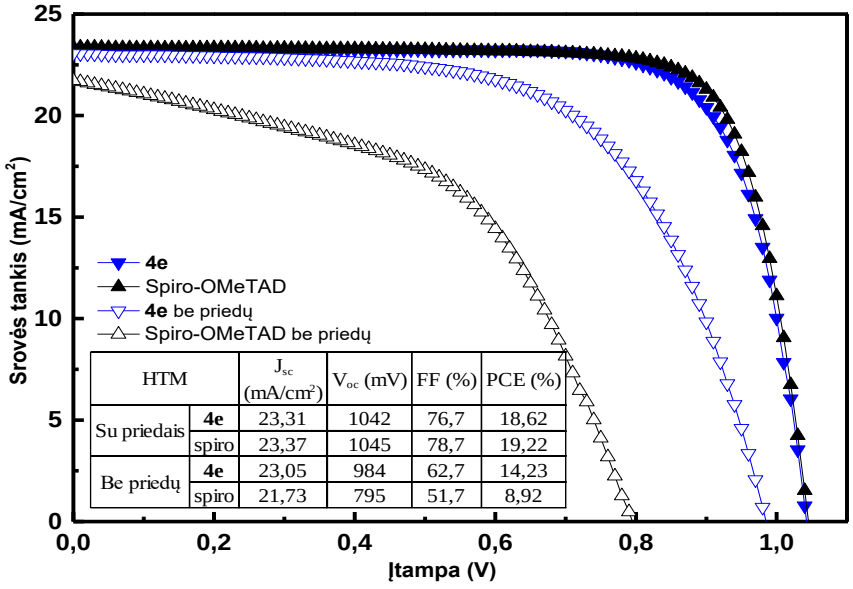

HTM		J_{sc} (mA/cm^2)	V_{oc} (mV)	FF (%)	PCE (%)
Su priedais	**4e**	23,31	1042	76,7	18,62
	spiro	23,37	1045	78,7	19,22
Be priedų	**4e**	23,05	984	62,7	14,23
	spiro	21,73	795	51,7	8,92

9 pav. Geriausiai veikiančių perovskitinių saulės elementų, kuriuose kaip skylių pernašos medžiagos naudojami junginiai **4e** ir *spiro*-OMeTAD, charakteristikos

Visi trys junginiai **4c–4e** buvo išbandyti kaip HTM optimizuotos architektūros perovskito saulės elementuose, kuriuos sudaro FTO, TiO_2 blokuojantis sluoksnis, mezoporinis TiO_2, amorfinis SnO_2, perovskitas, HTM, Au. Kaip šviesą sugeriantis sluoksnis buvo naudojamas mišraus $[(FAPbI_3)_{0,87}(MAPbBr_3)_{0,13}]_{0,92}(CsPbI_3)_{0,08}$ perovskito sluoksnis (9 pav.). Kaip tikėtasi, įrenginiai su junginiu **4e** buvo geriausi iš

trijų, jų energijos konversijos efektyvumas siekė 18,62 %. Pažymėtina, kad, tiriant priedų neturinčios kompozicijos perovskitinius saulės elementus, įrenginių su junginiais **4c** ir **4e** rezultatai buvo geresni nei įrenginių su *spiro*-OMeTAD. Šie įrenginiai taip pat generavo didesnę trumpojo jungimo srovę (J_{sc}) ir užpildos faktorių (*FF*).

Efektyviausių PSC su **4e** ir *spiro*-OMeTAD stabilumo tyrimas parodė, kad įrenginiai su **4e** po 700 valandų išlaikė >90 % pradinio efektyvumo, o įrenginių su *spiro*-OMeTAD efektyvumas sumažėjo iki 65 %.

5. Triogerio bazės karkasą turintys dažikliai įjautrintiems saulės elementams

Tarp tobulėjančių fotovoltinių technologijų kaip vienos perspektyviausių energijos gavimo įrenginių minimos dažikliais įjautrintos saulės celės (DSSC), kurios sulaukia nemažai dėmesio dar nuo Ru pagrindu veikiančių fotojautriklių išradimo [200, 201]. Įspūdingas 12,5 % celių efektyvumas, pasiektas su nauju bemetaliu alkoksisililkarbazolo dažikliu ADEKA-1, parodė, kad bemetaliai dažikliai gali būti perspektyvūs kaip celių jautrikliai norint pagaminti didelio našumo DSSC [207]. Įjautrinamųjų dažiklių kūrimas yra vienas iš svarbiausių būdų padidinti DSSC fotovoltinių prietaisų efektyvumą ir ilgaamžiškumą.

Pastebėta, kad dauguma jautriklių turi donoro-π-akceptoriaus (D-π-A) struktūras, kurios leidžia pasiekti efektyvų šviesos indukuojamą intramolekulinį krūvio perdavimą molekulėje [208–210]. Vis dėlto vienos 1D-π-1A sistemos dažiklis dažnai turi strypo formos struktūrą, kuri gali sukelti nepageidaujamą dažiklio agregaciją ir krūvio rekombinaciją [211]. Dažikliai, turintys dvi ar keletą inkarinių grupių, turi unikalų pranašumą, leidžiantį stipriau prisikabinti prie TiO_2 paviršiaus, taip pat pasižymi šviesos absorbcijos poslinkiu į raudonąją spektro pusę, efektyviu krūvininkų perdavimu [204, 213] ir fotosrovės generavimu [204, 214]. Vis dėlto buvo pastebėta, kad jei D-(π-A)$_2$ architektūros dažiklio molekulė yra strypo formos, tai gali sukelti nepageidaujamą dažiklių agregaciją, vykstančią dėl karboksirūgščių fragmentų, neprisitvirtinusių prie TiO_2 paviršiaus [217]. Šią problemą galima išspręsti suprojektavus molekulę su kampo formos molekuliniu karkasu, neleidžiančiu įgauti nepageidaujamos formos.

Šis skyrius skirtas bemetalių dažiklių **5A–5C** (10 pav.), turinčių Triogerio bazės karkasą su trifenilamino donorinėmis grupėmis ir akceptorines „inkaro“ funkciją atliekančias rodanino-3-acto rūgšties grupes, sintezei ir jų savybių tyrimui. Siekta ištirti šių junginių dvigubojo prisikabinimo prie TiO_2 substrato galimybes. Palyginimui buvo susintetinti dažiklių analogai **5D–5F**, turintys vieną inkarinę grupę.

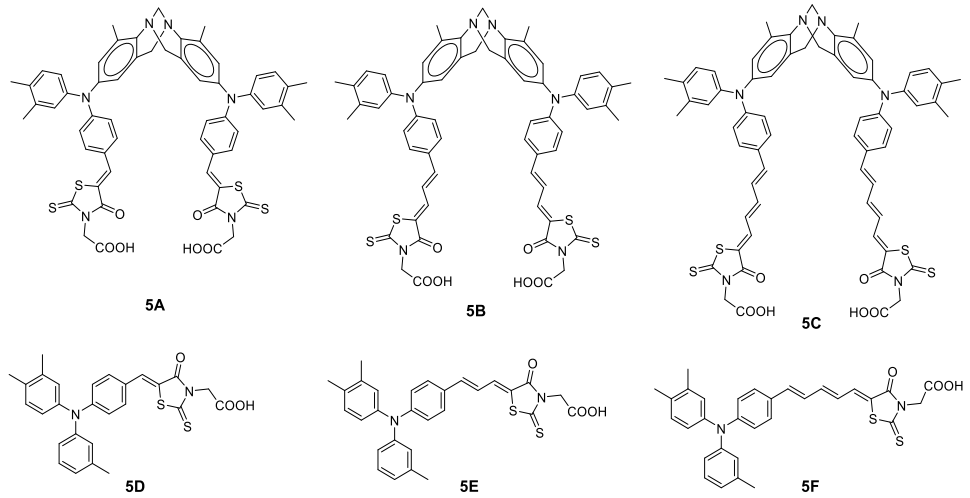

10 pav. Susintetintų ir ištirtų dažiklių **5A–5F** molekulinės formulės

5.1. Naujų Triogerio bazės karkasą turinčių dažiklių sintezė

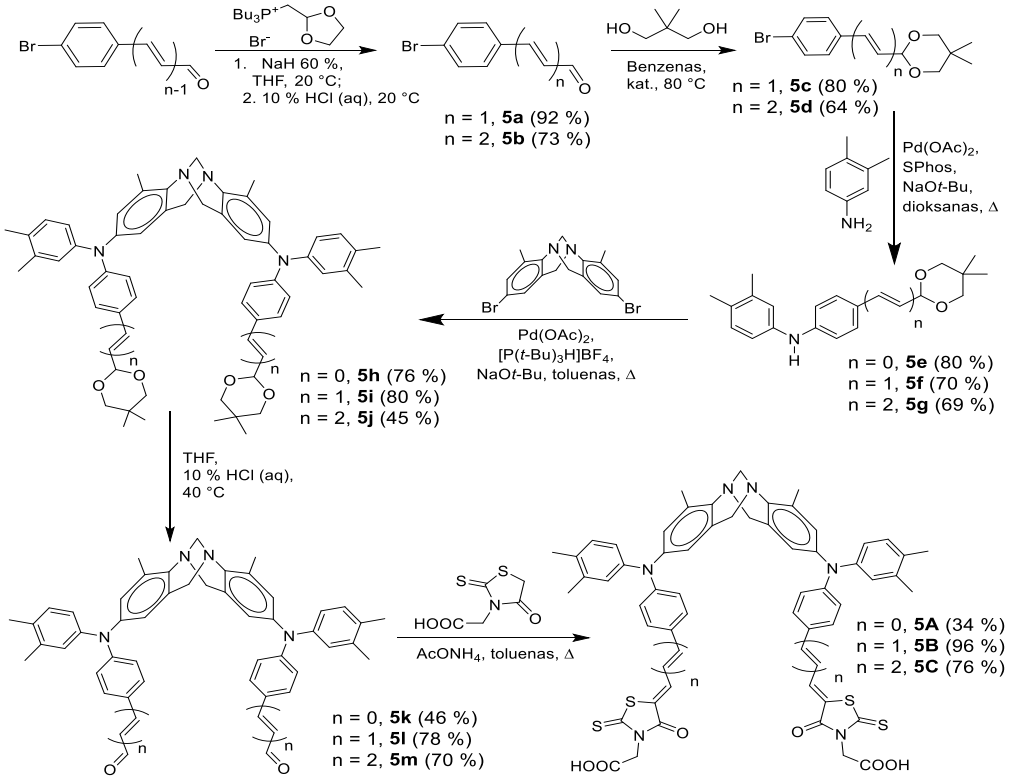

6 schema. Dvi inkarines grupes turinčių dažiklių su TB karkasu **5A–5C** sintezė

Naujų bemetalių dažiklių **5A–5C**, turinčių Triogerio bazės karkasą, sintezė atlikta pagal šešių pakopų metodiką (6 schema). Iš pradžių buvo atlikta Hornerio ir Wittigo kondensacija ir taip padidinta polivinilo grandinė (nuo n = 0 iki n = 2). Atliekant paladžio katalizuojamą kryžminę reakciją tarp užblokuotų aldehidų **5c**, **5d** ir 3,4-dimetilanilino gauti produktai su 70–80 % išeiga. Gautieji difenilaminai **5e**, **5f** ir **5g** dalyvavo reakcijoje su bromintu Triogerio bazės dariniu **1'**, naudojant paladžio(II) acetatą, tri-tret-butilfosfonio tetrafluorboratą ir natrio tret-butoksidą. Taip gauti TB karkasą turintys tarpiniai produktai **5h**, **5i** ir **5j**. Pašalinus apsauginę grupę, gauti dialdehidai **5k–5m**. Juos kondensuojant su rodanino-3-acto rūgštimi gauti tiksliniai dažikliai **5A**, **5B** ir **5C**.

Palyginimui analogiškai buvo susintetinti dažikliai **5D**, **5E** ir **5F**, turintys vieną inkarinę grupę. Iš pradžių pagal žinomą metodiką buvo susintetintas pirmtakas **5n** [220]. Kitame etape buvo gautas difenilaminas, turintis apsaugotą aldehido grupę. Jis buvo sujungtas su 3-jodtoluenu, pasitelkiant paladžiu katalizuojamą Buchwaldo ir Hartwigo C–N prijungimo reakciją. Taip gautas aldehidas **5o**. Šis aldehidas kondensuotas Knoevenagelio metodu su rodanino-3-acto rūgštimi ledinėje acto rūgštyje ir gautas dažiklis **5D**. Atitinkamai iš aldehido **5o** Hornerio ir Wittigo kondensacijos su tributil(1,3-dioksolan-2-ilmetil)fosfonio bromidu metu pavyko gauti aldehidą **5d** su 78 % išeiga. Papildomas vinilinimas ir vėliau vykdyta Knoevenagelio kondensacija leido gauti dažiklius **5E** ir **5F** (7 schema).

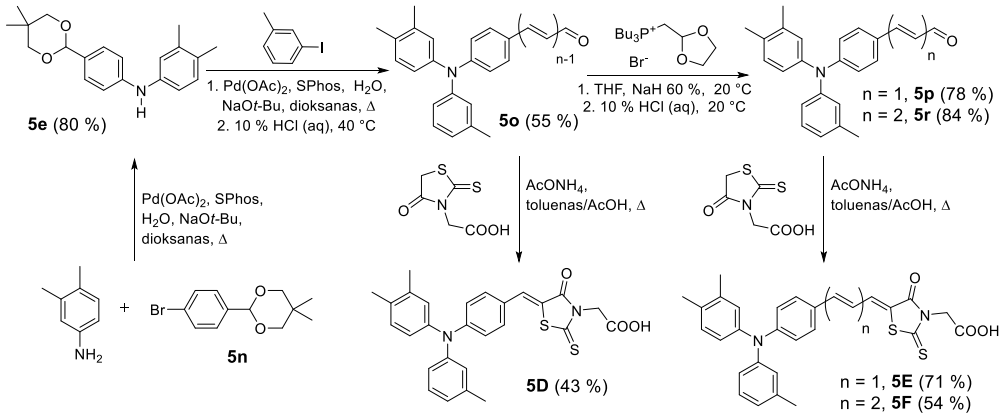

7 schema. Dažiklių **5D–5F**, turinčių vieną inkarinę grupę, sintezė

TB dažiklių struktūra buvo patvirtinta ^{1}H ir ^{13}C BMR spektroskopija, IR spektrais ir elementine analize.

5.2. Optinės savybės

Norint sužinoti, kokią įtaką polimetinų grandinių skaičius ir jų grandinės ilgis turi tiriamų dažiklių optinėms savybėms, buvo atlikti UV-Vis tyrimai su dvi inkarines grupes turinčiais dažikliais **5A–5C** ir jų monoakceptoriniais analogais **5D–3F**.

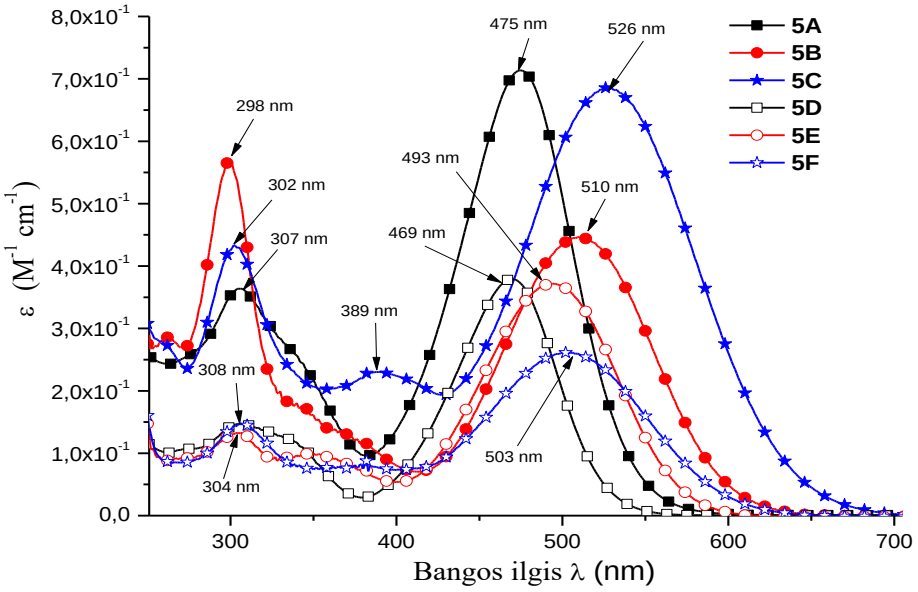

11 pav. Dažiklių **5A**–**5F** 10^{-4} M DMSO tirpaluose absorbcijos spektrai

Kaip matoma iš 11 pav., ir diinkarinių organinių dažiklių **5A**–**5C**, turinčių TB karkasą, ir monoinkarinių dažiklių **5D**–**5F** absorbcijos spektrai rodo dvi absorbcijos juostas, atitinkamai maždaug 270–350 nm ir 400–670 nm intervale. Intensyvios absorbcijos juostos regimosios šviesos intervale gali būti priskirtos intramolekuliniam krūvio perdavimui tarp trifenilamino donorinio ir akceptorinio rodanino-3-acto rūgšties fragmentų esant sužadintajai būsenai. Lyginant diinkarinių dažiklių **5A**–**5C** ir jų monoinkarinių analogų **5D**–**5F** optines savybes aiškiai matomi du efektai. Pirma, TB karkaso pagrindu pagaminti organiniai dažikliai, išskyrus **5B**, turi maždaug du kartus didesnius ekstinkcijos koeficientus (11 pav.), palyginti su monoinkariniais dažikliais. Antra, tik nereikšmingas, jei apskritai egzistuojantis, batochrominis poslinkis, pastebimas tarp diinkarinių dažiklių, palyginti su monoinkariniais, rodo, kad tarp dviejų chromoforų, esančių diinkariniuose dažikliuose, nėra struktūrinės nesužadintosios būsenos sąveikos. Tačiau dažiklių **5B** ir **5C** intramolekulinio krūvio perdavimo absorbcijos juostas lyginant su dažiklių **5E** ir **5F** juostomis aiškiai matoma ši sąveika. Tikriausiai taip yra dėl polimetinų grandinių prailginimo, kuris suteikia šioms dalims lankstumą ir tokiu būdu leidžia atsirasti tiesioginei sąveikai tarp dviejų inkarinių grupių TB karkasą turinčiuose dažikliuose.

5.3. Fotoelektrinės savybės

Siekiant termodinamiškai įvertinti galimus elektronų perdavimo iš sužadinto dažiklio molekulės į TiO_2 procesus, atlikti ciklinės voltamperometrijos (CV) matavimai (9 lent.). Dažiklių LUMO energijos lygmenys viršija TiO_2 (–4 eV) [159, 221] laidumo juostos ribą. Tai užtikrina palankią elektronų pernašą iš sužadintosios būsenos dažiklio į puslaidininkio laidumo juostą. Akivaizdus visų dažiklių HOMO lygmenų didesnis neigiamumas, palyginti su jodido ar trijodido potencialu (4,97 eV;

–0,54 V plg. su SHE) [222]. Vadinasi, termodinaminė varomoji jėga oksiduotų dažiklių regeneracijai yra pakankama.

9 lentelė. Fotoelektrinės dažiklių savybės

Dažiklis	$E_{0\text{–}0}$ (eV)[b]	$E_g^{\text{opt-film}}$ (eV)[c]	E_{HOMO} (eV)[a]	E_{LUMO} (eV)[a]	I_p (eV)[d]	EA (eV)[e]
5A	2,35	2,07	–5,62	–3,36	5,48	–3,41
5B	2,23	1,80	–5,58	–3,76	5,54	–3,74
5C	1,98	1,68	–5,51	–3,65	5,45	–3,77
5D	2,38	2,07	–5,70	–3,27	5,43	–3,36
5E	2,22	1,84	–5,64	–3,42	5,38	–3,54
5F	2,03	1,73	–5,59	–3,47	5,45	–3,72

CV matavimai atlikti su stiklo elektrodu dichlormetano tirpaluose, naudojant 0,1 M tetrabutilamonio heksafluorfosfatą kaip elektrolitą ir $Ag/AgNO_3$ kaip palyginamąjį elektrodą. Kiekvienas matavimas buvo kalibruotas naudojant feroceną (Fc). Potencialai apskaičiuoti plg. su Fc^+/Fc. Konversijos koeficientai: ferocenas DCM-SCE: 0,46 [162], SCE-SHE: 0,244 [163], SHE-vakuumas: 4,43 [164]. [a] E_{LUMO} apskaičiuota pagal lygtį $E_{LUMO} = I_p - E_g^{\text{otp-film}}$. [b] $E_{0\text{–}0} = 1240/\lambda$ sankirta. [c] Optinės draustinės juostos ($E_g^{opt\text{-}film}$) apskaičiuotos iš elektroninės absorbcijos spektrų plonose plėvelėse. [d] Kietosios būsenos junginių jonizacijos potencialas (I_p) buvo matuojamas fotoemisijos ore metodu iš plėvelių. [e] Elektronų gimiringumas (EA) apskaičiuotas pagal lygtį $EA = I_p - E_g^{\text{opt-film}}$.

Jonizacijos potencialas (I_p) buvo išmatuotas elektronų fotoemisijos ore metodu. Rezultatai pateikti 9 lentelėje. Išmatuotos I_p vertės yra šiek tiek mažesnės už HOMO lygmenis, nustatytus CV eksperimentais. Skirtumus galėjo lemti skirtingi matavimo metodai ir sąlygos (taikant CV metodą naudojami tirpalai, o fotoemisijos metodą – kietosios būsenos plėvelės).

5.4. Kvantinės chemijos skaičiavimai

Buvo atlikti TB fragmentą turinčių diinkarinių dažiklių kompiuterinio skaičiavimo tyrimai. Ištirti abu galimi TB dažiklio asocijuotos „uždaros“ ir „atviros“ – neasocijuotos formos rotamerai (12 pav.).

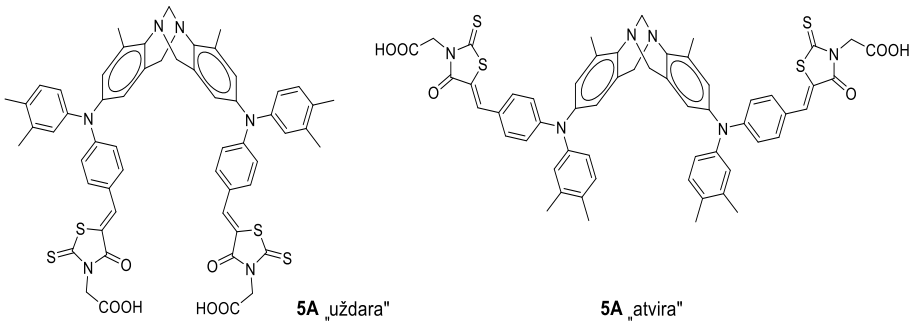

12 pav. Galimi TB dažiklio **5A** geometriniai rotamerai: „uždara“ ir „atvira“ forma

Šių junginių molekulinės struktūros buvo optimizuotos B3LYP/def2-SVP metodu. Stabilesnės („uždaros“) formos rodanino žiedas yra šiek tiek pasisukęs fenilgrupės, esančios trifenilamine, atžvilgiu ir tai rodo, kad tarp karboksirūgščių fragmentų gali būti vandenilio ryšių. Tai gali kliudyti veiksmingai abiejų inkaravimo grupių sąveikai su TiO_2. Optimizuotų „uždaros“ ir „atviros“ formų rotamerų, tarp kurių energijos skirtumas yra 14,9–16,4 kcal/mol, struktūros ir elektronų orbitalės pateiktos 10 lentelėje.

10 lentelė. Dvigubojo dažiklio **5A** optimizuotos struktūros ir elektronų orbitalės

Dažiklis	HOMO	LUMO
5A „uždara“	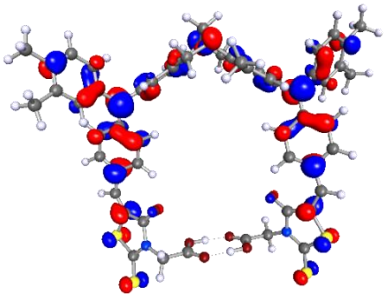	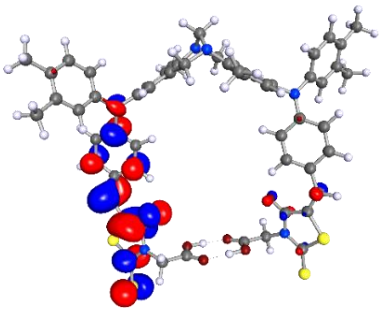
5A „atvira“	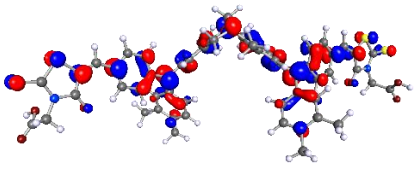	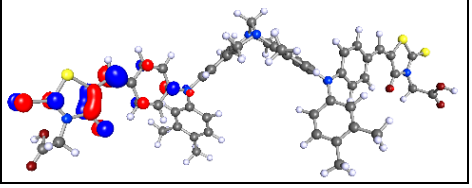

HOMO ir LUMO orbitalių išsidėstymas pateiktas 10 lentelėje. Pastebima, kad HOMO orbitalės yra pasklidusios per visą molekulę, šiek tiek pasislinkusios trifenilamino fragmentų link. LUMO orbitalės yra pasislinkusios rodanino fragmento link. Tai rodo dalinį HOMO ir LUMO krūvininkų pernašos pobūdį.

5.5. Dažikliais įjautrinti saulės elementai

Tiriamų dažiklių (**5A–5F**) fotovoltinis efektyvumas buvo įvertintas DSSC, naudojant jodido-trijodido elektrolitą, o gauti fotovoltiniai parametrai apibendrinti 11 lentelėje. Saulės celės, pagamintos naudojant dažiklį **5C** ir jo monoinkarinį analogą **5F**, turinčius ilgiausias polietino grandines, pasižymėjo platesne celės efektyvios sugerties juosta (400–700 nm), bet mažesnėmis sugerties vertėmis (apie 7 %), palyginti su kitais dažikliais (400–600 nm; 12–40 %), ir iš to kylančiomis mažesnėmis trumpojo jungimo srovės (J_{sc}) vertėmis (1,44 ir 1,12 mA/cm^2). Saulės celių, pagamintų su diinkariniais dažikliais, išskyrus **5C**, V_{oc} vertės buvo šiek tiek mažesnes nei tų, kurioms naudoti monoinkariniai dažikliai. Išanalizavus gautas optines savybes, galima daryti prielaidą, kad geriausi rezultatai buvo gauti naudojant dažiklį **5D**: užfiksuotas bendrasis konversijos efektyvumas (η), siekiantis 2,36 % (J_{sc} = 5,42 mA cm^{-2}, V_{oc} = 582 mV, FF = 0,75). Įdomu tai, kad dažikliuose **5A** ir **5B**

esančios papildomos akceptoriaus grupės neturėjo teigiamo poveikio prietaiso veikimui.

11 lentelė. Skirtingais dažikliais įjautrintų saulės elementų parametrai esant 100 mW·cm^{-2} AM1,5 G apšvietimui

Dažikliai	V_{oc} (mV)	J_{sc} (mA/cm^2)	*FF* (%)	η (%)
5A	548±3	4,30±0,06	75,9±1,7	1,79±0,05
5B	468±6	1,99±0,11	73,1±0,9	0,68±0,04
5C	460±0	1,44±0,04	74,9±0,2	0,50±0,02
5D	582±3	5,42±0,15	75,3±1,5	2,36±0,05
5E	482±3	2,52±0,13	75,2±0,7	0,91±0,06
5F	448±3	1,12±0,10	72,1±0,3	0,36±0,03
D35	775±10	11,17±0,05	73,5±1,2	6,35±0,03
N719	740±0	13,30±0,36	72,9±1,1	7,17±0,07

Apibendrinant šį skyrių galima konstatuoti, kad prailgintos polietino grandinės pasižymi lankstumu ir leidžia sąveikauti dviem chromoforams, o tai skatina šių Triogerio bazės dažiklių agregaciją ir mažina jų efektyvumą saulės elementuose.

6. Patobulinti TB karkasą turintys dažikliai įjautrintiems saulės elementams

Siekiant pagerinti anksčiau ištirtų dažiklių molekulinį dizainą, išvengiant lanksčios polietino grandinės trūkumų ir dėl jo kylančio akceptorinių grupių sukibimo, reikia rasti alternatyvų konjuguotąjį jungiamąjį fragmentą. Toks fragmentas turi būti standus, kad išspręstų lankstumo problemą ir galbūt suteiktų tam tikrą struktūrinį tūrį, taip sukurdamas erdvines kliūtis ir apribodamas akceptorinių grupių galimybę pasiekti vienai kitą. Šios struktūrinės modifikacijos turėtų padėti išspręsti agregatų susidarymo problemą ir kartu užtikrintų dviejų inkarinių grupių teikiamus privalumus, geresnį prisikabinimą prie titano dioksido sluoksnio ir galimai didesnį elektronų perdavimo efektyvumą. Jungiamaisiais fragmentais galėtų būti tiofeno junginiai, pasižymintys standumu ir naudingomis molekulinėmis savybėmis, suteikiamomis diinkariniams dažikliams. Jie pranoksta įprastą fenilgrupę arba kai kuriuos kitus jungiamuosius fragmentus [226]. Sudėtingesnis jungiamojo darinio variantas galėtų būti fenilhidrazono fragmentas, suteikiantis ilgesnę konjuguotąją sistemą ir papildomą struktūrinį tūrį.

Šiame skyriuje aprašoma naujų patobulintos struktūros A-π-D-π-A ir D-π-A tipo dažiklių sintezė ir tyrimas, papildantis dvigubųjų dažiklių temą.

6.1. Triogerio bazės karkasą ir tiofeno ar hidrazono fragmentą turinčių dažiklių sintezė

Abu tiofeno tarpinius fragmentus turintys junginiai, diinkarinis dažiklis **6f** ir jo analogas **6i**, buvo susintetinti pagal šešių reakcijos pakopų metodiką (8 schema).

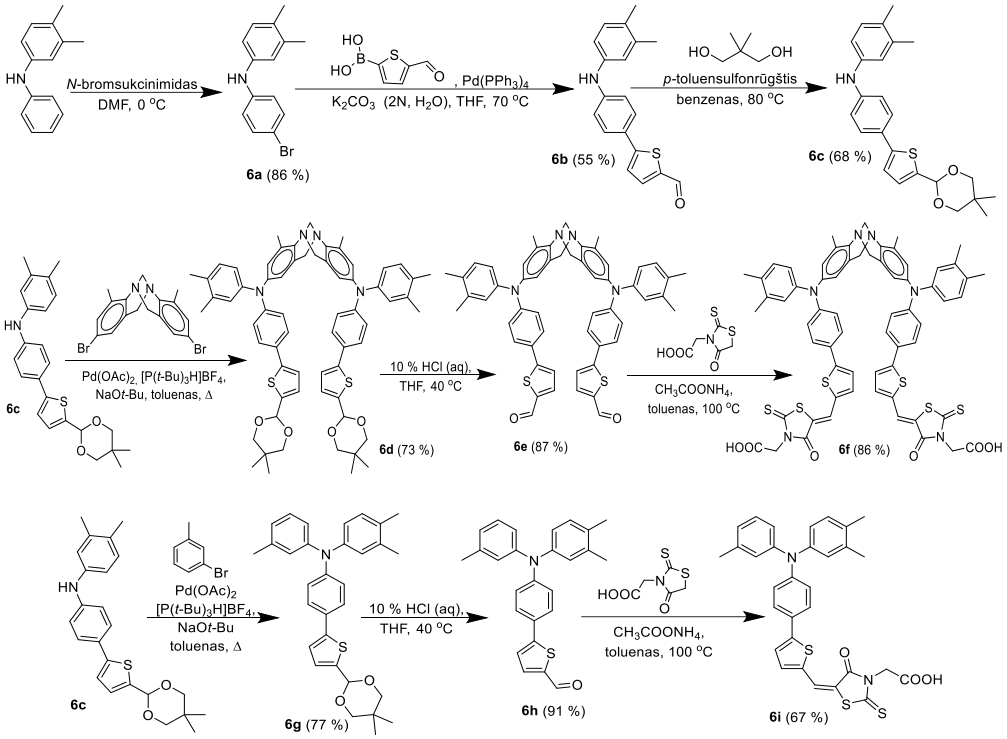

8 schema. Dažiklių su triofeno jungiamuoju fragmentu sintezė

Abiejų junginių sintezė prasideda sintetinant tuos pačius tarpinius junginius **6a**–**6c**. Jie vėliau prijungiami prie skirtingų aromatinių sistemų ir toliau naudojami atitinkamo dažiklio sintezei. Iš pradžių junginys **6a** buvo gautas iš 3,4-dimetil-*N*-fenilanilino brominimo reakcijoje su *N*-bromsukcinimidu. Šis junginys reagavo su (5-formiltiofen-2-il)boronine rūgštimi pagal Suzukio prijungimo metodiką, taip gautas aldehidas **6b**. Jis buvo toliau modifikuojamas blokuojant aktyviąją grupę *p*-toluensulfonine rūgštimi katalizuojama reakcija su 2,2-dimetil-1,3-propandioliu. Gautas produktas **6c** su 68 % išeiga. Difenilamino darinys **6c** reagavo su bromintu Triogerio bazės junginiu **1'** arba su 3-jodtoluenu, dalyvaujant paladžio (II) acetatui, tri-tret-butilfosfonio tetrafluorboratui ir natrio tret-butoksidui. Taip gauti tarpiniai produktai **6d** ir **6g**. Pašalinus apsauginę grupę, gauti aldehidai **6e** ir **6h**. Jie buvo kondensuoti su rodanino-3-acto rūgštimi. Taip susidarė TB karkasas ir tiofeniniai jungiamuosius fragmentus turintys dažikliai **6f** ir **6i**.

Jautrikliai, turintys fenilhidrazono jungiamuosius fragmentus, buvo susintetinti modifikuojant jau ištirtus aldehidus **5k** ir **5o** (9 schema). Jų reakcija su fenilhidrazinu leido gauti fenilhidrazonus **6j** ir **6n**. Šie junginiai buvo naudojami arilinimo reakcijose su **5n** (2-(4-bromfenil)-5,5-dimetil-1,3-dioksanu). Taip susintetinti hidrazonai su apsaugotomis aldehido funkcinėmis grupėmis, atitinkamai **6k** ir **6o**. Pašalinus apsaugines grupes, buvo gauti aldehido junginiai **6l** ir **6p**. Galiausiai vykstant aldehidų **6d** ir **6p** kondensacijai su rodanino-3-acto rūgštimi gauti tiksliniai dažikliai **6m** ir **6r**.

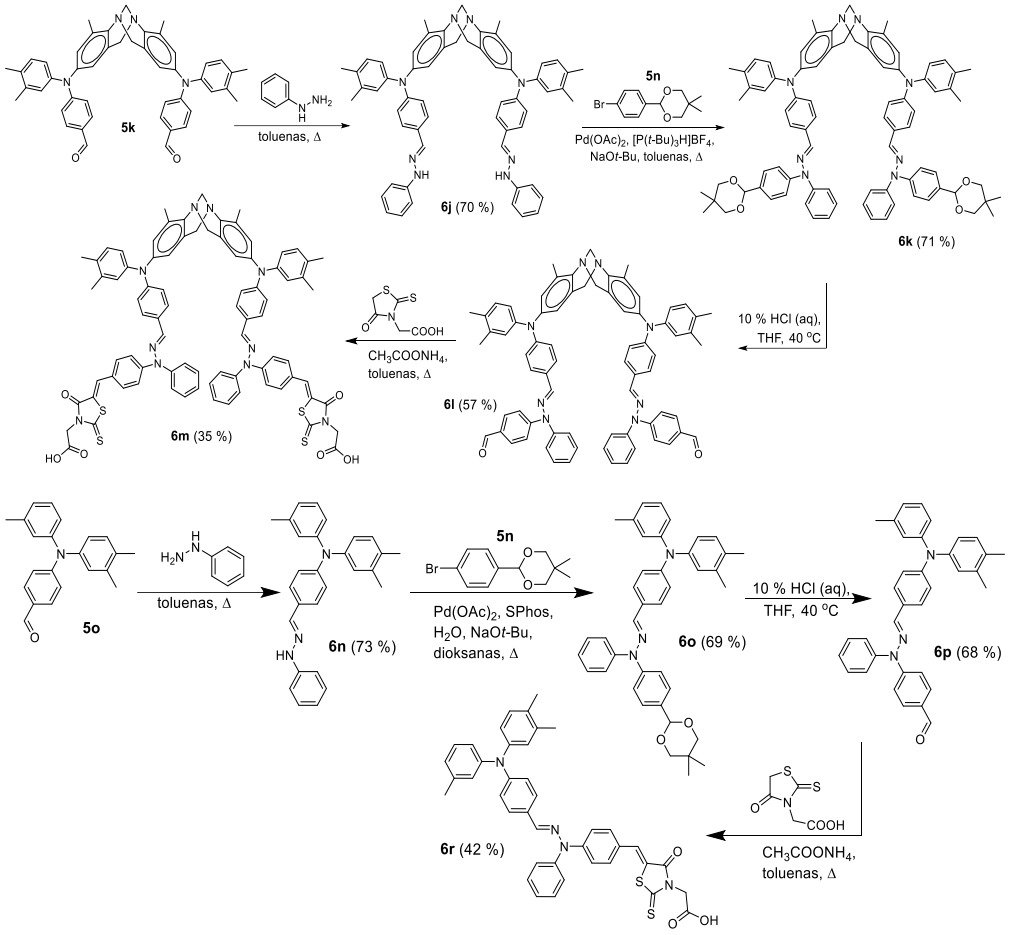

9 schema. Dažiklių su fenilhidrazono jungiamuoju fragmentu sintezė

TB dažiklių **6f**, **6i**, **6m** ir **6r** struktūra buvo patvirtinta ^{1}H ir ^{13}C BMR spektroskopija ir elementinės analizės metodu.

6.2. Optinės savybės

Norint ištirti ir įvertinti tiofeno ir hidrazono fragmentų, įterptų į molekulinę struktūrą, poveikį ir naujų dažiklių optines savybes, buvo atlikti diinkarinių dažiklių **6f** ir **6m** bei jų monoinkarinių analogų **6i** ir **6r** UV-Vis absorbcijos matavimai (13 pav.).

Kaip matoma 13 pav., abiejų diinkarinių TB karkasą turinčių organinių dažiklių **6f** bei **6m** ir monoinkarinių dažiklių **6i** bei **6r** absorbcijos spektrai rodo dvi skirtingas absorbcijos juostas, atitinkamai maždaug 270–340 nm ir 400–650 nm intervaluose. UV zonos juostos rodo didesnę absorbciją ilgesnių bangų pusėje, atitinkančią konjuguotosios sistemos π–π* elektronų perėjimus.

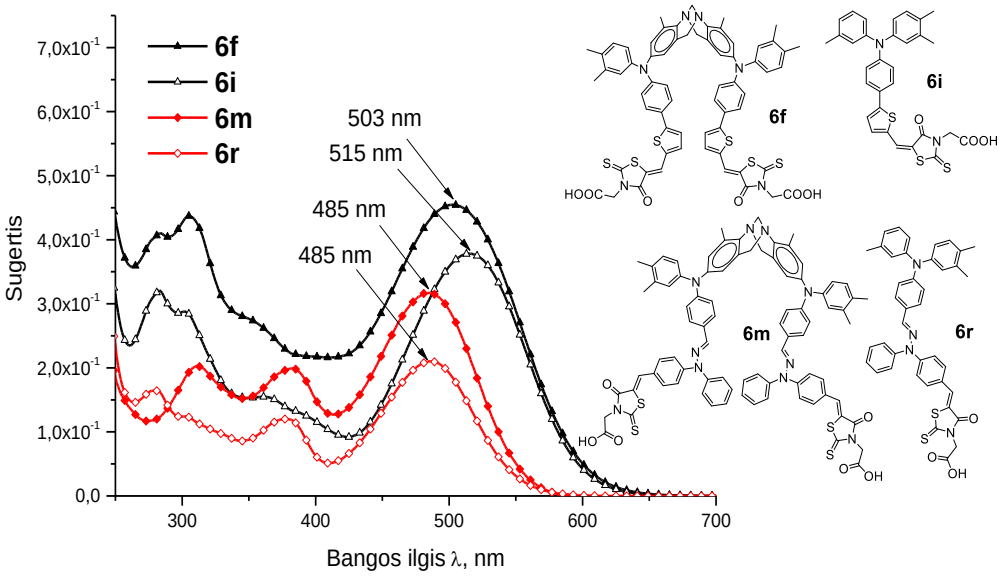

13 pav. Dažiklių **6f**, **6i**, **6m** ir **6r** 10^{-4} M DMSO tirpaluose sugerties spektrai

Įdomu tai, kad jautriklis **6m** ir jam gimininga monoinkarinis junginys **6r** turi silpną, bet aiškią papildomą absorbcijos juostą ties maždaug 385 nm, greičiausiai priklausančią fenilhidrazono fragmentui, esančiam šiuose dažikliuose. Intensyvios absorbcijos juostos regimosios šviesos intervale gali būti priskirtos intramolekuliniam krūvio perdavimui tarp trifenilamino donoro ir elektronus priimančio rodanino-3-acto rūgšties fragmento esant sužadintajai būsenai. Iš dažiklių **6f**, **6i**, **6m** ir **6r** absorbcijos spektrų aiškiai matyti, kad tiofeno jungiamąjį fragmentą turintys junginiai pasižymi labiau į raudonąją spektro dalį nutolusia šviesos sugertimi, besiskiriančia 18 ir 30 nm (atitinkamai di- ir monodažikliuose), palyginti su fenilhidrazono dažikliais. Vis dėlto lyginant dažiklių **6f** ir **6i** absorbcijos juostas aiškiai matyti, kad egzistuoja sugerties maksimumo poslinkis, lygus 12 nm, leidžiantis spręsti apie galimą dviejų chromoforų sąveiką šiame diinkariniame dažiklyje. Iš to galima daryti išvadą, kad tiofeno jungiamasis vienetas neapsaugo nuo dviejų molekulės akceptorių nepageidaujamos tarpusavio sąveikos. Toks poslinkis nebuvo pastebėtas tarp dažiklio **6m** ir jo monoanalogo **6r**. Tai rodo, kad fenilhidrazono intarpas suteikia norimas savybes ir trukdo sąveikai tarp dviejų chromoforų šiame dažiklyje. Galima konstatuoti, kad šie Triogerio bazės junginiai yra tinkami naudoti kaip dažikliai įjautrintiems saulės elementams.

7. Spinduoliai, turintys tetrafeniletenilo fragmentų ir Triogerio bazės karkasą

7.1. Naujų Triogerio bazės fragmentą turinčių spinduolių sintezė

Nauji Triogerio bazės junginiai, turintys tetrafeniletenilo (TPE) fragmentų, buvo susintetinti pasitelkiant Suzukio ir Miyauros arba Buchwaldo ir Hartwigo prijungimo reakcijas.

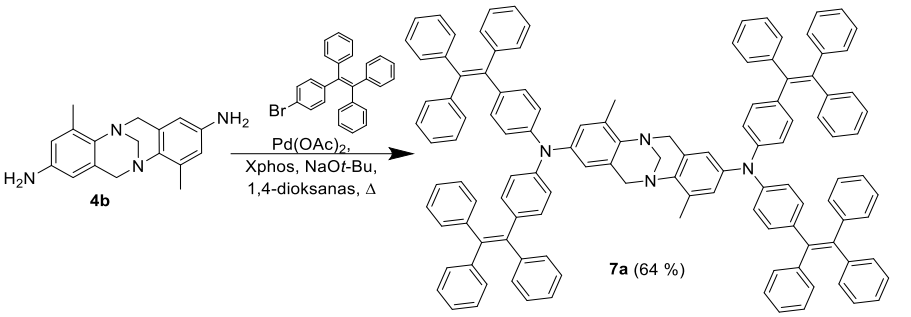

10 schema. Junginio **7a** sintezė

Junginys **7a**, kaip struktūriškai artimiausias anksčiau ištirtam junginiui **2b**, buvo susintetintas iš aminogrupių turinčio TB darinio **4b**, šiam reaguojant su bromintu TPE Buchwaldo ir Hartwigo prijungimo reakcijos sąlygomis (10 schema).

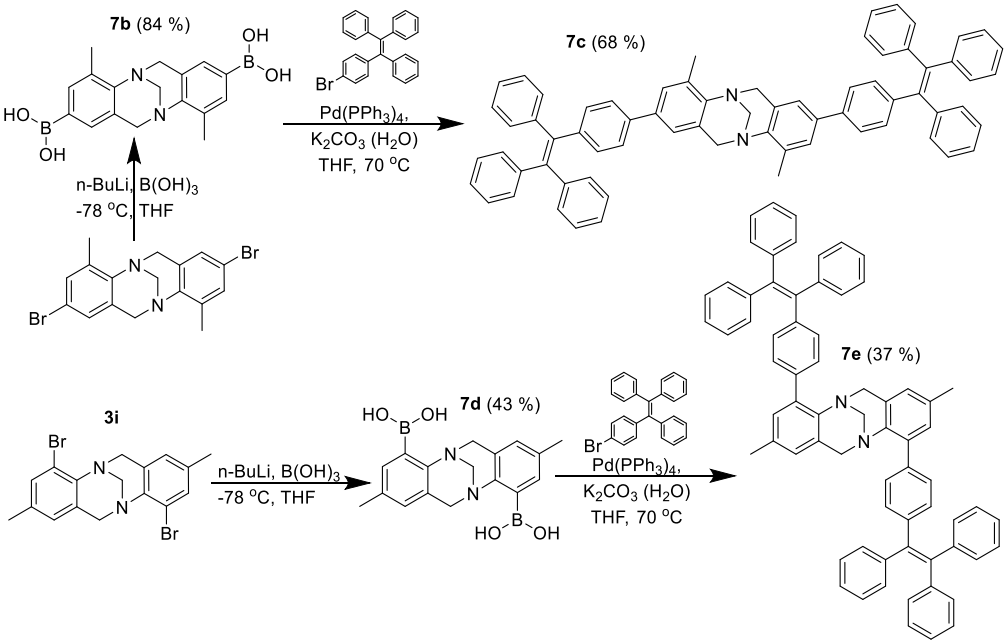

11 schema. Junginių **7b–7e** sintezė

Junginiai **7c** ir **7e**, turintys du TPE fragmentus, tiesiogiai sujungtus su Triogerio bazės karkasu, buvo susintetinti iš boroninę grupę turinčių TB junginių **7b** ir **7d**, šiems reaguojant pagal Suzukio ir Miyauros prijungimo metodiką su 1-(4-bromfenil)-1,2,2-trifenileteniu (11 schema).

Keturis TPE pakaitus turintis junginys **7g** buvo susintetintas per tarpinį boroninę grupę turintį TPE darinį **7f**. Šis vykdant Suzukio ir Miyauros prijungimo reakciją prijungtas prie bromu pakeisto TB karkaso **3j** (12 schema).

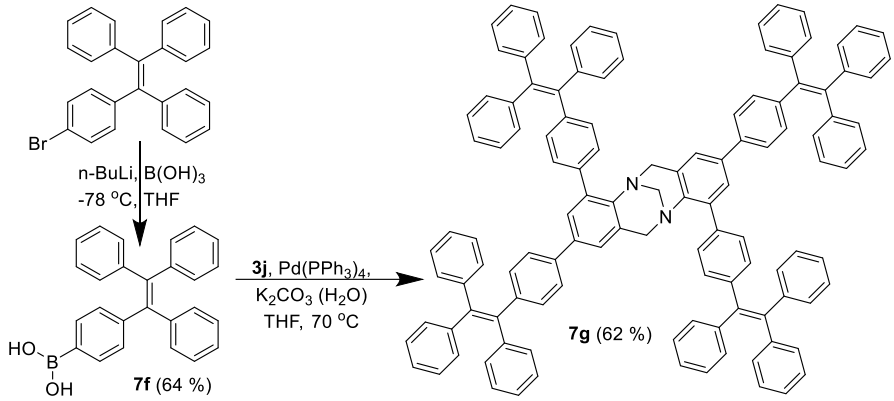

12 schema. Junginių **7f–7g** sintezė

Naujų Triogerio bazės darinių struktūra buvo patvirtinta ^{1}H ir ^{13}C BMR spektrais ir elementinės analizės metodu.

7.2. Terminės ir optinės savybės

Junginių **7a**, **7c**, **7e** ir **7g** DSC matavimai parodė, kad tiriami TB dariniai **7c** ir **7g** yra amorfiniai, o junginiai **7a** ir **7e** gali būti tiek kristalinės, tiek amorfinės būsenos (12 lent.). Junginio **7a** antrojo kaitinimo (aušinimo) ciklo metu kristalizacija nevyksta ir registruojama tik stiklėjimo temperatūra (T_g).

Junginių **7a**, **7c**, **7e** ir **7g** termogravimetrinė analizė parodė aukštą skilimo temperatūrą (12 lent.). Apskritai visi šios serijos junginiai pasižymi puikiu terminiu stabilumu – jų skilimo temperatūra viršija 400 °C. Tai leidžia patvirtinti, kad šių junginių terminis stabilumas nebus jų praktinį pritaikymą optoelektroniniuose įrenginiuose ribojantis veiksnys.

Buvo išmatuoti Triogerio bazės darinių **7a**, **7c**, **7e** ir **7g** UV-Vis absorbcijos spektrai THF tirpale (14 pav.) bei emisijos spektrai iš THF tirpalų ir grynosios medžiagos plėvelių (15 pav., 12 lent.).

12 lentelė. TB darinių terminės ir optinės savybės

Jung.	T_m [°C]	T_g [°C][b]	T_{dec} [°C][c]	λ_{max}^{abs} [nm][d]	ε [$M^{-1}cm^{-1}$]	THF tirpalas		Medžiagos plėvelė	
						λ_F (nm)[e]	Φ_F (%)[f]	λ_F (nm)[e]	Φ_F (%)[f]
7a	229[a]	187	455	304;368	73 518;52 599	511	0,03	526	4,2
7c	–	170	430	327	46 275	507	0,06	497	27,84
7e	338	325	413	322	36 693	509	0,07	494	17,05
7g	–	208	459	327	81 514	507	0,19	500	22,15

[a] Lydymosi temperatūra užfiksuota tik pirmojo kaitinimo metu; 10 K/min. [b] Nustatyta pagal DSC: kaitinimo greitis 10 K/min; N_2 atmosfera. [c] Skilimo pradžia (5 % masės nuostolis) nustatoma TGA: kaitinimo greitis, 10 K/min; N_2 atmosfera. [d] UV-Vis spektrai buvo užrašyti iš 10^{-4} M THF tirpalo. [e] Fluorescencijos maksimumai THF tirpale, grynosios medžiagos plėvelėje. [f] Fluorescencijos kvantinė išeiga THF tirpale, grynojoje plėvelėje.

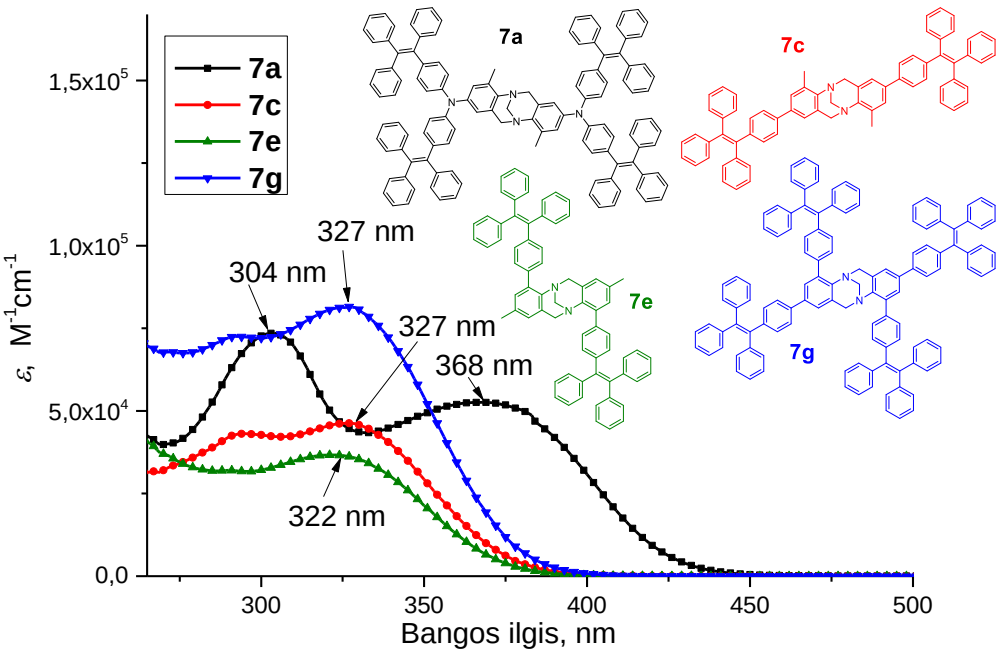

14 pav. Junginių **7a, 7c, 7e** ir **7g** UV-Vis spektrai THF tirpaluose ($c = 10^{-4}$ M)

UV-Vis absorbcijos spektrai rodo, kad junginio **7a** spektre yra du absorbcijos maksimumai, turintys didžiausias reikšmes esant 304 nm ir 368 nm. Šis darinys turi į ilgesnių bangų sritį labiausiai nutolusį sugerties maksimumą šioje junginių grupėje. Tai galimai rodo, kad jis pasižymi didžiausia konjuguotąja π-sistema. Junginys **7e** turi maksimalią sugerties reikšmę esant 322 nm, 5 nm hipsochrominį poslinkį, lyginant su junginiais **7c** ir **7g**. Šį reiškinį gali lemti sąveika ir erdviniai trikdžiai tarp TPE fragmento ir TB karkaso endoprotonų. Įdomu, kad darinio **7g** sugertis atrodo kaip junginių **7c** ir **7e** sugerčių suma tiek pagal absorbcijos intensyvumą, tiek pagal bangos ilgius, nefiksuojant jokio batochrominio poslinkio. Tai rodo, kad šie fragmentai nesąveikauja kaip viena konjuguotoji π-sistema.

Junginių **7c**, **7e** ir **7g** fluorescencijos spektrai ir kvantinės išeigos rodo tipinį agregacijos indukuotos emisijos (AIE) poveikį: nors prastai švyti tirpaluose, emisija labai padidėja esant kietajai būsenai (12 lent.). Šis reiškinys pastebimas ir junginyje **7a**, tačiau jis nepasižymėjo gera šviesos emisija nei tirpale, nei plėvelėse. Pažymėtina, kad didžiausias skirtumas tarp emisijos maksimumų tirpale ir esant kietajai būsenai yra matomas junginyje **7e**. Pagal tai, bei sumažėjusį kvantinį našumą, galima spręsti apie nepalankų agregatų susidarymą. Tai galima paaiškinti remiantis junginio **7e** struktūra: TPE fragmentai yra prijungti prie V formos TB karkaso šonų (4,10-padėtyse), o ne galų, todėl jie yra orientuoti panašiai į lygiagrečias linijas, nukreiptas į priešingus šonus nuo Triogerio bazės karkaso. Šie fragmentai neperėmė TB karkaso galų suteikiamos orientacijos ir nesudarė reikšmingo kampo vienas kito atžvilgiu.

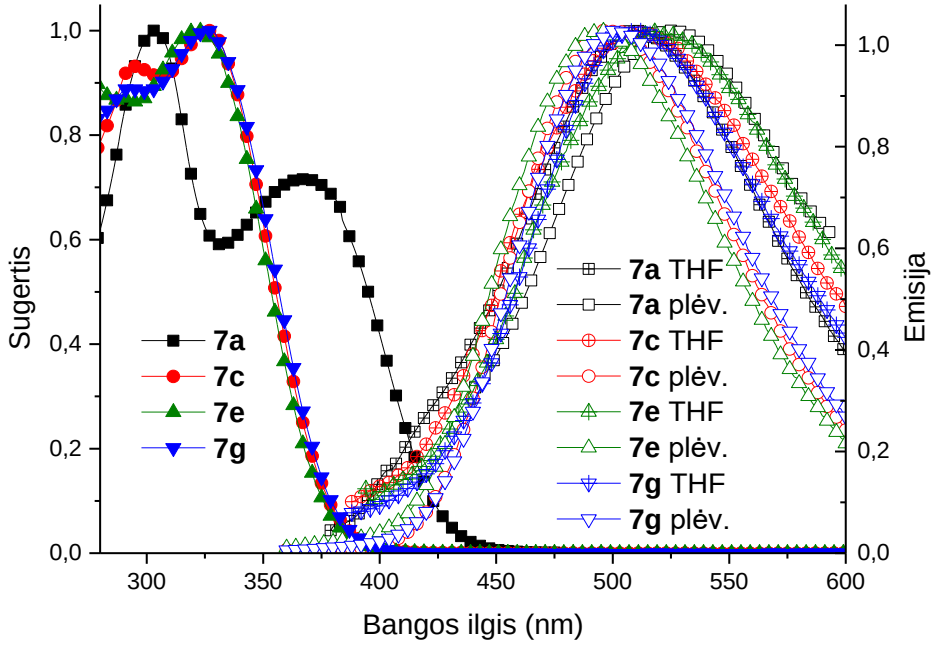

15 pav. Junginių **7a**, **7c**, **7e** ir **7g** sugerties (10^{-4} M THF tirpaluose) ir emisijos iš THF tirpalų (10^{-5} M) bei plėvelių spektrai

Junginys **7c** turi savo TPE fragmentus, prijungtus prie Triogerio bazės V formos karkaso galuose (2,8-padėtyse), dėl to jie yra orientuoti beveik statmenai vienas kitam. To rezultatas yra molekulinė struktūra, turinti aukščiausią kietosios būsenos kvantinį efektyvumą grupėje. Junginys **7g** turi dvi abiem būdais prijungtas TPE poras ir jo kvantinis efektyvumas yra artimas vidurkiui tarp dviejų ankstesnių molekulių. Tai rodo, kad jis irgi nukenčia nuo darinio **7e** turimų trūkumų, todėl galima daryti išvadą, kad du papildomi TPE fragmentai (palyginti su **7c**) yra labiau trūkumas nei privalumas.

7.3. Fotoelektrinės savybės

Junginių **7a**, **7c**, **7e** ir **7g** jonizacijos potencialai buvo išmatuoti fotoelektronų spektroskopijos ore metodu (13 lent.). Darinio **7a** I_p vertė yra 5,49 eV ir gali būti palyginta su išmatuotu junginio **2b** I_p (5,45 eV). Junginių **7c**, **7e** ir **7g** jonizacijos potencialai palyginti dideli, jų vertės yra atitinkamai 5,82 eV, 5,84 eV ir 5,76 eV. Tai galėjo lemti donorinių pakaitalų ar azoto atomų, jungiančių TPE fragmentus, nebuvimas arba tai, kad jų konjuguotoji π-sistema nėra pakankamai didelė.

Junginių **7a**, **7c**, **7e** ir **7g** nesužadintosios būsenos oksidacijos potencialai buvo išmatuoti taikant ciklinės voltamperometrijos metodą (13 lent.). Tiriant visus šiuos junginius pastebėta grįžtamoji oksidacija, tai rodo junginių elektrocheminį stabilumą. Tirpaluose atliktų CV matavimų rezultatai neblogai koreliuoja su jonizacijos potencialų matavimo duomenimis, gautais iš plėvelių. Tai rodo ribotą tarpmolekulinę sąveiką esant kietajai būsenai.

13 lentelė. Junginių **7a**, **7c**, **7e** ir **7g** energijos lygmenų duomenys [a]

Junginys	E_g^{opt} (eV)[b]	E_{HOMO} (eV)[c]	E_{LUMO} (eV)[d]	I_p (eV)[e]
7a	2,77	–4,90	–2,13	5,49
7c	3,12	–5,57	–2,45	5,82
7e	3,14	–5,36	–2,22	5,84
7g	3,11	–5,47	–2,36	5,76

[a] CV matavimai atlikti su stiklo elektrodu dichlormetano tirpaluose, naudojant 0,1 M tetrabutilamonio heksafluorfosfatą kaip elektrolitą ir $Ag/AgNO_3$ kaip palyginamąjį elektrodą. Kiekvienas matavimas buvo kalibruotas naudojant feroceną (Fc). Potencialai apskaičiuoti plg. su Fc^+/Fc. [b] Optinės draustinės juostos E_g^{opt} apskaičiuotos iš tirpalų absorbcijos spektrų. [c] Konversijos koeficientai: ferocenas DCM-SCE: 0,46 [162], SCE-SHE: 0,244 [163], SHE-vakuumas: 4,43 [164]. [d] E_{LUMO} apskaičiuota pagal lygtį $E_{LUMO} = I_p - E_g^{otp}$. [e] Kietosios būsenos junginių jonizacijos potencialas (I_p) buvo matuojamas fotoemisijos ore metodu iš plėvelių.

Įvertinant prieš tai išdėstytus faktus galima konstatuoti, kad susintetinti keturi nauji Triogerio bazės junginiai, turintys TPE šoninius pakaitus, yra termiškai stabilūs, tirpūs ir pasižymi AIE savybėmis, todėl juos galima naudoti formuojant kietojo kūno sluoksnį įrenginiuose. Šių junginių kvantinės išeigos nebuvo tokios didelės, kaip tikėtasi, tačiau tyrimai atskleidė tam tikrų struktūros ir savybių tarpusavio dėsningumų, kurie leidžia toliau tobulinti ir optimizuoti būsimų junginių molekulinį dizainą. Taip pat nustatyta, kad didžiausias kvantinis efektyvumas buvo gautas molekulėmis, kuriose TPE fragmentai yra prijungti prie TB karkaso 2,8-padėtyse, taip nukreipiant juos kampu vienas kito atžvilgiu. Kitokios molekulinės struktūros junginių kvantinis našumas buvo mažesnis netgi tada, kai prijungtų TPE fragmentų skaičius buvo dvigubai didesnis. Šie rezultatai leidžia daryti išvadą, kad Triogerio bazės molekulinis karkasas (jungiant pakaitus 2,8-padėtyse) yra tinkamas sintetinant spinduolius, pasižyminčius AIE savybėmis.

Pagrindiniai rezultatai ir išvados

1) Susintetintos mažamolekulės skyles pernešančios medžiagos, turinčios Triogerio bazės karkasu sujungtus trifenilamino fragmentus su skirtingais išoriniais pakaitais. Ištirtos šių junginių struktūrinės, terminės, optinės ir fotofizinės savybės. Nustatyta, kad:
   a) Triogerio bazės dariniai yra termiškai stabilūs, visų jų skilimo temperatūra viršija 370 °C;
   b) išmatuotos junginių **1b–1d** jonizacijos potencialo (5,25–5,34 eV) ir krūvininkų dreifinio judrio ($1{,}2\cdot10^{-5}$–$3{,}3\cdot10^{-4}$ cm^2/Vs) vertės rodo, jog šie junginiai tinkami naudoti optoelektronikoje.
2) Aldehidų kondensacijos būdu buvo susintetinti organiniai puslaidininkiai, turintys Triogerio bazės karkasą ir šoninius pakaitus su feniletenilfragmentais. Ištyrus šiuos junginius, nustatyta, kad:

a) Triogerio bazės junginių struktūrinis praplėtimas feniletenilgrupėmis išplečia konjuguotąją π-sistemą, suteikia jiems amorfiškumo, mažesnį jonizacijos potencialą (5,27–5,45 V) ir didelį skylių dreifinį judrį (0,002–0,011 cm^2/Vs);
b) perovskitinių saulės elementų, kuriuose naudojami susintetinti puslaidininkiai, energijos konversijos efektyvumas siekė 11,09 % (su junginiu **2c**, palyginti su 15,34 % naudojant *spiro*-OMeTAD). Tai rodo, kad šiuos junginius tinka naudoti optoelektronikos prietaisų gamyboje.

3) Susintetinti skyles pernešantys puslaidininkiai, turintys TPD struktūrinių fragmentų, sujungtų Triogerio bazės karkasu, o jų savybių tyrimas parodė, kad:
   a) Triogerio bazės karkasas kampu orientuoja prie jo prijungtus *p*-pakeistus TPD fragmentus vieną kito atžvilgiu, taip sudarydamas stabilius, amorfinius organinius puslaidininkius, kurie pasižymi dideliu krūvininkų judriu, siekiančiu iki 0,036 cm^2/Vs;
   b) pagaminti ir išmatuoti perovskitiniai saulės elementai su susintetintomis medžiagomis pasižymėjo gana dideliu konversijos efektyvumu: 14,6 % naudojant junginį **3h** (palyginti su 16,1 % naudojant *spiro*-OMeTAD) ir 17,91 % naudojant junginį **3l** (palyginti su 19,22 % naudojant *spiro*-OMeTAD). Taip įrodyta, jog šios grupės junginiai gali efektyviai atlikti skylių pernašos funkciją šiuose prietaisuose.
4) Susintetinti ir ištirti skyles pernešantys puslaidininkiai, turintys Triogerio bazės fragmentą ir per enamino grupę prijungtas difenilo atšakas. Nustatyta, kad:
   a) sintezės metodas, taikomas pasitelkiant enamino kondensaciją, leidžia gauti skyles pernešančius TB junginius, visiškai išvengiant poreikio naudoti paladžio katalizatorius, atitinkamus ligandus, taikyti inertines atmosferos sąlygas, taip pat išvengiant kruopštaus gryninimo šalinant paladžio liekanas, todėl šis metodas yra patrauklus komerciniu požiūriu;
   b) susintetintos skyles pernešančios medžiagos yra termiškai stabilios ir turi gana didelį dreifinį judrį (junginio **4e** – $3{,}35 \cdot 10^{-4}$ cm^2/Vs), todėl šie junginiai yra patrauklūs įvairioms optoelektronikos reikmėms;
   c) junginiai buvo išbandyti perovskitiniuose saulės elementuose ir gauti ypač geri rezultatai; didžiausiu energijos konversijos efektyvumu – 18,62 % – pasižymėjo elementai su metoksigrupių turinčiu junginiu **4e** (palyginti su 19,22 % naudojant *spiro*-OMeTAD) ir netgi viršijo *spiro*-OMeTAD prietaisų efektyvumą 1,6 karto, naudojant kompozicijas be priedų.
5) Suprojektuoti ir susintetinti dažikliai, turintys Triogerio bazės karkasą ir dvi rodanino-3-acto rūgšties akceptorines-inkarines grupes, prijungtas poli[n]enine grandine (n = 0–2). Taip pat susintetintos jų „pusinės“ versijos, turinčios vieną inkarinę grupę, ir šie dažikliai palyginti tarpusavyje. Prieita prie išvadų, jog:
   a) ultravioletinės ir regimosios šviesos sugerties spektrai rodo, jog dvigubųjų dažiklių absorbcijos maksimumai yra pasislinkę į raudonąją spektro pusę, lyginant su jų „pusinių“ analogų maksimumais. Šis skirtumas didėja su kiekvienu papildomu poli[n]eninės grandinės fragmentu. Taip didėja grandinių lankstumas ir kartu stiprėja dvigubųjų dažiklių inkarinių grupių tarpusavio sąveika;

b) dažikliais įjautrintų saulės celių bandymai parodė, kad lankstumas, kurį lemia ilgesnės polietino grandinės ir jų leidžiama sąveika tarp dviejų chromoforų, skatina agregatų susidarymą ir sumažina prietaiso efektyvumą. Geriausi rezultatai buvo gauti naudojant trumpos grandinės „pusinį“ dažiklį **5D**.

6) Suprojektuoti ir susintetinti TB dažikliai, turintys tiofeno arba fenilhidrazono jungiamuosius fragmentus, kuriais pakeistos lanksčios jungiamosios polietino grandinės. Šių dažiklių savybių tyrimas parodė, kad:
   a) nors tiofeno fragmentas suteikia geresnę šviesos sugertį dažikliams, palyginti su hidrazono junginiais, tačiau jis vis tiek nepašalina nepageidaujamos vidinės chromoforų sąveikos.
   b) dažiklio struktūroje esantis fenilhidrazono jungiamasis fragmentas eliminuoja sąveiką tarp dviejų chromoforų.
7) Susintetinti ir ištirti nauji Triogerio bazės junginiai su tetrafeniletenilo šoniniais pakaitais. Šie junginiai yra termiškai stabilūs, tirpūs ir pasižymi agregacijos indukuota emisija. Tai rodo, kad jie tinka naudoti gryniesiems kietosios būsenos sluoksniams formuoti šviesą spinduliuojančiuose įrenginiuose.

7. REFERENCES

1. OSTROVERKHOVA, Oksana. Organic optoelectronic materials: mechanisms and applications. *Chemical reviews*. 2016. Vol. 116, no. 22, p. 13279–13412.
2. SIEMINSKI, Adam. International energy outlook. *Energy Information Administration (EIA)*. 2014. Vol. 18.
3. LIU, Xuxu, CHEN, Huajie and TAN, Songting. Overview of high-efficiency organic photovoltaic materials and devices. *Renewable and Sustainable Energy Reviews* [online]. December 2015. Vol. 52, p. 1527–1538. DOI 10.1016/j.rser.2015.08.032. Available from: http://linkinghub.elsevier.com/retrieve/pii/S1364032115008783
4. JEON, Nam Joong, NA, Hyejin, JUNG, Eui Hyuk, YANG, Tae-Youl, LEE, Yong Guk, KIM, Geunjin, SHIN, Hee-Won, IL SEOK, Sang, LEE, Jaemin and SEO, Jangwon. A fluorene-terminated hole-transporting material for highly efficient and stable perovskite solar cells. *Nature Energy* [online]. 9 August 2018. Vol. 3, no. 8, p. 682–689. DOI 10.1038/s41560-018-0200-6. Available from: http://dx.doi.org/10.1038/s41560-018-0200-6
5. BERGESEN, Joseph D, TÄHKÄMÖ, Leena, GIBON, Thomas and SUH, Sangwon. Potential long-term global environmental implications of efficient light-source technologies. *Journal of Industrial Ecology*. 2016. Vol. 20, no. 2, p. 263–275.
6. DREYFUS, G and GALLINAT, C. Rise and Shine: Lighting the World with 10 Billion LED Bulbs. *US Department of Energy*. 2015. Vol. 7.
7. RAMÍREZ, Cristina L., PEGORARO, César, TRUPP, Leandro, BRUTTOMESSO, Andrea, AMOREBIETA, Valentín, VERA, D. Mariano A. and PARISE, Alejandro R. Charge transfer properties of Tröger base derivatives. *Physical Chemistry Chemical Physics* [online]. 2011. Vol. 13, no. 45, p. 20076. DOI 10.1039/c1cp22086a. Available from: http://xlink.rsc.org/?DOI=c1cp22086a
8. TRÖGER, Julius. Ueber einige mittelst nascirenden Formaldehydes entstehende Basen. *Journal für Praktische Chemie*. 1887. Vol. 36, no. 1, p. 225–245.
9. SPIELMAN, M A. The structure of Troeger's base. *Journal of the American Chemical Society*. 1935. Vol. 57, no. 3, p. 583–585.
10. WAGNER, E C. Condensations of Aromatic Amines with Formaldehyde in Media Containing Acid. III. The Formation of Tröger's Base. *Journal of the American Chemical Society*. 1935. Vol. 57, no. 7, p. 1296–1298.
11. PRELOG, V and WIELAND, P. Über die Spaltung der Tröger'schen Base in optische Antipoden, ein Beitrag zur Stereochemie des dreiwertigen Stickstoffs. *Helvetica Chimica Acta*. 1944. Vol. 27, no. 1, p. 1127–1134.
12. DOLENSKÝ, Bohumil, ELGUERO, José, KRÁL, Vladimír, PARDO, Carmen, VALIK, Martin, SYNTHESIS, The, TRO, A Mono, RESOLUTION, B Chiral and MOLECULAR, A. Current Tröger's base chemistry. *Advances in Heterocyclic Chemistry*. 2007. Vol. 93, no. 06, p. 1–56. DOI 10.1016/S0065-2725(06)93001-3.
13. LAYLIN, James K. *Nobel laureates in chemistry, 1901-1992*. Chemical Heritage Foundation, 1993. ISBN 0841226903.
14. LARSON, S B and WILCOX, C S. Structure of 5, 11-methano-2, 8-dimethyl-5, 6, 11, 12-tetrahydrodibenzo [b, f][1, 5] diazocine (Tröger's base) at 163 K. *Acta Crystallographica Section C*. 1986. Vol. 42, no. 2, p. 224–227.
15. WILEN, Samuel H, QI, Jian Zhong and WILLIARD, Paul G. Resolution,

asymmetric transformation, and configuration of Troeger's base. Application of Troeger's base as a chiral solvating agent. *The Journal of Organic Chemistry*. 1991. Vol. 56, no. 2, p. 485–487.

16. WILCOX, Craig S. Tröger's base analogs. New structural units for the preparation of chiral hosts and metal ligands. *Tetrahedron Letters* [online]. 1985. Vol. 26, no. 47, p. 5749–5752. DOI 10.1016/S0040-4039(00)98915-9. Available from: http://linkinghub.elsevier.com/retrieve/pii/S0040403900989159
17. PALIWAL, S, GEIB, S and WILCOX, C S. Molecular torsion balance for weak molecular recognition forces. effects of" Tilted-T" Edge-to-Face aromatic interactions on conformational selection and solid-state structure. *Journal of the American Chemical Society*. 1994. Vol. 116, no. 10, p. 4497–4498.
18. KIM, Eun-il, PALIWAL, Sunil and WILCOX, Craig S. Measurements of molecular electrostatic field effects in edge-to-face aromatic interactions and CH-π interactions with implications for protein folding and molecular recognition. *Journal of the American Chemical Society*. 1998. Vol. 120, no. 43, p. 11192–11193.
19. GREENBERG, Arthur, MOLINARO, Nicholas and LANG, Michael. Structure and dynamics of Troeger's base and simple derivatives in acidic media. *The Journal of Organic Chemistry*. 1984. Vol. 49, no. 6, p. 1127–1130.
20. HAMADA, Yasumasa and MUKAI, Shiho. Synthesis of ethano-Tröger's base, configurationally stable substitute of Tröger's base. *Tetrahedron: Asymmetry*. 1996. Vol. 7, no. 9, p. 2671–2674.
21. LENEV, Denis A, GOLOVANOV, Denis G, LYSSENKO, Konstantin A and KOSTYANOVSKY, Remir G. Configurationally stable methylates of methano-and ethano-Tröger bases. *Tetrahedron: Asymmetry*. 2006. Vol. 17, no. 15, p. 2191–2194.
22. MICHON, Christophe, SHARMA, Ankit, BERNARDINELLI, Gerard, FRANCOTTE, Eric and LACOUR, Jérôme. Stereoselective synthesis of configurationally stable functionalized ethano-bridged Tröger bases. *Chemical Communications*. 2010. Vol. 46, no. 13, p. 2206–2208.
23. SMITH, Lee Irvin and SCHUBERT, W M. Polyalkylbenzenes. XXXIV. 1 The Reaction between Polymethyl-p-methoxyanilines and Formaldehyde. *Journal of the American Chemical Society*. 1948. Vol. 70, no. 8, p. 2656–2661.
24. WEBB, Thomas H, SUH, Hongsuk and WILCOX, Craig S. Chemistry of synthetic receptors and functional group arrays. 16. Enantioselective and diastereoselective molecular recognition of alicyclic substrates in aqueous media by a chiral, resolved synthetic receptor. *Journal of the American Chemical Society*. 1991. Vol. 113, no. 22, p. 8554–8555.
25. BAG, Braja Gopal and MAITRA, Uday. A convenient method for the synthesis of Tröger's Base analogues. *Synthetic communications*. 1995. Vol. 25, no. 12, p. 1849–1856.
26. MILLER, Thomas R and WAGNER, E C. Some Analogs of Troeger's Base and Related Compounds 1. *Journal of the American Chemical Society* [online]. March 1941. Vol. 63, no. 3, p. 832–836. DOI 10.1021/ja01848a055. Available from: http://pubs.acs.org/doi/abs/10.1021/ja01848a055
27. HÄRING, Marc. Die Darstellung von 5, 11-Endomethylen-tetrahydrophenhomazinen und 5-Alkyl-tetrahydrophenhomazinen. *Helvetica Chimica Acta*. 1963. Vol. 46, no. 7, p. 2970–2982.

28. ADRIAN JR, James C and WILCOX, Craig S. Chemistry of synthetic receptors and functional group arrays. 19. General effects of binding site water exclusion on hydrogen bond based molecular recognition systems: a closed binding site is less affected by environmental changes than an open site. *Journal of the American Chemical Society*. 1992. Vol. 114, no. 4, p. 1398–1403.

29. HANSSON, Anna, JENSEN, Jacob, WENDT, Ola F and WÄRNMARK, Kenneth. Synthesis of Dihalo-Substituted Analogues of Tröger's Base from ortho-and meta-Substituted Anilines. *European Journal of Organic Chemistry*. 2003. Vol. 2003, no. 16, p. 3179–3188.

30. SALEZ, Hervé, WARDANI, Abderrahim, DEMEUNYNCK, Martine, TATIBOUET, Arnaud and LHOMME, Jean. Synthesis of tröger's base analogs derived from 3-aminoacridine and 10-aminobenzo [b][1, 7] phenanthroline. *Tetrahedron letters*. 1995. Vol. 36, no. 8, p. 1271–1274.

31. LI, Zhong, XU, Xiaoyong, PENG, Yanqing, JIANG, Zhaoxing, DING, Chuanyong and QIAN, Xuhong. An Unusual Synthesis of Tröger's Bases Using DMSO/HCl as Formaldehyde Equivalent. *Synthesis*. 2005. Vol. 2005, no. 08, p. 1228–1230.

32. BECKER, Daniel, FINNEGAN, Patricia M and COLLINS, Paul W. Isolation of a Highly Functionalized Troeger's Base Derivative via a Novel Reaction. *Tetrahedron letters*. 1993. Vol. 34, no. 12.

33. SATISHKUMAR, Sakilam and PERIASAMY, Mariappan. A convenient method for the synthesis and resolution of Tröger base. *Tetrahedron: Asymmetry*. 2006. Vol. 17, no. 7, p. 1116–1119.

34. SATISHKUMAR, Sakilam and PERIASAMY, Mariappan. Chiral recognition of carboxylic acids by Troeger's base derivatives. *Tetrahedron: Asymmetry*. 2009. Vol. 20, no. 19, p. 2257–2262.

35. BHUIYAN, M Delower H, MAHON, Andrew B, JENSEN, Paul, CLEGG, Jack K and TRY, Andrew C. Synthesis of Symmetric Dinitro-Functionalised Tröger's Base Analogues. *European Journal of Organic Chemistry*. 2009. Vol. 2009, no. 5, p. 687–698.

36. VARDELLE, Emilie, MARTIN-MINGOT, Agnès, JOUANNETAUD, Marie-Paule, JACQUESY, Jean-Claude and MARROT, Jérôme. An efficient access to new Tröger's bases using superacidic chemistry. *Tetrahedron Letters*. 2009. Vol. 50, no. 10, p. 1093–1096.

37. WU, Hui, ZHANG, Pu, SHEN, Yang, ZHANG, Fu-ren, WAN, Yu and SHI, Da-qing. Convenient Syntheses of Tröger's Base Derivatives in Ionic Liquids. *Synlett*. 2007. Vol. 2007, no. 02, p. 336–338.

38. CERRADA, Luisa, CUDERO, José, ELGUERO, José and PARDO, Carmen. Azolyl substituted Tröger's bases. *Journal of the Chemical Society, Chemical Communications*. 1993. No. 23, p. 1713–1714.

39. CUDERO, José, PARDO, Carmen, RAMOS, Mar, GUTIERREZ-PUEBLA, Enrique, MONGE, Angeles and ELGUERO, José. Synthesis and molecular structure of heterocyclic Tröger's bases derived from C-amino heterocycles. *Tetrahedron* [online]. 1997. Vol. 53, no. 6, p. 2233–2240. DOI 10.1016/S0040-4020(96)01125-8. Available from: http://www.sciencedirect.com/science/article/pii/S0040402096011258

40. JENSEN, Jacob and WÄRNMARK, Kenneth. Synthesis of Halogen Substituted

Analogues of Tröger's Base. *Synthesis*. 2001. Vol. 25012, no. 12, p. 1437–210. DOI 10.1055/s-2001-17525.

41. SERGEYEV, Sergey, SCHÄR, Michael, SEILER, Paul, LUKOYANOVA, Olena, ECHEGOYEN, Luis and DIEDERICH, François. Synthesis of trans-1, trans-2, trans-3, and trans-4 Bisadducts of C60 by Regio-and Stereoselective Tether-Directed Remote Functionalization. *Chemistry–A European Journal*. 2005. Vol. 11, no. 8, p. 2284–2294.
42. JENSEN, Jacob, STROZYK, Michal and WARNMARK, Kenneth. Influence of scale, stoichiometry and temperature on the synthesis of 2, 8-dihalo analogues of tröger's base from the corresponding anilines and paraformaldehyde. *Journal of heterocyclic chemistry*. 2003. Vol. 40, no. 2, p. 373–375.
43. BEW, Sean P, LEGENTIL, Laurent, SCHOLIER, Vincent and SHARMA, Sunil V. α-Amino acid Tröger base derivatives, possible conformationally restricted scaffolds? *Chemical Communications*. 2007. No. 4, p. 389–391. DOI 10.1039/b614371g.
44. KIEHNE, U., WEILANDT, T. and LÜTZEN, A. Diastereoselective Self-Assembly of Double-Stranded Helicates from Tröger's Base Derivatives. *Organic letters* [online]. March 2007. Vol. 9, no. 7, p. 1283–1286. DOI 10.1021/ol070048i. Available from: http://pubs.acs.org/doi/abs/10.1021/ol070048i
45. DIDIER, Delphine, TYLLEMAN, Benoît, LAMBERT, Natacha, VELDE, Christophe M L Vande, BLOCKHUYS, Frank, COLLAS, Alain and SERGEYEV, Sergey. Functionalized analogues of Tröger's base: scope and limitations of a general synthetic procedure and facile, predictable method for the separation of enantiomers. *Tetrahedron*. 2008. Vol. 64, no. 27, p. 6252–6262.
46. BHUIYAN, M Delower H, ZHU, Kai-Xian, JENSEN, Paul and TRY, Andrew C. Synthesis of Symmetric Diester-Functionalised Tröger's Base Analogues. *European Journal of Organic Chemistry*. 2010. Vol. 2010, no. 24, p. 4662–4670.
47. MALIK, Qasim M, IJAZ, Sadia, CRAIG, Donald C and TRY, Andrew C. Synthesis and reactivity of dimethoxy-functionalised Tröger's base analogues. *Tetrahedron*. 2011. Vol. 67, no. 32, p. 5798–5805.
48. DIDIER, Delphine and SERGEYEV, Sergey. Bromination and Iodination of 6H, 12H-5, 11-Methanodibenzo [b, f][1, 5] diazocine: A Convenient Entry to Unsymmetrical Analogs of Tröger's Base. *European journal of organic chemistry*. 2007. Vol. 2007, no. 23, p. 3905–3910.
49. FARRAR, W V. Reactions of formaldehyde with aromatic amines. *Journal of Applied Chemistry*. 1964. Vol. 14, no. 9, p. 389–399.
50. WAGNER, E C. A rationalization of acid-induced reactions of methylene-bis-amines, methylene-amines, and of formaldehyde and amines. *The Journal of Organic Chemistry*. 1954. Vol. 19, no. 12, p. 1862–1881.
51. RÚNARSSON, Ögmundur Vidar, ARTACHO, Josep and WÄRNMARK, Kenneth. The 125th anniversary of the Tröger's base molecule: Synthesis and applications of Tröger's base analogues. *European Journal of Organic Chemistry*. 2012. No. 36, p. 7015–7041. DOI 10.1002/ejoc.201201249.
52. ABELLA, Carlos A M, BENASSI, Mario, SANTOS, Leonardo S, EBERLIN, Marcos N and COELHO, Fernando. The mechanism of tröger's base formation probed by electrospray ionization mass spectrometry. *The Journal of organic*

chemistry. 2007. Vol. 72, no. 11, p. 4048–4054.

53. WAN, Yu, YUAN, Rui, ZHANG, Wei-chao, SHI, Yan-hui, LIN, Wei, YIN, Wei, BO, Rong-cheng, SHI, Jing-jing and WU, Hui. Two isolated intermediates of the Tröger's base: synthesis and mechanism. *Tetrahedron*. 2010. Vol. 66, no. 19, p. 3405–3409.

54. WEBB, Thomas H and WILCOX, Craig S. Improved synthesis of symmetrical and unsymmetrical 5, 11-methanodibenzo [b, f][1, 5] diazocines. Readily available nanoscale structural units. *The Journal of Organic Chemistry*. 1990. Vol. 55, no. 1, p. 363–365.

55. WEBER, Edwin, MÜLLER, Ute, WORSCH, Detlev, VÖGTLE, Fritz, WILL, Georg and KIRFEL, Armin. Quaternary Tröger bases as new inclusion hosts; the first X-ray structures of a Tröger base and of a dioxane clathrate. *Journal of the Chemical Society, Chemical Communications*. 1985. No. 22, p. 1578–1580.

56. BOND, Dianne R and SCOTT, Janet L. Clathrate formation with Troeger base analogues. *Journal of the Chemical Society, Perkin Transactions 2*. 1991. No. 1, p. 47–51. DOI 10.1039/p29910000047.

57. MICHON, Christophe, GONÇALVES-FARBOS, Maria-Héléna and LACOUR, Jérôme. NMR enantiodifferentiation of quaternary ammonium salts of Troeger base. *Chirality: The Pharmacological, Biological, and Chemical Consequences of Molecular Asymmetry*. 2009. Vol. 21, no. 9, p. 809–817.

58. COOPER, F C and PARTRIDGE, M W. 564. Cyclic amidines. Part V. 5: 11-endo-Substituted 5: 6: 11: 12-tetrahydro-2: 8-dimethylphenhomazines. *Journal of the Chemical Society (Resumed)*. 1957. P. 2888–2893.

59. JOHNSON, Roy A, GORMAN, Robert R, WNUK, Richard J, CRITTENDEN, Norman J and AIKEN, James W. Troeger's base. An alternate synthesis and a structural analog with thromboxane A2 synthetase inhibitory activity. *Journal of medicinal chemistry*. 1993. Vol. 36, no. 21, p. 3202–3206.

60. PERIASAMY, Mariappan, SURESH, Sundaram and SATISHKUMAR, Sakilam. Synthesis of new derivatives from a Tröger base via exchange of the methano bridge with carbonyl compounds. *Tetrahedron: Asymmetry*. 2012. Vol. 23, no. 2, p. 108–116.

61. REDDY, Manda Bhaskar, MANJULA, Alla, RAO, Bommena Vittal and SRIDHAR, Balasubramanian. Regioselective synthesis of dimethylamino- or arylalkylamino-"crowned" tröger's base analogues under Vilsmeier-Haack conditions. *European Journal of Organic Chemistry*. 2012. No. 2, p. 312–319. DOI 10.1002/ejoc.201100804.

62. MALIK, Qasim M, MAHON, Andrew B, CRAIG, Donald C and TRY, Andrew C. Reaction of Tröger's base analogues with Vilsmeier reagents. *Tetrahedron*. 2011. Vol. 67, no. 44, p. 8509–8514.

63. METLESICS, W, TAVARES, R and STERNBACH, L H. The Reduction Products of a Dibenzo [b, f][1, 5] diazocine1. *The Journal of Organic Chemistry*. 1966. Vol. 31, no. 10, p. 3356–3362.

64. ALBERT, Adrien and YAMAMOTO, Hiroshi. The structures of the anhydro-polymers of 2-aminobenzaldehyde. *Journal of the Chemical Society B: Physical Organic*. 1966. P. 956–963.

65. HARMATA, Michael and KAHRAMAN, Mehmet. Congeners of Troeger's base as

chiral ligands. *Tetrahedron: Asymmetry*. 2000. Vol. 11, no. 14, p. 2875–2879.

66. HARMATA, Michael, CARTER, Kevin W, JONES, Darin E and KAHRAMAN, Mehmet. The metallation of Troeger's base. *Tetrahedron letters*. 1996. Vol. 37, no. 35, p. 6267–6270.

67. HARMATA, Michael, RAYANIL, Kanok-On and BARNES, Charles L. Sequential Alkylation of Tröger's Base. An Approach to New Chiral Ligands. *Supramolecular Chemistry*. 2006. Vol. 18, no. 7, p. 581–586.

68. PEREIRA, Raul, ONDRISEK, Pavol, KUBINCOVÁ, Alžbeta, OTTH, Elisabeth and CVENGROŠ, Ján. Mild Stereoselective Intermolecular Acetoxylation and Azidation of α-C− H Bonds in Tröger's Bases. *Advanced Synthesis & Catalysis*. 2016. Vol. 358, no. 17, p. 2739–2744.

69. JENSEN, Jacob, STROZYK, Michal and WAERNMARK, Kenneth. Introduction of Terminal Alkynes into the 2-and 8-Positions of the Tröger's Base Core via Sonogashira Reaction of 2, 8-Diiodo-4, 10-dimethyl-6H, 12H-5, 11-methanodibenzo [b, f][1, 5] diazocine. *Synthesis*. 2002. Vol. 2002, no. 18, p. 2761–2765.

70. FAROUGHI, Masoud, JENSEN, Paul and TRY, Andrew C. Halogenation of Tröger's base analogues. *ARKIVOC*. 2009. Vol. 2009, no. Pt. ii, p. 269-280.

71. KIEHNE, Ulf and LÜTZEN, Arne. Synthesis of 2,8-Disubstituted Analogues of Troeger's Base. *Synthesis* [online]. 23 June 2004. Vol. 2004, no. 10, p. 1687–1695. DOI 10.1055/s-2004-829117. Available from: http://www.thieme-connect.de/DOI/DOI?10.1055/s-2004-829117

72. SOLANO, Carlos, SVENSSON, Daniel, OLOMI, Zarina, JENSEN, Jacob, WENDT, Ola F and WÄRNMARK, Kenneth. Introduction of Aromatic and Heteroaromatic Groups in the 2-and 8-Positions of the Tröger's Base Core by Suzuki, Stille and Negishi Cross-Coupling Reactions–A Comparative Study. *European journal of organic chemistry*. 2005. Vol. 2005, no. 16, p. 3510–3517.

73. HOF, Fraser, SCHÄR, Michael, SCOFIELD, Denise M, FISCHER, Felix, DIEDERICH, François and SERGEYEV, Sergey. Preparation of Tröger Base Derivatives by Cross-Coupling Methodologies. *Helvetica chimica acta*. 2005. Vol. 88, no. 8, p. 2333–2344.

74. DIDIER, Delphine and SERGEYEV, Sergey. Synthesis of symmetrical amino and aminomethyl derivatives of Tröger's base via Pd-catalyzed C–C and C–N bond formation. *Tetrahedron*. 2007. Vol. 63, no. 18, p. 3864–3869.

75. KIEHNE, Ulf, BRUHN, Torsten, SCHNAKENBURG, Gregor, FRÖHLICH, Roland, BRINGMANN, Gerhard and LÜTZEN, Arne. Synthesis, Resolution, and Absolute Configuration of Difunctionalized Tröger's Base Derivatives. *Chemistry - A European Journal* [online]. 9 May 2008. Vol. 14, no. 14, p. 4246–4255. DOI 10.1002/chem.200701960. Available from: http://doi.wiley.com/10.1002/chem.200701960

76. ARTACHO, Josep and WÄRNMARK, Kenneth. On the Synthesis of Asymmetric and Dissymmetric Amino Analogues of Tröger's Base. *Synthesis*. 2009. Vol. 2009, no. 18, p. 3120–3126.

77. KOSUGI, Masanori, KAMEYAMA, Masayuki and MIGITA, Toshihiko. Palladium-catalyzed aromatic amination of aryl bromides with N, N-di-ethylamino-tributyltin. *Chemistry Letters*. 1983. Vol. 12, no. 6, p. 927–928.

78. GURAM, Anil S and BUCHWALD, Stephen L. Palladium-catalyzed aromatic

aminations with in situ generated aminostannanes. *Journal of the American Chemical Society*. 1994. Vol. 116, no. 17, p. 7901–7902.

79. PAUL, Frederic, PATT, Joe and HARTWIG, John F. Palladium-catalyzed formation of carbon-nitrogen bonds. Reaction intermediates and catalyst improvements in the hetero cross-coupling of aryl halides and tin amides. *Journal of the American Chemical Society*. 1994. Vol. 116, no. 13, p. 5969–5970.

80. LOUIE, Janis and HARTWIG, John F. Palladium-catalyzed synthesis of arylamines from aryl halides. Mechanistic studies lead to coupling in the absence of tin reagents. *Tetrahedron Letters*. 1995. Vol. 36, no. 21, p. 3609–3612.

81. GURAM, Anil S, RENNELS, Roger A and BUCHWALD, Stephen L. A simple catalytic method for the conversion of aryl bromides to arylamines. *Angewandte Chemie International Edition in English*. 1995. Vol. 34, no. 12, p. 1348–1350.

82. JENSEN, Jacob, TEJLER, Johan and WÄRNMARK, Kenneth. General Protocols for the Synthesis of C 2-Symmetric and Asymmetric 2, 8-Disubstituted Analogues of Tröger's Base via Efficient Bromine− Lithium Exchanges of 2, 8-Dibromo-6 H, 12 H-5, 11-methanodibenzo [b, f][1, 5] diazocine. *The Journal of organic chemistry*. 2002. Vol. 67, no. 17, p. 6008–6014.

83. ARTACHO, Josep, NILSSON, Patrik, BERGQUIST, Karl-Erik, WENDT, Ola F and WÄRNMARK, Kenneth. The Synthesis and Characterization of all Diastereomers of a Linear Symmetrically Fused Tris-Tröger's Base Analogue: New Chiral Cleft Compounds. *Chemistry–A European Journal*. 2006. Vol. 12, no. 10, p. 2692–2701.

84. WEILANDT, Torsten, KIEHNE, Ulf, BUNZEN, Jens, SCHNAKENBURG, Gregor and LÜTZEN, Arne. Self-discriminating self-assembly of dinuclear heterochiral rhombs from tröger's base derived Bis(pyridyl) ligands. *Chemistry - A European Journal*. 2010. Vol. 16, no. 8, p. 2418–2426. DOI 10.1002/chem.200902993.

85. PARDO, Carmen, SESMILO, Esther, GUTIÉRREZ-PUEBLA, Enrique, MONGE, Angeles, ELGUERO, José and FRUCHIER, Alain. New chiral molecular tweezers with a bis-Tröger's base skeleton. *The Journal of organic chemistry*. 2001. Vol. 66, no. 5, p. 1607–1611.

86. VALIK, Martin, DOLENSKY, Bohumil, PETŘÍČKOVÁ, Hana and KRÁL, Vladimír. Regio-and Stereoselectivity in Preparation of Benzene Bridged Bis-and Tris-Tröger's Bases. *Collection of Czechoslovak chemical communications*. 2002. Vol. 67, no. 5, p. 609–621.

87. MAS, Thierry, PARDO, Carmen, SALORT, Francisca, ELGUERO, José and TORRES, M Rosario. A New Entry to Bis-Tröger's Bases. *European Journal of Organic Chemistry*. 2004. Vol. 2004, no. 5, p. 1097–1104.

88. MASA, Thierry, PARDO, Carmen and ELGUEROB, José. A shorter synthesis of symmetrical 2, 11-dimethyl-bis-Tröger's bases. A new molecular tweezer. *Arkivoc*. 2004. Vol. 4, p. 86–93.

89. HAVLÍK, Martin, DOLENSKÝ, Bohumil, KESSLER, Jiří, CÍSAŘOVÁ, Ivana and KRÁL, Vladimír. A new synthetic strategy to prepare throne and calix diastereoisomers of parallel tris-Tröger's bases. *Supramolecular Chemistry*. 2012. Vol. 24, no. 2, p. 127–134.

90. DOLENSKÝ, Bohumil, HAVLÍK, Martin and KRÁL, Vladimír. Oligo Tröger's bases—new molecular scaffolds. *Chemical Society Reviews* [online]. 2012. Vol. 41, no. 10, p. 3839. DOI 10.1039/c2cs15307f. Available from:

http://pubs.rsc.org/en/content/articlehtml/2012/cs/c2cs15307f

91. YASHIMA, Eiji, AKASHI, Mitsuru and MIYAUCHI, Noriyuki. Chiral Bis (1, 10-phenanthroline) with Tröger's Base Skeleton. Synthesis and Interaction with DNA. *Chemistry Letters*. 1991. Vol. 20, no. 6, p. 1017–1020.

92. ABONIA, Rodrigo, ALBORNOZ, Andrea, LARRAHONDO, Hector, QUIROGA, Jairo, INSUASTY, Braulio, INSUASTY, Henry, HORMAZA, Angelina, SÁNCHEZ, Adolfo and NOGUERAS, Manuel. Synthesis of pyrazole and pyrimidine Tröger's-base analogues. *Journal of the Chemical Society, Perkin Transactions 1* [online]. 2002. Vol. 4, no. 13, p. 1588–1591. DOI 10.1039/b200862a. Available from: http://xlink.rsc.org/?DOI=b200862a

93. WU, Hui, CHEN, Xiu-mei, WAN, Yu, YE, Ling, XIN, Hai-qiang, XU, Hua-hong, YUE, Cai-hui, PANG, Li-ling, MA, Rui and SHI, Da-qing. Stereoselective Mannich reactions catalyzed by Tröger's base derivatives in aqueous media. *Tetrahedron Letters*. 2009. Vol. 50, no. 9, p. 1062–1065.

94. BAILLY, Christian, LAINE, William, DEMEUNYNCK, Martine and LHOMME, Jean. Enantiospecific recognition of DNA sequences by a proflavine Tröger base. *Biochemical and biophysical research communications*. 2000. Vol. 273, no. 2, p. 681–685.

95. BALDEYROU, Brigitte, TARDY, Christelle, BAILLY, Christian, COLSON, Pierre, HOUSSIER, Claude, CHARMANTRAY, Franck and DEMEUNYNCK, Martine. Synthesis and DNA interaction of a mixed proflavine–phenanthroline Tröger base. *European journal of medicinal chemistry*. 2002. Vol. 37, no. 4, p. 315–322.

96. TATIBOUËT, Arnaud, DEMEUNYNCK, Martine, ANDRAUD, Chantal, COLLET, André and LHOMME, Jean. Synthesis and study of an acridine substituted Tröger's base: preferential binding of the (–)-isomer to B-DNA. *Chemical Communications*. 1999. Vol. 4200, no. 2, p. 161–162.

97. GASLONDE, Thomas, LÉONCE, Stéphane, PIERRÉ, Alain, PFEIFFER, Bruno, MICHEL, Sylvie and TILLEQUIN, François. Tröger's bases in the acronycine, benzo [a] acronycine, and benzo [b] acronycine series. *Tetrahedron letters*. 2011. Vol. 52, no. 34, p. 4426–4429.

98. DEMEUNYNCK, M, FONTAINE, C and LHOMME, J. 1H NMR study of heterocyclic symmetric and asymmetric Tröger's base analogs containing the acridine ring. *Magnetic resonance in chemistry*. 1999. Vol. 37, no. 1, p. 73–76.

99. DEMEUNYNCK, Martine, MOUCHERON, Cécile and KIRSCH-DE MESMAEKER, Andrée. Tetrapyrido [3, 2-a: 2′, 3′-c: 3 ″, 2 ″-h: 2‴, 3‴-j] acridine (tpac): a new extended polycyclic bis-phenanthroline ligand. *Tetrahedron letters*. 2002. Vol. 43, no. 2, p. 261–264.

100. TATAR, Ameneh, DOLENSKÝ, Bohumil, DVOŘÁKOVÁ, Hana and KRÁL, Vladimír. Selective formation of either Tröger's base or spiro Tröger's base derivatives from [2-aminoporphyrinato (2-)] nickel by choice of reaction conditions. *Tetrahedron Letters*. 2012. Vol. 53, no. 45, p. 6015–6017.

101. GOSWAMI, Shyamaprosad and GHOSH, Kumaresh. Molecular recognition: Chain length selectivity studies of dicarboxylic acids by the cavity of a new Troger's base receptor. *Tetrahedron letters*. 1997. Vol. 38, no. 25, p. 4503–4506.

102. ARRIBAS, Carlos Solano, WENDT, Ola F, SUNDIN, Anders P, CARLING, Carl-Johan, WANG, Ruiyao, LEMIEUX, Robert P and WÄRNMARK, Kenneth.

Formation of an heterochiral supramolecular cage by diastereomer self-discrimination: fluorescence enhancement and C 60 sensing. *Chemical Communications*. 2010. Vol. 46, no. 24, p. 4381–4383.

103. LEMAUR, Vincent, CORNIL, Jérôme, DIDIER, Delphine, MUJAWASE, Aline and SERGEYEV, Sergey. A Joint Theoretical and Experimental Insight into the Electronic Structure of Chromophores Derived from 6H, 12H-5, 11-Methanodibenzo [b, f][1, 5] diazocine. *Helvetica chimica acta*. 2007. Vol. 90, no. 11, p. 2087–2095.

104. ADRIAN JR, James C and WILCOX, Craig S. Chemistry of synthetic receptors and functional group arrays. 10. Orderly functional group dyads. Recognition of biotin and adenine derivatives by a new synthetic host. *Journal of the American Chemical Society*. 1989. Vol. 111, no. 20, p. 8055–8057.

105. GOSWAMI, Shyamaprosad, GHOSH, Kumaresh and DASGUPTA, Swagata. Troger's base molecular scaffolds in dicarboxylic acid recognition. *The Journal of organic chemistry*. 2000. Vol. 65, no. 7, p. 1907–1914.

106. HANSSON, Anna P, NORRBY, Per-Ola and WÄRNMARK, Kenneth. A bis (crown-ether) analogue of Tröger's base: Recognition of achiral and chiral primary bisammonium salts. *Tetrahedron letters*. 1998. Vol. 39, no. 25, p. 4565–4568.

107. CROSSLEY, Maxwell J, HAMBLEY, Trevor W, MACKAY, Lindsey G, TRY, Andrew C and WALTON, Robin. Porphyrin analogues of Tröger's base: large chiral cavities with a bimetallic binding site. *Journal of the Chemical Society, Chemical Communications*. 1995. No. 10, p. 1077–1079.

108. CROSSLEY, Maxwell J, MACKAY, Lindsey G and TRY, Andrew C. Enantioselective recognition of histidine and lysine esters by porphyrin chiral clefts and detection of amino acid conformations in the bound state. *Journal of the Chemical Society, Chemical Communications*. 1995. No. 18, p. 1925–1927.

109. REEK, Joost N H, CROSSLEY, Maxwell J, SCHENNING, Albert P H J, BOSMAN, Anton W and MEIJER, E W. Templated assembly of a molecular capsule. *Chemical Communications*. 1998. No. 1, p. 11–12.

110. BROTHERHOOD, Peter R, WU, Richard A-S, TURNER, Peter and CROSSLEY, Maxwell J. Cavity effect amplification in the recognition of dicarboxylic acids by initial ditopic H-bond formation followed by kinetic trapping. *Chemical communications*. 2007. No. 3, p. 225–227.

111. BHAYANA, Brijesh and WILCOX, Craig S. A minimal protein folding model to measure hydrophobic and CH–π effects on interactions between nonpolar surfaces in water. *Angewandte Chemie*. 2007. Vol. 119, no. 36, p. 6957–6960.

112. HOF, Fraser, SCOFIELD, Denise M, SCHWEIZER, W Bernd and DIEDERICH, François. A weak attractive interaction between organic fluorine and an amide group. *Angewandte Chemie*. 2004. Vol. 116, no. 38, p. 5166–5169.

113. FISCHER, Felix Raoul, SCHWEIZER, W. Bernd and DIEDERICH, François. Substituent effects on the aromatic edge-to-face interaction. *Chemical Communications* [online]. 2008. Vol. 2, no. 34, p. 4031. DOI 10.1039/b809058k. Available from: http://xlink.rsc.org/?DOI=b809058k

114. GOLDBERG, Yuri and ALPER, Howard. Transition metal complexes of Tröger's base and their catalytic activity for the hydrosilylation of alkynes. *Tetrahedron letters*. 1995. Vol. 36, no. 3, p. 369–372.

115. MINDER, B, SCHÜRCH, M, MALLAT, T and BAIKER, A. Chiral nitrogen

compounds as new modifiers for the enantioselective hydrogenation of ethyl pyruvate. *Catalysis letters*. 1995. Vol. 31, no. 2–3, p. 143–151.

116. SHEN, Yu-Mei, ZHAO, Mei-Xin, XU, Jiaxi and SHI, Yian. An amine-promoted aziridination of chalcones. *Angewandte Chemie*. 2006. Vol. 118, no. 47, p. 8173–8176.

117. XU, Feng, TILLYER, Richard D, TSCHAEN, David M, GRABOWSKI, Edward J J and REIDER, Paul J. Enantioselective 1, 4-addition of aryllithium reagents to α, β-unsaturated tert-butyl esters in the presence of chiral additives. *Tetrahedron: Asymmetry*. 1998. Vol. 9, no. 10, p. 1651–1655.

118. CUENÚ, Fernando, ABONIA, Rodrigo, BOLAÑOS, Alberto and CABRERA, Armando. Synthesis, structural elucidation and catalytic activity toward a model Mizoroki–Heck C–C coupling reaction of the pyrazolic Tröger's base Pd 4 Cl 8 (PzTB) 2 complex. *Journal of Organometallic Chemistry*. 2011. Vol. 696, no. 9, p. 1834–1839.

119. TATIBOUËT, A, DEMEUNYNCK, M and LHOMME, J. Synthesis of polyfunctionalized Troeger's base analogs derived from ethacridine (6, 9-diamino-2-ethoxyacridine). *Synthetic communications*. 1996. Vol. 26, no. 23, p. 4375–4395.

120. TATIBOUËT, Arnaud, DEMEUNYNCK, Martine, SALEZ, Hervé, ARNAUD, Roger, LHOMME, Jean and COURSEILLE, Christian. Synthesis and physico-chemical properties of an acridine analog of the Troger's base. *Bulletin de la Société chimique de France*. 1997. Vol. 5, no. 134, p. 495–501.

121. VEALE, Emma B and GUNNLAUGSSON, Thorfinnur. Synthesis, photophysical, and DNA binding studies of fluorescent Troger's base derived 4-amino-1, 8-naphthalimide supramolecular clefts. *The Journal of organic chemistry*. 2010. Vol. 75, no. 16, p. 5513–5525.

122. ELMES, Robert B. P., ERBY, Marialuisa, BRIGHT, Sandra A., WILLIAMS, D. Clive and GUNNLAUGSSON, Thorfinnur. Photophysical and biological investigation of novel luminescent Ru(ii)-polypyridyl-1,8-naphthalimide Tröger's bases as cellular imaging agents. *Chemical Communications* [online]. 2012. Vol. 48, no. 20, p. 2588. DOI 10.1039/c2cc17274g. Available from: http://xlink.rsc.org/?DOI=c2cc17274g

123. BANERJEE, Swagata, VEALE, Emma B., PHELAN, Caroline M., MURPHY, Samantha A., TOCCI, Gillian M., GILLESPIE, Lisa J., FRIMANNSSON, Daniel O., KELLY, John M. and GUNNLAUGSSON, Thorfinnur. Recent advances in the development of 1,8-naphthalimide based DNA targeting binders, anticancer and fluorescent cellular imaging agents. *Chemical Society Reviews* [online]. 2013. Vol. 42, no. 4, p. 1601. DOI 10.1039/c2cs35467e. Available from: http://xlink.rsc.org/?DOI=c2cs35467e

124. MANDA, Bhaskar Reddy, ALLA, Manjula, GANJI, Roopa Jones and ADDLAGATTA, Anthony. Discovery of Tröger's base analogues as selective inhibitors against human breast cancer cell line: Design, synthesis and cytotoxic evaluation. *European journal of medicinal chemistry*. 2014. Vol. 86, p. 39–47.

125. KHOSHBIN, Meisa S, OVCHINNIKOV, Maxim V, MIRKIN, Chad A, GOLEN, James A and RHEINGOLD, Arnold L. Metallomacrocycles incorporating a hemilabile Troeger's base derived ligand. *Inorganic chemistry*. 2006. Vol. 45, no. 6, p. 2603–2609.

126. KIEHNE, Ulf, WEILANDT, Torsten and LÜTZEN, Arne. Self-Assembly of

Dinuclear Double-and Triple-Stranded Helicates from Bis (bipyridine) Ligands Derived from Tröger's Base Analogues. *European Journal of Organic Chemistry*. 2008. Vol. 2008, no. 12, p. 2056–2064.

127. WEILANDT, Torsten, KIEHNE, Ulf, SCHNAKENBURG, Gregor and LÜTZEN, Arne. Diastereoselective self-assembly of dinuclear heterochiral metallosupramolecular rhombs in a self-discriminating process. *Chemical Communications*. 2009. No. 17, p. 2320–2322.

128. DALLA FAVERA, Natalia, KIEHNE, Ulf, BUNZEN, Jens, HYTTEBALLE, Sophie, LÜTZEN, Arne and PIGUET, Claude. Intermetallic interactions within solvated polynuclear complexes: A misunderstood concept. *Angewandte Chemie*. 2010. Vol. 122, no. 1, p. 129–132.

129. SERGEYEV, Sergey. Recent Developments in Synthetic Chemistry, Chiral Separations, and Applications of Tröger 's Base Analogues. *Helvetica Chimica Acta* [online]. March 2009. Vol. 92, no. 3, p. 415–444. DOI 10.1002/hlca.200800329. Available from: http://doi.wiley.com/10.1002/hlca.200800329

130. YUAN, Chunxue, XIN, Qian, LIU, Huijun, WANG, Lei, JIANG, Minhua and TAO, Xutang. Λ-shaped optoelectronic materials based on Tröger's base. *Science China Chemistry* [online]. 9 April 2011. Vol. 54, no. 4, p. 587–595. DOI 10.1007/s11426-011-4224-z. Available from: http://link.springer.com/10.1007/s11426-011-4224-z

131. YUAN, Chun-Xue, TAO, Xu-Tang, REN, Yan, LI, Yang, YANG, Jia-Xiang, YU, Wen-Tao, WANG, Lei and JIANG, Min-Hua. Synthesis, structure, and aggregation-induced emission of a novel lambda (Λ)-shaped pyridinium salt based on tröger's base. *The Journal of Physical Chemistry C*. 2007. Vol. 111, no. 34, p. 12811–12816.

132. XI, He, YUAN, Chun-Xue, LI, Ye-Xin, LIU, Yang and TAO, Xu-Tang. Crystal structures and solid-state fluorescence of BODIPY dyes based on Λ-shaped Tröger's base. *CrystEngComm* [online]. 2012. Vol. 14, no. 6, p. 2087. DOI 10.1039/c2ce06260g. Available from: http://xlink.rsc.org/?DOI=c2ce06260g

133. XIN, Qian, TAO, Xu-Tang, WANG, Fu-Zhi, SUN, Jian-Liang, ZOU, De-Chun, WANG, Fa-Jun, LIU, Hui-Jun, LIU, Zhi, REN, Yan and JIANG, Min-Hua. Fluorene-based Tröger's base analogues: Potential electroluminescent materials. *Organic Electronics*. 2008. Vol. 9, no. 6, p. 1076–1086.

134. NEOGI, Ishita, JHULKI, Samik, GHOSH, Avijit, CHOW, Tahsin J. and MOORTHY, Jarugu Narasimha. Bifunctional organic materials for OLEDs based on Tröger's base: Subtle structural changes and significant differences in electroluminescence. *Organic Electronics* [online]. December 2014. Vol. 15, no. 12, p. 3766–3772. DOI 10.1016/j.orgel.2014.10.030. Available from: http://dx.doi.org/10.1016/j.orgel.2014.10.030

135. RAMÍREZ, Cristina L., PROCACCINI, Raúl, CHESTA, Carlos A., PARISE, Alejandro R. and VERA, D. Mariano A. Selective charge transfer in donor/acceptor systems bridged by Tröger base derivatives. *Organic Electronics* [online]. October 2013. Vol. 14, no. 10, p. 2564–2572. DOI 10.1016/j.orgel.2013.06.024. Available from: http://linkinghub.elsevier.com/retrieve/pii/S1566119913003078

136. WEISS, David S. and ABKOWITZ, Martin. Advances in Organic Photoconductor Technology. *Chemical Reviews* [online]. 13 January 2010. Vol. 110, no. 1, p. 479–526. [Accessed 21 February 2018]. DOI 10.1021/cr900173r. Available from: http://pubs.acs.org/doi/abs/10.1021/cr900173r

137. KIM, Hobeom, LIM, Kyung-Geun and LEE, Tae-Woo. Planar heterojunction

organometal halide perovskite solar cells: roles of interfacial layers. *Energy & Environmental Science*. 2016. Vol. 9, no. 1, p. 12–30.

138. YU, Ze and SUN, Licheng. Recent Progress on Hole-Transporting Materials for Emerging Organometal Halide Perovskite Solar Cells. *Advanced Energy Materials* [online]. June 2015. Vol. 5, no. 12, p. 1500213. DOI 10.1002/aenm.201500213. Available from: http://doi.wiley.com/10.1002/aenm.201500213

139. ALLARD, Sybille, FORSTER, Michael, SOUHARCE, Benjamin, THIEM, Heiko and SCHERF, Ullrich. Organic semiconductors for solution-processable field-effect transistors (OFETs). *Angewandte Chemie International Edition*. 2008. Vol. 47, no. 22, p. 4070–4098.

140. SHIROTA, Yasuhiko and KAGEYAMA, Hiroshi. Charge carrier transporting molecular materials and their applications in devices. *Chemical reviews*. 2007. Vol. 107, no. 4, p. 953–1010.

141. STROHRIEGL, Peter and GRAZULEVICIUS, Juozas V. Charge-Transporting Molecular Glasses. *Advanced Materials*. 2002. Vol. 14, no. 20, p. 1439–1452.

142. SEK, Danuta, GRABIEC, Eugenia, JANECZEK, Henryk, JARZABEK, Bozena, KACZMARCZYK, Bozena, DOMANSKI, Marian and IWAN, Agnieszka. Structure–properties relationship of linear and star-shaped imines with triphenylamine moieties as hole-transporting materials. *Optical Materials*. 2010. Vol. 32, no. 11, p. 1514–1525.

143. BARONAS, Paulius, KAZLAUSKAS, Karolis, GRUODIS, Alytis, JANKAUSKAS, Vygintas, TOMKEVICIENE, Ausra, SIMOKAITIENE, Jurate, GRAZULEVICIUS, Juozas Vidas and JURSENAS, Saulius. High-triplet-energy carbazole and fluorene tetrads. *Journal of Luminescence*. 2016. Vol. 169, p. 256–265.

144. MALINAUSKAS, Tadas, TOMKUTE-LUKSIENE, Daiva, SENS, Rüdiger, DASKEVICIENE, Maryte, SEND, Robert, WONNEBERGER, Henrike, JANKAUSKAS, Vygintas, BRUDER, Ingmar and GETAUTIS, Vytautas. Enhancing Thermal Stability and Lifetime of Solid-State Dye-Sensitized Solar Cells via Molecular Engineering of the Hole-Transporting Material Spiro-OMeTAD. *ACS Applied Materials & Interfaces* [online]. 3 June 2015. Vol. 7, no. 21, p. 11107–11116. DOI 10.1021/am5090385. Available from: http://xlink.rsc.org/?DOI=C6RA09878A

145. ABATE, Antonio, PAEK, Sanghyun, GIORDANO, Fabrizio, CORREA-BAENA, Juan-Pablo, SALIBA, Michael, GAO, Peng, MATSUI, Taisuke, KO, Jaejung, ZAKEERUDDIN, Shaik M and DAHMEN, Klaus H. Silolothiophene-linked triphenylamines as stable hole transporting materials for high efficiency perovskite solar cells. *Energy & Environmental Science*. 2015. Vol. 8, no. 10, p. 2946–2953.

146. NEOGI, Ishita, JHULKI, Samik, RAWAT, Madhu, ANAND, R S, CHOW, Tahsin J and MOORTHY, Jarugu Narasimha. Organic amorphous hole-transporting materials based on Tröger's Base: alternatives to NPB. *RSC Advances*. 2015. Vol. 5, no. 34, p. 26806–26810.

147. NEOGI, Ishita, JHULKI, Samik, GHOSH, Avijit, CHOW, Tahsin J. and MOORTHY, Jarugu Narasimha. Amorphous Host Materials Based on Tröger's Base Scaffold for Application in Phosphorescent Organic Light-Emitting Diodes. *ACS Applied Materials & Interfaces* [online]. 11 February 2015. Vol. 7, no. 5, p. 3298–3305. DOI 10.1021/am508004n. Available from: http://pubs.acs.org/doi/10.1021/am508004n

148. BORSENBERGER, P M, PAUTMEIER, L, RICHERT, R and BÄSSLER, H. Hole transport in 1, 1-bis (di-4-tolylaminophenyl) cyclohexane. *The Journal of chemical physics*. 1991. Vol. 94, no. 12, p. 8276–8281.

149. VERES, Janos, OGIER, Simon D, LEEMING, Stephen W, CUPERTINO, Domenico C and MOHIALDIN KHAFFAF, S. Low-k insulators as the choice of dielectrics in organic field-effect transistors. *Advanced Functional Materials*. 2003. Vol. 13, no. 3, p. 199–204.

150. THELAKKAT, Mukundan. Star-Shaped, Dendrimeric and Polymeric Triarylamines as Photoconductors and Hole Transport Materials for Electro-Optical Applications. *Macromolecular Materials and Engineering* [online]. 1 July 2002. Vol. 287, no. 7, p. 442. DOI 10.1002/1439-2054(20020701)287:7<442::AID-MAME442>3.0.CO;2-H. Available from: http://doi.wiley.com/10.1002/1439-2054%2820020701%29287%3A7%3C442%3A%3AAID-MAME442%3E3.0.CO%3B2-H

151. MALINAUSKAS, Tadas, DASKEVICIENE, Maryte, BUBNIENE, Giedre, PETRIKYTE, Ieva, RAISYS, Steponas, KAZLAUSKAS, Karolis, GAIDELIS, Valentas, JANKAUSKAS, Vygintas, MALDZIUS, Robertas, JURSENAS, Saulius and GETAUTIS, Vytautas. Phenylethenyl-substituted triphenylamines: Efficient, easily obtainable, and inexpensive hole-transporting materials. *Chemistry - A European Journal*. 2013. Vol. 19, no. 44, p. 15044–15056. DOI 10.1002/chem.201204064.

152. JEON, Nam Joong, LEE, Hag Geun, KIM, Young Chan, SEO, Jangwon, NOH, Jun Hong, LEE, Jaemin and SEOK, Sang Il. o-Methoxy substituents in spiro-OMeTAD for efficient inorganic–organic hybrid perovskite solar cells. *Journal of the American Chemical Society*. 2014. Vol. 136, no. 22, p. 7837–7840.

153. NUKADA, K, SATO, K and AKASAKI, Y. Substituent Effects on Drift Mobility of Benzidine Series Hole Transport Materials. *Electrophotography*. 1991. Vol. 30, p. 16–21.

154. ZHAO, Hongda, TANJUTCO, Christine and THAYUMANAVAN, S. Design and synthesis of stable triarylamines for hole-transport applications. *Tetrahedron Letters*. 2001. Vol. 42, no. 27, p. 4421–4424.

155. SUZUKI, Ken, KOBAYASHI, Tohru, NISHIKAWA, Takenobu, HORI, Yoji and HAGIWARA, Toshimitsu. *2, 2 (diarlyl) vinylphosphine compound, palladium catalyst thereof, and process for producing arylamine, diaryl, or arylalkyne with the catalyst*. 24 September 2002. Google Patents.

156. DEMEUNYNCK, Martine and TATIBOUËT, Arnaud. Chapter 1 Recent developments in Tröger's base chemistry. In : GRIBBLE, Gordon W and GILCHRIST, Thomas L B T - Progress in Heterocyclic Chemistry (eds.), *A Critical Review of the 1998 Literature preceded by two Chapters on Current Heterocyclic Topics* [online]. Elsevier, 1999. p. 1–20. [Accessed 21 February 2018]. ISBN 0959-6380. Available from: https://www.sciencedirect.com/science/article/pii/S0959638099800038

157. BUBNIENE, Giedre, MALINAUSKAS, Tadas, DASKEVICIENE, Maryte, JANKAUSKAS, Vygintas and GETAUTIS, Vytautas. Easily functionalizable carbazole based building blocks with extended conjugated systems for optoelectronic applications. *Tetrahedron*. 2010. Vol. 66, no. 17, p. 3199–3206. DOI 10.1016/j.tet.2010.02.086.

158. MALINAUSKAS, Tadas, TOMKUTE-LUKSIENE, Daiva, DASKEVICIENE, Maryte, JANKAUSKAS, Vygintas, JUSKA, Giedrius, GAIDELIS, Valentas, ARLAUSKAS, Kestutis and GETAUTIS, Vytautas. One small step in synthesis, a big leap in charge mobility: diphenylethenyl substituted triphenylamines. *Chemical communications (Cambridge, England)* [online]. 2011. Vol. 47, no. 27, p. 7770–2. DOI 10.1039/c1cc12700d. Available from: http://www.ncbi.nlm.nih.gov/pubmed/21643601

159. BRAUKYLA, Titas, SAKAI, Nobuya, DASKEVICIENE, Maryte, JANKAUSKAS, Vygintas, KAMARAUSKAS, Egidijus, MALINAUSKAS, Tadas, SNAITH, Henry J. and GETAUTIS, Vytautas. Synthesis and Investigation of the V-shaped Tröger′s Base Derivatives as Hole-transporting Materials. *Chemistry - An Asian Journal* [online]. 20 July 2016. Vol. 11, no. 14, p. 2049–2056. [Accessed 21 February 2018]. DOI 10.1002/asia.201600474. Available from: http://doi.wiley.com/10.1002/asia.201600474

160. MALINAUSKAS, Tadas, DASKEVICIENE, Maryte, BUBNIENE, Giedre, PETRIKYTE, Ieva, RAISYS, Steponas, KAZLAUSKAS, Karolis, GAIDELIS, Valentas, JANKAUSKAS, Vygintas, MALDZIUS, Robertas and JURSENAS, Saulius. Phenylethenyl-Substituted Triphenylamines: Efficient, Easily Obtainable, and Inexpensive Hole-Transporting Materials. *Chemistry-A European Journal*. 2013. Vol. 19, no. 44, p. 15044–15056.

161. TONG, Hui, DONG, Yongqiang, HONG, Yuning, HÄUSSLER, Matthias, LAM, Jacky W Y, SUNG, Herman H-Y, YU, Xiaoming, SUN, Jiaxin, WILLIAMS, Ian D and KWOK, Hoi Sing. Aggregation-induced emission: effects of molecular structure, solid-state conformation, and morphological packing arrangement on light-emitting behaviors of diphenyldibenzofulvene derivatives. *The Journal of Physical Chemistry C*. 2007. Vol. 111, no. 5, p. 2287–2294.

162. CONNELLY, Neil G and GEIGER, William E. Chemical redox agents for organometallic chemistry. *Chemical Reviews*. 1996. Vol. 96, no. 2, p. 877–910.

163. PAVLISHCHUK, Vitaly V and ADDISON, Anthony W. Conversion constants for redox potentials measured versus different reference electrodes in acetonitrile solutions at 25 C. *Inorganica Chimica Acta*. 2000. Vol. 298, no. 1, p. 97–102.

164. REISS, Howard and HELLER, Adam. The absolute potential of the standard hydrogen electrode: a new estimate. *The Journal of Physical Chemistry*. 1985. Vol. 89, no. 20, p. 4207–4213.

165. ALLARD, Sybille, FORSTER, Michael, SOUHARCE, Benjamin, THIEM, Heiko and SCHERF, Ullrich. Organic Semiconductors for Solution-Processable Field-Effect Transistors (OFETs). *Angewandte Chemie International Edition* [online]. 19 May 2008. Vol. 47, no. 22, p. 4070–4098. DOI 10.1002/anie.200701920. Available from: http://doi.wiley.com/10.1002/anie.200701920

166. SONNTAG, Martin, KREGER, Klaus, HANFT, Doris, STROHRIEGL, Peter, SETAYESH, Sepas and DE LEEUW, Dago. Novel star-shaped triphenylamine-based molecular glasses and their use in OFETs. *Chemistry of materials*. 2005. Vol. 17, no. 11, p. 3031–3039.

167. TONG, Qing-Xiao, LAI, Shiu-Lun, CHAN, Mei-Yee, LAI, Ka-Ho, TANG, Jian-Xin, KWONG, Hoi-Lun, LEE, Chun-Sing and LEE, Shuit-Tong. High T g triphenylamine-based starburst hole-transporting material for organic light-emitting devices. *Chemistry of Materials*. 2007. Vol. 19, no. 24, p. 5851–5855.

168. NALWA, Hari Singh. Handbook of organic conductive molecules and polymers. *Handbook of organic conductive molecules and polymers*. 1997. P. 87.

169. SALIBA, Michael, ZHANG, Wei, BURLAKOV, Victor M, STRANKS, Samuel D, SUN, Yao, BALL, James M, JOHNSTON, Michael B, GORIELY, Alain, WIESNER, Ulrich and SNAITH, Henry J. Plasmonic-Induced Photon Recycling in Metal Halide Perovskite Solar Cells. *Advanced Functional Materials*. 2015. Vol. 25, no. 31, p. 5038–5046.

170. SAPAROV, Bayrammurad and MITZI, David B. Organic–inorganic perovskites: structural versatility for functional materials design. *Chemical reviews*. 2016. Vol. 116, no. 7, p. 4558–4596.

171. SALIBA, Michael, MATSUI, Taisuke, SEO, Ji-Youn, DOMANSKI, Konrad, CORREA-BAENA, Juan-Pablo, NAZEERUDDIN, Mohammad Khaja, ZAKEERUDDIN, Shaik M, TRESS, Wolfgang, ABATE, Antonio and HAGFELDT, Anders. Cesium-containing triple cation perovskite solar cells: improved stability, reproducibility and high efficiency. *Energy & Environmental Science*. 2016. Vol. 9, no. 6, p. 1989–1997.

172. SALIBA, Michael, MATSUI, Taisuke, DOMANSKI, Konrad, SEO, Ji-Youn, UMMADISINGU, Amita, ZAKEERUDDIN, Shaik M, CORREA-BAENA, Juan-Pablo, TRESS, Wolfgang R, ABATE, Antonio and HAGFELDT, Anders. Incorporation of rubidium cations into perovskite solar cells improves photovoltaic performance. *Science*. 2016. Vol. 354, no. 6309, p. 206–209.

173. BURSCHKA, Julian, DUALEH, Amalie, KESSLER, Florian, BARANOFF, Etienne, CEVEY-HA, Ngoc-Lê, YI, Chenyi, NAZEERUDDIN, Mohammad K and GRÄTZEL, Michael. Tris (2-(1 H-pyrazol-1-yl) pyridine) cobalt (III) as p-type dopant for organic semiconductors and its application in highly efficient solid-state dye-sensitized solar cells. *Journal of the American Chemical Society*. 2011. Vol. 133, no. 45, p. 18042–18045.

174. JAEGER, Claus, BILKE, Roland, HEIM, Michael, HAARER, Dietrich, KARICKAL, Harridas and THELAKKAT, Mukundan. Novel hole transporting poly (triphenyldiamine) s for application in hybrid solar cells. In : *Organic Photovoltaics*. International Society for Optics and Photonics, 2001. p. 104–112.

175. KIM, Hui-Seon, LEE, Chang-Ryul, IM, Jeong-Hyeok, LEE, Ki-Beom, MOEHL, Thomas, MARCHIORO, Arianna, MOON, Soo-Jin, HUMPHRY-BAKER, Robin, YUM, Jun-Ho and MOSER, Jacques E. Lead iodide perovskite sensitized all-solid-state submicron thin film mesoscopic solar cell with efficiency exceeding 9%. *Scientific reports*. 2012. Vol. 2, p. 591.

176. ZHOU, Huanping, CHEN, Qi, LI, Gang, LUO, Song, SONG, Tze-bing, DUAN, Hsin-Sheng, HONG, Ziruo, YOU, Jingbi, LIU, Yongsheng and YANG, Yang. Interface engineering of highly efficient perovskite solar cells. *Science*. 2014. Vol. 345, no. 6196, p. 542–546.

177. NISHIMURA, Hidetaka, ISHIDA, Naoki, SHIMAZAKI, Ai, WAKAMIYA, Atsushi, SAEKI, Akinori, SCOTT, Lawrence T and MURATA, Yasujiro. Hole-transporting materials with a two-dimensionally expanded π-system around an azulene core for efficient perovskite solar cells. *Journal of the American Chemical Society*. 2015. Vol. 137, no. 50, p. 15656–15659.

178. MARINOVA, Nevena, TRESS, Wolfgang, HUMPHRY-BAKER, Robin, DAR, M Ibrahim, BOJINOV, Vladimir, ZAKEERUDDIN, Shaik Mohammed,

NAZEERUDDIN, Mohammad Khaja and GRÄTZEL, Michael. Light harvesting and charge recombination in CH3NH3PbI3 perovskite solar cells studied by hole transport layer thickness variation. *ACS nano*. 2015. Vol. 9, no. 4, p. 4200–4209.

179. KWON, Young Soo, LIM, Jongchul, SONG, Inwoo, SONG, In Young, SHIN, Won Suk, MOON, Sang-Jin and PARK, Taiho. Chemical compatibility between a hole conductor and organic dye enhances the photovoltaic performance of solid-state dye-sensitized solar cells. *Journal of Materials Chemistry*. 2012. Vol. 22, no. 17, p. 8641–8648.

180. MA, Shuying, ZHANG, Hua, ZHAO, Ning, CHENG, Yibing, WANG, Mingkui, SHEN, Yan and TU, Guoli. Spiro-thiophene derivatives as hole-transport materials for perovskite solar cells. *Journal of Materials Chemistry A*. 2015. Vol. 3, no. 23, p. 12139–12144.

181. SARAGI, T P I, SPEHR, T, SIEBERT, A, FUHRMANN-LIEKER, T and SALBECK, J. Spiro Compounds for Organic Optoelectronic. *Chem. Rev.* [online]. 2007. Vol. 107, no. mmCmm, p. 1011–1065. DOI 10.1021/cr0501341. Available from: http://pubs3.acs.org/acs/journals/doilookup?in_doi=10.1021/cr0501341

182. BRAUKYLA, Titas, SAKAI, Nobuya, DASKEVICIENE, Maryte, JANKAUSKAS, Vygintas, KAMARAUSKAS, Egidijus, KOMSKIS, Regimantas, MALINAUSKAS, Tadas, JURSENAS, Saulius, SNAITH, Henry J. and GETAUTIS, Vytautas. V-Shaped Hole-Transporting TPD Dimers Containing Tröger's Base Core. *The Journal of Physical Chemistry C* [online]. 18 May 2017. Vol. 121, no. 19, p. 10267–10274. DOI 10.1021/acs.jpcc.6b11880. Available from: http://pubs.acs.org/doi/10.1021/acs.jpcc.6b11880

183. CEKAVICIUTE, M, SIMOKAITIENE, J, JANKAUSKAS, V, RAISYS, S, KAZLAUSKAS, K, JURSENAS, S and GRAZULEVICIUS, J V. Structure–Properties Relationship of Phenylethenyl-Substituted Triphenylamines. *The Journal of Physical Chemistry C*. 2013. Vol. 117, no. 16, p. 7973–7980.

184. REGHU, Renji R, SIMOKAITIENE, Jurate, GRAZULEVICIUS, Juozas V, RAISYS, Steponas, KAZLAUSKAS, Karolis, JURSENAS, Saulius, JANKAUSKAS, Vygintas and REINA, Antonio. Synthesis and properties of hole-transporting triphenylamine-derived dendritic compounds. *Dyes and Pigments*. 2015. Vol. 115, p. 135–142.

185. TERRY, G C, UFFINDELL, V E and WILLETS, F W. Triplet state of triphenylamine. *Nature*. 1969. Vol. 223, no. 5210, p. 1050.

186. BAGNICH, Sergey A, ATHANASOPOULOS, Stavros, RUDNICK, Alexander, SCHROEGEL, Pamela, BAUER, Irene, GREENHAM, Neil C, STROHRIEGL, Peter and KÖHLER, Anna. Excimer formation by steric twisting in carbazole and triphenylamine-based host materials. *The Journal of Physical Chemistry C*. 2015. Vol. 119, no. 5, p. 2380–2387.

187. RAISYS, S., KAZLAUSKAS, K., DASKEVICIENE, M., MALINAUSKAS, T., GETAUTIS, V., JURSENAS, S., MERTZ, J., TRETIAK, S., BLANCHARD-DESCE, M., JURSENAS, S., GETAUTIS, V., BELJONNE, D. and SAMUEL, I. D. W. Exciton diffusion enhancement in triphenylamines via incorporation of phenylethenyl sidearms. *Journal of Materials Chemistry C* [online]. 2014. Vol. 2, no. 24, p. 4792. DOI 10.1039/c4tc00262h. Available from: http://xlink.rsc.org/?DOI=c4tc00262h

188. MENKE, Torben, RAY, Debdutta, KLEEMANN, Hans, HEIN, Moritz P, LEO, Karl

and RIEDE, Moritz. Highly efficient p-dopants in amorphous hosts. *Organic Electronics*. 2014. Vol. 15, no. 2, p. 365–371.

189. MIMAITE, Viktorija, GRAZULEVICIUS, Juozas Vidas, LAURINAVICIUTE, Rasa, VOLYNIUK, Dmytro, JANKAUSKAS, Vygintas and SINI, Gjergji. Can hydrogen bonds improve the hole-mobility in amorphous organic semiconductors? Experimental and theoretical insights. *Journal of Materials Chemistry C* [online]. 2015. Vol. 3, no. 44, p. 11660–11674. DOI 10.1039/C5TC02534F. Available from: http://xlink.rsc.org/?DOI=C5TC02534F

190. KERUCKAS, Jonas, LYGAITIS, Ramunas, SIMOKAITIENE, Jurate, GRAZULEVICIUS, Juozas Vidas, JANKAUSKAS, Vygintas and SINI, Gjergji. Influence of methoxy groups on the properties of 1, 1-bis (4-aminophenyl) cyclohexane based arylamines: experimental and theoretical approach. *Journal of Materials Chemistry*. 2012. Vol. 22, no. 7, p. 3015–3027.

191. GUDEIKA, Dalius, GRAZULEVICIUS, Juozas Vidas, SINI, Gjergji, BUCINSKAS, Audrius, JANKAUSKAS, Vygintas, MIASOJEDOVAS, Arunas and JURSENAS, Saulius. New derivatives of triphenylamine and naphthalimide as ambipolar organic semiconductors: Experimental and theoretical approach. *Dyes and Pigments*. 2014. Vol. 106, p. 58–70.

192. CHUEH, Chu-Chen, LI, Chang-Zhi and JEN, Alex K-Y. Recent progress and perspective in solution-processed Interfacial materials for efficient and stable polymer and organometal perovskite solar cells. *Energy & Environmental Science*. 2015. Vol. 8, no. 4, p. 1160–1189.

193. ZHOU, Zhongmin, PANG, Shuping, LIU, Zhihong, XU, Hongxia and CUI, Guanglei. Interface engineering for high-performance perovskite hybrid solar cells. *Journal of Materials Chemistry A*. 2015. Vol. 3, no. 38, p. 19205–19217.

194. KAZIM, Samrana, NAZEERUDDIN, Mohammad Khaja, GRÄTZEL, Michael and AHMAD, Shahzada. Perovskite as light harvester: a game changer in photovoltaics. *Angewandte Chemie International Edition*. 2014. Vol. 53, no. 11, p. 2812–2824.

195. YANG, Woon Seok, NOH, Jun Hong, JEON, Nam Joong, KIM, Young Chan, RYU, Seungchan, SEO, Jangwon and SEOK, Sang Il. High-performance photovoltaic perovskite layers fabricated through intramolecular exchange. *Science*. 2015. Vol. 348, no. 6240, p. 1234–1237.

196. SALIBA, Michael, ORLANDI, Simonetta, MATSUI, Taisuke, AGHAZADA, Sadig, CAVAZZINI, Marco, CORREA-BAENA, Juan-Pablo, GAO, Peng, SCOPELLITI, Rosario, MOSCONI, Edoardo and DAHMEN, Klaus-Hermann. A molecularly engineered hole-transporting material for efficient perovskite solar cells. *Nature Energy*. 2016. Vol. 1, no. 2, p. 15017.

197. DASKEVICIENE, Maryte, PAEK, Sanghyun, WANG, Zhiping, MALINAUSKAS, Tadas, JOKUBAUSKAITE, Gabriele, RAKSTYS, Kasparas, CHO, Kyung Taek, MAGOMEDOV, Artiom, JANKAUSKAS, Vygintas, AHMAD, Shahzada, SNAITH, Henry J., GETAUTIS, Vytautas and NAZEERUDDIN, Mohammad Khaja. Carbazole-based enamine: Low-cost and efficient hole transporting material for perovskite solar cells. *Nano Energy* [online]. 2017. Vol. 32, no. January, p. 551–557. DOI 10.1016/j.nanoen.2017.01.015. Available from: http://dx.doi.org/10.1016/j.nanoen.2017.01.015

198. PUODZIUKYNAITE, E, BURBULIS, E, GRAZULEVICIUS, J V, GETAUTIS, V and JANKAUSKAS, J. Carbazole-based bis (enamines) as effective charge-

transporting amorphous molecular materials. *Synthetic Metals*. 2008. Vol. 158, no. 21–24, p. 993–998.

199. BRAUKYLA, Titas, XIA, Rui, DASKEVICIENE, Maryte, MALINAUSKAS, Tadas, GRUODIS, Alytis, JANKAUSKAS, Vygintas, ROLDÁN-CARMONA, Cristina, MOMBLONA, Cristina, GETAUTIS, Vytautas, and NAZEERUDDIN, Mohammad Khaja. Inexpensive Hole Transporting Materials Derived from Tröger's Base Afford Efficient and Stable Perovskite Solar Cells. *Angewandte Chemie* [online]. 2019. DOI 10.1002/anie.201903705. Available from: https://doi.org/10.1002/anie.201903705

200. NAZEERUDDIN, Mohammad K, DE ANGELIS, Filippo, FANTACCI, Simona, SELLONI, Annabella, VISCARDI, Guido, LISKA, Paul, ITO, Seigo, TAKERU, Bessho and GRÄTZEL, Michael. Combined experimental and DFT-TDDFT computational study of photoelectrochemical cell ruthenium sensitizers. *Journal of the American Chemical Society*. 2005. Vol. 127, no. 48, p. 16835–16847.

201. NAZEERUDDIN, Mohammad K, PECHY, Peter, RENOUARD, Thierry, ZAKEERUDDIN, Shaik M, HUMPHRY-BAKER, Robin, COMTE, Pascal, LISKA, Paul, CEVEY, Le, COSTA, Emiliana and SHKLOVER, Valery. Engineering of efficient panchromatic sensitizers for nanocrystalline TiO2-based solar cells. *Journal of the American Chemical Society*. 2001. Vol. 123, no. 8, p. 1613–1624.

202. YELLA, Aswani, LEE, Hsuan-Wei, TSAO, Hoi Nok, YI, Chenyi, CHANDIRAN, Aravind Kumar, NAZEERUDDIN, Md Khaja, DIAU, Eric Wei-Guang, YEH, Chen-Yu, ZAKEERUDDIN, Shaik M and GRÄTZEL, Michael. Porphyrin-sensitized solar cells with cobalt (II/III)–based redox electrolyte exceed 12 percent efficiency. *science*. 2011. Vol. 334, no. 6056, p. 629–634.

203. YELLA, Aswani, MAI, Chi-Lun, ZAKEERUDDIN, Shaik M, CHANG, Shu-Nung, HSIEH, Chi-Hung, YEH, Chen-Yu and GRÄTZEL, Michael. Molecular engineering of push–pull porphyrin dyes for highly efficient dye-sensitized solar cells: The role of benzene spacers. *Angewandte Chemie International Edition*. 2014. Vol. 53, no. 11, p. 2973–2977.

204. DAI, Xue-Xin, FENG, Hao-Lin, CHEN, Wen-Jia, YANG, Yi, NIE, Le-Bin, WANG, Lingyun, KUANG, Dai-Bin, MEIER, Herbert and CAO, Derong. Synthesis and photovoltaic performance of asymmetric di-anchoring organic dyes. *Dyes and Pigments*. 2015. Vol. 122, p. 13–21.

205. ZHANG, Fan, LUO, Yan-hong, SONG, Jin-sheng, GUO, Xiao-zhi, LIU, Wei-li, MA, Chun-ping, HUANG, Yong, GE, Mao-fa, BO, Zhishan and MENG, Qing-Bo. Triphenylamine-based dyes for dye-sensitized solar cells. *Dyes and Pigments*. 2009. Vol. 81, no. 3, p. 224–230.

206. HAGFELDT, Anders, BOSCHLOO, Gerrit, SUN, Licheng, KLOO, Lars and PETTERSSON, Henrik. Dye-sensitized solar cells. *Chemical reviews*. 2010. Vol. 110, no. 11, p. 6595–6663.

207. KAKIAGE, Kenji, AOYAMA, Yohei, YANO, Toru, OTSUKA, Takahiro, KYOMEN, Toru, UNNO, Masafumi and HANAYA, Minoru. An achievement of over 12 percent efficiency in an organic dye-sensitized solar cell. *Chemical Communications*. 2014. Vol. 50, no. 48, p. 6379–6381.

208. BAHETI, Abhishek, JUSTIN THOMAS, K R, LI, Chun-Ting, LEE, Chuan-Pei and HO, Kuo-Chuan. Fluorene-based sensitizers with a phenothiazine donor: effect of mode of donor tethering on the performance of dye-sensitized solar cells. *ACS*

applied materials & interfaces. 2015. Vol. 7, no. 4, p. 2249–2262.

209. LIANG, Mao and CHEN, Jun. Arylamine organic dyes for dye-sensitized solar cells. *Chemical Society Reviews*. 2013. Vol. 42, no. 8, p. 3453–3488.

210. MISHRA, Amaresh, FISCHER, Markus K R and BÄUERLE, Peter. Metal-free organic dyes for dye-sensitized solar cells: From structure: Property relationships to design rules. *Angewandte Chemie International Edition*. 2009. Vol. 48, no. 14, p. 2474–2499.

211. JIA, Hailang, SHEN, Kang, JU, Xuehai, ZHANG, Mingdao and ZHENG, Hegen. Enhanced performance of dye-sensitized solar cells with Y-shaped organic dyes containing di-anchoring groups. *New Journal of Chemistry*. 2016. Vol. 40, no. 3, p. 2799–2805.

212. OOYAMA, Yousuke and HARIMA, Yutaka. Photophysical and Electrochemical Properties, and Molecular Structures of Organic Dyes for Dye-Sensitized Solar Cells. *ChemPhysChem*. 2012. Vol. 13, no. 18, p. 4032–4080.

213. TIAN, Haining, YANG, Xichuan, CHEN, Ruikui, ZHANG, Rong, HAGFELDT, Anders and SUN, Licheng. Effect of different dye baths and dye-structures on the performance of dye-sensitized solar cells based on triphenylamine dyes. *The Journal of Physical Chemistry C*. 2008. Vol. 112, no. 29, p. 11023–11033.

214. REN, Xiaoming, JIANG, Shenghui, CHA, Mingyang, ZHOU, Gang and WANG, Zhong-Sheng. Thiophene-bridged double D-π-A dye for efficient dye-sensitized solar cell. *Chemistry of Materials*. 2012. Vol. 24, no. 17, p. 3493–3499.

215. ABBOTTO, Alessandro, MANFREDI, Norberto, MARINZI, Chiara, DE ANGELIS, Filippo, MOSCONI, Edoardo, YUM, Jun-Ho, XIANXI, Zhang, NAZEERUDDIN, Mohammad K and GRÄTZEL, Michael. Di-branched di-anchoring organic dyes for dye-sensitized solar cells. *Energy & Environmental Science*. 2009. Vol. 2, no. 10, p. 1094–1101.

216. SIROHI, Reenu, KIM, Dong Hee, YU, Soo-Chang and LEE, Sang Hee. Novel di-anchoring dye for DSSC by bridging of two mono anchoring dye molecules: a conformational approach to reduce aggregation. *Dyes and Pigments*. 2012. Vol. 92, no. 3, p. 1132–1137.

217. URNIKAITE, Simona, MALINAUSKAS, Tadas, BRUDER, Ingmar, SEND, Robert, GAIDELIS, Valentas, SENS, Rüdiger and GETAUTIS, Vytautas. Organic Dyes with Hydrazone Moieties: A Study of Correlation between Structure and Performance in the Solid-State Dye-Sensitized Solar Cells. *The Journal of Physical Chemistry C* [online]. 17 April 2014. Vol. 118, no. 15, p. 7832–7843. DOI 10.1021/jp500527d. Available from: http://pubs.acs.org/doi/abs/10.1021/jp500527d

218. FAROUGHI, Masoud, TRY, Andrew C and TURNER, Peter. 2, 4, 8, 10-Tetrabromo-6H, 12H-5, 11-methanodibenzo [b, f][1, 5] diazocine. *Acta Crystallographica Section E: Structure Reports Online*. 2006. Vol. 62, no. 9, p. o3893–o3894.

219. URNIKAITE, Simona, BRAUKYLA, Titas, MAGOMEDOV, Artiom, KAMARAUSKAS, Egidijus, MALINAUSKAS, Tadas and GETAUTIS, Vytautas. A structural study of Troger's base scaffold-based dyes for DSSC applications. *Dyes and Pigments* [online]. August 2017. Vol. 143, p. 48–61. DOI 10.1016/j.dyepig.2017.04.012. Available from: http://linkinghub.elsevier.com/retrieve/pii/S0143720816315091

220. LEE, Min-Woo, CHA, Su-Bong, YANG, Su-Jin, PARK, Se-Woong, KIM, Kyung-Kon, PARK, Nam-Gyu and LEE, Duck-Hyung. Synthesis of Organic Dyes with Linkers Between 9,9-Dimethylfluorenyl Terminal and α-Cyanoacrylic Acid Anchor, Effect of the Linkers on UV-Vis Absorption Spectra, and Photovoltaic Properties in Dye-Sensitized Solar Cells. *Bulletin of the Korean Chemical Society* [online]. 20 October 2009. Vol. 30, no. 10, p. 2269–2279. DOI 10.5012/bkcs.2009.30.10.2269. Available from: http://koreascience.or.kr/journal/view.jsp?kj=JCGMCS&py=2009&vnc=v30n10&sp=2269

221. QIN, Peng, TETREAULT, Nicolas, DAR, M Ibrahim, GAO, Peng, MCCALL, Keri L, RUTTER, Simon R, OGIER, Simon D, FORREST, Neil D, BISSETT, James S and SIMMS, Michael J. A novel oligomer as a hole transporting material for efficient perovskite solar cells. *Advanced Energy Materials*. 2015. Vol. 5, no. 2.

222. LEBLANC, S E and FOGLER, H Scott. The role of conduction/valence bands and redox potential in accelerated mineral dissolution. *AIChE journal*. 1986. Vol. 32, no. 10, p. 1702–1709.

223. PARTHASARATHY, Venkatakrishnan, PANDEY, Ravindra, STOLTE, Matthias, GHOSH, Sampa, CASTET, Frédéric, WÜRTHNER, Frank, DAS, Puspendu Kumar and BLANCHARD-DESCE, Mireille. Combination of Cyanine Behaviour and Giant Hyperpolarisability in Novel Merocyanine Dyes: Beyond the Bond Length Alternation (BLA) Paradigm. *Chemistry–A European Journal*. 2015. Vol. 21, no. 40, p. 14211–14217.

224. DOLEZEL, Jan, HIRSOVA, Petra, OPLETALOVA, Veronika, DOHNAL, Jiri, MARCELA, Vejsova, KUNES, Jiri and JAMPILEK, Josef. Rhodanineacetic acid derivatives as potential drugs: preparation, hydrophobic properties and antifungal activity of (5-arylalkylidene-4-oxo-2-thioxo-1, 3-thiazolidin-3-yl) acetic acids. *Molecules*. 2009. Vol. 14, no. 10, p. 4197–4212.

225. PENG, Bo, YANG, Siqi, LI, Lanlan, CHENG, Fangyi and CHEN, Jun. A density functional theory and time-dependent density functional theory investigation on the anchor comparison of triarylamine-based dyes. *The Journal of chemical physics*. 2010. Vol. 132, no. 3, p. 34305.

226. SIVANADANAM, Jagadeeswari, GANESAN, Paramaguru, GAO, Peng, NAZEERUDDIN, Mohammad K. and RAJALINGAM, Renganathan-. Impact of π Spacers on the Optical, Electrochemical and Photovoltaic performance of D-(π-A) 2 Based Sensitizers. *ChemistrySelect* [online]. 24 May 2018. Vol. 3, no. 19, p. 5269–5276. DOI 10.1002/slct.201800977. Available from: http://doi.wiley.com/10.1002/slct.201800977

227. BENDER, Vitor C, MARCHESAN, Tiago B and ALONSO, J Marcos. Solid-state lighting: a concise review of the state of the art on LED and OLED modeling. *IEEE Industrial Electronics Magazine*. 2015. Vol. 9, no. 2, p. 6–16.

228. HONG, Yuning, LAM, Jacky W Y and TANG, Ben Zhong. Aggregation-induced emission. *Chemical Society Reviews* [online]. 2011. Vol. 40, no. 11, p. 5361–5388. DOI 10.1039/C1CS15113D. Available from: http://dx.doi.org/10.1039/C1CS15113D

229. ZHAO, Zujin, LAM, Jacky W. Y. and TANG, Ben Zhong. Tetraphenylethene: a versatile AIE building block for the construction of efficient luminescent materials for organic light-emitting diodes. *Journal of Materials Chemistry* [online]. 2012. Vol. 22, no. 45, p. 23726. DOI 10.1039/c2jm31949g. Available from:

http://xlink.rsc.org/?DOI=c2jm31949g

230. LUO, Jingdong, XIE, Zhiliang, LAM, Jacky W Y, CHENG, Lin, CHEN, Haiying, QIU, Chengfeng, KWOK, Hoi Sing, ZHAN, Xiaowei, LIU, Yunqi and ZHU, Daoben. Aggregation-induced emission of 1-methyl-1, 2, 3, 4, 5-pentaphenylsilole. *Chemical communications*. 2001. No. 18, p. 1740–1741.

231. ZHAO, Zujin, W. Y. LAM, Jacky and ZHONG TANG, Ben. Aggregation-Induced Emission of Tetraarylethene Luminogens. *Current Organic Chemistry* [online]. 1 November 2010. Vol. 14, no. 18, p. 2109–2132. DOI 10.2174/138527210793351571. Available from: http://www.eurekaselect.com/openurl/content.php?genre=article&issn=1385-2728&volume=14&issue=18&spage=2109

232. DE MELLO, John C, WITTMANN, H Felix and FRIEND, Richard H. An improved experimental determination of external photoluminescence quantum efficiency. *Advanced materials*. 1997. Vol. 9, no. 3, p. 230–232.

233. MIYAMOTO, Eiichi, YAMAGUCHI, Y and YOKOYAMA, M. Ionization potential of organic pigment film by atmospheric photoelectron emission analysis. *Electrophotography*. 1989. Vol. 28, p. 364–370.

234. CARDONA, Manuel and LEY, Lothar. Photoemission in solids I. *Photoemission in Solids I: General Principles*. 1978.

235. VAEZI-NEJAD, S M. Xerographic time of flight experiment for the determination of drift mobility in high resistivity semiconductors. *International Journal of Electronics Theoretical and Experimental*. 1987. Vol. 62, no. 3, p. 361–384.

236. CHAN, ARCHIE Y C and JUHASZ, C. Xerographic-mode transient charge technique for probing drift mobility in high-resistivity materials. *International Journal of Electronics Theoretical and Experimental*. 1987. Vol. 62, no. 4, p. 625–632.

237. WOJCIECHOWSKI, Konrad, LEIJTENS, Tomas, SIPROVA, Svetlana, SCHLUETER, Christoph, HÖRANTNER, Maximilian T, WANG, Jacob Tse-Wei, LI, Chang-Zhi, JEN, Alex K-Y, LEE, Tien-Lin and SNAITH, Henry J. C60 as an efficient n-type compact layer in perovskite solar cells. *The journal of physical chemistry letters*. 2015. Vol. 6, no. 12, p. 2399–2405.

238. AHLRICHS, Reinhart, BÄR, Michael, HÄSER, Marco, HORN, Hans and KÖLMEL, Christoph. Electronic structure calculations on workstation computers: The program system turbomole. *Chemical Physics Letters*. 1989. Vol. 162, no. 3, p. 165–169.

239. LEE, Chengteh, YANG, Weitao and PARR, Robert G. Development of the Colle-Salvetti correlation-energy formula into a functional of the electron density. *Physical review B*. 1988. Vol. 37, no. 2, p. 785.

240. BECKE, Axel D. Density-functional thermochemistry. III. The role of exact exchange. *The Journal of chemical physics*. 1993. Vol. 98, no. 7, p. 5648–5652.

241. SCHÄFER, Ansgar, HORN, Hans and AHLRICHS, Reinhart. Fully optimized contracted Gaussian basis sets for atoms Li to Kr. *The Journal of Chemical Physics*. 1992. Vol. 97, no. 4, p. 2571–2577.

242. WEIGEND, Florian and AHLRICHS, Reinhart. Balanced basis sets of split valence, triple zeta valence and quadruple zeta valence quality for H to Rn: Design and assessment of accuracy. *Physical Chemistry Chemical Physics*. 2005. Vol. 7, no. 18,

p. 3297–3305.

243. STEFFEN, Claudia, THOMAS, Klaus, HUNIAR, Uwe, HELLWEG, Arnim, RUBNER, Oliver and SCHROER, Alexander. TmoleX—a graphical user interface for TURBOMOLE. *Journal of computational chemistry*. 2010. Vol. 31, no. 16, p. 2967–2970.

244. KODERA, T. and TORIZUKA, K. (Mitsubishi Paper Mills, Ltd.) Jpn. Kokai Tokkyo Koho. JP 11043458. 1999. Jpn. Kokai Tokkyo Koho.

245. HWANG, Seok-Hwan, KIM, Young-Kook, LEE, Chang-Ho, LEE, Seok-Jong, YANG, Seung-gak and KIM, Hee-Yeon. Phenylcarbazole-based compound and organic electroluminescent device employing the same. 20080107919. September 2008. US Patent.

246. SEKI, M. and UENO, K. Materials for Organic Electroluminescent Devices. JP 2008288270. 2008. Japan.

247. KUHN, A., BRUDER, Ingmar, SENS, Rüdiger, PSCHIRER, Neil Gregory and ERK, Peter. Dye-sensitized Solar Cell with Oxide Semiconductors. 2012104742. 2012. WO Patent.

248. ŠTURALA, Jiří and CIBULKA, Radek. Synthesis of symmetrical dinitro-and diamino-substituted Tröger's base analogues. *European Journal of Organic Chemistry*. 2012. No. 36, p. 7066–7074. DOI 10.1002/ejoc.201201188.

249. YUAN, Wang Zhang, LU, Ping, CHEN, Shuming, LAM, Jacky W.Y. Y, WANG, Zhiming, LIU, Yang, KWOK, Hoi Sing, MA, Yuguang and TANG, Ben Zhong. Changing the Behavior of Chromophores from Aggregation-Caused Quenching to Aggregation-Induced Emission: Development of Highly Efficient Light Emitters in the Solid State. *Advanced Materials* [online]. 8 March 2010. Vol. 22, no. 19, p. 2159–2163. DOI 10.1002/adma.200904056. Available from: http://doi.wiley.com/10.1002/adma.200904056

250. POULSEN, Pernille H, FEU, Karla Santos, PAZ, Bruno Matos, JENSEN, Frank and JØRGENSEN, Karl Anker. Organocatalytic Asymmetric 1, 6-Addition/1, 4-Addition Sequence to 2, 4-Dienals for the Synthesis of Chiral Chromans. *Angewandte Chemie*. 2015. Vol. 127, no. 28, p. 8321–8325.

8. CURRICULUM VITAE

Personal information

Name, Surname	Titas Braukyla
Date of birth	1988 08 04
Place of birth	Lithuania
Nationality	Lithuanian
e-mail	t.braukyla@gmail.com, titas.braukyla@ktu.lt

Education

2013–2019	Kaunas University of Technology - PhD studies, Chemistry
2012 autumn	University of Applied Sciences Upper Austria (FH OÖ), ERASMUS exchange program. Bio- and Environmental Technology
2011–2013	Kaunas University of Technology - Master of Engineering Sciences, Chemical Engineering
2007–2011	Kaunas University of Technology - Bachelor of Chemistry, Applied Chemistry
1999–2007	Marijampolės marijonų secondary school, Marijampolė, secondary school
1995–1999	„Želmenėliai", Marijampolė, primary school

Work experience

2018.04–present	Junior researcher of the project
2015.07–2017.09	Project Engineer
2016.07–2017.02	Junior researcher of the project
2013.09–2015.03	Junior researcher of the project

Languages

Lithuanian - mother tongue. English (C2), German (B1), Russian (A2).

Scientific work

2013.09 - present Research in the scientific group of prof. dr. Vytautas Getautis. Aims of the work: synthesis and characterization of novel stable organic photosemiconductors and dyes forthe applications in electronics (PSC, DSSC, OLED).

2012.09-12 Research work in the scientific group of prof. dr. Alexander Jäger (Upper Austria University Of Applied Sciences)
Aims of the work: Conversion of plant biomass into biodiesel via biotechnological pathway.

2008–2011 5 times participant of the Research council of Lithuania projects „*Student scientific practice", „Student scientific research"* and *„ Promoting student research activities"*.

9. LIST OF AUTHOR'S PUBLICATIONS AND CONFERENCES

Publications in peer-reviewed journals

1. Braukyla, Titas; Sakai, Nobuya; Daškevičienė, Marytė; Jankauskas, Vygintas; Kamarauskas, Egidijus; Malinauskas, Tadas; Snaith, Henry J.; Getautis, Vytautas. Synthesis and investigation of the V-shaped Trogers base derivatives as hole-transporting materials // Chemistry - An Asian journal. Weinheim : Wiley-Blackwell. ISSN 1861-4728. eISSN 1861-471X. 2016, Vol. 11, iss. 14, p. 2049-2056. DOI: 10.1002/asia.201600474. [Current Contents; Scopus; Compendex; MEDLINE; Chemical abstracts; Science Citation Index Expanded (Web of Science)] [IF: 4,083; AIF: 5,649; quartile: Q1 (2016, InCites JCR SCIE)]
2. Urnikaitė, Simona; Braukyla, Titas; Magomedov, Artiom; Kamarauskas, Egidijus; Malinauskas, Tadas; Getautis, Vytautas. A structural study of Troger's base scaffold-based dyes for DSSC applications // Dyes and pigments. Oxford : Elsevier. ISSN 0143-7208. eISSN 1873-3743. 2017, vol. 143, p. 48-61. DOI: 10.1016/j.dyepig.2017.04.012. [Academic Search Research & Development; Academic Search Complete; Scopus; Science Citation Index Expanded (Web of Science)] [IF: 3,767; AIF: 2,926; quartile: Q1 (2017, InCites JCR SCIE)]
3. Braukyla, Titas; Sakai, Nobuya; Daskeviciene, Maryte; Jankauskas, Vygintas; Kamarauskas, Egidijus; Komskis, Regimantas; Malinauskas, Tadas; Jursenas, Saulius; Snaith, Henry J.; Getautis, Vytautas. V-shaped hole-transporting TPD dimers containing Troöger's base core // Journal of physical chemistry C. Washington, NW : American Chemical Society. ISSN 1932-7447. eISSN 1932-7455. 2017, vol. 121, iss. 19, p. 10267-10274. DOI: 10.1021/acs.jpcc.6b11880. [Scopus; Science Citation Index Expanded (Web of Science)] [IF: 4,484; AIF: 5,412; quartile: Q1 (2017, InCites JCR SCIE)]
4. Braukyla, Titas; Xia, Rui; Daskeviciene, Maryte; Malinauskas, Tadas; Gruodis, Alytis; Jankauskas, Vygintas; Fei, Zhaofu; Momblona, Cristina; Roldán-Carmona, Cristina; Dyson, Paul J.; Getautis, Vytautas; Nazeeruddin, Mohammad Khaja. Inexpensive hole transporting materials derived from Tröger's base afford efficient and stable perovskite solar cells // Angewandte chemie international edition. Weinheim : Wiley-VCH. ISSN 1433-7851. eISSN 1521-3773. 2019, vol. 00, p. 1-8. DOI: 10.1002/anie.201903705. [PubMed; Scopus; Science Citation Index Expanded (Web of Science)] [IF: 12,257; AIF: 5,880; quartile: Q1 (2018, InCites JCR SCIE)]

Presentations in conferences

2019.07.09 Conference „*13th International Conference on Optical Probes of Organic and Hybrid Optoelectronic Materials and Applications 2019*", Vilnius, Lithuania. Poster presentation „Hole-transporting enamines with Tröger's base scaffold for application in perovskite solar cells"

2019.05.16 Conference „*Chemistry & Chemical Technology 2019*", Vilnius, Lithuania. Poster presentation „Hole-transporting materials for perovskite solar cells containing Tröger's base core and enamine–linked diphenyl moieties"

2017.09.01 Conference „*ECME 2017 - 14th European Conference on Molecular Electronics*", Dresden, Germany. Poster presentation „*V-Shaped Hole-Transporting Materials Containing Tröger's Base Core and TPD-Type Branches"*

2017.04.28 Conference „*Chemistry & Chemical Technology 2017*", Kaunas, Lithuania. Oral presentation „*Synthesis and investigation of V-shaped hole-transporting TPD dimers containing Tröger`s base core"*

2017.03.14 Conference "*Open readings 2017*", Vilnius, Lithuania. Poster presentation „*Synthesis and investigation of V-shaped hole-transporting materials containing Tröger`s base core and TPD-type branches*"

2016.07.03 Conference "*Balticum Organicum Syntheticum 2016*", Riga, Latvia. Poster presentation "Synthesis of V-shaped hole-transporting materials containing Tröger`s base core and phenylethenyl branches*"*

2016.06.12 International summer school „*Advanced Perovskite, Hybrid and Thin-film Photovoltaics*", Krutyn, Poland. Poster presentation "*Novel V-shaped hole-transporting materials containing Tröger`s base core and phenylethenyl branches*"

2016.04.28 Conference „*Chemistry & Chemical Technology 2016*", Vilnius, Lithuania. Poster presentation „*Synthesis and investigation of V-shaped hole-transporting materials containing Tröger`s base core and phenylethenyl branches*"

2015.06.18 41st Lithuanian National Conference of Physics, Vilnius, Lithuania. Poster presentation *„Naujų molekulinių stiklų su Trögerio bazės fragmentu krūvio pernašos savybės"*

2014.07.07 Conference "*Balticum Organicum Syntheticum 2014*", Vilnius, Lithuania. Poster presentation "Synthesis of molecular glasses containing Tröger's base fragment*"*

2014.04.25 Conference „*Chemistry & Chemical Technology 2014*", Kaunas, Lithuania. Oral presentation „*Synthesis and investigation of novel molecular glasses containing Tröger's base fragment"*

10. ACKNOWLEDGEMENTS

My greatest appreciation regarding this dissertation is addressed to Prof. Dr. V. Getautis for giving me an opportunity to work in his research group, for his ideas, supervision, helpful advices during my research and studies, and for encouragement to carry on to the finish.

My sincere appreciations are to Dr. T. Malinauskas and Dr. M. Daškevičienė (Department of Organic Chemistry, KTU) for their helpful advice, lab wisdom, and support.

I would like to thank Prof. Dr. H. J. Snaith, Dr. N. Sakai (Department of Physics, Clarendon Laboratory, University of Oxford) and Prof. Dr. M. K. Nazeeruddin, Dr. R. Xia, Dr. C. Roldán-Carmona, and Dr. C. Momblona (Group for Molecular Engineering of Functional Materials, Institute of Chemical Sciences and Engineering, EPFL) for the fabrication and characterization of the PSCs.

I kindly thank to Dr. B. Barvainienė, A. Urbonavičienė, Dr. I. M. Liutvinienė, Dr. A. Pukalskas, Dr. D. Rosliuk, Dr. P. P. Danilovas, Dr. J. Simokaitienė, Dr. G. Ragaitė, and A. Bieliauskas (Faculty of Chemical Technology, KTU) for their help with elemental analysis, IR, UV/Vis, FL, MS, DSC, TGA, NMR measurements.

I thank Dr. G. Bagdžiūnas (Department of Polymer Chemistry and Technology, KTU) for the X-ray crystallography analysis.

I am grateful to Prof. Habil. Dr. V. Gaidelis, Dr. V. Jankauskas, and Dr. A. Gruodis (Department of the Solid State Electronics, Vilnius University) for the measurements of ionization potentials, charge carrier mobilities, molecular calculations and structure optimizations. Prof. Habil. Dr. S. Juršėnas and R. Komskis (Institute of Applied Research, Vilnius University) is acknowledged for the measurements of PL quantum yields and exciton lifetimes.

I am really thankful to my colleagues: Dr. S. Urnikaitė, Dr. I. Petrikytė, A. Magomedov, E. Kasparavičius, M. Steponaitis, Dr. G. Bubnienė, Dr. J. Ardaravičienė (Department of Organic Chemistry, KTU) and others for their assistance, consultations, encouragement, pieces of advice and a kind word in a lab.

I am also thankful to people who contributed to this dissertation indirectly, through the work of their own: workgroup of Prof. Dr. K. Warnmark (Lund University) for their scientific discoveries and publications, and for the reported convenient synthetic method that was essential for my work; workgroup of Prof. Dr. A. Lützen (Uni Bonn) for inspiringly well developed and precisely described method to obtain diamino-TB compounds; T. Reznor (NIN) for a work that was of a great use and inspiration during the research and writing of this dissertation.

My warm thanks to my friends and former fellow PhD students: Dr. T. Matulaitis (University of St Andrews) and Dr. N. Kukhta (Durham University) for their sincere friendship, support, pieces of advice, and sharing the spark of scientific interest during all the years of studies.

Most of all, I owe my loving thanks to my family, and especially to my wife Julija, for the support, love, encouragement, understanding and patience during the time of bringing this scientific work to fruition.

SL344. 2019-06-17, 26,5 leidyb. apsk. l. Tiražas 12 egz. Užsakymas 136.
Išleido Kauno technologijos universitetas, K. Donelaičio g. 73, 44249 Kaunas
Spausdino leidyklos „Technologija“ spaustuvė, Studentų g. 54, 51424 Kaunas